Multi-Scale Laboratory Characterisation of Soft Calcareous Mudstone

David J. Simpson

BSc (Hons) Geology

MSc Engineering Geology

A thesis submitted for the degree of Doctor of Philosophy in the

School of Civil Engineering and Geosciences

Newcastle University

Newcastle

NE1 7RU

November 2015

ABSTRACT

The construction industry of Abu Dhabi is thriving and its coastline has some of the most ambitious structures in the world. Whilst the sub-surface evaporitic and calcareous soft rocks of this region are of great geological interest, they are relatively poorly understood from a geotechnical engineering perspective, forcing foundation designs to be overly conservative.

Understanding a lithology's' stiffness at small strains is of great importance for the accurate estimation of ground movements around excavations and foundations, and yet post-SI laboratory testing programmes in this part of the world tend to centre around basic rock mechanics practices such as UCS tests. These procedures are generally unsuitable due to the friable and moisture sensitive nature of the native lithologies, and rarely obtain parameters representative of in-situ behaviour. Measuring the development of local strains on samples is particularly problematic due to these physical attributes.

The calcareous mudstones of this thesis have mechanical and structural characteristics falling between that of soil and rock and as such require a geotechnical testing approach that combines methods from both soil and rock mechanics disciplines. A custom framework has been developed that acts as a methodology for the laboratory testing of a soft calcareous mudstone. The mineralogical, micro-structural and mechanical characteristics of this lithology are examined via a suite of testing techniques, including XRD, SEM, advanced triaxial, DIC and Bender Elements along with industry standard procedures. Shearing, tensile and consolidation behaviours are explored.

Examination of the micro-macro scale features of this material show it to be highly structured, with strength and stiffness being controlled by inter-granular bonding of Dolomite grains, as well as by mean effective stress state and rate of strain. The presence of fibrous Palygorskite acts to reduce the degree of bonding, causing specimens rich in this clay mineral to behave more mechanically ductile.

ACKNOWLEDGEMENTS

I would firstly like to thank the academic, administrative and technical staff at Newcastle University for their help and generosity throughout the writing of this thesis, always making time to answer questions or otherwise assist in the smooth running of the project. I would also like to thank the staff at Buro Happold, GDS, AEG, Cundall and Dunelm for the parts they have played throughout the last four years and for helping me achieve the goals of this research project.

I would like to thank my supervisors Dr Mohamed Rouainia and Dr Paul Hughes for their constant reassurance and guidance.

A big thank you also goes to Stuart Patterson and Fred Beadle for making my time in the lab so memorable and for all of their help, input and encouragement throughout the years.

Thanks to my family and friends for their support and patience, especially during the difficult final year of this project. Notably, I would like to thank my mother for her love and reassurance along with her inspirational display of strength, courage and positivity in the face of extreme adversity.

Finally I would like to thank my son Nathaniel for uplifting me without even knowing he was doing it and Leilani for being a fantastic and loving mother to him.

NOMENCLATURE

A	= Area of Sample	mm^2, m^2
B	= Skempton B Value for Saturation	%
c’	= Cohesion	kPa, MPa
Cc	= Compression Index	-
Cs	= Swelling Index	-
CL	= Low Plasticity	-
CI	= Intermediate Plasticity	-
CH	= High Plasticity	-
c_u	= Undrained Shear Strength	kPa, MPa
D	= Diameter of Sample	mm, m
d_{10}	= Diameter of particles at 10% cumulative percentage passing	µm, mm
d_{30}	= Diameter of particles at 30% cumulative percentage passing	µm, mm
d_{50}	= Diameter of particles at 50% cumulative percentage passing	µm, mm
d_{60}	= Diameter of particles at 60% cumulative percentage passing	µm, mm
DIC	= Digital Image Correlation	-
E	= Young’s Modulus	kPa, MPa
E_{sec}	= Secant Young’s Modulus	kPa, MPa
E_{tan}	= Tangent Young’s Modulus	kPa, MPa
e	= Void Ratio	Dimensionless
e_0	= Initial Void Ratio	Dimensionless
F	= Force	N, kN
G_s	= Specific Gravity	Dimensionless
G	= Shear Modulus	kPa, MPa
G_{sec}	= Secant Shear Modulus	kPa, MPa
G_{tan}	= Tangent Shear Modulus	kPa, MPa
G_0	= Initial Shear Modulus	MPa
I_{d1}	= Durability Index (first cycle)	%
I_{d2}	= Durability Index (second cycle)	%
J	= Cross Anisotropic Modulus	kPa, MPa

K_0	= In-situ Coefficient of Earth Pressure	Dimensionless
K	= Bulk Modulus	kPa, MPa
k	= Coefficient of Permeability	m/s
log	= Logarithm to the Base 10	N/A
L	= Length of Sample	mm, m
L_0	= Initial Length of Sample / Initial Gauge Length	mm, m
M	= Mass of Sample	g, kg
n	= Porosity	Dimensionless
p	= Mean Total Stress	kPa, MPa
p’	= Mean Effective Stress	kPa, MPa
p'_0	= Initial Mean Effective Stress	kPa, MPa
p_c	= Pre-consolidation Pressure	kPa, MPa
PSD	= Particle Size Distribution	-
q	= Deviatoric Stress	kPa, MPa
q_{max}	= Maximum Deviatoric Stress	kPa, MPa
R	= Ratio of Tensile Strength to UCS	-
SEM	= Scanning Electron Microscopy	-
Sr_i	= Initial Degree of Saturation	%
Ts	= Travel Time	ms
u	= Pore Water Pressure	kPa, MPa
UCS	= Uniaxial Compressive Strength	kPa, MPa
v	= Poisson’s Ratio	Dimensionless
V	= Volume of Sample	mm^3, m^3
Vs	= Seismic Velocity	m/ms
w_0	= Initial Moisture Content	%
XRD	= X-Ray Diffraction	-
ε_a	= Axial Strain	%
ε_r	= Radial Strain	%
ε_s	= Shear Strain	%
ε_v	= Volumetric Strain	%
σ_1	= Major Principal Stress	kPa, MPa
σ_3	= Minor Principal Stress, also Cell Pressure	kPa, MPa
σ_a	= Total Axial Stress	kPa, MPa
σ'_a	= Effective Axial Stress	kPa, MPa

σ_r	= Total Radial Stress, also Cell Pressure	kPa, MPa
σ'_r	= Effective Radial Stress	kPa, MPa
σ_t	= Tensile Stress	kPa, MPa
ϕ’	= Friction Angle	Degrees
ρ	= Bulk Density	Mg/m^3
ρ_d	= Dry Density	Mg/m^3
ρ_s	= Particle Density	Mg/m^3
ρ_w	= Density of Water	Mg/m^3
‰	= Permille (parts per thousand)	-

CONTENTS

LIST OF FIGURES

LIST OF TABLES

CHAPTER 1. INTRODUCTION

1.1. RESEARCH RATIONAL

Many of the coastal areas of Abu Dhabi in the United Arab Emirates (UAE) are heavily built up urban conurbations and Abu Dhabi Island is home to some of the tallest buildings in the world. The young 'soft rocks' that make up the sub-surface of this part of the Middle East are well studied from a geological standpoint, however research into their complex mechanical behaviour is less common and only a handful of publications exist (Cook, 1999); (Epps, 2011). In addition to this, their unique physical characteristics make the application of many standard laboratory testing methodologies inappropriate, particularly regarding their sensitivity to changing moisture contents which can make them problematic to handle if not prepared correctly.

Since the end of the Palaeozoic, the climate of the UAE has remained broadly similar to the one in which it is seen today, with its solid and drift geology defined by repeated cycles of glacio-eustatic triggered marine transgressions in and around the Arabian Gulf and subsequent sub-aerial erosion and transportation (Walkden & Williams, 1998); (ASP, 2001); (Epps, 2010). These cycles have allowed the formation of vast expanses of carbonate and evaporite sediments to form from the Gulf's saline waters, including: fossiliferous limestone and dolomite along with siltstones, sandstones and interbedded gypsum, halite and anhydrite as well as the calcareous mudstones studied within this thesis (Walkden & Williams, 1998); (Evans, 2011).

These mudstones were likely to have been deposited within a low energy but chemically dynamic hyper saline environment, and are predominantly biogenic / chemical in origin, as opposed to purely detrital. In lithologies such as these, the time gap between the formation of clasts and their bonding agents can be small, or even occur contemporaneously and weak cementicious bridges may precipitate within voids far more rapidly than, for example, iron oxide or alumina bonds will form in terrestrial and freshwater sediments, introducing a degree of structure that needs to be taken into account when attempting to characterise their behaviour (Epps, 2011); (Truong, et al., 2012). Sediments formed in hyper saline waters are noted to be particularly sensitive to changing physicochemical environments which can cause problems during routine geotechnical laboratory tests which typically demand full saturation in order to assess effective parameters, or else require samples to be dry in the case of many rock testing

procedures (Burland & Lord, 1970); (Hawkins, 2000). In addition to this, the calcareous mudstones studied are highly friable, making the measurement of local deformations difficult using standard strain gauges designed for application with hard rocks.

A significant volume of work undertaken by UK consultants is procured in the Middle East and the long term construction programmes for countries such as Abu Dhabi indicate that this will continue to be the case for some time to come.

One of the major challenges of working in the region is developing effective project designs in ground conditions that are both aggressive and susceptible to variations in the sub-surface groundwater regime. Beyond this it is also apparent that the geotechnical properties of strata encountered are often poorly understood and that current testing procedures are lacking in terms of their applicability to soft rocks, leading to potentially conservative foundation solutions.

An improved appreciation of ground behaviour in Abu Dhabi will enable UK consultants to offer Middle Eastern clients more efficient design solutions and potentially enable them to obtain a greater percentage of the consultancy market. It will also ensure that inherent ground related risks are better addressed and thereby reduce the likelihood of claims against designers.

In light of the scale of the recent urban development being carried out around the coastline of Abu Dhabi, coupled with the lack of current publications concerning the properties of the sub-surface deposits, it has been deemed that further research is required in order to gain a more thorough understanding of the physical behaviour of these calcareous mudstones.

This thesis presents both the methodologies and findings of a custom suite of characterisation, optical and mechanical tests carried out upon one extensively occurring soft rock lithology from the Abu Dhabi coastline in order to assess and characterise its physical and petrographic properties, with a particular focus on the small strain stiffness behaviour of this lithology in triaxial compression. This is of particular relevance to the design of tall buildings and underground structures in the region. Ultimately, the lithology assessed within this thesis is broken down into sub-types (namely Type A and Type B), in order to rationalise its diverse mechanical and physical properties and aid in the prediction of its likely behaviour based upon known index characteristics.

1.1.1. *BACKGROUND - SOFT ROCKS*

The importance of distinguishing between soil and rock is known to all engineers involved with the ground, as typically, both the physical and engineering properties of the two materials are very different (Matthews, et al., 2006); (Haberfield, 2000), and an artificial boundary has been drawn between these two broad material types that few practicing geotechnical engineers are able to cross with confidence, generally preferring to specialise in either rock or soil mechanics (Hawkins, 2000); (Haberfield, 2000).

Soil mechanics, being closely related to and associated with the activities of civil engineering, has historically dealt with shallow near surface ground materials with a focus on the problems surrounding wet or soft deposits, with site investigations being typically carried out using cable percussive means and laboratory testing focused on obtaining properties such as plasticity, grain size distribution, relative densities, shear strength, friction angle, cohesion, compressibility and permeability (Haberfield, 2000).

Usually, testing is carried out upon samples devoid of macro features such as cracks or cobbles that might result in unlikely or unrealistic outcomes or cause pre-emptive failures. This is particularly true of triaxial testing. When discontinuities are considered, these tend to be fissures associated with stress release or drying (Hawkins, 2000).

Rock mechanics, however, was borne through the mining industry where emphasis was placed upon gaining access to underground mineral and metal deposits, and as such a good knowledge of the planes of weakness and orientation of jointing was essential. This is reflected in modern day site investigations where logging of rotary cores tends to focus upon the degree of weathering and the angles of discontinuities (Haberfield, 2000). An understanding of the orientation and roughness of in-situ discontinuities and fractures are often considered more important than a rock's intact strength, as in most cases these are weaker and more prone to failure than the solid rock itself, and as such much attention is given to bedding plane and stress induced joint orientation and frequency (Hawkins, 2000). Where material intact properties are considered, they are generally assumed to be elastic, isotropic and homogeneous (Corthesy, et al., 2003). In-situ measurements, descriptions and rock mass classifications are used as much as laboratory testing, however common tests carried out are point load tests, Brazilian Tensile tests and unconfined compressive strength (UCS) tests. These tests are quick and simple, but do provide good baseline values from which empirical estimations of overall engineering performance may be made (Agustawijaya, 2007).

The geological cycle describes the idealised theoretical process of soil lithifying into rock and rock weathering into soil (Dobereiner & Freitas, 1986); (Haberfield, 2000), however, a 'grey area' exists between these two generalised extremes (Figure 1.1), housing a group of materials that do not fit into the well-established and convenient categories of soil / rock engineering (Hawkins, 2000); (Haberfield, 2000); (Bromhead & Patel, 2000). These materials are known as soft rocks.

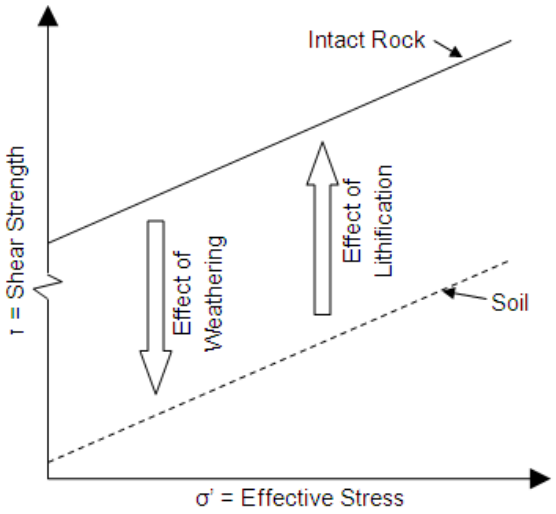

Figure 1.1: Difference between soil and rock in terms of shear strength envelopes. Adapted from (Vaughan, 1993).

Soft rocks have, in the past, been treated as 'special cases', and have been dealt with via the application of whichever discipline is better known to those working on a given project or by using the convention that appears to better suit the problematic material (Johnston, 1991); (Vaughan, 1993).

However attempting to treat these intermediate materials in a traditional manner has often lead to heavily over-engineered and highly conservative geotechnical solutions, being neither economically nor environmentally sustainable and even on a few rarer occasions this approach has resulted in designs that are marginal or unsafe (Haberfield, 2000). For example, soft rocks found in areas where soils are predominant may be treated like stiff clays or dense sands, giving little allowance for their more brittle, stiffer nature. Likewise, soft rocks located in areas generally characterised by hard rock's may be treated as if very weak or weathered, not allowing for the higher compressibility's possible nor the influence of pore water pressures or degree of saturation (Johnston, 1991); (Agustawijaya, 2007); (Haberfield, 2000).

To combat this, soft rocks are increasingly being treated as a new sub-category of geotechnical engineering with designated societies and conferences emerging. Soft rock

is becoming an umbrella term for lithologies which do not fully obey the established trends of either soil or rock mechanics.

Soft rock lithologies may be as varied as those of both soils and rocks, as due to the wide range of natural processes occurring above and below ground, almost any rock or soil type may, at some time during its transition through the rock cycle, fall within the category of 'soft rock' (Johnston, 1991); (Aversa, et al., 1993); (Corthesy, et al., 2003):

Strong rocks may, over time, become 'soft' as a result of weathering processes including stress release, frost disintegration or chemical decay (Thompson & Leach, 1988); (Hawkins, 2000), whilst soils may become hardened by consolidation, aging, structuring and cementation via various chemical and / or physical processes (Dobereiner & Freitas, 1986); (Hawkins, 2000); (Bromhead & Patel, 2000); (Cecconi & Viggiani, 2001); (Truong, et al., 2012), causing them to no longer owe their strength solely to their particle size distribution, void ratio and stress history (Leroueil & Vaughan, 1990); (Bica, et al., 2008).

Mechanically, soft rocks may behave primarily like a rock or a soil, however often exhibit aspects of both depending upon on the degree of weathering / cementation and other factors including; percentage saturation, pore-water chemistry, rate of applied stress, confining pressure, temperature and mineralogy. As such, classification using one technique in isolation is difficult and there exist many schemes that have attempted to define the mechanical boundaries between soils, rocks and soft rocks (Dobereiner & Freitas, 1986); (Johnston, 1991); (Cook, 1999); (Agustawijaya, 2007); (Epps, 2011).

Most schemes rely on the findings of Uniaxial Compressive Strength (*UCS*) tests, however other properties such as undrained compressive shear strength (*Cu*), tensile strength and even the degree of submerged disintegration have historically been employed. Soft rocks tend to be described based on their intact properties (as are soils) rather than the strength of their discontinuities, however a number of schemes have also considered Rock Mass Index observations (Hawkes & Mellor, 1970); (Fookes & Higginbottom, 1975); (Brown, 1981); (Dobereiner & Freitas, 1986); (Hoek & Brown, 1988); (Johnston, 1991); (Hawkins & Pinches, 1992); (Kim, et al., 1994); (Okubo & Fukui, 1996); (Hoek, et al., 1998); (Cook, 1999); (Hawkins, 2000); (Corthesy, et al., 2003); (Coviello, et al., 2005); (Agustawijaya, 2007); (Zhang, et al., 2010); (Epps, 2011). However it is worth noting that there is no consensus regarding a definition of

soft rocks at this time as the concept of hard soils / soft rocks is still in its infancy (Hawkins, 2000); (Corthesy, et al., 2003).

This thesis explores the current understanding of soft rocks via literature review and highlights some of the inherent ambiguity surrounding them that has led to such debate within the academic and industrial communities, as well as assessing the role of various factors affecting a key performance characteristic of geo-materials: stiffness.

1.1.2. *BACKGROUND - SMALL STRAIN STIFFNESS THEORY*

Historically there has often been noted a discrepancy between the high stiffness of geo-materials measured in-situ and the relatively low stiffness's obtained from laboratory testing. It is now well understood that this is largely due to small strain stiffness behaviour; the tendency for geo-materials to display high stiffness's that decrease rapidly with small increases in strain.

Three distinct regions of stiffness – strain behaviour exist: very small strains (<0.001% strain where stiffness is constant), small strains (between 0.001 and 1% strain where considerable stiffness degradation occurs with increasing strain) and large strains (>1% strain where stiffness is reduced to a nominal value) (Atkinson & Sallfors, 1991); (Finno & Kim, 2011); (Clayton, 2011). Whilst the majority of commercial testing tends to focus on the behaviour of geo-materials at large strains, the programme of mechanical characterisation of the soft calcareous mudstones within this thesis focuses primarily upon stiffness at small strains.

The importance of accurately measuring soil stiffness, from very small strains through to failure, is well recognised (Barla, et al.). Soil stiffness's measured locally often exceed those taken from traditional laboratory testing by an order of magnitude within the small strain range; putting results more in line with stiffness's observed from in-situ / field measurements and seismic testing. This trend has also been found to be true for soft rocks, and like soils, the typical ground strains that develop within such materials rarely exceed 0.1% under normal working loads (Kim, et al., 1994) making rigorous investigation into soft rock behaviour at small strains important for many building projects, as it is within this range that the strains applicable to the most geotechnical structures fall (Figure 1.2).

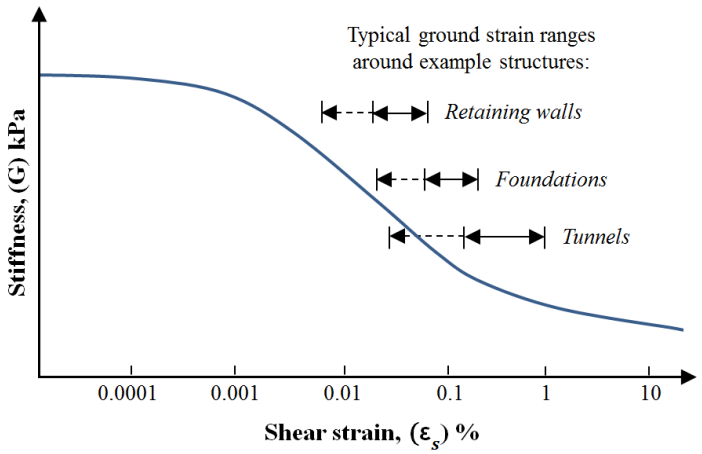

Figure 1.2: Shear stiffness relationship to shear strain alongside example structures (Clayton, 2011)

The examination of the small strain stiffness behaviour of soils continues to close the gap between laboratory and field measurements of stiffness with a large amount of work having been undertaken in this area (Jardine , et al., 1985); (Jardine, et al., 1986); (Burland, 1989); (Atkinson & Sallfors, 1991); (Jardine, 1992); (Puzrin & Burland, 1998); (Atkinson, 2000); (Clayton & Heymann, 2001); (Gasparre, 2005); (Heymann, et al., 2005); (Gasparre & Coop, 2006); (Finno & Kim, 2011); (Truong, et al., 2012). However, comparatively minimal research has been carried out to investigate similar properties of soft rocks.

Due to the problems associated with the recovery of soft rocks through drilling, including their tendency to become damaged by the drilling process, along with natural inter-sample variability and the difficulty of testing friable rock samples in the laboratory, the majority of existing published work on soft rocks tends to focus on laboratory manufactured / artificially cemented specimens rather than field derived natural sample cores.

This thesis will predominantly carry out tests on undisturbed natural core samples supplied from two site investigations in Abu Dhabi, assessing their small and very small strain stiffness behaviour with respect to their stress state and mineralogical make up as well as obtaining a number of index properties for use in design.

1.2. AIM

This research aims to characterise the physical, mineralogical and mechanical properties of a soft calcareous mudstone from Abu Dhabi using a micro to macro scale approach, ultimately relating its lithological and structural features to its engineering behaviour.

1.3. OBJECTIVES

This aim will be achieved by carrying out a series of objectives:

1. To review existing literature on the topics of; typical soft rock mechanical behaviour from small through to large strains, the sedimentary and chemical environment under which calcareous mudstones are formed and also the current testing apparatus and procedures most commonly applied to soft rocks in order to contextualise the materials tested within this thesis and assess the most suitable means of assessing their properties in the laboratory;

2. To establish a repeatable framework for the assessment of mineralogy and structure of calcareous soft rocks using laboratory techniques;

3. To develop a methodology for the measurement of local stresses and strains that takes into account the natural weaknesses and sensitivity to moisture contents that this lithology presents in both compression and tension;

4. To define the mineralogy and fabric / structure of the calcareous mudstone samples (pre-shearing) via various micro-scale optical techniques with a focus on sensitive and dissolvable minerals;

5. To characterise the soft rock's mechanical response to stress at both large and small strains including their strength and stiffness dependence upon confining pressure and strain rate along with their behaviour in tension;

6. To link the findings of the mechanical testing programme to the findings of the petrographic analysis to develop a full micro to macro characterisation of the soft calcareous mudstone, ultimately classifying them accordingly, and;

7. To draw conclusions regarding the physical behaviour of soft calcareous mudstone from Abu Dhabi and propose recommendations for the geotechnical testing of soft rocks in the laboratory.

1.4. SCOPE

A review of literature has revealed a lack of research into the mechanical properties of soft calcareous rocks originating from Abu Dhabi. These materials are young and display behavioural properties akin to both soil and rock, creating problems for routine geotechnical design and laboratory testing alike.

Scanning electron microscope (SEM) techniques will be used to assist in the characterisation of the fabric and structure of these difficult materials pre-shearing. X-ray diffraction techniques will also be used to improve understanding of the mineralogy of the soft rock and its cementation. A suite of standard characterisation tests from both soil and rock mechanics will be performed on the soft calcareous mudstones based upon their suitability in order to further characterise their behaviour.

A methodology for the testing of soft rocks in triaxial / Brazilian laboratory tests will be developed that takes into account the friable and sensitive nature of calcareous mudstone with a particular focus on the development of local strains.

Hall Effect local strain gauges will be used in triaxial apparatus in order to measure the response of samples subjected to a number of stress states. Bender Elements will be employed in a single test in order to assess the initial shear modulus (G_0) of the sample. Triaxial experiments carried out within this thesis are limited to compressive tests under drained conditions. In unconfined conditions a new method will be used, namely digital image correlation (DIC) to assist in the measurement of localised strain developments during indirect tensile strength testing. Odometers will be used to observe and measure consolidation characteristics in addition to assessing structural features.

All samples tested within this thesis originated from two site investigations (namely the Yas Mina SI and the NBAD SI) and were recovered via rotary coring technique. Samples were packaged and stored in Abu Dhabi prior to being transported to the UK. A limited number of samples were available throughout this project and as such the experimental programme needed to be carefully pre-planned and staggered in such a way as to maximise the amount and variability of tests that could be carried out. This thesis is primarily laboratory focused and does not analyse any data derived from in-situ field testing, nor does it include any simulated or modelled testing.

It is anticipated this research will ultimately aid in the design of more economical foundations and add to the present literature by examining a material of long standing

geological interest within a geotechnical context. This research project will also assist the wider geotechnical community by providing experimental results that can be used to validate and calibrate existing models concerning the small strain stiffness degradation and yielding of soft rocks.

It is hoped that by linking the calcareous mudstones' engineering properties to its lithological characteristics, it may be possible to develop a framework explaining the materials' mechanical behaviour based upon its stress state and index properties.

CHAPTER 2. LITERATURE REVIEW

2.1. CHAPTER 2 INTRODUCTION

The previous chapter set out the aim, objectives and scope of this research project and introduced several key themes that flow throughout it, including the problems surrounding soft rock testing and small strain stiffness theory.

This chapter explores the current understanding of the definition of soft rocks and the ambiguity that surrounds them. Small strain stiffness theory is discussed along with factors known to influence the strength and stiffness of hard soils and soft rocks from small through to large strains, an understanding of which is crucial for the interpretation of mechanical testing data and ultimately for the classification of tested materials.

The purpose of this chapter is to provide context for the project and also to ensure that practices and theories are up to date. Additionally, this chapter aims to identify a research gap, justifying the need for research into the mechanical behaviour of soft calcareous rocks.

Descriptions of the two sites of interest are presented in Chapter 3 along with a brief review of the geological setting of the study area. Assessments of the applicability of several local strain measuring devices are reviewed in Chapter 4 along with other laboratory testing specific observations and developments.

2.2. SOFT ROCKS

2.2.1. *ORIGIN OF SOFT ROCKS*

The geological cycle describes the process of soils lithifying into rocks and rocks weathering into soils (Haberfield, 2000). This continuous cycle can be seen pictorially within Figure 2.1. Located centrally between the two extremes of hard rocks and soft soils is the diffusely bounded region of ‘soft rock’, an emerging material type that does not fully obey the accepted trends of either soil or rock mechanics.

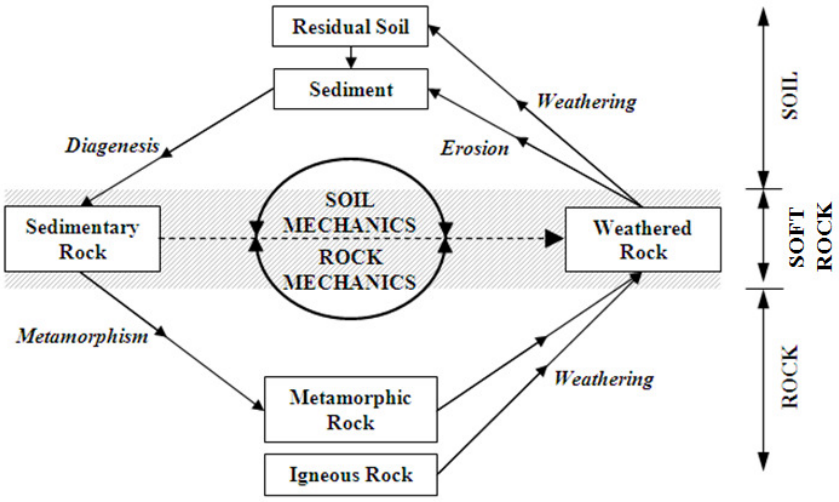

Figure 2.1: Schematic representing the formation of soft rock. Adapted from (Dobereiner & Freitas, 1986).

Grain size, texture, mineralogy, cementation and colour of soft rocks can be as varied as that of both hard rocks and soils and as such exclusive categorisation based upon these properties is difficult. Soft rocks may behave primarily like a rock or a soil, however often exhibit aspects of both due to the degree of weathering / cementation and other factors including; percentage saturation, rate of applied stress, confining pressure, temperature, mineral content and grain size distribution (Dobereiner & Freitas, 1986); (Agustawijaya, 2007); (Epps, 2011).

Throughout the literature there are many types of soft rocks studied and their origins are diverse. Aversa, et al (1993) and Cortesy, et al (2003) state that soft rocks can include; mudstone, sandstone, shale, pyroclastics, carbonates and evaporites, (of which the carbonate and evaporite deposits are noted as being geo-mechanically some of the most complex), however due to the wide range of natural processes occurring above and below ground, almost any rock or soil type may, at some time during its existence, fall under the heading of ‘soft rock’.

For example strong rocks may, over time, become considered ‘soft’ as a result of advanced weathering processes including stress release, frost disintegration or chemical decay. In layered sedimentary rocks, the pattern in which the strata succumbs to weathering can often be inverted, with ‘soft rocks’ occurring deeper in a stratigraphy than hard rocks of the same sequence.

Keuper Marl deposits, for example, have been observed by Thompson & Leach (1988) to display six distinct weathering grades, inter-fingered amongst one another, ranging in strength from that of moderately strong rock through to stiff residual soils. Some strata

are most accurately characterised using soil mechanics whilst others by rock mechanics, although superficially the materials are fundamentally similar.

Another example of this pattern was seen by Hawkins (2000) in the Triassic Mudrocks of Aust, along the Severn Estuary. Whilst much of this material comprises cemented bands, with rock mass strengths ≈12 MPa, the overall behaviour is dominated by the presence of soft rocks, lowering the rock mass strength to <1 MPa.

Weathering processes easily exploit sedimentary rocks, as they generally have a higher permeability and void ratio than their metamorphic and igneous counterparts, and whilst it is true that most 'soft rocks' are sedimentary (and often fine grained), many metamorphic and igneous rocks may also be affected in similar ways (Hawkins, 2000). The granites of Devon and Cornwall, for example, will weather into China Clay having been weakened by hydrothermal activity (Hawkins, 2000).

When viewed from a desk study perspective, soft rock types may be assumed, quite incorrectly, to be more competent than they are in reality. This is usually based upon misconceptions surrounding their pre-weathered / altered strengths.

Likewise soils, at the opposite end of the cycle, may become hardened by consolidation, causing water expulsion and densification along with particle re-alignment and aging to the point that they fall within a strength range usually associated with weak rocks. Other soils may become structured, adding to their strength and stiffness, as inter-particulate bonding develops or as they become rapidly cemented by various chemical and physical processes (Dobereiner & Freitas, 1986); (Hawkins, 2000); (Bromhead & Patel, 2000); (Cecconi & Viggiani, 2001); (Truong, et al., 2012).

Many studies have been carried out by various authors on soils developing structure, for example London Clay, Bothkennar Clay and Vallericca Clay, and the behaviour of such materials is of great interest to the geotechnical community. Many authors consider micro-structured / structured soils to fall within the definition of soft rocks as they no longer owe their strength solely to their PSD, void ratio and stress history, key characteristics of soil behaviour (Leroueil & Vaughan, 1990); (Bica, et al., 2008).

A third type of soft rock origin exists, that of the young cemented materials deposited within calcareous / hyper saline environments. These materials differ from structured soils for a number of reasons. Firstly, the particulate material may originate from biogenic or chemical activity, as opposed to a purely detrital formation. Secondly, the

time gap between the formation of particulate material and its bonding can be small (or even occur contemporaneously). Salts, for example halite, will precipitate out of evaporating water to form weak cementicious bridges more rapidly than iron oxide or alumina bonds will form. This occurs across vast areas in Sabkha regions, often displaying a random spatial distribution of saline cement due to the distribution of capillary forces (Epps, 2011); (Truong, et al., 2012). Calcareous soft rocks form in waters that are chemically active and dynamic, accelerating lithification compared to that of terrestrial and freshwater sediments. Young calcareous / evaporite rocks are rapidly becoming considered as classic examples of soft rocks (Truong, et al., 2012), and are complex from an engineering perspective as they are particularly sensitive to changing physicochemical environments:

Chalk in Britain from the Upper Cretaceous, for example, has low unconfined compressive strengths and is usually treated as a rock. When tested in UCS they fail in a brittle manner, however when subject to high confining stress or sheared at low strain rates they behave in a ductile and 'soil like' way, losing their brittle behaviour (Burland & Lord, 1970); (Hawkins, 2000).

Also Cook (1999), during several site investigations within the UAE, noted the tendency for the exposed young and seemingly hard calcareous rocks at the base of excavations to deteriorate rapidly and exhibit soil like behaviour following overburden pressure release and dewatering, undergoing swelling, losing strength and becoming ductile.

Hawkins (2000) suggests that soft rocks should not be thought of as an extension of soil and rock behaviour, but as a category unto themselves, requiring new methods of testing, apparatus and analysis.

2.2.2. *DEFINITIONS OF SOFT ROCK*

Upon encountering soft rocks, engineers will often attempt to characterise them as either a soil or rock. In soil mechanics, the descriptive terms 'hard' or 'very stiff' are often applied to soft rock materials in order to simplify their behaviour, and terms such as 'weathered' and 'weak' are used in rock mechanics. In practice these terms are not wholly appropriate.

Weathered rock may include materials exhibiting a wide strength range, from 'fresh' to 'fully weathered' and 'residual soil'. A rock may be weak due to its intact mechanical

behaviour or that of the jointed rock mass, whereas soft rock is solely a description of intact properties. Likewise, hard and very stiff have specific meanings in soil mechanics which preclude the brittle properties of rocks (Johnston, 1991); (Hawkins, 2000).

Calcareous soft rocks present additional problems in terms of categorisation, as their lithological names can create false understandings of their behaviour (Cook, 1999). By referring to calcareous materials as mudstone, sandstone or siltstone, engineers may fail to understand the significantly weaker behaviour of their calcareous counterparts.

Many schemes attempt to define the mechanical boundaries of soft rocks and even specifically those of soft calcareous rocks (Cook, 1999). Most use UCS strength, however other properties such as undrained cohesion (Cu), tensile strength and even Rock Mass Index observations have been considered. Some of the most popular methods / schemes relate to the following properties:

- Disintegration in water
- Uniaxial Compressive Strength
- Tensile Strength
- Degree of Cohesion
- Ductility
- Rock Mass Index

Disintegration in Water

It has historically been accepted that a soil, when immersed in water, will disintegrate over time, whereas rocks will not. Whilst broadly true, soft rocks do not adhere to this trend. In an attempt to simplify the categorisation of soft rocks, Dobereiner & Freitas (1986) subjected soft sandstone samples to this rule of thumb. Mixed results were found as some lithologies disintegrated whereas others did not; making sole use of this test ambiguous for classifying the soft rocks in their study.

Based on the results of over 400 UCS tests on Calcareous soft rocks, Cook (1999) proposed that the soil to rock boundary should be unique for each lithology. By noting strength changes of calcareous sandstones, siltstones and mudstones following submersion in water, Cook (1999) was able to draw a line between what constituted as soil and what should be considered as rock, effectively negating the term soft rock (or ‘between ground’, as Cook himself proposed the intermediate lithologies be referred). The findings of Cook’s work are presented as Table 2.1:

Table 2.1: Boundary between soil - rock for some calcareous materials. (Cook, 1999).

Rock Type	UCS strength marking soil/rock boundary (MPa)
Calcarenite	0.5
Calcareous Sandstone	1.0
Calcareous Siltstone / Mudstone	***2.0***

These demarcations were taken from the point, directly below which, the materials were unable to remain intact following submersion in water. Cook speculated that the results may vary if salinity was introduced to the water and recommended that a period of 3 days submersion should be sufficient to observe disintegration.

Cook (1999) states that the calcareous rocks of Abu Dhabi degraded over time when exposed to humid air in addition to the rapid degradation they underwent when fully submerged in water. This study is of particular interest, as the lithologies assessed originate from similar locations within Abu Dhabi to those of this project.

Uniaxial Compressive Strength (UCS)

The upper and lower UCS strength boundaries of 'soft rock' have been debated by a number of authors over the past 40 years and numerous classifications have emerged.

Fookes & Higginbottom (1975) inferred the boundary between soil and rock to be between 0.3 and 1.25 MPa UCS during work with carbonate sediments. Epps, (2011) suggests the boundary between unconsolidated and cemented sediments to be between 0.6 and 1.25 MPa UCS.

Early mentions of 'soft rocks' within the literature have referred to them as having UCS values of less than 25MPa (Bieniawski, 1973). Clarke & Walker (1977) used the term 'slightly indurated / hard to moderately weak' following their work on carbonate sediments, classifying them as falling between 0.3 and 12.5 MPa UCS strength (Cook, 1999).

The ISRM (1981) classification scheme for soil and rocks shows an overlap between very stiff to hard soils and extremely weak and very weak rocks, as shown in Figure 2.2.

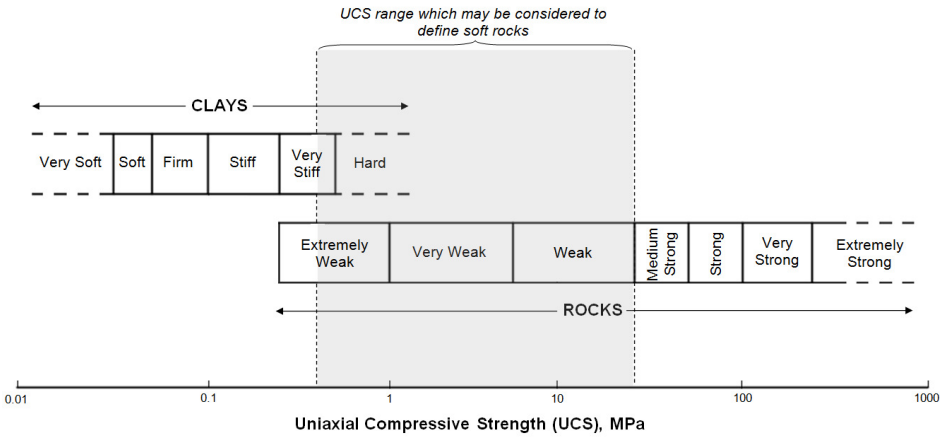

Figure 2.2: ISRM classification scheme adapted from (Brown, 1981) and (Johnston, 1991) to show the strength range adopted for use within this project.

This overlap, occurring between the range of 0.5 and 25MPa intact UCS, has been considered the definition of soft rocks for many authors, as suggested by Johnston (1991) and Dobereiner & Freitas, (1986). Despite this rising consensus, soft rocks have since been described as having UCS values of less than 10 MPa (Kim, et al., 1994), or as having a UCS of less than 20 MPa (Agustawijaya, 2007); (Zhang, et al., 2010).

This is not a new problem, as arriving at a consensus for strength terminology and standardisation has been historically difficult. Figure 2.3 shows an example of this with regards rock mechanics, showing the changing boundaries of strength based upon USC performance through the years and with respect to various society's perspectives:

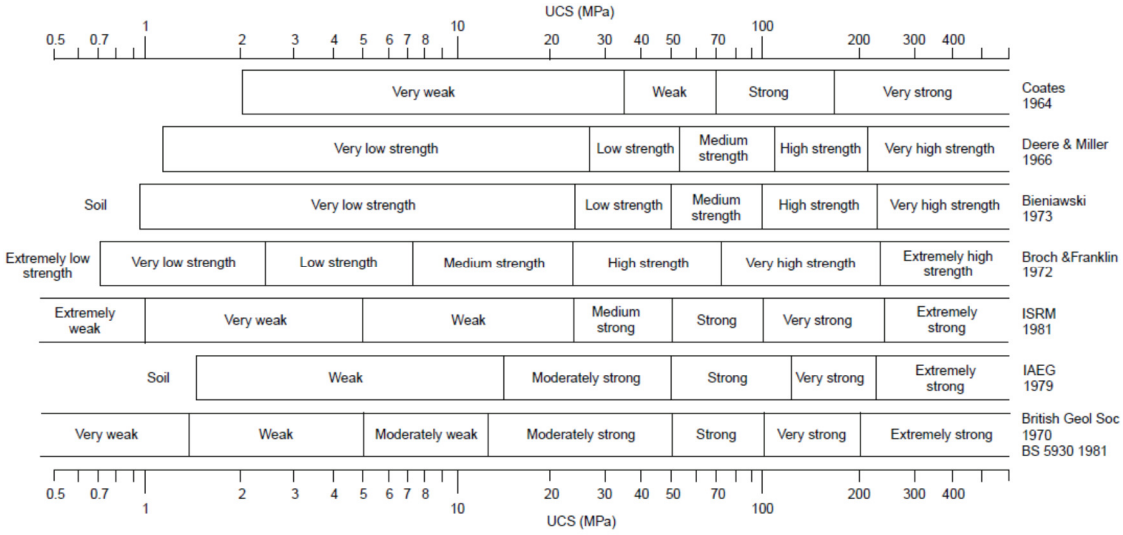

Figure 2.3: Various rock strength classification schemes through time.

These schemes highlight that terminology changes meaning through time and even with respect to geographic location, with a 'very weak' material in 1964 being classified as anything up to moderately strong by the 1980s.

From a domestic perspective, the upper and lower boundary of soft rocks can be drawn with reference to BS5930. Whilst UCS is used to define the upper regions of moderately weak rocks, the lower boundary of hard soil strength is more logically obtained by means of undrained triaxial tests (Table 2.2).

This method was adopted by (Hawkins & Pinches, 1992) and (Hawkins, 2000) and has the advantage of acknowledging that reliable UCS values obtained from soil testing is unlikely, whilst recognising that materials with UCS values greater than 10MPa may behave in a predominantly 'rock like' way with respect to strength, presenting a realistic transition between soil and rock strength.

Table 2.2: Definition of soft rocks using British scheme with soft rocks highlighted in grey. As proposed by (Hawkins, 2000) and (Hawkins & Pinches, 1992).

Cu	<20 kPa	Very Soft
Cu	20-40 kPa	Soft
Cu	40-80 kPa	Firm
Cu	80-160 kPa	Stiff
Cu	160-320 kPa	Very Stiff
Cu	**320-640 kPa**	**Hard**
UCS	**1.25-2.5 MPa**	**Very Weak Rock**
UCS	**2.5-5.0 MPa**	**Weak**
UCS	**5.0-10.0 MPa**	**Moderately Weak**
UCS	10-50 MPa	Moderately Strong
UCS	50-100 MPa	Strong
UCS	100-200 MPa	Very Strong
UCS	>200 MPa	Extremely Strong

Tensile Strength

By definition, the tensile strength of a material is the maximum stress it can undergo before failure in a purely tensile state. This is often considered the most critical mechanical parameter in rock mechanics as it is generally significantly lower than any given rock's shear strength (Coviello, et al., 2005).

Obtaining this parameter is notoriously difficult however, and the method best suited to reliably determining it has been the focus of much debate within the scientific community for some time (Chen & Hsu, 2001) resulting in many methods and practices, both directly and indirectly including the Direct Pull Test, Brazilian Disk Test, Three and Four Point Bending Tests and the Ring Test. However due to numerous practical

difficulties, specifically the ease and cost of sample preparation alongside problems associated with the reliable transfer of tensile stresses during uniaxial tensile testing, more attention tends to be directed to indirect methods such as the Brazilian Test.

The ratio of UCS to tensile strength at failure of soft rocks is noted to be lower than that of hard rocks. Coviello, et al (2005) found ratios of between 4.9 and 6.2 during their testing of Calcerenite, a soft rock material with a UCS ≈4 MPa.

Similar trends were found during preliminary testing at Newcastle University on both moderately strong Springwell Sandstone (with UCS ≈50 MPa) and weak artificial rock (UCS ≈ 4 MPa). Brazilian tensile testing was carried out revealing ratios of 12 and 5 respectively for the two materials.

Within this context, soft rocks are characterized by low ratios (R) of UCS to Tensile Strength (TS). Strong rocks, such as granite or gneiss may have an R of 25-35 and well cemented sandstones an R of 13-21. According to Okubo & Fukui (1996), ratios between UCS and TS for hard rock should fall between 8 and 27, depending upon lithology. Soft rocks, however, tend to have a UCS to TS ratio of less than 10 or even as low as 3-5 in the case of calcareous rocks and evaporites ((Coviello, et al., 2005); (Hoek, 2007); (Cai, 2010)). Whilst not commonly used as an aid to definition, low UCS / tensile strength ratios are indeed indicative of soft rocks.

Cohesion

Whilst Hawkes & Mellor (1970) defined rocks as being any naturally occurring ground material displaying cohesion enough to allow UCS testing. Later researchers suggest a cohesion of above 0.3 MPa could be considered a rock (Cook, 1999).

Ductility

Hawkins (2000), states that a rock may be considered soft when plastic deformation becomes prevalent over elastic-brittle failure, particularly at low confining pressures. This is repeated by Cortesy, et al (2003), whilst studying evaporites, shale and Molassic sandstones, stating that soft rocks are characterised by high pre-failure ratios of non-elastic to elastic behaviour.

Unlike hard rocks, which are assumed to behave in an elastic-brittle manner, soft rocks will often experience ductile failure (even at relatively low confining pressures). That is not to say elastic-brittle failure mechanisms do not occur within soft rock masses, only

that the transition to ductile-plastic failure occurs at lower stresses than in competent hard rock, (often within engineering induced stress change ranges).

Rock Mass Index Observations – Geological Strength Index Diagram

Hoek, et al (1998) attempted to accommodate 'soft rock' into the pre-existing Geological Strength Index (GSI) diagram, a rock mass scale based on visual examination, by the addition of a sub-division.

The original GSI, as published earlier by Hoek & Brown (1988), contained four categories to describe rocks of varying strength (Hawkins, 2000). These were: Blocky, Very Blocky, Blocky / Disturbed and Disintegrated. However in light of the findings of an investigation in Athens, where the Athens Schist Formation is extensively researched, the GSI was extended to contain a fifth category; Foliated / Laminated / Sheared.

2.2.3. *ADOPTED DEFINITION OF SOFT ROCK*

The difficulty in classifying soft rocks arises from their origin. As soft rocks are an intermediate, transitional material, the boundaries of what constitutes a soft rock are naturally blurred and diffuse (Haberfield, 2000) and lithology specific.

Attempting to classify soft rocks within existing descriptive categories is not possible, however whilst a universal consensus is yet to be met, several definitions have been considered. The majority of these schemes use UCS values as they are derived from a simple and widely used laboratory rock strength test.

Johnston (1991) suggests that the all-encompassing term 'soft rock' be adopted for natural materials with UCS values of between 0.5 and 20 MPa, whilst knowledge of this material type continues to grow. Hawkins (2000) disagrees, stating that as the term 'soft' is already used in BS5930 to describe soils of between 20-40 kPa Cu, applying the term to rocks of low strength may be misleading. By considering undrained shear strengths, Hawkins (2000) adopts the strength range 320kPa Cu to 10 MPa UCS. Several authors, including Cook (1999) prefer terms such as 'between ground' and 'transitions materials' and attempt to retain the classic division between soil and rock, (albeit lithology specifically), removing the complication of introducing a third field of geotechnics.

In order to maintain consistency within this thesis, the following definition has been adopted, based upon the scheme proposed by Hawkins (2000):

Geo-material with strength values of between 320 kPa Cu and 10 MPa UCS will be considered 'soft rock'.

Although; Cortesy, et al (2003) reiterate there is no definitive consensus regarding a definition and that any adopted scheme should be used only as a guide (Hawkins, 2000).

2.3. SOFT ROCK STIFFNESS

2.3.1. *LINEAR STIFFNESS*

Understanding and predicting the way in which the ground reacts to construction is the chief role of a geotechnical engineer. To achieve this, many properties of the ground (and how they change with stress and time) must be defined (Matthews, et al., 2006). One of the most important properties for solving ground-structure interaction problems is stiffness, and this holds true for soil, rock and soft rock (Heymann, 1998); (Vardanega & Bolton, 2011).

Stiffness is the relationship, or ratio, between the stress (σ) applied to a material and the strain (ε) it causes. Many materials are assumed to have a linear elastic stress response, in that they rebound back to their original size and shape upon removal of stress, or else fail in a brittle manner if their strength is exceeded (Whitlow, 2001). Historically, computational analyses used to solve ground–structure interaction problems such as settlement are commonly based on theories assuming linear elasticity (Jardine, et al., 1986).

Young's Modulus (E), also called the Stiffness Modulus and the Modulus of Elasticity, is defined as the gradient of the linear elastic stress-strain relationship of a given material and is calculated using equation 2.1:

$$E = \frac{\Delta \sigma}{\Delta \varepsilon} \qquad 2.1$$

The greater the stiffness of the material, the greater the Young's Modulus (Figure 2.4).

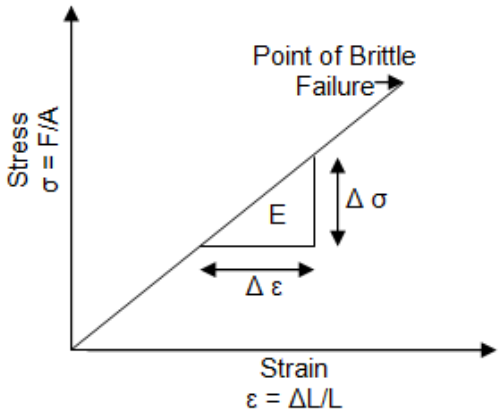

Figure 2.4: Simplified linear elastic stress strain (adapted from Wood, 2004)

Linear elastic models are a simplification of the reality when applied to soil and rock. Whilst it is attractive to generalise soil stress-strain performance into idealised linear elastic behaviour, geomaterials are not perfectly isotropic, as the method of sedimentation (generally as thin laterally continuous layers) produces cross-anisotropic fabrics (Pennington, et al., 1997). Also, the presence of compressible void spaces and weak inter-particle bonds need to be taken into consideration (Heymann, 1998).

In reality, it is known that the stress–strain relationship of geo-materials is highly non-linear. Atkinson (2000) highlighted that one of the major problems in ground engineering prior to the 1980's was the discrepancies observed between the results of traditional laboratory measurements and the back calculated soil stiffness recorded in the field. Jardine *et al* (1986) stated that stiffnesses calculated from traditional laboratory testing are usually much lower than those observed in the field, and Burland and Hancock (1977) stated that the behaviour of soils around excavations could not be due to or explained by simple linear elastic analysis.

Initially it was thought that these discrepancies observed in laboratory testing were caused by sample disturbance during excavation, transport and preparation (Heymann, 1998), however it was later discovered that they could be remediated through an understanding of non-linear stiffness, and in particular, the behaviour of geo-material stiffness within the small strain range.

2.3.2. *NON-LINEAR STIFFNESS*

Initial attempts to understand the true stiffness of soils were undertaken by Simpson *et al* (1979), who showed that instead of using the traditional linear elastic theory, the errors between observed field measurements and laboratory experiments could be reduced by applying a bi-linear stress-strain law with a high initial stiffness.

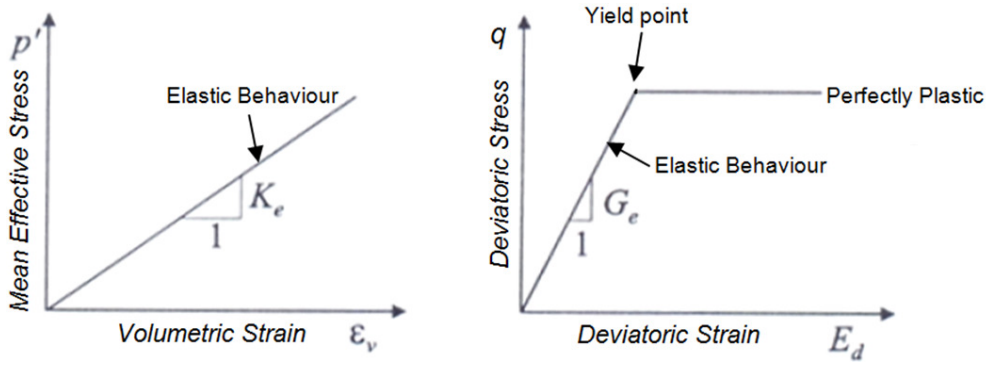

Figure 2.5: Bi-Linear stress strain model (adapted from Potts and Zdravkovic, 1999)

This model was improved upon over time (and with advances in electronic instrumentation, (Potts & Zdrakovic, 1999)), and it was realised that the relationships between stresses and strains are not bi-linear, but are in fact almost continuously non-linear and that some yielding occurs well within the state boundary surface of soils (and soft rocks) where material behaviour changes from elastic and recoverable to inelastic and irrecoverable (Burland, 1989); (Leroueil & Vaughan, 1990); (Mohsin, 2008).

This non-linearity can be demonstrated by looking at the work of Atkinson (2000). In his work he described the Young's Modulus of a material at the start of loading as E_0. The stiffness of a material displaying non-linear properties can be expressed as both tangent Young's Modulus (E_t) or secant Young's Modulus (E_s) as shown in Figure 2.6 and Figure 2.7, and provide different stiffness for any given strain level, with secant usually being higher as seen in Figure 2.8. Secant is often convenient (and is the most commonly reported of the two within the literature) due to its relative simplicity in calculations using raw laboratory testing data, which often contain some degree of data scatter, complicating the derivation of tangential stiffness (Vardanega & Bolton, 2011).

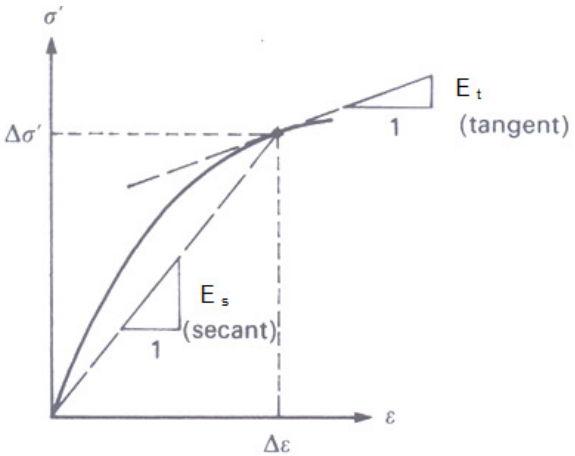

Figure 2.6: Stress vs strain highlighting tangent and secant stiffness (adapted from Whitlow, 2001)

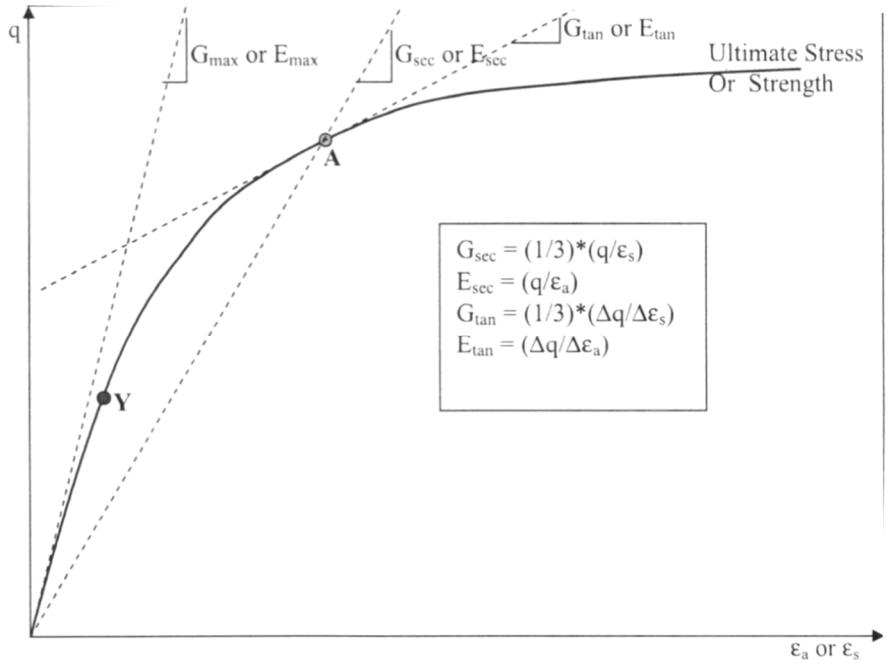

Figure 2.7: Deviator Stress vs Stress plot highlighting both secant and tangent stiffness at point A and maximum stiffness (prior to yield at point Y). (Mohsin, 2008).

Figure 2.8 shows how the secant and tangent values of stiffness vary with strain and also shows stiffness to be much higher in the very small and small strain ranges than the large strain range.

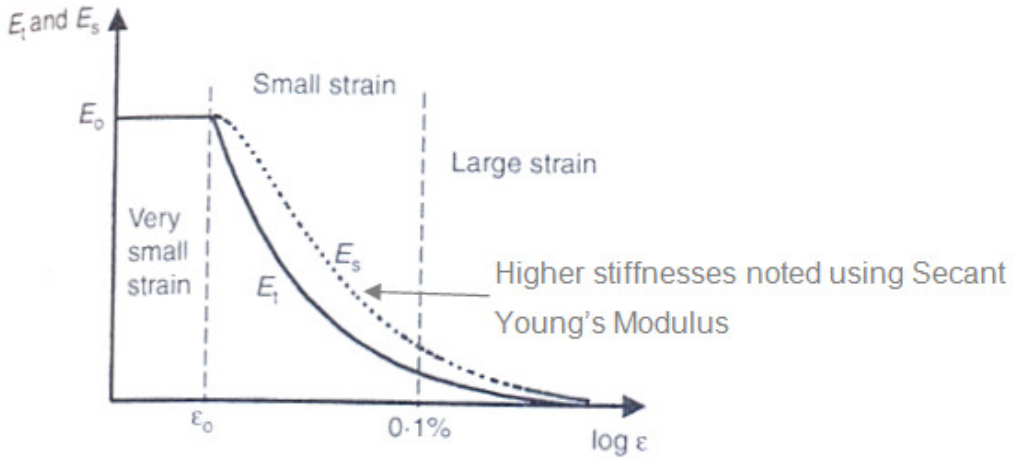

Figure 2.8: Diagram showing the variation in stiffness between Et and Es plots (adapted from Atkinson, 2000)

Typically Young's Modulus is used to quantify the behaviour of non-compressible materials, whereas soils and to a lesser extent rocks are compressible due to the presence of voids and the ability of particles to move relative to one another allowing geo-materials to strain both volumetrically and in shear. Although hard rocks stiffness will often be assigned a Young's Modulus (E) and Poisson's Ratio (v).

2.3.3. *STIFFNESS OF COMPRESSIBLE MATERIALS*

When a material, for example metal, is subject to a force it will deform (Donaghe, et al., 1988), although it will retain its original volume throughout this shearing (Figure 2.9):

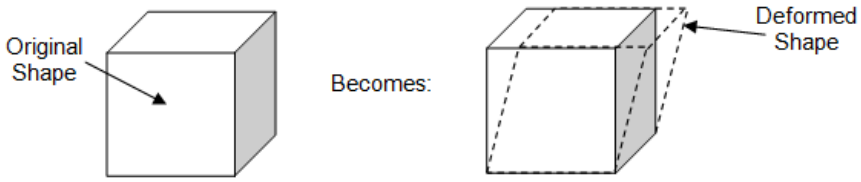

Figure 2.9: Diagram showing exaggerated non-compressible deformation.

When a soil sample is subject to compressional forces, the soil particles can rearrange and fill spaces previously occupied by air or water, (given that pore pressures are allowed to drain as a function of porosity and permeability). Particles may even be crushed or deformed during this process over a longer period of time (creep and secondary consolidation). This means that in addition to the sample being deformed (sheared) the sample will also strain volumetrically. It should be noted at this point that the sign convention of strains in geotechnical engineering are positive for compressive strains and negative for extensional strains. Figure 2.10 shows there is both a shear strain (ε_s) element and a volumetric strain (ε_v) element of soil deformation.

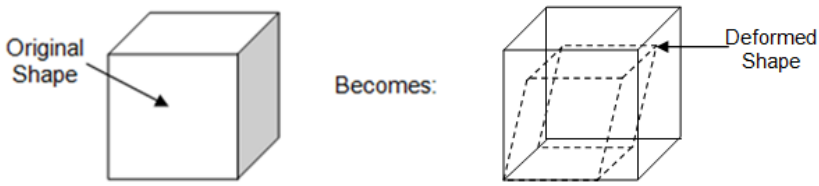

Figure 2.10: Diagram showing exaggerated compressible deformation.

The volumetric strain component is calculated using the equation 2.2:

$$\varepsilon_v = \frac{\Delta V}{V_0} \qquad 2.2$$

Where ΔV is the change in volume and V_o is the original volume (note also that sign convention has reductions in volume expressed as positive volumetric strains). In triaxial testing, volumetric strains (ε_v) may be inferred from measured back volume change, inferred from calculations assuming a Poisson's ratio, or else calculated using local strain measurement data (if absolute axial strain (ε_a) and radial strains (ε_r) are known, as shown in equation 2.3):

$$\varepsilon_v = \varepsilon_a + (2 \times \varepsilon_r) \qquad 2.3$$

If radial strains are not known, they can be found using the relationship between volumetric strains and axial strains in drained testing (equation 2.4 (Muir Wood, 1990)):

$$\varepsilon_r = \frac{\left(-\Delta V/V_0\right) + \left(\Delta L/L_0\right)}{2} \qquad 2.4$$

Mean effective stress (p') can then be plotted against ε_v to obtain K, the Bulk Modulus or volumetric stiffness modulus (equation 2.5).

$$K = \frac{\Delta p'}{\Delta \varepsilon_v} \qquad 2.5$$

Where p' is calculated using equation 2.6:

$$p' = \frac{\sigma_1' + \sigma_2' + \sigma_3'}{3} \qquad 2.6$$

In triaxial, (σ_1') is the effective axial stress and (σ_2') and (σ_3') are the effective radial stress. Figure 2.11 shows a plot of p' vs ε_v (p'_0 is the initial mean effective stress):

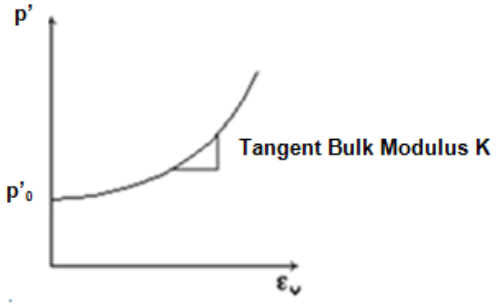

Figure 2.11: Mean effective stress - volumetric strain, bulk modulus measured as tangent

The shear strain component is represented by the angle γ, shown in Figure 2.12:

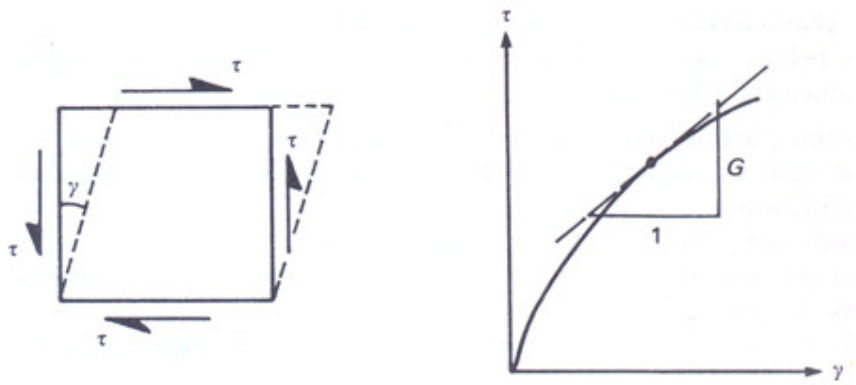

Figure 2.12: Diagram showing shear stress - strain relationships (adapted from Whitlow, 2001)

Also shown in Figure 2.12 is the shear stress (τ) vs shear strain (γ) graph, from which the gradient can be taken at any point along the curve. This is known as the Shear Modulus (G), or modulus of rigidity (equation 2.7).

$$G = \frac{\Delta \tau}{\Delta \gamma} \qquad 2.7$$

In triaxial testing, equation 2.8 is used to calculate shear strains (ε_s):

$$\varepsilon_s = \left(\frac{2}{3}\right) \times (\varepsilon_a - \varepsilon_r) \qquad 2.8$$

Deviator stress in triaxial apparatus is calculated using equation 2.9:

$$q = \sigma^1 - \sigma^3 \qquad 2.9$$

Where (σ^1) or (σ_a) is the total axial stress and (σ^3) or (σ_r) is the total radial stress allowing the triaxial shear modulus to be calculated using equation 2.10:

$$G = \frac{\Delta q}{(3 \times \Delta \varepsilon_s)} \qquad 2.10$$

In an idealised isotropic and elastic soil the three stiffness moduli of E, G and K, can all be related to one another using the following equations (2.11 and 2.12) (Puzrin & Burland, 1998); (Atkinson, 2000); (Mohsin, 2008):

$$G = \frac{E}{2 \times (1 + v)} \qquad 2.11$$

$$K = \frac{E}{3 \times (1 - [2 \times v])} \qquad 2.12$$

Which, in a material with Poisson's ratio of 0.5, shows that 3G = E and K is infinite.

In the example of an elastic isotropic soil, the shear and volumetric stiffness's can be considered as decoupled, that is to say operating in isolation from one another and not altering one another as they develop. This behaviour can be seen in Figure 2.13.

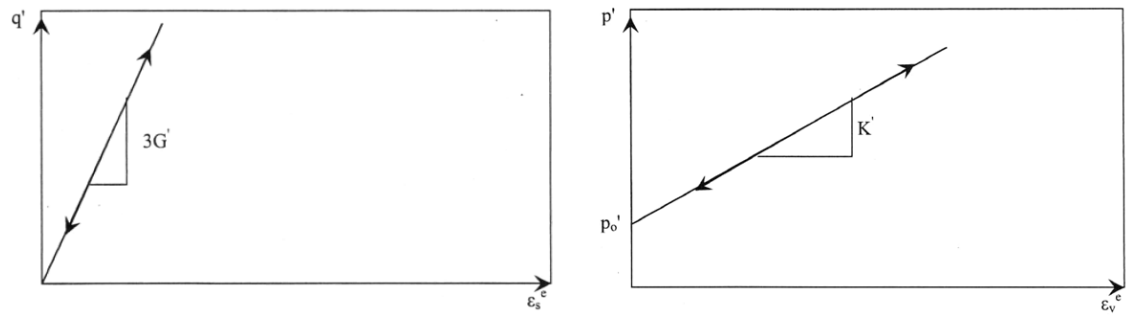

a) b)

Figure 2.13: Idealised elastic shear and volumetric strain during a) loading and unloading and, b) swelling / compression (Mohsin, 2008).

In terms of a coupling matrix, elastic deformation can be expressed as the following constitutive formula (equation 2.13), with the coupling moduli (J_1' and J_2') are equal to zero (Graham & Houlsby, 1983); (Puzrin & Burland, 1998); (Mohsin, 2008):

$$\begin{Bmatrix} \Delta q \\ \Delta p' \end{Bmatrix} = \begin{bmatrix} 3G' & 0 \\ 0 & K' \end{bmatrix} \begin{Bmatrix} \Delta \varepsilon_s \\ \Delta \varepsilon_v \end{Bmatrix} \qquad 2.13$$

Where non-elastic deformation is taking place however, the various moduli are closely linked to one another, giving rise to a degree of coupling. This can be seen in equation :

$$\begin{Bmatrix} \Delta q \\ \Delta p' \end{Bmatrix} = \begin{bmatrix} 3G' & J_1' \\ J_2' & K' \end{bmatrix} \begin{Bmatrix} \Delta \varepsilon_s \\ \Delta \varepsilon_v \end{Bmatrix} \qquad 2.14$$

Where shear stiffness is intrinsically linked to deviator stress and shear strain, bulk stiffness linked to mean effective stress and volumetric strain and the remaining paired stresses and strains are linked to one another in the following manner (equations 2.15-2.18):

$$3G' = \frac{\Delta q}{\Delta \varepsilon_s} \qquad 2.15$$

$$K' = \frac{\Delta p'}{\Delta \varepsilon_v} \qquad 2.16$$

$$J_1' = \frac{\Delta q}{\Delta \varepsilon_v} \qquad 2.17$$

$$J_2' = \frac{\Delta p'}{\Delta \varepsilon_s} \qquad 2.18$$

It should be noted that for an elasto plastic soil where the coupling moduli are equal (J_1' = J_2') equation 2.13 can be simplified during both undrained loading (as $\Delta\varepsilon_v = 0$) and isotropic compression (as $\Delta\varepsilon_s = 0$) (Mohsin, 2008). Typical stress-strain relationships for both undrained shearing and isotropic compression are shown in Figure 2.14 along with an unload / reload loop.

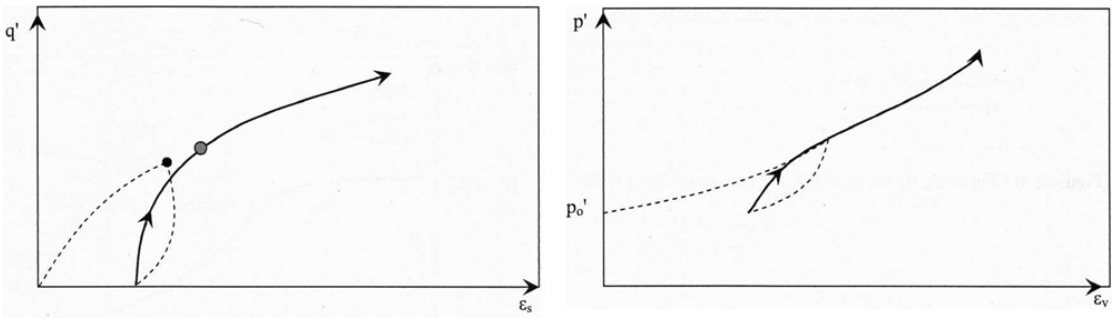

a) b)

Figure 2.14: a) Typical shearing and b) compression behaviour of soils (Mohsin, 2008).

These various moduli (Young's, Shear, Bulk and coupling moduli) are all used in quantifying the stiffness of geo-materials. Assessing the shear stiffness of soft rocks from small strains through to large strains is one of the primary focuses of the mechanical testing programme of this research project.

2.3.4. *SMALL STRAIN STIFFNESS THEORY*

Routine commercial triaxial tests on soils will often strain samples up to 20% axial strain, utilising externally measured axial displacements and axial loads (externally implying 'outside of the cell') to form stiffness estimates. These tests will not allow for the existence of bedding errors and will calculate diametric strains using assumed values of Poisson's ratio. The progressive volumetric deformation of samples throughout saturation and consolidation stages will be calculated via back volume change rather than measured directly, relying upon further assumptions of full saturation and in practice, volume changes occurring during saturation are discounted using standard methods. Results from such tests will often be grossly inaccurate, underestimating stiffnesses and strengths of materials by up to an order of magnitude; however will often suffice for the majority of simple designs where rough estimates of undrained shear strengths or ultimate failure loads are all that is required.

By carrying out experimentation utilising local strain measuring devices, higher stiffnesses can be recorded than are possible when using externally emplaced apparatus, especially at low strain levels. The examination of locally measured strains of soils at small strains and their associated high stiffnesses has been the focus of much research over the past few decades (Jardine , et al., 1985); (Jardine, et al., 1986); (Burland, 1989); (Atkinson & Sallfors, 1991); (Jardine, 1992); (Puzrin & Burland, 1998); (Atkinson, 2000); (Clayton & Heymann, 2001); (Gasparre, 2005); (Heymann, et al., 2005); (Gasparre & Coop, 2006); (Finno & Kim, 2011); (Truong, et al., 2012), although comparatively minimal research has investigated similar properties of soft rocks.

Three regions of strain behaviour based upon the stiffness degradation of various natural and artificial soils have been classified. These are: very small strain (where stiffness using Young's Modulus is approximately constant, $E_0 = E_t = E_s$ up to 0.001%), small strain (between 0.001% and 0.1% strain where stress-strain behaviour is non-linear but unload-reload cycles form closed hysteresis loops) and large strain (greater than 0.1% strain which is the focus of the majority of routine geotechnical laboratory testing outside of research). The definitive boundaries between these strain regions, (linked to the Y1, Y2 and Y3 yield surfaces in p - q stress space), have been greatly debated within the literature, with authors using the magnitude of shear strain development, significant deviations of volumetric straining and arbitrary generalised axial strains to mark the transition between the very small / small / large strain boundaries (Jardine , et

al., 1985); (Burland, 1989); (Puzrin & Burland, 1998); (Atkinson & Sallfors, 1991); (Silvestri & d'Onofrio, 2000); (Finno & Kim, 2011); (Clayton, 2011).

For the purposes of this project, the small and large strain regions adopted by Atkinson & Sallfors (1991) along with other authors including Finno & Kim (2011) have been used.

These strain regions are superimposed upon an example of a hard soil's stiffness degradation, that of Glacial Till, in Figure 2.15. These results were determined via a series of triaxial drained and undrained compressional tests incorporating local strain gauges. The diagram shows the typical initial high shear stiffness of geomaterials within the small strain range followed by its rapid deterioration as plastic strains develop. The diagram also highlights that in order to obtain G_0 and very small strain stiffness (apparent linear behaviour) in the laboratory, bender elements or resonant column apparatus need to be employed, as local gauges such as LVDT's and Hall Effect gauges have a minimum operational range (Finno & Kim, 2011).

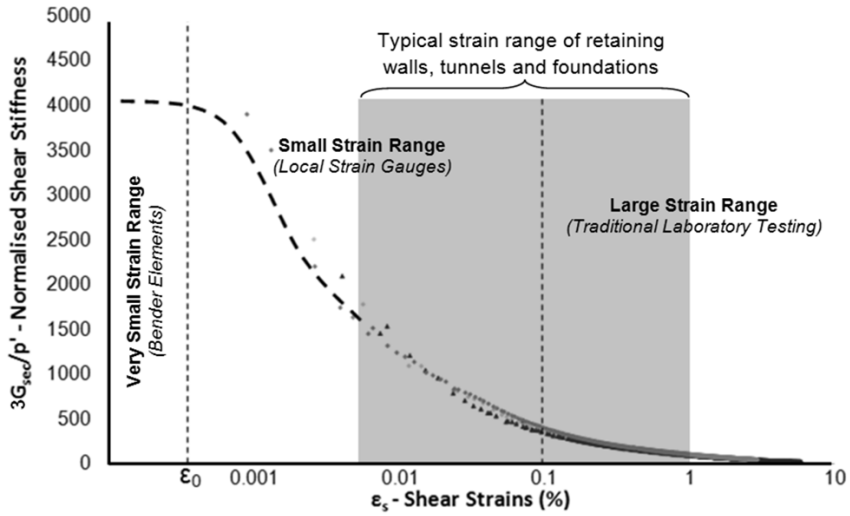

Figure 2.15: Strain regions adapted from Atkinson & Sallfors (1991), superimposed upon results of tests carried out on Glacial Till (Simpson & Rouainia, 2011).

Once small strain stiffness is accounted for, results fall more in line with stiffness observed in-situ / from field measurements and seismic testing (Clayton & Khatrush, 1986); (Heymann, 1998); (Atkinson, 2000); (Clayton & Heymann, 2001); (Heymann, et al., 2005); (Kim & Finno, 2011).

This is because, with the exception of the ground directly in contact with structures / excavations, studies have shown that the majority of the ground strains at very low levels. Puzrin & Burland, (1998) went as far as to state that ground engineering

problems are dominated by small strain behaviour. This trend has also been found to be true for soft rocks, and like soils, the typical ground strains that develop within such materials rarely exceed 0.1% under normal working loads (Kim, et al., 1994). Burland (1989) stated that field measurements taken around displacements of foundations and excavations are often within the small strain range, and that even when high bearing pressures are applied (as measured in his example of a 'tall hotel' in Berlin), vertical strains rarely exceed 0.1% and have a maximum of 0.3%. Research carried out on tunnels by Burland (1989) has shown that except directly above the crown of the tunnel, vertical displacements are less than 0.05%.

This premise can be seen in Figure 2.16, where strain contours under a) a rigid foundation and b) around a retaining wall b) are superimposed upon the surrounding ground. The very high strains measured at the edge of rigid foundations may be associated with softening of the ground at the base of the foundations in much the same way that bedding errors form during triaxial testing (Burland, 1989).

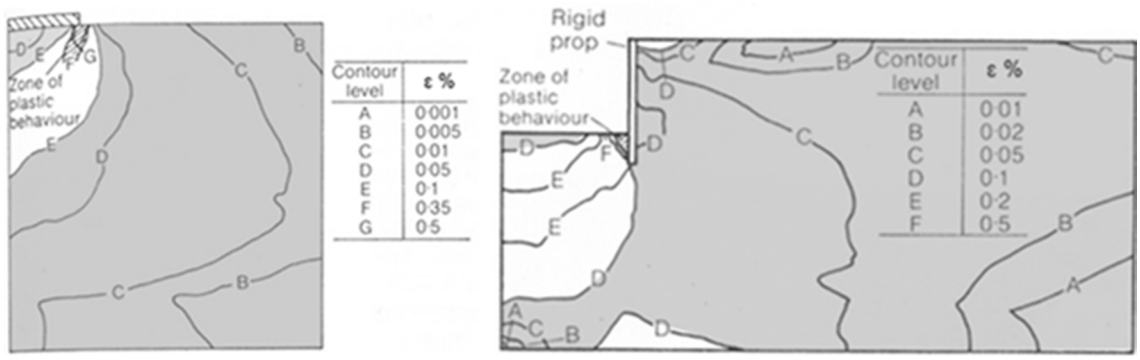

a) b)

Figure 2.16: Ground strain contours measured beneath a) a rigid foundation and b) retaining wall. Ground dominated by small strain is shaded. Adapted from (Jardine, et al., 1986).

The fact that much of the ground strain around well-designed structures falls within the small strain range makes studying the small strain stiffness properties of soft / weak rocks, and those factors which affect such properties, relevant and applicable for many geotechnical projects (increasingly so as the sensitivity of the project rises).

It is also important that small strain stiffness degradation is not just measured or observed, but incorporated into models and designs. Mohsin, (2008) presented the following diagram (Figure 2.17) to explain the difference between measured strains in the laboratory taking into account small strains (line OYA) and that predicted using an elastic-plastic model (line O'Y'A'). By assuming a moderately stiff elastic behaviour prior to yield (O'-Y') the elasto-plastic model initial underestimates, then over estimates

stiffness with increasing shear strain compared to that of the actual laboratory / field data. Post yield (at Y and Y') the simplified model's stiffness rapidly drops as the stress-strain slope gradient sharply changes. Mohsin, (2008) also noted that post yield, simplified models explain the behaviour of soils quite adequately, however, due to the presence of non-linearity within the small strain range, they fail to accurately model the behaviour pre-yield, which is of far greater importance for the majority of design.

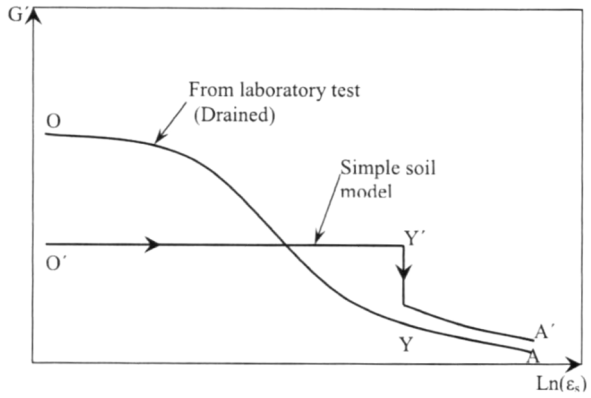

Figure 2.17: Shear stiffness behaviour of a soil tested within the laboratory and that of a simplified elastic-plastic model. (Mohsin, 2008).

Figure 2.18 shows the discrepancies between assuming linear elasticity during calculations, allowing for small strain stiffness and the actual settlements measured in-situ at the Jubilee Line, London Underground. Whilst an error still exists between actual and calculated settlements, by incorporating small strains into the model the calculated stiffnesses are closer than those predicted assuming only linear elastic behaviour.

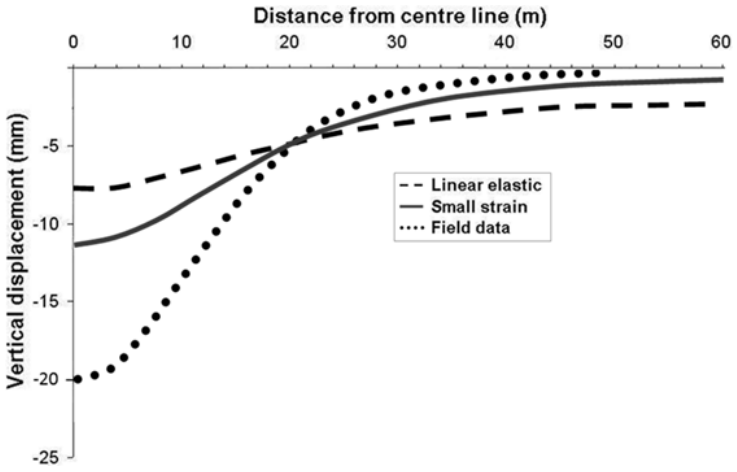

Figure 2.18: Diagram showing the trend of ground settlements above the Jubilee Line, using both Linear Elastic and Small Strain calculations along with actual measured data.

2.4. FACTORS AFFECTING PERFORMANCE OF SOFT ROCK

The behaviour of geo-materials is complex and dependent upon a wide range of factors. Several particularly important variables have been isolated for study and each is addressed in turn within the context of small strain stiffness, and to a lesser degree the tensile strength and one-dimensional compressibility of soft rocks. These variables include:

- Compressibility and Void Ratio
- Effective Confining Stress
- Structure
- In-Situ Discontinuities and Fractures
- Moisture Content and Saturation
- Mineralogy and Micro Fabric
- Influence of Strain Rate
- Cyclic / Dynamic Loading
- Influence of Aging
- Stress Path Direction and Recent Stress History
- Anisotropy

2.4.1. *COMPRESSIBILITY AND VOID RATIO*

The relationship between void ratio and strength / stiffness is already well known within soil mechanics, and understanding this key index property is crucial in order to accurately predict a soil's mechanical reaction to stress (Heymann, 1998); (Bica, et al., 2008).

In loose or unstructured / uncemented materials subjected to load / stress strains develop mainly via inter-particulate sliding. Voids become compressed and pore-fluids / pressures are dissipated and replaced by solid materials at a rate defined as a function of the given material's permeability and number of allowable drainage pathways. Dense geomaterials, however, strain mostly via particle deformation and (in shear) volumetric dilation, a much more energy intensive process as often demonstrated in shear box apparatus.

An inverse relationship between a given geo-material's void ratio and its strength may be drawn and as such, stiffness tends to increase as void ratio decreases (Heymann, 1998); (Vardanega & Bolton, 2011).

Soft clays undoubtedly have a much higher compressibility potential than hard rocks, however if the compressibility of a material is normalised against its strength, the resulting values become nearly constant for all natural geomaterials. Skempton (1961) showed that for a variety of materials ranging from soft clay through to dense sand, concrete and ultimately solid quartz crystals, the compressibility of the material skeleton displayed a broad range of results (over five orders of magnitude), however the compressibility of the solid materials alone (with zero void space) ranged only from 1.4 to 2.7 $x10^{-8}$ kPa^{-1}. This can be seen in Table 2.3.

Table 2.3: Compressibility of skeleton and solid material. Adapted from (Haberfield, 2000); (Skempton, 1961) and (Johnston, 1991)

Material	Skeleton Compressibility ($x10^{-8}$ kPa^{-1}) [C]	Solid Compressibility ($x10^{-8}$ kPa^{-1}) [C_s]	C_s / C
Soft Clay	60000	2.0	0.00003
Stiff Clay	7500	2.0	0.00025
Loose Sand	9000	2.7	0.0003
Dense Sand	1800	2.7	0.0015
Mudstone (MW)	600	2.7	0.0045
Mudstone (SW)	150	2.7	0.018
Vermont Marble	17	1.4	0.08
Quincey Granite	7.5	1.9	0.25
Quartzitic Sandstone	5.8	2.7	0.47
Quartz	2.7	2.7	1

In practice during the isotropic compression of a sample, dry density will converge towards (but never reach) the particle density of a mono-mineralic material as void ratio decreases, thus increasing stiffness.

Void ratio is most commonly thought of with respect to its relationship with vertical stress within oedometer / one-dimensional consolidation. By understanding a material's bulk density, dry density and particle density alongside moisture content and saturation ratio, void ratio can be plotted against log vertical stress in order to assess the degree of over-consolidation (via the identification of a geo-materials pre-consolidation stress) or the existence of structure (by characterising the structure permitted space via comparisons with remoulded materials). Some authors argue that over-consolidation is itself a form of structure (Kavvandas & Anagnostopoulos, 1998); (Bica, et al., 2008).

These yield parameters during one dimensional consolidation are well known to occur within soils and are routinely assessed during laboratory testing; however they also hold true for soft rocks (and to a lesser extent hard rocks).

All geomaterials may display both normally consolidated (plastic) and over consolidated (apparent elastic) behaviour, provided the magnitude of applied stress is

great enough or small enough, as seen in Figure 2.19, despite being properties which are generally associated only with soils.

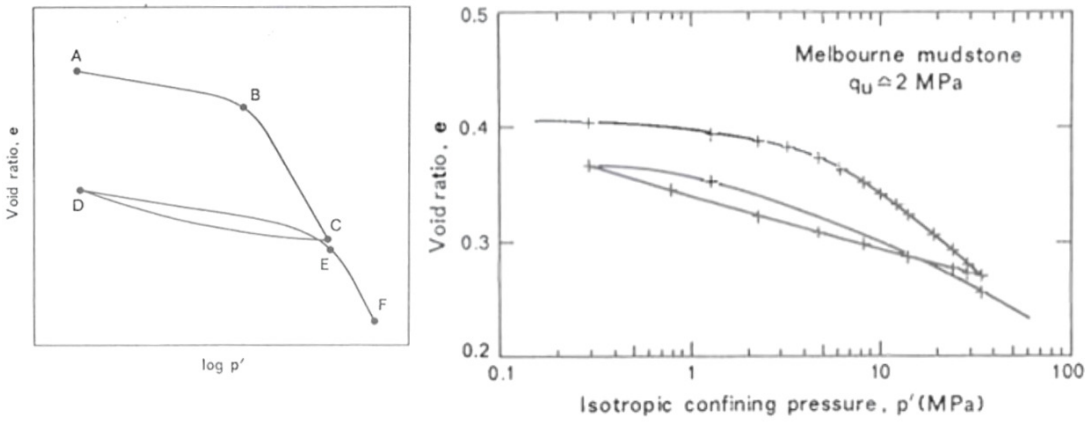

a) b)

Figure 2.19: a) Typical e-log p' curve for a clay material and b) compression characteristics of a Mudstone. From (Johnston, 1991)

Within the elastic over-consolidated zone, (A-B on Figure 2.19), geo-materials tend to display peak strengths and are volumetrically dilatant. Within the plastic normally consolidated zone however (B-C on Figure 2.19), geo-materials tend to be ductile and volumetrically contractant. These zones are separated by a yield point, which in soil mechanics is termed the pre-consolidation stress (or structural yield if structure is present), and in rock mechanics the brittle-ductile transition zone (Haberfield, 2000); (Nygard, et al., 2006).

As soft rocks mechanical properties fall between those of soils and rocks, it is not surprising that their strength and stiffness dependency with void ratio is also located between that of the two generalised material types. Void ratio is important within soft rocks; however the degree of structure / cement present is an equally important controlling factor (often allowing soft rocks to reach impossibly high void ratios compared to their un-cemented equivalents or even significantly reduced void ratios if secondary in-filling has occurred) (Heymann, 1998); (Bica, et al., 2008).

2.4.2. *EFFECTIVE CONFINING STRESS*

Generally speaking, the higher the mean effective stress subjected to a sample, the higher its stiffness / strength (Heymann, 1998); (Kate & Gokhale, 1998) as seen in Figure 2.20, however the way in which a sample yields / fails with changes in effective confining stress conditions is quite complex.

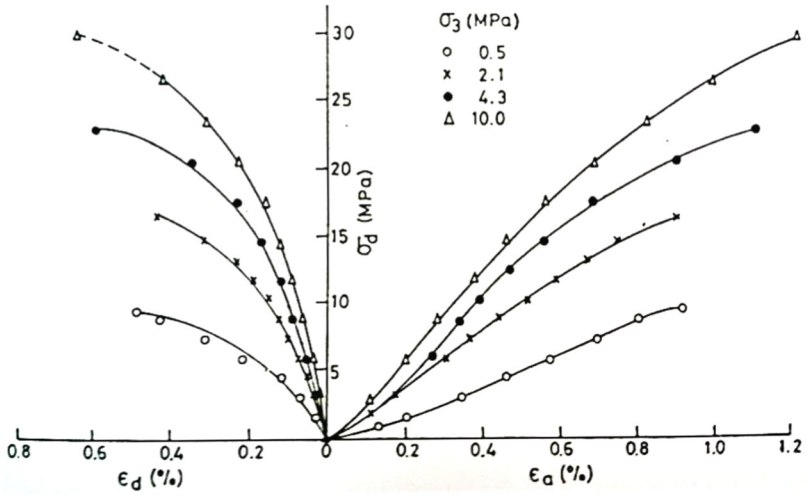

Figure 2.20: Stress strain response of a saturated soft sandstone at increasing cell pressures. From (Kate & Gokhale, 1998).

The effect of increasing radial stress upon a sample of London Clay (between 0.38 and 4.4 MPa) and Carara Marble (between 23 and 326 MPa) are shown in Figure 2.21.

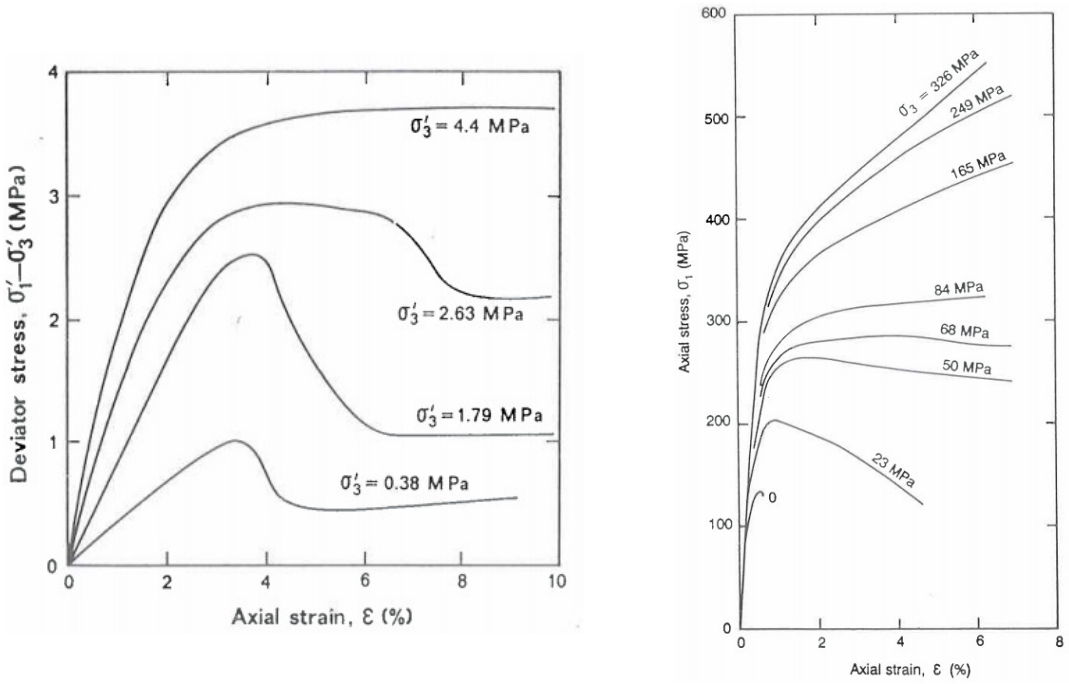

a) b)

Figure 2.21: Stress strain curves for a) London Clay (Bishop, et al., 1965) and b) Carrara Marble, (Karman, 1911); (Johnston, 1991).

Aside from the markedly higher stresses involved in the rock testing experiment, the stress strain response to loading under increasing confining pressures are highly comparable in both the soil and rock. Lower pressures show typical over-consolidated strain-softening behaviour with curves showing defined peaks, and then as the maximum overburden pressure (for soils) or the brittle-ductile transition pressure (for

rock) is approached, the response becomes that of normally-consolidated ductile strain-hardening. The only major difference between the soil and rock behaviours in Figure 2.21, is that soil stiffness increases with mean effective stress whilst the rock stiffness is seen to be constant until yielding regardless of p', as exemplified in Figure 2.22

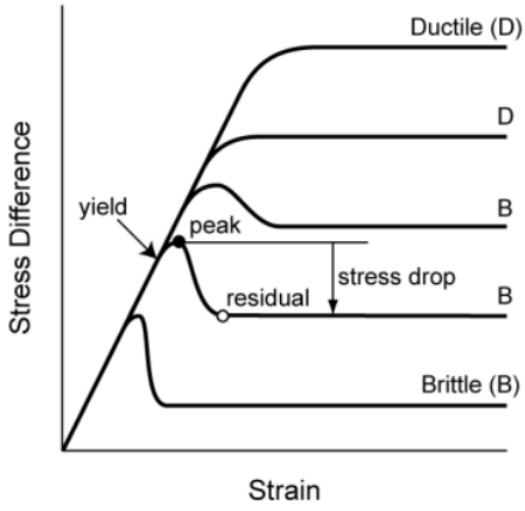

Figure 2.22: Brittle-ductile transition of rock (Schopfer, et al., 2013) after (Mogi, 1974) .

This common ground between soil and rock was also noted by Aversa, et al (1993) in their study of structured soft clays and pyroclastic rocks which also showed that strain softening and strain hardening responses to stress occur in both soil and soft rock, governed by confining pressure. A similar study carried out by Cecconi & Viggiani (2001) examining the structure of pyroclastic soft rocks, states that at low confining pressures the material behaves in a brittle rock like manner whilst at high confining pressures soil-like ductility is observed. This is also echoed by Kate & Gokhale (1998) who add that the transition from brittle to ductile behaviour in soft sandstones at high confining pressures occurs regardless of the degree of saturation (although the degree of saturation does influence the maximum strength parameters), by Carter, et al (2000) in their study of calcareous sandstones, Nygard, et al (2006) in their study of marine mudstones and has been successfully modelled by Schopfer, et al (2013).

Leroueil (2000) presents findings from a study originally carried out by Nishi, et al (1989) showing how confining pressure dependent initial shear stiffness G_0 is, and highlighting that this becomes increasingly true as a material becomes weakened by weathering, as shown in Figure 2.23 (due to de-structuring / breakage of bonding). Similar findings were observed by Ismail, et al (2001) during testing upon artificially cemented calcareous soils showing those cemented with gypsum displayed stiffness

behaviour that was highly confining pressure dependant, (although the general consensus for structured materials is that they become confining pressure dependant only once cementicious bonds have broken (Cuccovillo & Coop, 1997); (Hird & Chan, 2008); (Trhlikova, et al., 2012); (Truong, et al., 2012)).

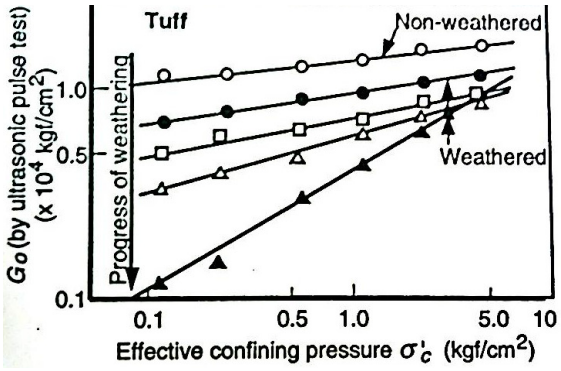

Figure 2.23: Effect of confining pressure upon G_0 at varying stages of weathering. From (Nishi, et al., 1989).

Sun, et al, (2004) carried out testing upon weak and weathered soft rock in triaxial apparatus, namely a weathered porphyrite, taken from a dam site in Hyogo, Japan. High quality rotary core samples were tested at a variety of confining pressures and results generally showed that both saturated and partially saturated sample strength was highly confining pressure dependent.

This pressure dependence also manifests in the form of volumetric straining, whereby samples tested at higher confining stresses behave in a contractant manner where as they move towards dilatant behaviour at lower pressures (similar to the behaviour of loose compared to dense non-cohesive soil) as shown in Figure 2.24.

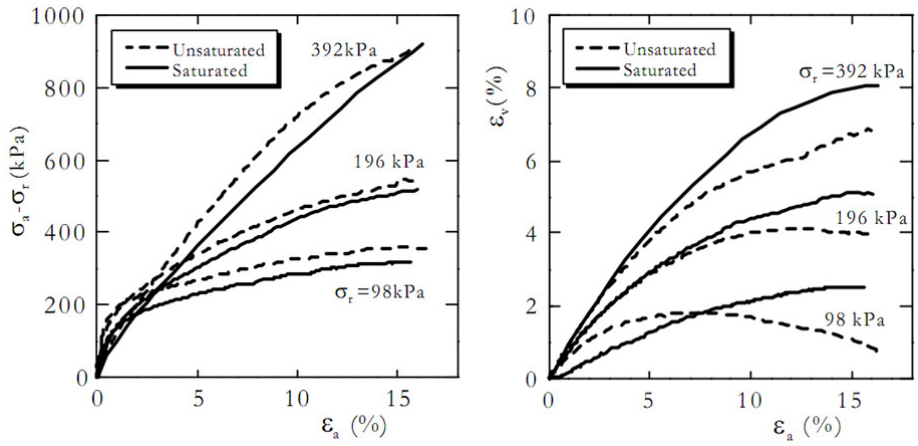

a) b)

Figure 2.24: a) Deviator stress vs axial strain and b) volumetric strain vs axial strain, showing strength dependence upon confining stress and water content. From (Sun, et al., 2004)

Whilst this behaviour is well documented in soils, it is not usually seen in rocks. This is due to the strength of the bonding and fabric of a rock being so much higher than the stresses being imposed upon them under normal working loads. The structural yield point of hard rocks is usually so high that minor fluctuations and variations in confining stress does little to influence the material's overall strength, however in the case of soft rocks this structural yielding point occurs at significantly lower stress states and is therefore more important to geotechnical design as the structure may yield under normal working loads.

The isotropic yield stress of chalk is shown in Figure 2.25 along with stiffness of the material at large (0.1%), small (0.01%) and very small (0.001%) axial strain (using strain ranges defined by Clayton & Heymann (2001)). This material yielded structurally at approximately 2900 kPa, at which point large volumetric straining occurred (up to 10%) along with a long period of creeping (2 weeks until creep stopped) (Clayton & Heymann, 2001).

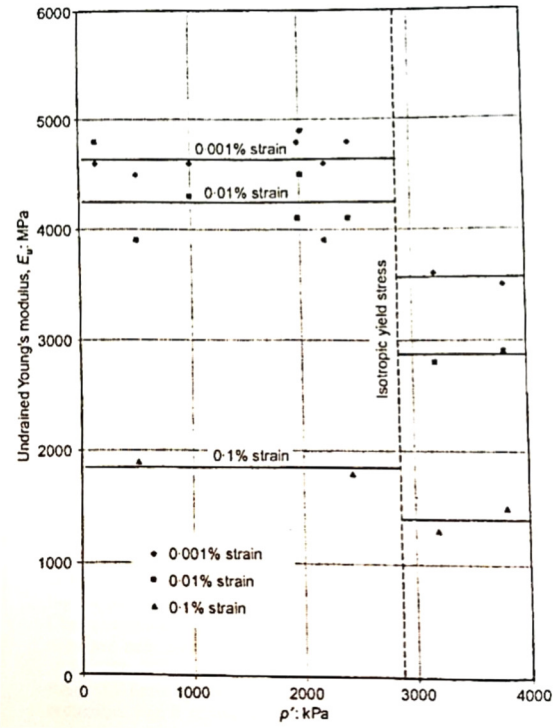

Figure 2.25: Isotropic yield stress of Chalk. From (Clayton & Heymann, 2001)

Figure 2.26 shows the effect of increasing cell pressure on a soft rock beyond the point that the structural yield takes place in terms of sets of pre and post de-structuring Mohr Circles. It can be seen that the lower stress circles (below 400 kPa) have more apparent

cohesion than those at greater pressures, due entirely to the loss of structure (breakage of bonding) brought about by isotropic increases in effective cell pressure.

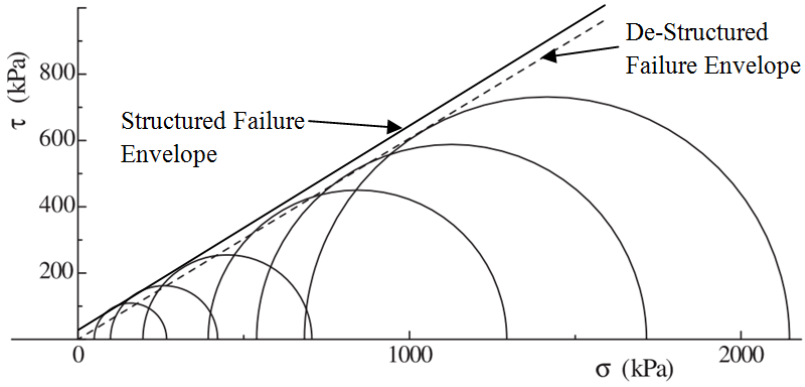

Figure 2.26: Loss of strength due to structural breakdown with increasing cell pressure. From (Sun, et al., 2006)

In reality even hard rocks have a radial pressure dependant stress response, but the pressures needed to observe such dependency would have to be very high, for example measured in terms of hundreds of MPa rather than the kPa ranges carried out by Sun, et al (2006) (from approximately 100 – 700 kPa) which are more easily achievable in most triaxial cells.

Additionally, by analysing samples within a rock-mechanics framework, a non-linear Hoek-Brown failure envelope may be more applicable (Figure 2.27) and may account for the apparent curvilinear shape of the failure bounding surface.

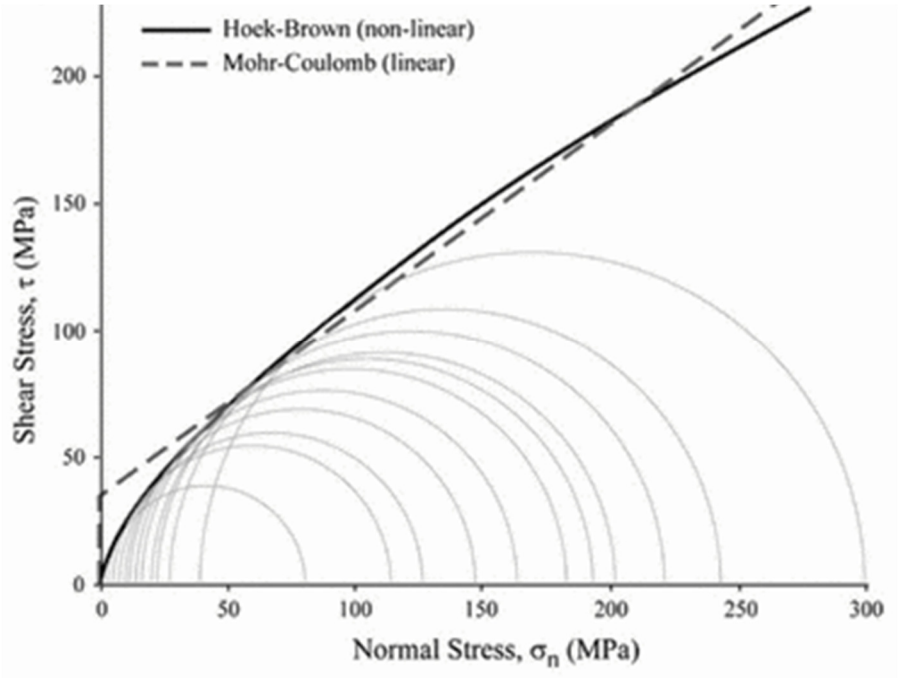

Figure 2.27: Mohr-Coulomb failure envelope and Hoek-Brown envelope (Eberhardt, 2012)

The relationship that structured soft rock has with confining pressure is complicated. At low pressures the sample may be significantly stiffer than an equivalent unbound material, perhaps even brittle in nature, however as radial stress rises and bonding breaks down, the behaviour of soft rock returns to stress response similar to that of a soil (ductile) or a reconstituted material of similar grain size distribution and void ratio (Vatsala, et al., 2001).

2.4.3. *STRUCTURE*

It is well known that structure is a key component governing the mechanical behaviour of rocks; however, Leroueil, et al (1984) and later Leroueil & Vaughan (1990) amongst other authors demonstrated that soil behaviour may also be significantly influenced by structure. The presence of structure affects the manner in which a soil will respond to stress in a way that cannot solely be accounted for by void ratio and stress history, the theory of which can be seen diagrammatically in Figure 2.28 a) and during oedometer testing of Vallericca Clay in Figure 2.28 b), where yielding occurs at a higher pressure than would be anticipated for a given void ratio and pre-consolidation pressure (Aversa, et al., 1993); (Vatsala, et al., 2001); (Amorosi & Rampello, 1998); (Leroueil, 2000); (Gasparre, 2005); (Gasparre, et al., 2007); (Amorosi & Rampello, 2007); (Bica, et al., 2008); (Trhlikova, et al., 2012).

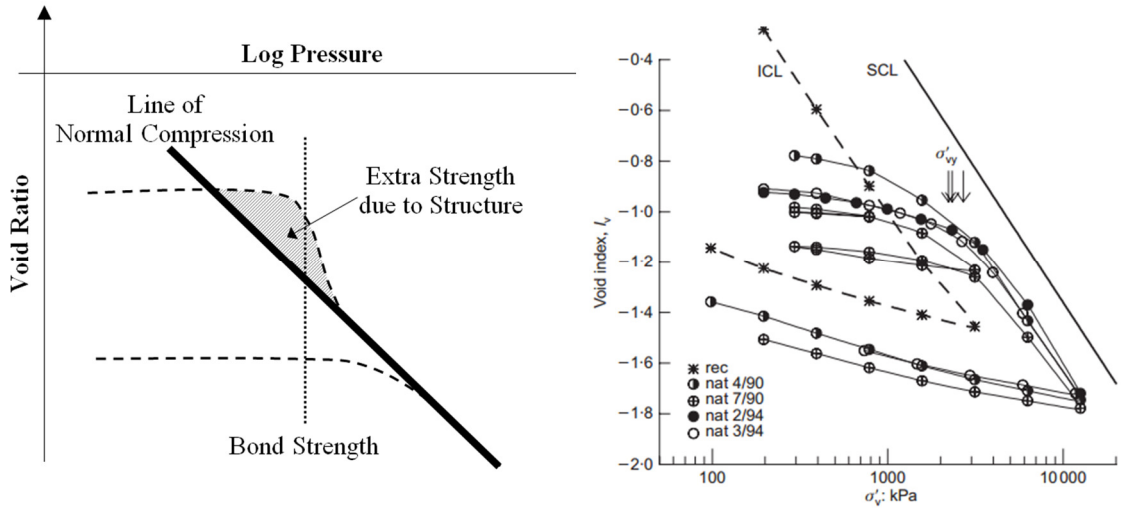

a) b)

Figure 2.28: a) Influence of structure during consolidation both in theory and, b) from testing carried out on Vallerica Clay. Adapted from (Aversa, et al., 1993); (Amorosi & Rampello, 2007).

This concept is now well accepted and much research has been carried out within the past three decades focusing on understanding the role that structure plays in a variety of soils from around the world, including famously Bothkennar Clay, Vallericca Clay and

London Clay. The structure of these materials has been assessed throughout the whole strain range, often with reference to the material's reconstituted counterpart for comparison (Leroueil, et al., 1984); (Leroueil & Vaughan, 1990); (Puzrin & Burland, 1998); (Leroueil, 2000); (Amorosi & Rampello, 2007); (Gasparre, 2005); (Gasparre, et al., 2007); (Trhlikova, et al., 2012).

Structure is a term used to describe the way in which the orientation and organisation of particles within a geomaterial contribute towards its strength and stiffness, and encapsulated within this term are both fabric and bonding. The higher the degree of structure within a given sample of soil, the higher it's strength / stiffness in comparison to the same material in its un-structured, re-constituted state (assuming that the mean effective stress or vertical stress conditions under which the material is being tested are not greater than those required to cause yielding of the structure) (Mitchell, 1976); (Amorosi & Rampello, 1998); (Heymann, 1998); (Gasparre, 2005); (Amorosi & Rampello, 2007); (Epps, 2011); (Trhlikova, et al., 2012).

Fabric describes the homogeneity / heterogeneity of a material, its layering, bedding and also the distribution of discontinuities, fractures and imperfections. The fabric developed is dependent upon the environment within which a material is deposited, as this governs the rate of deposition and the amount of disturbance to which particles are subjected. Changing stress states may also alter the fabric of a sample, for example causing a sample to become denser or introducing a level of anisotropy or over-consolidation (Amorosi & Rampello, 1998); (Kavvandas & Anagnostopoulos, 1998); (Gasparre, 2005); (Amorosi & Rampello, 2007).

Typical micro scale clay fabric clasifications include; cardhouse, bookhouse, honeycombe, dispersed, turbostratic and stack. Heymann (1998) states that the lower the degree of fabric present in the sample, (therefore the more homogeneous the sample), the higher its stiffness apparently becomes; however it is difficult to totally isolate the effects of fabric on stiffness during testing. Heterogeneous samples are also more affected by sample disturbance than homogeneous samples so may lose strength and stiffness characteristics more rapidly during transportation and recovery (Sides & Barden, 1970); (Gasparre, 2005).

Bonding describes the inter-particulate forces at work within a geomaterial which are not purely frictional (Gasparre, 2005); (Amorosi & Rampello, 2007). Bonding of geomaterials develops via several means including the; deposition of material from

solution into void spaces, cold welding at inter-particle contacts, attractive forces (usually only applicable to clays), re-crystallisation due to weathering and the accretion of material at particle contacts (often simplified as 'cementation') (Heymann, 1998); (Amorosi & Rampello, 2007); (Truong, et al., 2012). The higher the degree of bonding present, the stiffer a given sample becomes. Well bonded samples are also noted to suffer less from sample disturbance than weakly bonded or totally unbonded samples following recovery. Once a level of stress great enough to cause the destruction of these inter-particle bonds is introduced to a sample, the sample will start to undergo 'de-bonding', an irreversible process (Amorosi & Rampello, 2007). Samples will also display increasingly higher tensile strengths as their bonding increases.

Bonding develops over time as part of the process of ageing. The smaller the particle sizes, the faster bonding appears to develop, as seen by Mesri et al (1990) during testing on clays, silts and sands, who suggested that finer grained samples have more contact points between grains than coarser samples and therefore can more easily develop inter-particle bonds. It is also noted that SEM analysis is a useful tool in order to superficially assess the extent that bonding has developed (Amorosi & Rampello, 2007).

Malandraki & Toll (1996) showed that materials with various structural strength display different patterns of small strain stiffness degradation, as seen in Figure 2.29 (Jardine, 1992). Figure 2.29 highlights that an un-bonded, structure-less sample will yield and display the greatest drop in stiffness once the linear elastic zone of the soil is exceeded (at Y1). Structured soils and soft rocks will both also yield at this Y1 elastic zone limit, however the greatest loss of initial stiffness is located directly following the de-structuring of that material along that given stress path (which occurs at the onset of plastic straining due to the breakage of bonds). A characteristic two-fold stiffness drop is often seen in soft rocks (Figure 2.29). Furthermore, the strain quantity required to exceed this elastic zone increases as structure strength increases. Bond breakdown / de-structuration, is noted to occur during shearing and even during isotropic compression provided radial stresses become great enough (Amorosi & Rampello, 1998); (Leroueil, 2000).

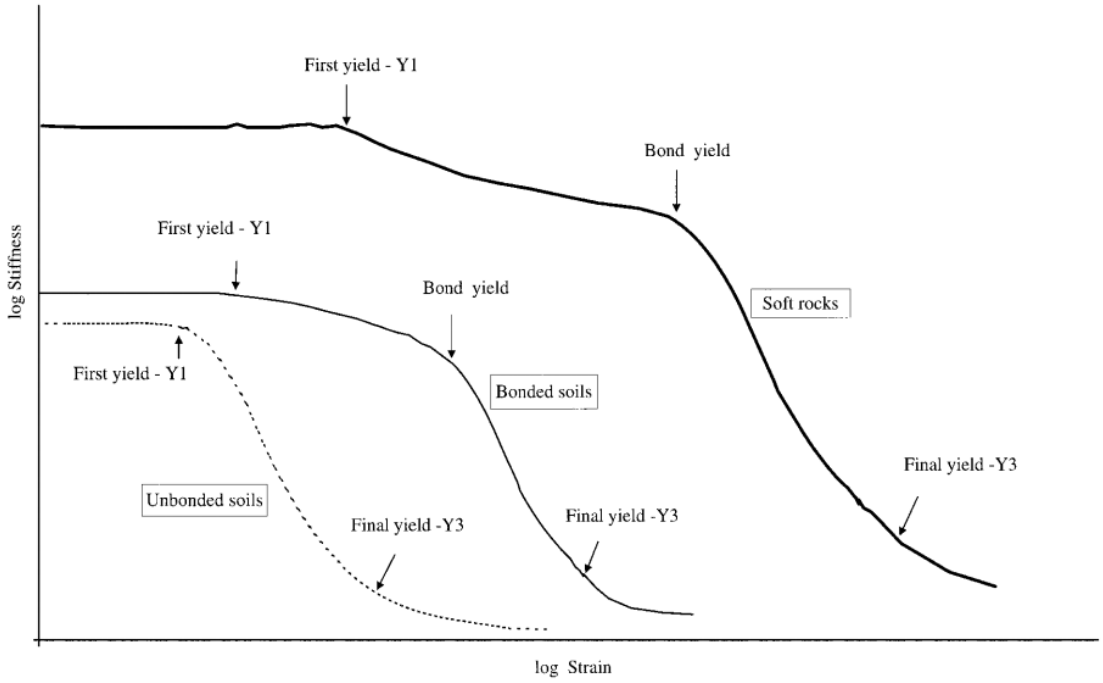

Figure 2.29: Yield points for a variety of materials. From Malandraki & Toll (2001)

This bond yield point re-emerges and becomes important once more if the orientation of the stress path is changed, meaning that a loss of structural bonds in one direction does not necessarily mean that unbroken bonds do not exist, showing that the yielding of a bonded / structured material is highly anisotropic.

Leroueil, et al, (1984) understood that structure (both fabric and bonding) would deteriorate with increased sample disturbance, and categorised materials based upon the amount of disturbance they had undergone in relation to their remaining strength. Samples which retain their in-situ strength along with good bonding and structure are termed 'Intact'. Soils which have lost their intact structure via an increase in stress are known as 'de-structured', whilst materials which have been disturbed fully are known as 'remoulded'. Soils which have had all structure removed, for example heavily disturbed soils or remoulded samples, will follow the over-consolidated line until the pre-consolidation state (P_c') is reached during compression. De-structuring has been observed to occur during swelling in materials that exhibit very weak bonding, however can occur to some degree accidently during sampling, storage and transportation of samples meaning it may never be quantified during testing. This has been observed within Glacial Tills that have been roughly handled, or stored in such a manner that drying and desiccation related shrinkage was able to take place prior to shearing.

Soils which retain structure, when compressed uni-axially via oedometer, can reach states considered 'impossible' for that of structure-less materials, in that they may

continue to react to stress in a similar manner to an over-consolidated material (elastically) even after their pre-consolidation stress is reached. The soil will then yield as structural bonds break down and return to a reference state similar to that observed during normally consolidated behaviour, re-joining the line of virgin / normal / intrinsic compression line, akin to that of its equivalent remoulded material (Leroueil & Vaughan, 1990); (Burland, 1990); (Aversa, et al., 1993); (Amorosi & Rampello, 1998); (Leroueil, 2000); (Vatsala, et al., 2001); (Amorosi & Rampello, 2007).

This extra strength due to the presence of structure in a soil is known as structure permitted space during one-dimensional compression (Heymann, 1998), (although the presence of structure also increases shear strength). This 'structure permitted strength' only holds true for structured materials that are considered 'intact', as defined by Leroueil, et al, (1984) and is most evident at lower pressures (especially in soils with high void ratios).

There is some debate within the literature concerning the effect that intact structure has on G_0 with respect to effective confining stress. Some authors report a G_0 dependency on confining pressure throughout the whole stress range, whilst others say that prior to structural yield G_0 is independent of confining pressure. It is likely that both cases may be true and that they rely on other factors such as mineralogy of both the grains and bonding agents along with the level / rate of applied stress and if the sample is prone to creep (Cuccovillo & Coop, 1997); (Hird & Chan, 2008); (Trhlikova, et al., 2012); (Truong, et al., 2012).

A case study that exemplifies the role of structure in soils is that of the Pappadai Clay. Pappadai Clay is a material which is known to be over-consolidated and who's geological pre-consolidation stress is also known (vertical effective stress at depth of sample = 415 kPa and known P_c' =1300). One dimensional consolidation tests were carried out on this material and also compared to fully reconstituted material properties. Testing revealed that yield occurred at around 2600 kPa, twice that of the known P_c', an extra layer of strength attributed entirely to the presence of structure, as shown in Figure 2.30.

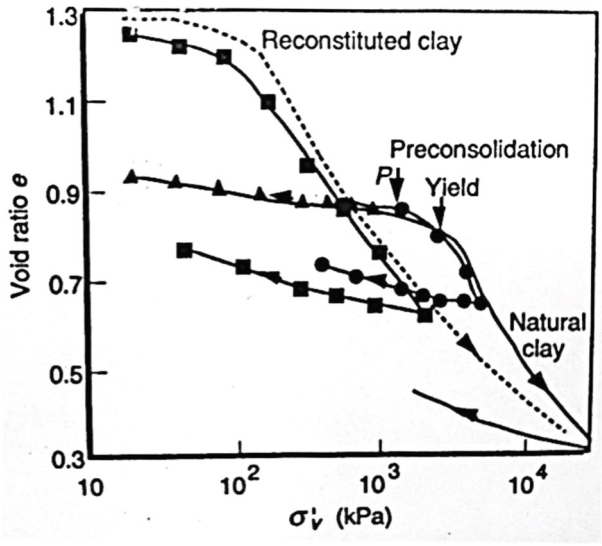

Figure 2.30: Consolidation behaviour of natural structured Pappadai Clay and remoulded equivalent. P signifies geological Pre-consolidation pressure. Adapted from (Leroueil, 2000)

The role of structure is even more apparent in soft rocks where the strength of the bonds developed may be much higher than that ever seen in a soil. At stress levels lower than those required to cause de-structuring, bonding is the over-riding factor controlling stiffness and strength of soft rocks, however isolating the role of structure in a soft rock is substantially more difficult than it is for a soil. Because a soil's structure will readily break down with increased disturbance without fundamentally altering the particulate properties (for example grain size distribution, angularity etc…), the effect of structure on a given soil can be conveniently assessed via comparisons to its fully disturbed / remoulded state. Such relationships between intact and remoulded strength are much more problematic to obtain for soft rocks, however, as the process used to disturb the material often requires the generation of high stresses and will potentially irreversibly modify the material behaviour (Amorosi & Rampello, 1998); (Aversa & Evangelista, 1998); (Cecconi & Viggiani, 2001); (Clayton & Heymann, 2001).

Aversa, et al (1993) attempted to isotropically de-structure a pyroclastic soft rock during triaxial testing. Samples were de-structured by being subjected to very high (up to 60 MPa) confining pressures in isotropic conditions, beyond the point of bond breakage. They observed that structure permitted space was not encountered at high pressures, as the radial stress increased beyond the materials structural yield causing de-bonding. De-structured samples had significant reductions in peak strength and stiffness compared to intact samples, however displayed similar residual strength (Figure 2.31). Intact samples dilated volumetrically, whilst de-structured samples were contractant.

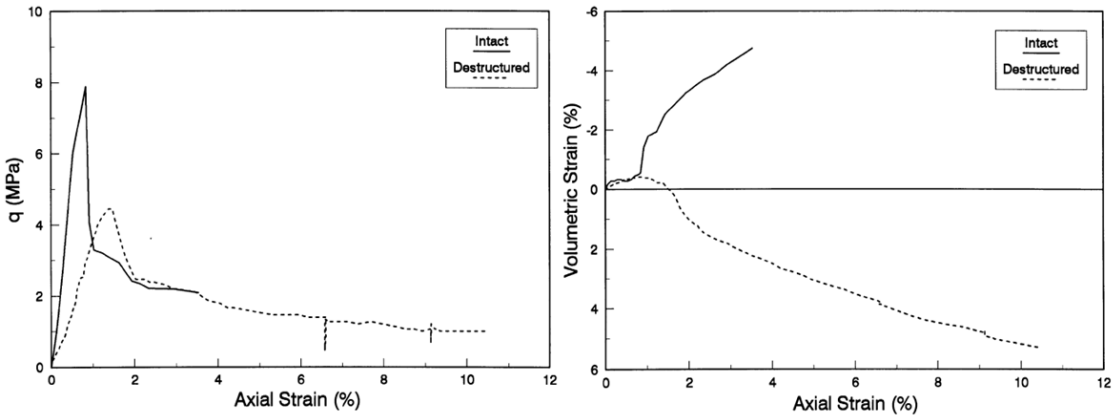

a) b)

Figure 2.31: Comparison between intact and de-structured samples of pyroclastic rock in terms of a) deviatoric stress - axial strain and b) volumetric strains – axial strain. Adapted from (Aversa & Evangelista, 1998).

Cuccovillo & Coop, (1997) carried out similar testing on intact and de-structured samples of calcarenite, a calcareous soft rock, in order to explore the role that bonding played upon stiffness throughout a wide strain range. Results of this research can be seen as Figure 2.32.

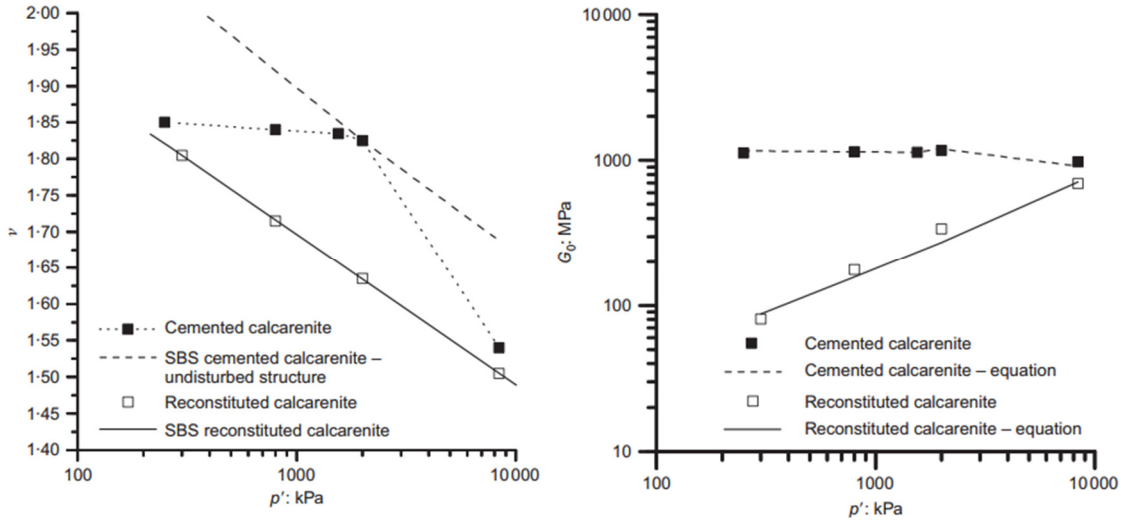

a) b)

Figure 2.32: Comparison between intact and de-structured samples of calcarenite in terms of a) void ratio – mean effective stress b) G_0 – mean effective stress. Adapted from (Cuccovillo & Coop, 1997) and (Trhlikova, et al., 2012).

It should be noted that de-structuration tests on soft rocks such as these are rare within the literature as research laboratories often lack the equipment required to obtain such high cell pressures within triaxial apparatus, although some soft rocks may isotropically de-structure (or de-bond) at lower stresses making their examination easier.

Cecconi & Viggiani (2001) also observed that the behaviour of a structured soft rock is highly reliant upon the isotropic confining pressures at which they were tested. At low stresses, brittle 'rock-like' behaviour is observed whilst at higher stresses; ductile 'soil-like' behaviour becomes prevalent (Nova & Parma, 2011). The confining pressure at which structure will yield may be quite low for soils, however will increase through soft rock and ultimately into hard rocks, depending upon the bonding mechanisms (Heymann, 1998). This concept has been covered in an earlier section.

The point at which a structured soft rock changes from 'rock-like' to 'soil-like' behaviour may be of great importance, especially if it occurs at stress levels likely to be encountered due to the emplacement of realistic engineering loads. As such, the examination of the brittle-ductile transition stress is a key concern for this research. In addition to this, as the on-set and accumulation of plastic straining causes the breakdown of structural bonds, it is therefore suggested that strain controlled testing (rather than stress controlled tests) should be adopted (Leroueil, 2000); (Amorosi & Rampello, 2007). The quantification of structure is also important and as such oedometer testing along with intrinsic / remoulded testing has been considered.

2.4.4. *IN-SITU DISCONTINUITIES / FRACTURES*

Fractures and jointing / bedding discontinuities are considered to be a key characteristic affecting the overall strength of a hard rock mass. The stresses or loads required to cause failure within discontinuities can be several orders of magnitude lower than those needed to cause a shearing failure within the intact rock, and as such it becomes vitally important that the nature (origin, persistence, smoothness and water bearing characteristics) and orientation of these potential failure planes are understood fully and accounted for in designs within hard rock (Hawkins, 2000).

Discontinuities within soil layers are generally assumed not to exist in the majority of circumstances and soils tested are often treated as being homogeneous for the purposes of characterisation and during analytical calculations. This is reflected in the most common tests carried out in geotechnical soil laboratories throughout the UK, where samples are all but required to contain no pre-determined failure planes or uncharacteristically large grains that might void results.

In reality however, soils are every bit as affected by the presence and orientation of fractures and defects as rocks are, as shown in Figure 2.33:

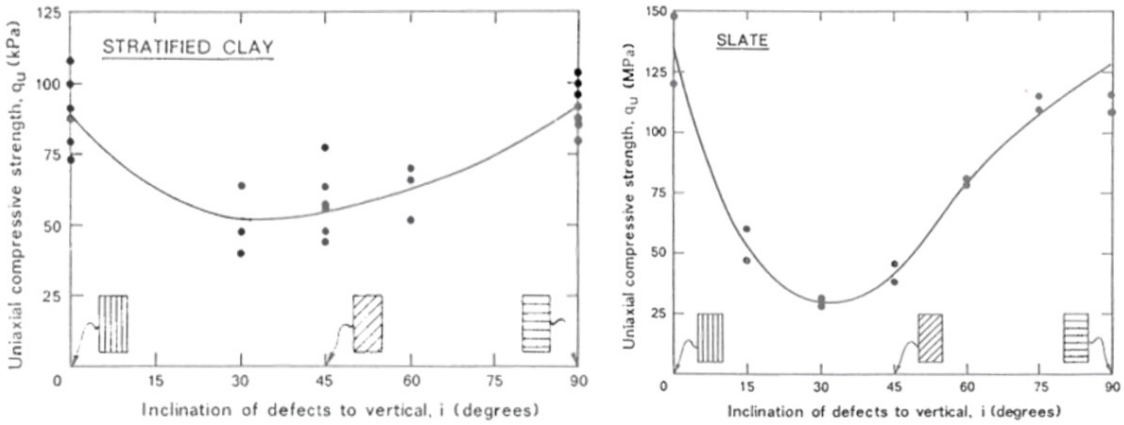

a) b)

Figure 2.33: Influence of the orientation of pre-existing defects on strength during compressional loading of a) stratified clay (Lo & Milligan, 1967) and b) slate (Hoek, 1965); (Johnston, 1991).

These diagrams demonstrate that, whilst the presence of discontinuities within rock have a more pronounced effect on their compressive strength, unfavourably orientated defects within a soil may still lower uniaxial compressive strength by around 25%. However, because a soil's shear / compressive strength may often be tens of MPa less than that of rock, the existence of such imperfections usually has little influence on geotechnical design, as a drop in undrained shear strength of 30 kPa within a soil, for example, is negligible compared to a potential drop of hundreds of MPa with a rock mass due to a critically inclined defect (Haberfield, 2000).

Gasparre (2005) also noted the effect of discontinuities within soils on a laboratory scale during her work on London Clay. Sample size was noted to have an inverse effect on sample strength, in that; larger samples displayed lower strengths than smaller samples of the same material. Whilst at first this seems counter-intuitive, one must remember that larger samples have an increased likelihood of containing unseen internal discontinuities that would be more easily identified within smaller samples, voiding them prior to testing. This was also observed by Clayton et al (1994) whilst testing chalk samples both in the laboratory and in-situ, where the small laboratory samples had apparent higher stiffnesses than those measured in the field, simply because the large scale fractures and discontinuities were not present in the laboratory sized samples.

At low radial stresses, some materials show an initial increase in stiffness rather than the expected linear elastic response within the very small strain range (Figure 2.34). This is thought to be due to the closure of micro-cracks between well bonded areas of the sample causing the material to behave more competently (Clayton & Heymann, 2001). This also shows the influence discontinuities may have on a sample. This behaviour is

not to be confused with the initial increase in secant stiffness observed as a result of data scatter and an inappropriate shear stage starting point during the analysis of triaxial data.

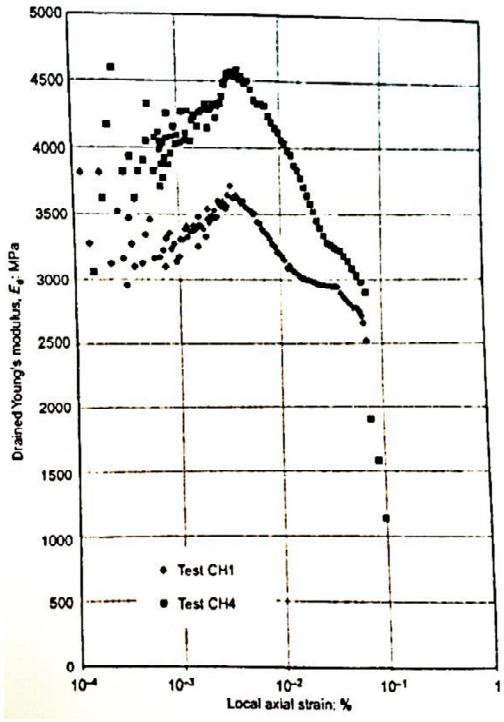

Figure 2.34: Micro-crack closure increasing very small strain stiffness of chalk. From (Clayton & Heymann, 2001).

This closure of micro-cracks can occur in tests that require increasing radial stress, potentially masking the true behaviour of a material's intact strength by generating a false confining pressure dependant relationship (Ismail, et al., 2001). Micro-cracks were observed by Cortesy, et al, (2003) during cyclic testing of soft rocksalt samples, where pronounced hysteresis loops developed between loading cycles (Figure 2.35). This was thought to be due to micro-cracks opening and closing as stress was applied / removed.

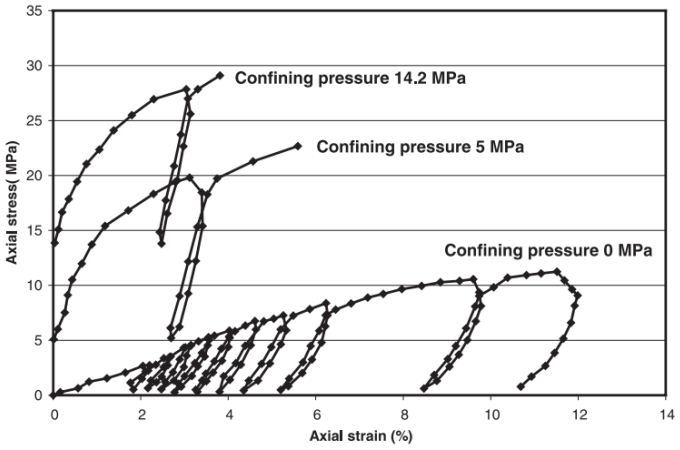

Figure 2.35: Micro-cracks causing hysteresis during cyclic loading of rocksalt. From (Corthesy, et al., 2003).

Large cracks and fissures / discontinuities may entirely control the failure behaviour of a soft rock and so need to be accounted for during testing and any pre-existing fractures measured prior to the test commencing. For the purpose of this thesis, the effect of discontinuities will be minimised by selecting only intact samples and those that do not contain any pervasive jointing / flaws.

2.4.5. *MOISTURE CONTENT / SATURATION*

Tests carried out by Sun, et al., (2004) and (2006) focused upon the role of confining pressure on soft rock strength, however also demonstrated that water content plays an equally important role. Saturated samples were found to have lower cohesion than partially saturated samples and displayed lower peak and initial strengths. These findings are echoed by both Heymann (1998) and Leroueil (2000), who state that the stiffness of cohesive soil is noted to decrease as the degree of saturation increases.

Internal friction angles were found not to change with water content (Figure 2.36).

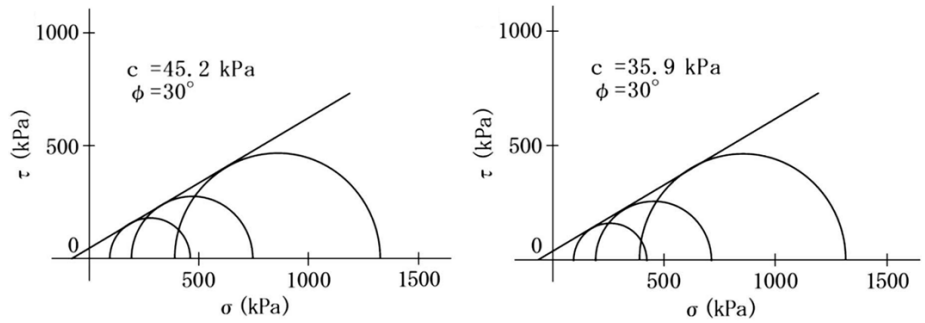

a) b)

Figure 2.36: Weak weathered rock shear strengths when a) partially saturated and b) fully saturated. From (Sun, et al., 2006).

A study examining soft sandstone carried out by Kate & Gokhale (1998) exploring the reliance of stiffness on degree of saturation highlighted that samples at 100% saturation (Sr = 1) undergo larger amounts of strain both axially and radially at a given stress level in triaxial apparatus than those samples at lower Sr values, as seen in Figure 2.37:

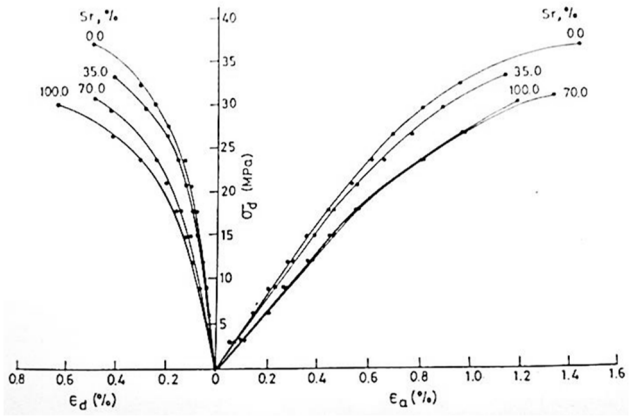

Figure 2.37: Stress strain curves for soft rock samples at various degrees of saturation in Triaxial apparatus. From (Kate & Gokhale, 1998).

It should be noted that the increased curvature of the stress-strain relationship in Figure 2.37 as deviatoric stress rises indicates that the soft rocks response is becoming more ductile for that given level of applied stress with increased water content.

The importance of saturation is well known in the field of soil mechanics, where materials often strain and compress under loading to extents that significantly high porewater pressures are able to develop (relative to the strength of the material in question). This means that the principle of effective stress becomes very important and is a key consideration when dealing with saturated soils. The presence of water, however, is rarely mentioned in relation to hard rocks (with the exception of water flow within fractures, jointing and bedding in-situ) and laboratory based rock mechanics often deals only in terms of total stresses (Haberfield, 2000).

Soft rocks are an intermediate material and therefore can react in a more ‘soil like’ way with regards to the presence of porewater than would be expected for equivalent harder lithologies, being susceptible to processes such as swelling. Chiu, et al., (1983) and later Kate & Gokhale (1998) and Cook (1999) state that the degree of saturation of a soft rock can significantly influence both the measured stiffness and strength properties.

Cook (1999) reviewed a number of studies relating to the moisture content of soft rocks and showed that typically a dry sample’s UCS will be 2 to 3 times higher than that of its saturated equivalent. Ratios of UCS dry to UCS wet of 4 were found for the calcareous rocks he studied which is particularly interesting due to the geographical area of the samples’ origin being similar to those tested for this research. Figure 2.38 shows this trend of high UCS with low moisture content for calcarenites.

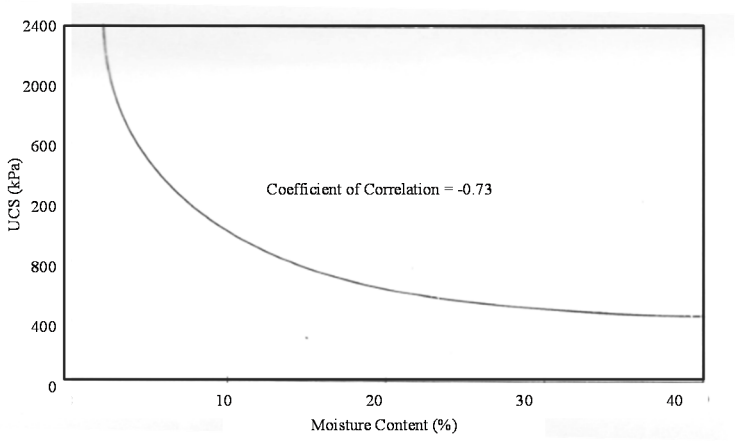

Figure 2.38: UCS values plotted against moisture content. Adapted from (Cook, 1999).

Although strength increases, dryer samples become friable and brittle. Cook (1999) goes on to state that samples should be tested soon after being retrieved from the ground, as a time gap between recovery and testing may cause unrepresentative results.

However, it should be noted that in the interests of obtaining effective stress parameters, fully saturated samples are considerably easier to work with than partially saturated samples as pore pressures and volume changes are measurable.

2.4.6. *MINEROLOGY AND MICRO FABRIC*

A good knowledge of the mineralogy of a sample is very important as, particularly in sedimentary rocks, the stiffness and strength of the minerals making up the grains / crystals and notably the cementation plays a large role in governing the overall stiffness and strength of a material (Heymann, 1998). This is true from coarse grained rocks through to fine grained rocks.

The importance of mineral strength is evidenced on a basic level by Mohs Scale of Mineral Hardness, developed by Friedrich Mohs in 1802 and still forms a crucial (albeit crude) part of petrographic analysis and identification on a hand-specimen level as taught to geologists early into their studies.

In soil mechanics, the mineralogy of granular soils is less important in terms of strength and stiffness of in-situ materials, however the presence or absence of certain minerals (for example gypsum) may govern the degree to which localised dissolution may occur or the degree to which inter-granular bonds / cementation may be present. In cohesive soils, the type and nature of the clay minerals present will influence shrink and swell properties as well as plasticity indices, a key factors controlling clay behaviour.

X-Ray Diffraction (XRD), in particular the powder diffraction method, is ideally suited for the characterization and identification of polycrystalline phases. As the majority of minerals may be described as being crystalline, they me be uniquely identified by their emission, or rather refraction, of constructive interference (well defined, in-phase X-ray beams) when exposed to an incoming concentrated X-ray beam (Ewald, 1962). Amorphous minerals cannot be identified in this manner as the scatter of resultant X-rays is too great, with too little repetition to re-enforce any discernable patterns (Sarsfield, et al., 2006). This means that in the majority of geology related applications, XRD can be employed as a useful means of qualitatively or even semi- quantitatively assessing the distribution of minerals present with a high degree of success.

The mineralogy of fine grained soft rocks, such as mudstone or shale, has a great influence on their geomechanical behaviour, as shown by Dobereiner & Freitas (1986). Interestingly, their study found that this was not the case with coarser grained materials, such as weak sandstones, where regardless of the lithology of the individual grains, mechanical behaviour was not seen to vary, indicating a greater role of the strength of the cementing agents than the grains themselves.

Work carried out by Ismail, et al (2001) demonstrated the role of cement mineralogy in the yielding and post-yielding behaviour of artificially cemented calcareous sands. By creating a series of samples bonded with a variety of agents manufactured to comparable density and uniaxial compressive strength, the influence of cement could be isolated. Their work revealed that soils bonded with Portland cement yielded in a ductile manner before becoming dilatant at low effective confining stress (less than 800 kPa') whereas those cemented using gypsum or calcite tended to fail in a brittle mode at equivalent σ_3'.

However, the mere presence of a bonding / cementing agent is not necessarily enough to add to a geomaterials stiffness, as the bonds must be intact and forming cementicious bridges between grains in order to add additional rigidity (Heymann, 1998). Analysing the extent to which this is occurring in a sample (even an artificial laboratory made sample) is difficult without the use of advanced optical tools. Typically studies attempting to investigate the qualitative mineralogical fabric of a sample will make use of techniques such as Scanning Electron Microscopy (SEM) and thin sections.

SEMs focus a beam of electrons onto an object and, by measuring the back scatter of the emission with a synchronised detector, are able to form a very clear, high resolution

image capable of extraordinary magnification (Specification, 2010). SEM has been frequently used in the broader field of geology for some time, for example its extensive use in micropalaeontology, however only recently has this method been implemented for use in geotechnical situations.

Clayton, et al (2004), for example, used this method to analyse the size and shape of particles within gold tailings. Due to the clarity of the images, the roughness and angularity of the particles could be seen on a scale not possible using conventional methods. This allowed the conclusion to be drawn that the microscopic properties of the tailings governed the materials mass characteristics and overall physical behaviour.

SEM was also used to great effect by Kate & Gokhale (1998) in their study on the influence of moisture content on soft sandstones and by Bromhead & Patel (2000) during their investigation of 'locked' sandstone with zero cement.

The most common application of SEM in a geotechnical context is assessing the spatial distribution of cement (Ismail, et al., 2001); (Amorosi & Rampello, 2007). If cementing agents are adhering only to the outside of grains or within void spaces they may not contribute towards a material's overall strength. If, however, cement has formed bridges between particles, the material's mechanical behaviour will have irreversibly changed, becoming more brittle, stronger and stiffer.

The possible presence of dissolvable minerals such as halite or gypsum within a soft rock within this thesis adds an additional purpose of an SEM investigation, as by assessing the relative spatial distribution of dissolvable particles within a soil skeleton the material's potential for localised dissolution may be found. As with cement distribution, if the dissolvable minerals have formed cementicious bridges between grains, effectively cementing the material, their dissolution will cause a structural failure, reverting the material to a weaker, more ductile configuration (shown diagrammatically in Figure 2.39).

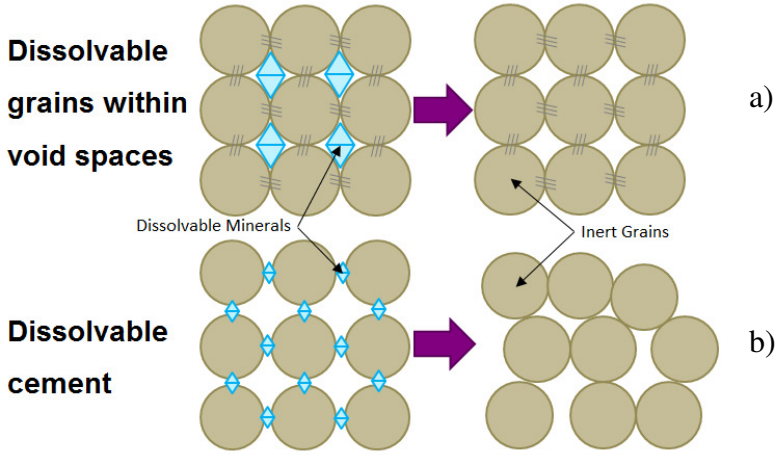

Figure 2.39: a) Dissolvable material precipitated within voids. b) Dissolvable material acting as cement.

Techniques such as SEM and XRD can provide an overall view of the mineralogical makeup of a sample, identifying the presence and type of dissolvable minerals, clay minerals, cementing agents and/or other micro-features that may be controlling factors of a material's behaviour.

2.4.7. *STRESS / STRAIN RATE*

The rate of applied stress is a factor that needs to be considered for all geotechnical laboratory experimentation and testing, as this variable is capable of altering measured strengths and stiffnesses substantially if not properly accounted for (d'Onofrio, et al., 1999); (Silvestri & d'Onofrio, 2000); (Vardanega & Bolton, 2011). Typical routine testing of both soils and rocks will strain samples several times faster than strains generated during construction, decreasing the accuracy and relevance of results.

General findings from the literature show that higher strengths and stiffnesses are measured as the rate of deformation increases as shown in Figure 2.40. This property is however complicated by the generation of excess pore water pressures at higher strain rates (Richardson & Whitman, 1963); (Leroueil, 2000); (Silvestri & d'Onofrio, 2000); (Vardanega & Bolton, 2011).

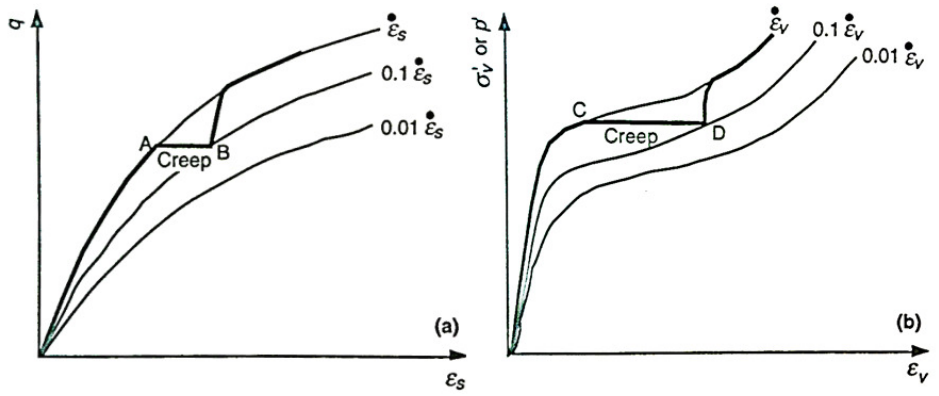

Figure 2.40: Stress strain curves showing strain rate dependency in a) shear behaviour and b) bulk behaviour. From (Leroueil, 2000) testing of natural clays.

In order to account for the presence of porewater within soils testing, drained triaxial tests must be carried out at a rate of strain fast enough to eliminate the effect of creep (30 to 100 times faster than creep rates is often quoted), however slow enough that porewater pressures are able to fully dissipate (generating pore pressures of no more than 4% of the current mean effective stress, according to British Standards). Failure to do this may result in localised drops in effective stress, causing pre-emptive and unrepresentative failure. Likewise, undrained tests must be performed in such a manner that uneven internal porewater pressures do not build. This is often checked with the use of mid-height pressure probes, or else if such apparatus is not available, a rate of strain is selected that is assumed to allow pressures to fully equilibrate based on the response measured at the top and bottom of the sample (Gasparre, 2005); (Gasparre & Coop, 2006).

As the rate of porewater dissipation is a function of permeability, over-consolidated fine grained samples with low void ratios are particularly sensitive to shearing rates, meaning that all stages of testing and consolidation must be performed slow enough not to generate unwanted localised stresses. Provided that conditions of satisfactory drainage are met, observations within the literature indicate that an increase in strain rate will result in higher measured stiffness's. Although Ismail, et al (2001) stated that no such relationship was observed during their experimentation on artificially bonded sands, perhaps owing to very high permeability.

Strain rate effects are similar to (and in fact related to in terms of viscosity theories) the role of temperature on strength (Leroueil, 2000). The role of temperature becomes substantially more complex when evaporite / salt is being tested, however generally the stiffness of a material at a given strain will decrease as temperature increases. The role

of temperature on soft rock stiffness was tested by Zhang et al (2010) however it was found that the temperature required in order to observe a change from brittle to ductile behaviour was at least in excess of 60 degrees Celsius (their study's maximum temperature). Likewise during the testing of soft rocks fast strain rates are more likely to produce brittle behaviour whilst slow strain rates will produce ductile behaviour even for the same sample (Zhang, et al., 2010).

In soil mechanics, BS1377 standards on triaxial testing calculates the maximum allowable strain rate of a soil based upon observed behaviour during consolidation, meaning that the strain rate will be a function of that material's specific permeability. In rock mechanics however, where pore pressures are not generally taken into account (and samples are often tested dry), stress / strain rates are selected using a less sample specific method.

Current ISRM guidance states that during UCS testing, load will be increased at a constant rate until the occurrence of a failure within 5 – 15 minutes of the test start OR alternatively the uni-axial pressure be increased at a constant rate of between 0.5 – 1.0 MPa until failure. For strong rocks, these two methods provide comparable results, however as stated by Johnston (1991) the same cannot be said for soft rocks. This is because in order to allow failure to occur within the 5 – 15 minute guidelines, stress must be applied at a substantially slower rate than 0.5 – 1.0 MPa and if the 0.5 – 1.0 MPa guidelines are adopted, soft rocks will fail within seconds of the test commencing. Similar issues apply during the testing of soft rocks in Brazilian tensile apparatus.

The role of stress / strain rate is considered to be an important factor in governing the stiffness of soft rocks and their transition from brittle to ductile behaviour, and as such has been selected to form part of the proposed testing program. As this research project is examining the behaviour of a low permeability soft rock type (calcareous mudstone), careful consideration of appropriate strain rates must be had.

2.4.8. *CYCLIC / DYNAMIC LOADS*

Cyclic / dynamic loading and the resulting influence this has on a geo-material stiffness, is similar and related to the influence of strain rate within static loading tests.

Dynamic loading encompasses any form of applied stress on a given unit of material that is not static or constant, and included within this broad definition is cyclic loading.

Static loading can be thought of as a permanent load. A small building foundation or embankment, for example, will exert a near constant and permanently unchanging load upon the ground below it. Traditional soil testing tends to assume this is the case, especially within the UK, and that the peak shear strength / stiffness of a material can be utilised in geotechnical design.

During cyclic loading however, the peak shear strength and stiffness characteristics of a material will degrade over time, as more loading cycles are introduced (Ansal, et al., 2001). Common geotechnical problems where this may be applicable include petrol tanks, wind turbines and railway tracks, where the load imposed upon the ground below them fluctuates over time as the tank is filled and emptied, the wind blows harder or softer or as the train traffic is busy or quiet.

Leroueil (2000) presents findings from Yokohama Siltstone (Figure 2.41) showing the dependence strength has upon number of loading cycles. As the number of cycles increase, maximum normalised deviator stress decreases.

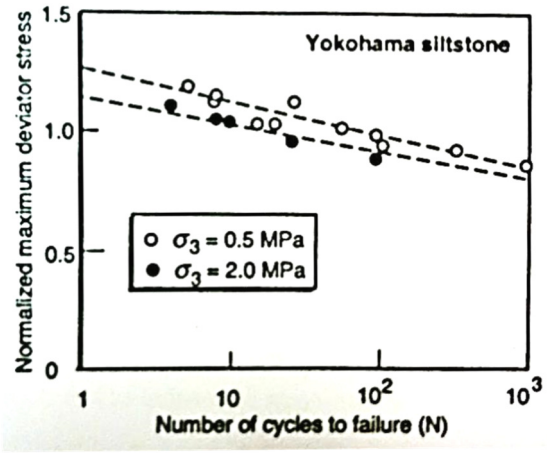

Figure 2.41: Maximum normalised deviatoric stress as a function of number of cycles to failure. From (Leroueil, 2000).

Curiously these findings, originally published by Yoshinaka & Osanda (1995), display a counter-intuitive relationship between fatigue / accumulation of cycles and confining stress, in that; as the confining stress increases, the normalised deviatoric stress required to cause failure for a given number of cycles decreases, perhaps due to materials shifting from brittle to ductile behaviour.

Niemunis et al (2004) state that settlements of foundations experiencing cyclic loads should be looked upon as long term soils-structure interaction problems, as settlements continue to occur well beyond those expected of comparable static loads (this can be

seen in Figure 2.42 and parameters are often derived from multi-stage oedometer testing).

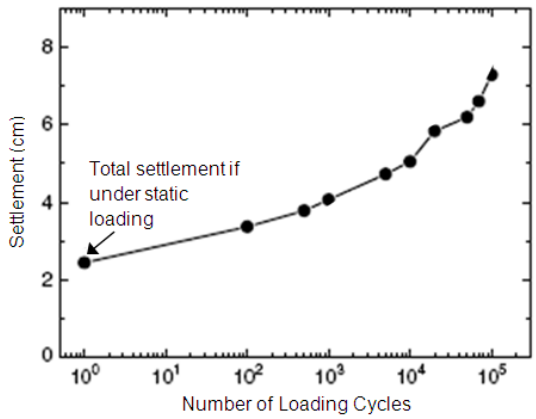

Figure 2.42: Settlement of strip footing bearing upon sand subject to cyclic loading. Adapted from (Niemunis, et al., 2004).

Earthquakes are another example of cyclic loading and, being common throughout much of the world, are a huge factor influencing the way in which safe yet economic structures and foundations are designed (Ansal, et al., 2001).

Shear stiffness of soils and soft rocks degrade with increased strain amplitude in much the same manner as that of small strain stiffness. This degradation can be broken into three phases, with thresholds marking the boundaries between each. These three stages can be seen in Figure 2.43.

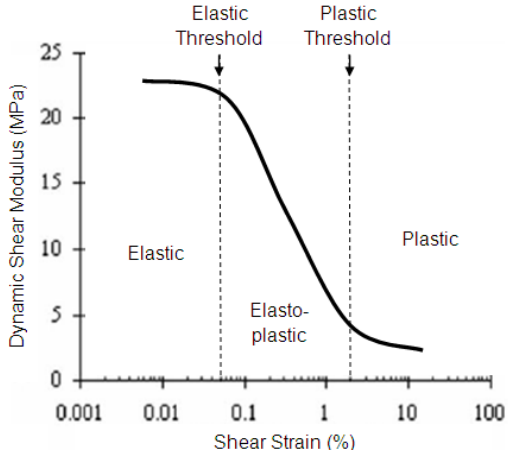

Figure 2.43: Dynamic shear modulus degradation stages and thresholds. Adapted from (Ansal, et al., 2001).

Firstly, if the strain amplitude introduced by the cyclic loading is small enough, the material will behave elastically. No long term shear stiffness degradation will be incurred, regardless of the number of loading cycles. This is comparable to very small strain linear elastic behaviour observed during static testing.

Once the elastic threshold is exceeded by the strain amplitude however, the material will start to behave elasto-plastically. Cyclic loading will lead to increased pore pressures, strain softening and inter-particle structure breakdown. Stiffness will gradually deteriorate with increased number of cycles, in a similar fashion to small strain stiffness deteriorating with increased strain during static tests. This behaviour is not limited to totally saturated soils / soft rocks, as (Peth & Horn, n.d.) found in their testing of partially saturated sands, where cohesion (and therefore shearing resistance) was witnessed to be gradually lost due to inter-particulate fluctuations from positive pore pressures to negative pore pressures (suction).

Finally, when the plastic threshold is exceeded, the material will undergo large strains and will experience yet further stiffness degradation due to structure breakdown and rising pore pressures. Extreme scenarios may even lead to liquefaction, caused by pore pressures exceeding total stresses leading to negative effective stress conditions (Peth & Horn, n.d.).

The effect of cyclical loading upon rock is greatly controlled by the material's original properties. If the stress induced is small and the material stiff, the strength degradation may be negligible (or simply cause brittle fracturing if load exceeds the material strength), however if the rocks in question behave in a soil like ductile manner, as many soft rocks have been observed to, the deterioration in stiffness moduli per load cycle may be quite pronounced.

2.4.9. *AGEING / CREEP*

Ageing is the term given to the mechanisms that occur in geomaterials over time when held at a steady stress state. Ageing is generally accepted to comprise of both creep and the development of bonding and can therefore be thought of as the initial stage in the generation of structure (and shares some overlap between those properties). Heymann (1998) notes that aging always increases the stiffness of a geomaterial as creep takes place (further consolidating the sample), and as bonding starts to develop.

Creep is a common process in soil behaviour, however unlike hard rock's (which do not reorganise their grain/crystal structure upon being exposed to normal working loads) soft rocks may also undergo creep, and Corthesy et al (2003) state that this process is even more pronounced in evaporite deposits.

Salts, when subjected to a constant load, will eventually reach a steady-state strain rate (the speed of which is controlled to some degree by temperature and humidity) (Corthesy, et al., 2003); (Berest, et al., 2010); (Truong, et al., 2012). Samples will continuously creep in a manner very unlike soil or other soft rock lithologies, except those containing significant quantities of salts. This behaviour is difficult to record in the laboratory given the material's highly sensitive nature to heat and moisture and some papers report carrying out testing on such materials at the bottom of mines, as temperature / humidity control rooms are insufficiently stable (a point re-iterated by Gasparre & Coop, (2006) when carrying out highly sensitive very small strain probing of London Clay). In addition to this, very accurate measurements of strain are required and when measuring creep in salt samples and the load applied must remain absolutely constant (Berest, et al., 2010).

Creep rates vary within soft rock samples subject to changes in stress, dependent upon a number of factors including mineralogy and stress state / stress history, and its extent is often not easy to measure. A sample which has undergone isotropic consolidation to a given mean effective stress in triaxial apparatus may be followed by a period of secondary consolidation which is observable if a rest period is allowed. Likewise a sample that has been subjected to a deviator stress then unloaded or allowed to rest may also undergo creep. Bishop & Lovenbury (1969) examined the creep characteristics of London Clay and state that there does not appear to be any deviatoric stress levels that creep does not occur to at least some degree.

Clayton & Heymann (2001) demonstrated that a sample of clay subject to three identical stress paths would produce the same initial stiffness and degree of stiffness degradation each time (as opposed to degrading due to cyclic straining), providing that creep was allowed to stop (upon returning the its isotropic stress state) before the next path was followed. This was also observed by Heymann (1998) in his investigation into the stiffness of London Clay at very small strains, and he also states that creep (once accounted for properly) can override the effects of recent stress history, although this point is still debated.

A study carried out by Leonards & Ramiah (1959) on the time related effect on clays indicated that allowing rest periods during consolidation caused sample stiffness to rise and the yield stresses to increase even if creep was disallowed. This showed that some degree of structure (fabric) develops during rest periods in testing, often to the extent

that structure permitted space may be observed in oedometer compression, even without the associated consolidation.

Whilst both creep and the development of bonds add to geomaterial stiffness, separating these two components of ageing is difficult (Heymann, 1998). The effect of ageing can develop quickly, often within engineering timescales, although will always be most pronounced when allowed to occur for prolonged periods of time. During laboratory testing, several authors have stated that allowing creep rates to drop below 0.001% per hour is acceptable for assuming the effects of creep to have become negligible (Kim & Finno, 2011), and that subsequent straining rates should be at least 30 times faster than creep rates at a given mean effective stress (although other authors recommend 100 times faster (Jardine, 1992); (Gasparre, 2005); (Gasparre & Coop, 2006)). Furthermore, suggestions are made that creep should be allowed to reduce for a week following consolidation and prior to shearing.

Whilst testing pure salt samples is not a part of this project, soft rocks from the UAE contain a percentage of evaporite minerals within their composition which may potentially alter their creep behaviour (Zhang, et al., 2010). Creep is an important property to consider during advanced triaxial testing, as failure to properly account for its presence can lead to inaccuracies in stiffness measurements particularly within the small strain range (Clayton & Heymann, 2001); (Heymann, et al., 2005). Testing should allow creep rates to subside to negligible levels, or in the case of materials that continue to exhibit steady strain rates, shear testing should be carried out at rates significantly higher than those of the observed steady creep.

2.4.10. *STRESS PATH DIRECTION AND RECENT STRESS HISTORY*

The specific stiffness response of a given geomaterial upon introduction to a stress, is controlled by many factors, however some of the most important (outside of mineralogy, void ratio and moisture content) are those of the orientation / coordinates of the current stress path within a stress space with respect to its recent stress history.

The location and orientation of the current stress path during shearing is important, as when a material is sheared from an initial stress space close to its yield surface, its stiffness response will change depending upon whether the stress path is moving away from (stiffer response) or towards (less stiff response) the yield surface (Heymann, 1998); (Finno & Kim, 2011). This is because plastic strains begin to become prevalent

closer to the yield surface and the geomaterial gradually starts to undergo permanent deformation.

The effect of proximity to the yield surface is more pronounced once large strains start to develop (Finno & Kim, 2011). If the distance needed to travel in stress space towards the yield surface is long then stiffer responses are observed, however at small strains it appears that the effect of recent stress history, (not proximity to the yield surface) is most important.

Recent stress history can be defined as the current stress path direction in relation to its most recent previous stress path, denoted by the angle (θ) between current and recent stress paths (Finno & Kim, 2011); (Finno & Cho, 2010). Whilst Heymann (1998) and Clayton & Heymann (2001) dispute the importance of recent stress history, claiming that the effects observed during testing may be accounted for by creep and proximity to the yield surface, the general consensus for materials that have no bonding at all is that the orientation of the stress path and its relation to recent stress history can have a very large influence on the small strain stiffness of a sample (Jardine, 1992); (Finno & Kim, 2011).

General findings have indicated that the closer to an angle (θ) of 180 degrees (total stress path reversal) between the outgoing stress path and the incoming stress path (recent stress history), the stiffer the soil response to stress will be. For example, a soil which has been subject to compressional forces in its recent past will respond in a stiffer manner to extensional testing than it will to compressional testing. Likewise, a sample which has been subjected to extensional forces in its recent past will respond in a stiffer manner to compressional testing than it will to extensional testing (Gasparre, 2005); (Finno & Kim, 2011); (Finno & Cho, 2010); (Kim & Finno, 2011). This concept is demonstrated in Figure 2.44. Whilst at a first glance these scenarios may seem interesting only in an academic sense, in reality understanding the effect of recent stress history is very important as cases of 180 degree stress path reversal (or high θ rotations) are common during the processes of construction, excavation and demolitions (Finno & Kim, 2011).

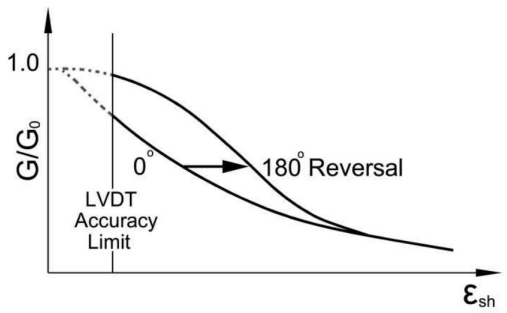

Figure 2.44: Conceptual diagram showing the effect of stress path rotation from angle of recent stress history on small strain stiffness. (Finno & Cho, 2010).

This effect is most pronounced within the small strain range and only once the Y2 yield surface has been engaged (Gasparre, 2005); (Finno & Kim, 2011). Once large strains start to develop, the stiffness of the soil converges to a similar value, regardless of the angle between current and recent stress paths. Finno & Kim (2011) found results matched this conceptual ideal during their later testing of Chicago Glacial Clays using Bender Elements in Triaxial apparatus, as shown in Figure 2.45.

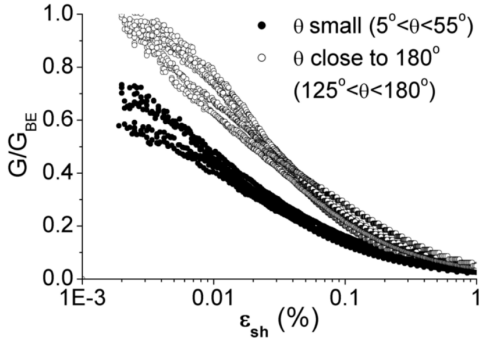

Figure 2.45: The effect of recent stress history (Finno & Kim, 2011).

In order to address some of the concerns regarding the effect of recent stress history raised by Clayton & Heymann (2001), Finno & Kim (2011) allowed creep to stop entirely prior to testing and between stress probes and always sheared samples at a rate high enough (always at least 30 times greater than creep rates, in some cases up to 100 times higher) to negate the effect of creep. They also noted that within very small strains (less than 0.002% prior to engaging the Y1 surface) stiffness does not appear to be affected by recent stress history.

Choosing the rate to which a sample should be exposed to stress or strain is difficult, as tests must be quick enough to negate creep, but slow enough that no uneven or excess porewater pressures build up within the sample. This is especially true of low permeability materials such as clay or mudstones.

For heavily structured materials, such as many rocks or soft rocks, the re-orientation of the stress path has little to no effect on the observed stiffness of that material, providing that not enough stress has been present to cause de-structuring (Clayton & Heymann, 2001). This also applies to bonded soil samples and Clayton & Heymann (2001) found that natural materials with even weak bonding will not display any effects of recent stress history provided that the structural yield surface is not crossed, and concluded that modern soil models may be simplified not to incorporate the effect of recent stress history providing the strains likely to be encountered were only 'modest' and that soil structure was likely to remain intact.

Finno & Kim (2011) concluded that both the recent stress history and current stress path direction / proximity to the yield surface affect the shear stiffness deterioration with strain, however stated that the angle of the recent stress history appeared to have a more pronounced effect. In soft rocks with structure present, strains not great enough to cause de-structuring / de-bonding will not be affected by recent stress history, however once the material's bonding has yielded, the effect and importance of recent stress history and stress path direction may come into play.

Without multiple identical samples (or the use of artificial samples), exploring the effect of stress path reversals is difficult. Multiple tests cannot be carried out on the same sample without fundamentally altering its stiffness and comparing results following different stress paths from samples whose geographical spatial distribution is large would confuse interpretation.

2.4.11. *ANISOTROPY*

Geomaterials, unlike manmade building materials such as metals and plastics, are always heterogeneous if viewed from a great enough, or indeed fine enough scale. The most outwardly homogeneous sandstone will appear heterogeneous once bedding and fracturing is taken into account, and even well sorted clays will be heterogeneous on the particulate level. However this level of heterogeneity does not necessarily translate into geomaterials behaving anisotropically with regard to response to stress. Two types of anisotropy are accepted to exist, inherent anisotropy (the anisotropy present within a sample in its original environment of deposition / in-situ) and induced anisotropy (caused by changing stress conditions, effectively over-riding the inherent anisotropy, mainly via volumetric strain onset) (Leroueil & Hight, 2002); (Bica, et al., 2008).

A remoulded soil that has been isotropically consolidated, will be isotropic in structure and fabric on a particulate level and therefore respond to stress in an (induced) isotropic manner. Samples which have been consolidated to in-situ (K_0) conditions however will have particulate structure aligned at right angles to the direction of the highest stress (induced anisotropy), and will therefore respond differently to an applied stress depending upon its orientation (Kim & Finno, 2011).

Kim & Finno (2011) carried out a series of experiments on Chicago Clays in order to examine their anisotropic nature. Findings showed that the greatest changes in anisotropy occur as irrecoverable plastic deformations develop (coincident with the Y2 surface defined by (Jardine, 1992)). This study also showed that ratios of horizontal to vertical shear stiffnesses were different in materials with different over-consolidation ratios (OCR), with lightly over-consolidated and normally consolidated materials having values of between 1.2 – 1.7 and heavily over-consolidated materials having values of higher than 2.2.

Anisotropy is closely linked to the existence of structure within soils, especially at a granular level, as it includes particle alignment and over-consolidation. Corthesy, et al, (2003) stated that soft rocks, or at least the rocksalt, potash, shale and sandstones that their research covered, could always be thought of as being anisotropic at a granular scale due to the presence of micro-cracking, the random orientation of crystals and variations in mineral content (Bica, et al., 2008).

Whilst micro-anisotropy is a factor controlling the mechanical behaviour of soft rocks, a much greater strength / stiffness reliance is placed on the inherent macro-anisotropic nature of materials, namely the orientation of pre-existing fractures and discontinuities. This is particularly true within soft rocks of sedimentary origin that have a distinct orientation of deposition (Hoek, 1965); (Lo & Milligan, 1967); (Johnston, 1991); (Bica, et al., 2008).

In order to assess anisotropy in the laboratory, either samples must be available which have been recovered from numerous angles / orientations (for example sample cores recovered from a large block at different orientations with respect to bedding), or else by using local gauges capable of measuring properties at defined orientations (such as bender elements mounted in both the horizontal and vertical positions during the assessment of G_0).

2.5. CHAPTER SUMMARY

Johnston (1991) recognises a very profound and important theory, that all rocks and soils, whilst having an enormous range of possible geotechnical properties, appearances and age, are all fundamentally similar in behaviour to one another, and that they all fit within the same school of thought as opposed to requiring discrete sciences of soil / rock mechanics. This he termed as the 'Geotechnical Spectrum'.

Geo-materials ranging from the softest wet clay to the strongest granite fit into the geotechnical spectrum and obey the same laws. The only difference being scale, with one end of the spectrum controlled by pore pressures and void ratios and the other by structure and discontinuities (Haberfield, 2000). This has been demonstrated through literature review by looking at the role that properties such as in-situ discontinuities and fractures play on overall material strength of both soil and rocks as well as examining key performance characteristics such as compressibility and strength.

Soft rocks have been found to have a strength dependence on confining pressure and water content that falls between that of soil and rock and to have failure mechanisms ranging from brittle to plastic under stress state changes small enough to be encountered given normal working loads (Johnston, 1991); (Aversa & Evangelista, 1998); (Sun, et al., 2004). In addition, the role of water content and degree of saturation were examined along with mineralogy, micro fabric, structure, confining stress, strain rate, stress path direction and recent stress history on the overall performance of soft rock with a particular focus on their effect on small strain stiffness behaviour with each variable either lowering or raising maximum stiffness as they vary.

As of yet there is no official definition which may be used to classify materials as soft rock (with soft rock materials instead often being treated as either soil or rock), however it is clear that transitional materials exist and that they cannot be studied within the laboratory appropriately by sole use of conventional methods from one discipline alone. For the purpose of this thesis, the definition of soft rock defined by Hawkins (2000) will be used. It is also important to note that no definitive framework for the testing of soft rocks exists to date.

Current thinking puts high emphasis on the characterisation of geomaterials pre-failure stress strain relationships, as these are often more crucial to design than properties of materials at failure. Research into the small and very small strain stiffness of geomaterials is helping to lessen the errors observed between ground strains measured

in-situ and those predicted based upon routine laboratory testing, which often underestimate stiffnesses within the small strain range by an order of magnitude. The importance of research into small strain stiffness behaviour is becoming increasingly well recognised in both industrial application and academic research of all geomaterials, including soft rocks (Burland, 1989); (Viggiani & Atkinson, 1995); (Barla, et al., 2000); (Silvestri & d'Onofrio, 2000); (Gasparre, 2005); (Gasparre & Coop, 2006).

In normally consolidated soil, its mechanical behaviour is a reflection of its PSD, particle shape, mineralogy and void ratio (Epps, 2011). Its small strain stiffness behaviour will be dependent upon these properties and will vary as a function of the imposed mean effective stress and rate of strain during testing. Complications arise once structure / anisotropies are present, as behaviour begins to deviate away from simple generalised patterns. The degree of over-consolidation, size of the structural yield surface and orientation of stresses become increasingly important factors, each being complicated further by their relationship to the stress state in which the material is being tested and its stress history.

To combat this myriad of variables, many studies adopt the use of artificial samples or fully remoulded samples. Assessing the role that cement plays on the strength and stiffness of artificial samples, for example, is common within the literature, as by directly controlling the PSD, percentage cement composition, void ratio / dry density and moisture contents of samples within a testing program it is possible to locate an individual variable and assess it in isolation with great repeatability. Often unstructured clays will have an element of induced anisotropy introduced to them by artificial consolidation within triaxial apparatus to a known pre-consolidation pressure, rather than relying upon their natural ‘remembered’ stress history. The use of artificial samples is attractive from a cost and convenience perspective also, as using undisturbed samples first requires an expensive drilling or trial pitting program as well as giving rise to the possibility (or even probability) of inter-sample variability (Amorosi & Rampello, 2007). Comparatively few studies are carried out assessing undisturbed properties of natural samples, even fewer still on intact calcareous soft rocks.

To date, very little information is documented regarding the behaviour of the calcareous mudstones around Abu Dhabi’s coastline, despite heavy urban development taking place in this part of the world. By testing natural soft rock cores, as opposed to artificial samples, results within this thesis will be more relevant to prospective development around this area than would their artificial counterparts.

To this end, the natural soft calcareous mudstones of this thesis will be tested with a combined approach of both traditional and advanced soil and rock testing procedures in order to better understand the full range of materials properties these soft rocks exhibit.

Techniques such as XRD and SEM will be employed to assist in the mineralogical and micro-structural characterisation of these materials pre-shearing along with standard procedures from both soil and rock testing disciplines to generate a thorough physical characterisation.

Ultimately, a mechanical assessment using; oedometer, indirect tensile and advanced triaxial tests will complete the micro-to-macro scale characterisation of these poorly understood materials, with the mechanical testing program having a particular focus on small strain stiffness (and an assessment of the degree to which these materials' stiffness is dependent upon strain rate and mean effective stress).

Traditional views and practices surrounding the distinct categories of soil and rock have led to very different approaches in managing these materials (Bromhead & Patel, 2000). This is seen at all stages of examination, from initial site investigation and logging methods all the way through to laboratory testing procedure and computer modelling (few models exist that incorporate soft rocks). The difference in treatment of materials above and below the soil/rock interface is "staggering" (Haberfield, 2000); (Truong, et al., 2012). Even the international technical societies for soil and rocks are distinct and operate independently with little or no interaction, further enforcing the widely held opinion that soil and rock fall under disparate disciplines. However, if soft rock behaviour is to be fully understood, it is critical that they are not simply treated as 'very hard soils' or 'very weak rocks', but instead confronted using a combined approach. Johnston (1991) and Haberfield (2000) have stated that by bridging the gap and bringing together the two sciences of soil and rocks into a complete and continuous understanding of natural geo-materials, it is plausible that much will be gained for geo-mechanics as a whole.

CHAPTER 3. SITE DESCRIPTION AND GEOLOGICAL SETTING

3.1. CHAPTER 3 INTRODUCTION

The previous chapter identified a gap in research with regard to soft rock's mechanical behaviour via literature review. It also defined small strain stiffness and presented the current thinking regarding the definition of soft rocks and those factors which affect their strength and stiffness.

This chapter briefly examines the geology of the area of interest and provides location plans of the two sites the calcareous mudstone samples examined in this thesis originated.

The purpose of this chapter is to provide a geographical and geological context for this research.

3.2. THE GEOLOGY OF ABU DHABI ISLAND

The geological history of the United Arab Emirates (UAE) is not a focus of this research; however, in the interests of adding context to the work being carried out, some key points are presented here along with a brief summary of the geology of Abu Dhabi Island and the origin of the calcareous mudstones tested within this project.

3.2.1. *THE UNITED ARAB EMIRATES*

Prior to the 1950's the geology of the UAE, formally known as the Trucial Coast, was only discussed with respect to its rich oil bearing Jurassic rock formations, namely the Diyab, Arab and Hith formations (Al Suwaidi, et al., 2011). However in more recent times, as the wealth of the region has expanded and the scale of construction projects increased, interest in the surface and shallow sub-surface deposits has also grown (Alsharhan & Kendall, 2011); (Epps, 2011); (Evans, 2011). This is particularly true of the young sediments and soft rocks that make up the coastal areas of the UAE, and whilst these areas are well studied from a geological standpoint, research into the mechanical behaviour of the soft rocks making up these coastal zones is less common and only a handful of publications exist (Epps, 2011).

The UAE resides upon a large body of continental rock which forms part of the Arabian Platform and has been relatively stable since the Cambrian with the exception of the formation of the Arabian\Persian Gulf (noted not to be a true ocean basin (Interact, 2011)). The Arabian Plate disconnected from the African Plate approximately 25 million years ago, forming the Red Sea, followed by the Afro-Arabian plates moving south and becoming glaciated. However, since the end of the Palaeozoic, the UAE has remained within climates similar to the one in which it is seen today, with its solid and drift geology defined by repeated cycles of marine transgressions in and around the Arabian Gulf (caused by glacio-eustatic processes) and sub-aerial erosion and transportation (Walkden & Williams, 1998); (ASP, 2001); (Epps, 2010). At times the Gulf has been totally dry, (for example during the last glacial maxima), allowing carbonate sediments to be transported from its bed inland (Teller, et al., 2000).

The Persian / Arabian Gulf is an asymmetric and elongated foreland basin, as seen in Figure 3.1. The Arabian side of the Gulf is gently sloping and shallow, with average depths of 35m (maximum of 100m), with extensive flat landward areas that historically flooded repeatedly to 1000km inland of the present day coastline during times of relatively high sea levels (evidenced by relic beach ridges found several kilometres inland (Kirkham, 2011)). These transgressions are supposedly responsible for the great flood of Sumerian legend, 'The Deluge', along with 'Noah's Flood' (Teller, et al., 2000); (Evans, 2011); (Alsharhan & Kendall, 2011); (Kendall & Alsharhan, 2011).

Figure 3.1: Map of the Persian / Arabian Gulf showing bathymetric provinces and water depth contours. Adapted from Alsharhan & Kendall, (2011).

This history of marine transgressions has allowed the formation of vast expanses of carbonate and evaporite sediments from the Gulf's saline waters, including: fossiliferous limestone and dolomite (representing the reservoir rocks for the majority of the UAE's oil reserves), calcareous shale; siltstone; mudstone; sandstone; and interbedded gypsum, halite and anhydrite (Walkden & Williams, 1998); (Evans, 2011).

Evaporites are a major part of the geology of the UAE, both at depth and at the surface, and much of the topographical highs and several of the offshore islands have been formed as a result of rising salt domes (salt diapirisms) at depths of approximately 6,000 meters, originating from the Cambrian Hormuz salt basin (Al Suwaidi, et al., 2011). Evaporites are also responsible for sealing many of the local, highly prolific, oil deposits. Salts are seen at surface in the form of vast Sabkhat (plural of Sabkha), the Arabic name for salt flats, formed by shallow salty groundwater rising through loose drift deposits by capillary action and precipitating within the void spaces following evaporation, effectively cementing the soils and forming impermeable surfaces prone to flooding. These Sabkhat have been famous from a geological perspective since the 1960s when they were first studied, with some reaching tens of kilometres in length and up to 15km wide (Evans, 2011); (Sepmstrata, 2011); (Alsharhan & Kendall, 2011); (Kirkham, 2011). These evaporites can be highly sensitive to changing groundwater salinity and flow conditions.

The Gulf itself receives virtually no runoff water from the Arabian Peninsula to the south, instead taking in water draining from the Zagros Mountains to the north. The present day salinity of the Gulf waters is between 37 and 40‰, and even reaching as high as 50‰ in locally shallow, sheltered regions. This high salinity, coupled with the high average summer daily temperatures of 35^{o}C within the UAE (average winter temperatures of 18^{o}C) allows carbonate sediments to continue to form today (Teller, et al., 2000); (Kendall & Alsharhan, 2011).

The majority of the surface of the present day UAE is covered by laterally extensive sandy deserts and intricate patterns of windblown dunes. These deposits are young, geologically speaking, and were formed as a result of sub-aerial erosion and subsequent deposition in a hot climate with very low precipitation rates (<100mm/yr.) (Teller, et al., 2000). Whilst being visually breath taking, with some dunes measuring between 50 and 100m in height, they pose significant engineering problems for structures such as roads (Tobin, 1980). The aeolian dunes are mainly composed of quartz grains, although increasing amounts of detrital carbonates become present with increasing proximity to

the Arabian Gulf, particularly within 40km of the Gulf coast (Teller, et al., 2000). Superficial deposits are often thick, almost totally covering the bedrocks below, even at coastal areas (Interact, 2011).

The only large expanses of 'hard' rock seen at the surface of the UAE are the ophiolites found within the Hajar Mountains, being comprised of the igneous rocks, mantle material and oceanic crusts thrust over the Arabian Plate in nappes, and are some of the most studied ophiolites in the world (ASP, 2001). A few localised exposures of Miliolite Sandstone can occasionally be seen around the coastal regions, (named after the chambered benthic foraminifera 'Miliola' that commonly occur within them) and formations of very young Holocene soft rocks known as 'Caprocks' are present around the shallow lagoons and tidal flats, having been cemented in-situ (Teller, et al., 2000); (Evans, 2011); (Kendall & Alsharhan, 2011).

3.2.2. *ABU DHABI ISLAND*

Abu Dhabi itself is the largest of the seven emirates, occupying around 85% of the total surface area of the UAE, as seen in Figure 3.2. Geologically, Abu Dhabi lies within a large syncline with few rock exposures. Like much of the UAE, the effect of rising salt domes can be seen in the form of hydrocarbon traps and on-land superficial deposits are consistent with the general trend of the UAE mentioned previously including dunes, windblown sediments and closer to the Arabian Gulf, Sabkha's (ASP, 2001).

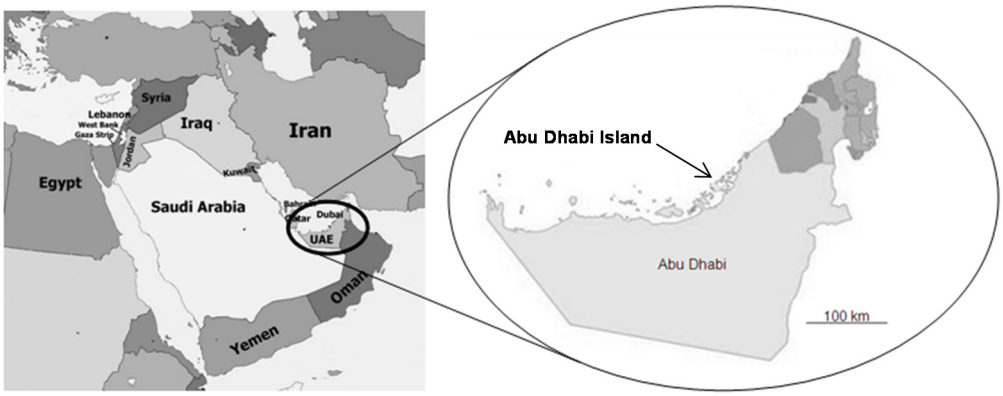

Figure 3.2: Map showing size of Abu Dhabi in comparison to other emirates. Adapted from pictures found at (uaetourguide, 2011).

The capital city of both Abu Dhabi and of the whole of the UAE is also called Abu Dhabi, which resides along the northern coast of the Abu Dhabi emirate on a T-shaped island forming part of a complex of barrier islands known as the Great Pearl Bank Barrier (Epps, 2010); (Kendall & Alsharhan, 2011). Architecturally, Abu Dhabi is highly developed, as shown in Figure 3.3, and has some of the tallest buildings in the

world, calling for precise and accurate understanding of the sediments and soft rocks upon which they found (Cook, 1999).

Figure 3.3: Aerial photograph of present day Abu Dhabi Island taken from Google Earth.

The area of the Arabian Gulf around Abu Dhabi is a young, shallow (<20m depth) and highly saline environment, in fact Abu Dhabi's original name was 'Milh', meaning 'salt', presumably referring to the vast Sabkha salt flats the saline Gulf has formed inland (Teller, et al., 2000); (Interact, 2011). Daily humidity ranges between 40% during the day and 90% at night and summer temperatures can reach as high as 45^{o}C. The majority of the deposits making up the coastline of Abu Dhabi are of Pleistocene to Holocene in age and are mainly carbonate sediments (Cook, 1999); (Epps, 2010); (Kendall & Alsharhan, 2011). Abu Dhabi Island is located at latitude of approximately 24^{o}N and the formation of evaporite deposits and calcite / dolomite dominated lithologies are common in shallow marine areas in tropical / subtropical regions such as this (Ismail, et al., 2002); (Alsharhan & Kendall, 2011).

Evans, et al., (1973) and later Epps, (2010) and Alsharhan & Kendall, (2011) (and Kendall & Alsharhan, (2011)) were able to divide these natural calcareous sediments into several categories or sub-environments, based upon their relative locations and the factors influencing their formation (excluding the anthropomorphically engineered fills). By and large the type and spatial distribution of the sediments in this area are governed by the prevailing wind direction ('The Shamal', the strong north-westerly wind (Evans, 2011); (Alsharhan & Kendall, 2011)), and the topographical orientation of the coastline; however several distinct sedimentary environments exist surrounding the island complex. These sub-environments are; frontal beaches and dunes, the tidal deltas, lagoonal channels and associated terraces, the intertidal flats and the vast Sabkha

regions, and study of these modern sediments is important as they are highly analogous to the soft rocks found at depth (Alsharhan & Kendall, 2011). The topographical extent of these sub-environments can be seen in Figure 3.4.

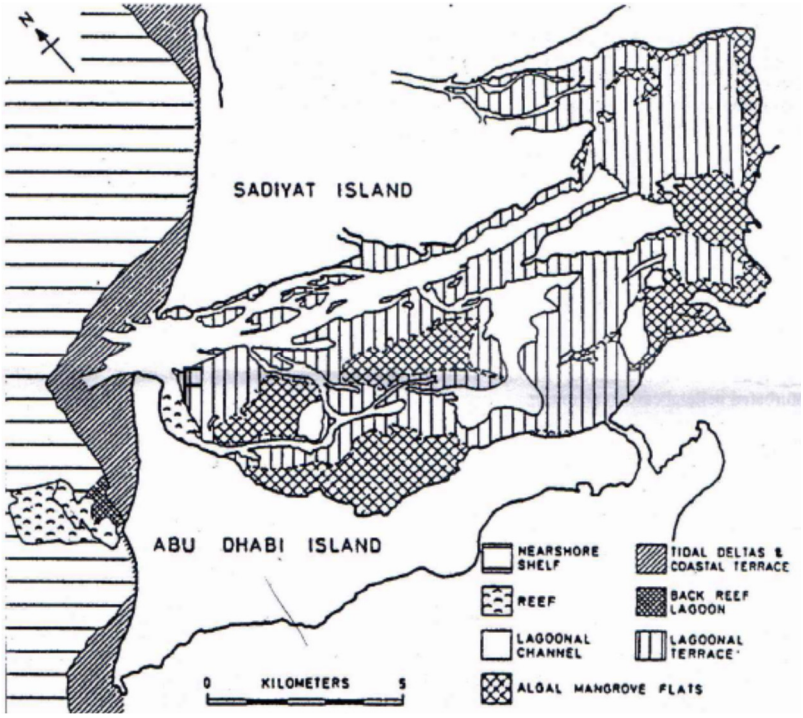

Figure 3.4: Sub-environments around the Abu Dhabi Island Barrier Complex (adapted from (Evans , et al., 1973) (Epps, 2010)).

Formed via the accretion of sediments around a core of Pleistocene calcareous sandstones (Miliolite Sandstone), the island itself has more recently been subject to the influence of rising sea levels (Evans, 2011). Prior to the heavy development seen today, the island's centre comprised of dunes of bioclastic and oolitic sand sized sediments along with frontal beaches made up of similar materials (along with more coarsely grained shell fragments) around the island's rim (Al Suwaidi, et al., 2011). Sea level is noted to have remained constant since the early Holocene allowing these sediments to extend / prograde seawards (Epps, 2010). Much of the modern day island is underlain by dredged engineering fill.

North and north-east of the island, the tidal delta is made up of fine to medium grained, uniformly graded sediments. These sediments include oolitic sands, skeletal debris, pellets and composite grains. This tidal delta is also noted to be prograding seaward (Epps, 2010); (Evans, 2011).

Behind the barrier island lie the lagoonal areas (or 'Khors'). These comprise of lagoonal channels and associated lagoon terraces. These lagoons form a large area of the

landward barrier complex. The lagoonal channels, whilst only making up only a small part of the lagoonal topographical area, may be deep and tend to contain a more mixed sedimentary composition. Sands with coarse gravel including clasts of Miliolite Sandstone are common, as are fragments of younger and poorly cemented soft rocks. At the landward side of the lagoons carbonate muds become more common along with cyanobacterial mats (and grains displaying varying degrees of micrite envelopes) and carbonate sands start to become increasingly common to the north. The lagoonal terraces cover the majority of the lagoon surface area and often contain bare rock at the surface. This rock may be in the form of exposures of Pleistocene Miliolite Sandstone or the very young submarine hardground, 'Caprock', which has been cemented in-situ and are underlain by soft sediments (Cook, 1997); (Epps, 2010); (Evans, 2011); (Kendall & Alsharhan, 2011); (Epps, 2011); (Kirkham, 2011).

These young 'Caprocks' are quite extensive, particularly around the Abu Dhabi island complex, and can cause a number of engineering problems. Often occurring as calcarenite, these Holocene well cemented soft rocks require robust approaches during piling and site investigation, only to give way to very soft materials directly underlying them. SPT 'n' values are noted to peak within this thin 'Caprock' layer before undergoing a significant deterioration within a relatively small increase in depth, even within the same lithological unit. This is thought to be due to the cementing mechanisms within the shallow rocks (<10mbgl) being primarily aragonite (with ρ_s of 2.94 Mg/m^3 and Moh's hardness of 3.5 to 4.0), whereas below this layer the cementing agent changes to predominantly magnesium rich calcite (having comparatively lower mineralogical strength properties, with ρ_s of 2.71 Mg/m^3 and only having hardness's of 3 on the Moh's scale). This gives a distinctive reversed strength profile with depth, as shown in Figure 3.5 (Cook, 1997); (Epps, 2010); (Evans, 2011); (Epps, 2011).

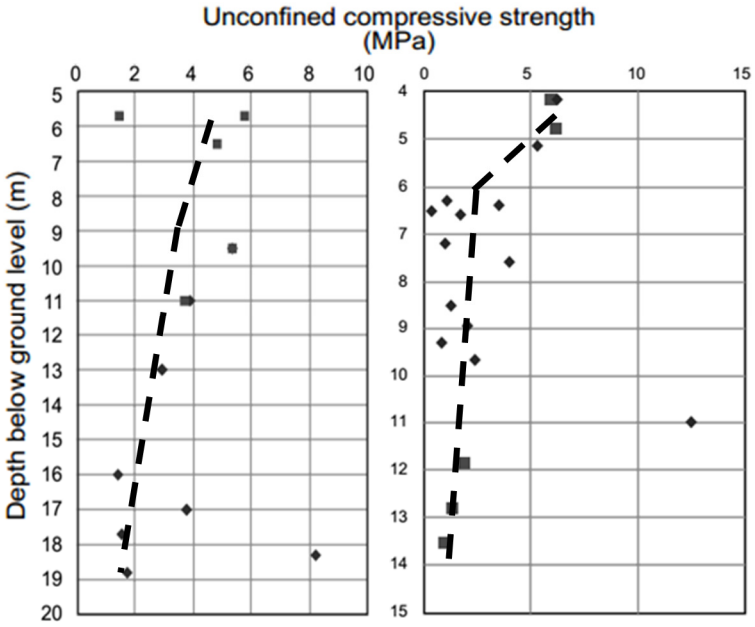

Figure 3.5: UCS strength decreasing with increasing depth through 'Caprock' layer, Abu Dhabi. Adapted from (Epps, 2011).

Adjacent to the lagoonal areas are intertidal flats. These areas are only intermittently submerged in seawater allowing for the growth of Blue Green Algae (cyanobacterial mats) and mangroves. In these areas amongst the carbonate sands and skeletal debris are finer carbonate muds (Epps, 2010); (Epps, 2011).

Finally Sabkhat are found on the most landward edges of the lagoonal areas. These Sabkhat are in the form of flat plains of salt encrusted sediments directly above the shallow water table, which by a process of capillary action and subsequent evaporation has led to the precipitation of salts including halite, gypsum and anhydride. Halite has been found to precipitate to depths of a metre within a Sabkha and gypsum layers and nodules are common at similar depths. Anhydrite is thought to form both from the dehydration of gypsum and from direct precipitation from the saline groundwater (Epps, 2010); (Evans, 2011); (Alsharhan & Kendall, 2011); (Kirkham, 2011).

These sub-environment areas can be seen clearly in diagrammatic cross section, Figure 3.6.

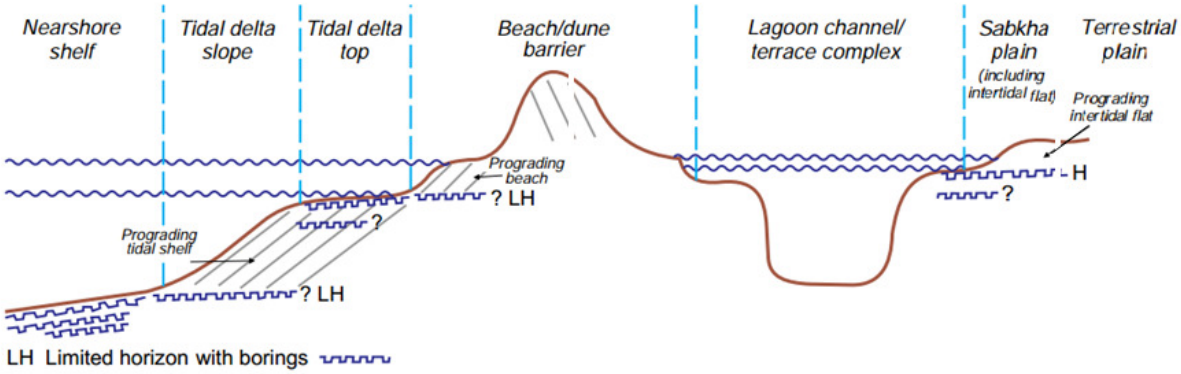

Figure 3.6: Cross section across Abu Dhabi island showing depositional sub-environments. Adapted from (Evans , et al., 1973), (Epps, 2010) and (Epps, 2011).

Broadly speaking, the shallow near surface sediments of the Abu Dhabi coast fall into the following categories, depending upon their sub-environmental zonation: carbonate mud, carbonate silt and carbonate sand (including oolitic sands and bioclastics). Likewise, their deeper and relatively older cemented soft rock equivalents can be categorised as: carbonate/calcareous mudstone (calcilutite), carbonate/calcareous siltstone (calcisiltite) and carbonate/calcareous sandstone (calcarenite) (Fookes & Higginbottom, 1975); (Epps, 2011).

The two sites studied during this research are situated within close proximity to one another and borehole locations across the two areas fall within the presented modern day sub-environments.

3.3. SITE DESCRIPTIONS

Samples were provided by Fugro Middle East (FMF) on behalf of Buro Happold for testing within this research project. Samples arose from two site investigations in Abu Dhabi, namely the Yas-Mina Natural Gas Pipeline Project (located on the islands surrounding the north of Abu Dhabi Island) and the National Bank of Abu Dhabi (NBAD) Global Head Quarters Building (located on Al Maryah Island, formerly known as Sowwah Island). The two sites are close to one another, from a geological standpoint, and they are both underlain by similar superficial deposits (locally, made ground) and solid geology. The locations of the two sites in relation to one another are presented in Figure 3.7. Details of the two site investigations are briefly discussed in the following sub-chapters, although specific information pertaining to the mechanical behaviour of the soft rocks encountered are discussed more thoroughly in Chapters 6 and 7 with reference to the results of this research project's laboratory testing programme.

Figure 3.7: Site location plan for the Yas Mina and NBAD site investigations.

Taking suitably sized core samples of undisturbed soft rock is difficult in all but the most highly weathered mudstones and siltstones, as large grains / clasts or even fragments of the rock itself which have fractured during the drilling process can cause the material to be returned in a damaged or even totally disturbed state, even when using techniques such as open drive samplers or rotary drilling equipment (Holden & Yilmaz, 1988). Rotary drilling of weathered Keuper Marls, for example, rarely provides samples suitable for testing, even when cored in small runs using plastic core liners (Terzagi, et al., 1996). The means of recovery, storage and transportation of samples from the two sites is also discussed within the following sub-chapters.

3.3.1. *YAS-MINA NATURAL GAS PIPELINE PROJECT*

This site investigation was undertaken to assess ground conditions for a proposed gas pipeline. The path of this pipeline is roughly east-west and spans much of Sadiyat Island. Work comprised eight boreholes (including three off-shore) to depths of 20mbgl, whose locations can be seen in Figure 3.8.

Figure 3.8: Borehole location plan of Yas Mina site investigation, Abu Dhabi. Aerial photograph taken from Google Earth

The boreholes undertaken during this investigation were distributed over a long, narrow stretch of land, and the nature of the paleogeography (comprising islands, lagoons and channels) resulted in a laterally discontinuously layered geology. Creating an absolute cross sectional representation of the geology along the entire path of the proposed pipeline is impossible with the information provided, however two cross sections have been produced depicting generalised ground conditions around the areas of BH-5 and BH-8 (Cross Section A-A') and BH-38 and BH-39 (Cross Section B-B'). These are presented as Figure 3.9. Generalised ground conditions encountered can be summarised as follows:

From ground level to 3.0-9.0mbgl a medium dense to dense, poorly graded silty SAND with occasional cemented layers is encountered, overlaying weak to very weak SANDSTONE / CALCARENITE layers to between 15.0-17.0mbgl. Below this a weak MUDSTONE, inter-bedded with gypsum, is encountered to 20.0mbgl where the boreholes terminated.

All on-land rotary boreholes were advanced using an ARDCO XV, whilst off-shore boreholes were carried out using a PILCON 3. Both methods used a mud flush and produced cores of approximately 76mm diameter (meaning that minimal re-shaping was required before triaxial testing was undertaken). Cores were generally carried out in run lengths of 2.50m, with total core recovery (TCR) of between 90-95% within beds where sub-samples were taken.

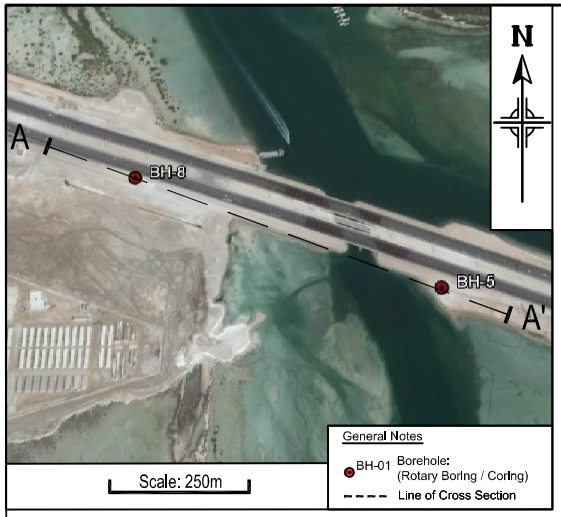

Key:

- Sand (Confirmed in Borehole)
- Calcarenite / Sandstone (Confirmed in Borehole)
- Calcareous Mudstone (Confirmed in Borehole)
- Gypsum (Confirmed in Borehole)
- Sand (Interpretative Extrapolation)
- Calcarenite / Sandstone (Interpretative Extrapolation)
- Calcareous Mudstone (Interpretative Extrapolation)
- Gypsum (Interpretative Extrapolation)

General Notes

- Inferred Strata Boundary
- Proven Strata Boundary
- Indicative Groundwater Level

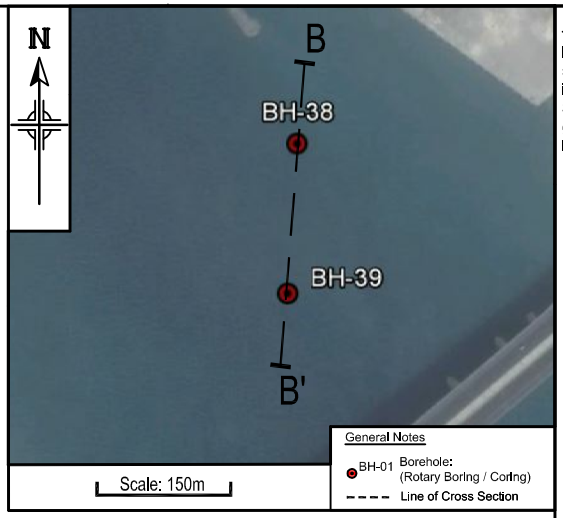

Indicative Only

29.3x Vertical Exaggeration

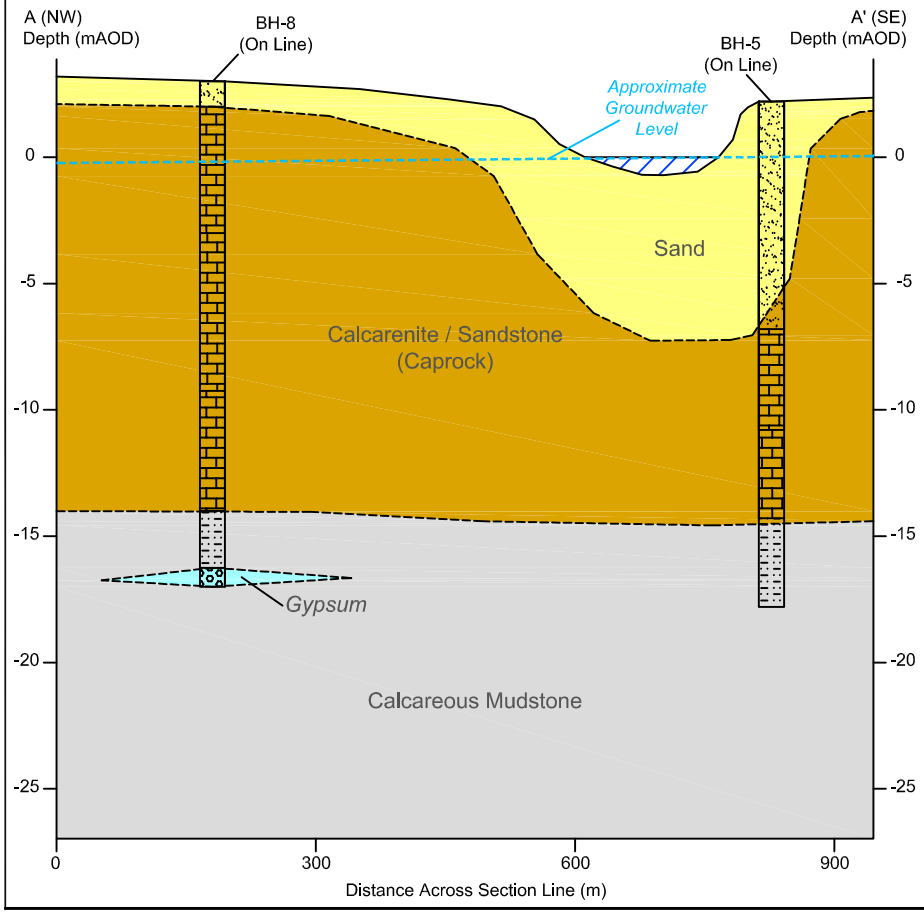

10.5x Vertical Exaggeration

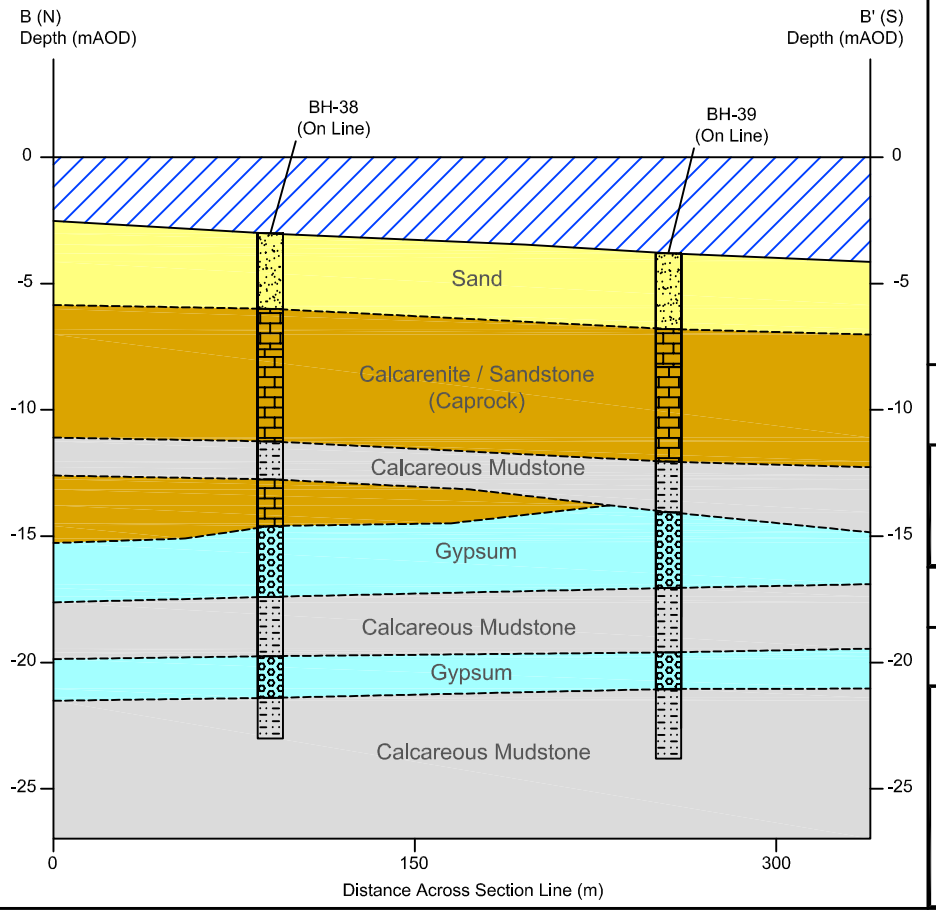

Notes

It should be noted that, whilst presented as separate strata within the NBAD ground investigation borehole logs, the Calcareous Sandstones and Calcarenites have been grouped together (as shown upon the Interpretative cross sections).

Site:
Yas Mina Natural Gas Pipeline Project

Title:
Interpretative Geological Cross Sections
Cross Section A - A'
&
Cross Section B - B'

Figure Number:
Figure 3.9

Scale:
As Shown

Newcastle University
School of Civil Engineering &Geosciences
School of Civil Engineering and Geosciences,
Newcastle University,
Newcastle,
NE1 7RU

Borehole coordinates are provided in Table 3.1 along with details of elevations and groundwater depths. Core sub-samples were recovered from all boreholes at a variety of depths in order to target several lithologies, however sub-samples of the lithology studied in this thesis (calcareous mudstone) were only recovered from five of the eight positions (namely BH-5,6,8,38 and 39). In addition to this, samples of groundwater were also recovered for chemical analysis.

Table 3.1: Summary of boreholes undertaken during the Yas Mina SI.

Borehole Number:	Universal Transverse Mercator (UTM) Coordinates:	Latitude and Longitude Coordinates:	Borehole Elevation (masl)	Total Boring Depth (mbgl)	Depth to Groundwater (mbgl)
BH-2	N 2712091 E 254101	24°30'11.22"N 54°34'23.97"E	3.0	20.0	2.65
BH-5	N 2714125 E 248633	24°31'14.13"N 54°31'8.56"E	2.0	20.0	3.70
BH-6	N 2714174 E 248495	24°31'15.64"N 54°31'3.63"E	1.0	20.0	3.50
BH-8	N 2714351 E 248052	24°31'21.14"N 54°30'47.79"E	2.0	20.0	N.E.
BH-16	N 2717200 E 243307	24°32'50.87"N 54°27'57.47"E	1.0	20.0	N.E.
BH-19	N 2717315 E 242193	24°32'53.94"N 54°27'17.82"E	2.0	20.0	N.E
BH-38 (offshore)	N 2714941 E 236973	24°31'33.67"N 54°24'14.04"E	0.0	20.0	3.00 (A.S.B.L)
BH-39 (offshore)	N 2714776 E 236845	24°31'28.23"N 54°24'9.61"E	0.0	20.0	3.80 (A.S.B.L)

Samples were wrapped in layers of plastic film, tin-foil and sack cloth before being sealed with a hard setting wax. Cores were also labelled with depth, borehole number, site name and finally wrapped in more layers of plastic film to retain in-situ moisture contents (Figure 3.10 a). All 14 cores from the Yas-Mina site were then packed into a vertical standing core box along with the samples of bottled natural groundwater and held firmly in place with Styrofoam and cuts of corrugated cardboard (Figure 3.10 b).

a) b)

Figure 3.10: Example of a) sample packaging and b) upright standing corebox.

3.3.2. *NATIONAL BANK OF ABU DHABI GLOBAL HQ*

This site investigation was carried out in order to assess ground conditions and establish a geological profile in preparation for the proposed development; the National Bank of Abu Dhabi, a 170m high super structure complete with a 28m deep, 8 level basement. The site is located on Al Maryah Island which is connected to Abu Dhabi Island (and Reem Island) by bridges (Fugro Middle East, 2013).

The scope of work comprised five boreholes, four of which were drilled to 60mbgl and one (BH-05) to 80mbgl. In addition to this three shallow trial pits were excavated. Core sub-samples were recovered for specialist testing at Newcastle University from the five boreholes at a variety of depths. All boreholes were located within close proximity to one another, as shown in Figure 3.11 (although it should be noted that engineering logs for BH-05 were not available for review in conjunction with this thesis).

Figure 3.11: Borehole location plan of NBAD site investigation, Abu Dhabi. Aerial photograph taken from Google Earth.

Two cross sections (Cross Section C-C' and Cross Section D-D') have been produced depicting generalised ground conditions beneath the site. These are presented as Figure 3.12. Ground conditions are broadly described within this site investigation as being 9-11m thickness of medium dense, silty, gravelly, fine to medium siliceous carbonate SAND overlaying approximately 10m of extremely weak to very weak SANDSTONE / CALCARENITE. The deepest layer encountered is described as an extremely weak to very weak SILTSTONE interbedded with gypsum and mudstone, which continues to the full depth of the exploration holes (60-80mbgl) (Fugro Middle East, 2013).

Key:

Vertical Exaggeration: x 1.75

- Sand (Confirmed in Borehole)
- Calcarenite (Confirmed in Borehole)
- Calcareous Siltstone (Confirmed in Borehole)
- Calcareous Mudstone (Confirmed in Borehole)
- Gypsum (Confirmed in Borehole)
- Groundwater Level (Confirmed in Borehole)
- Sand (Interpretative Extrapolation)
- Calcarenite (Interpretative Extrapolation)
- Calcareous Siltstone (Interpretative Extrapolation)
- Calcareous Mudstone (Interpretative Extrapolation)
- Gypsum (Interpretative Extrapolation)

General Notes

- Inferred Strata Boundary
- Proven Strata Boundary
- Indicative Groundwater Level

Indicative Only

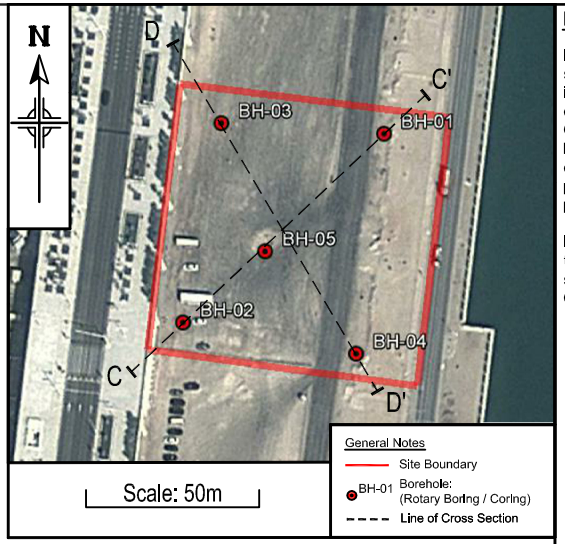

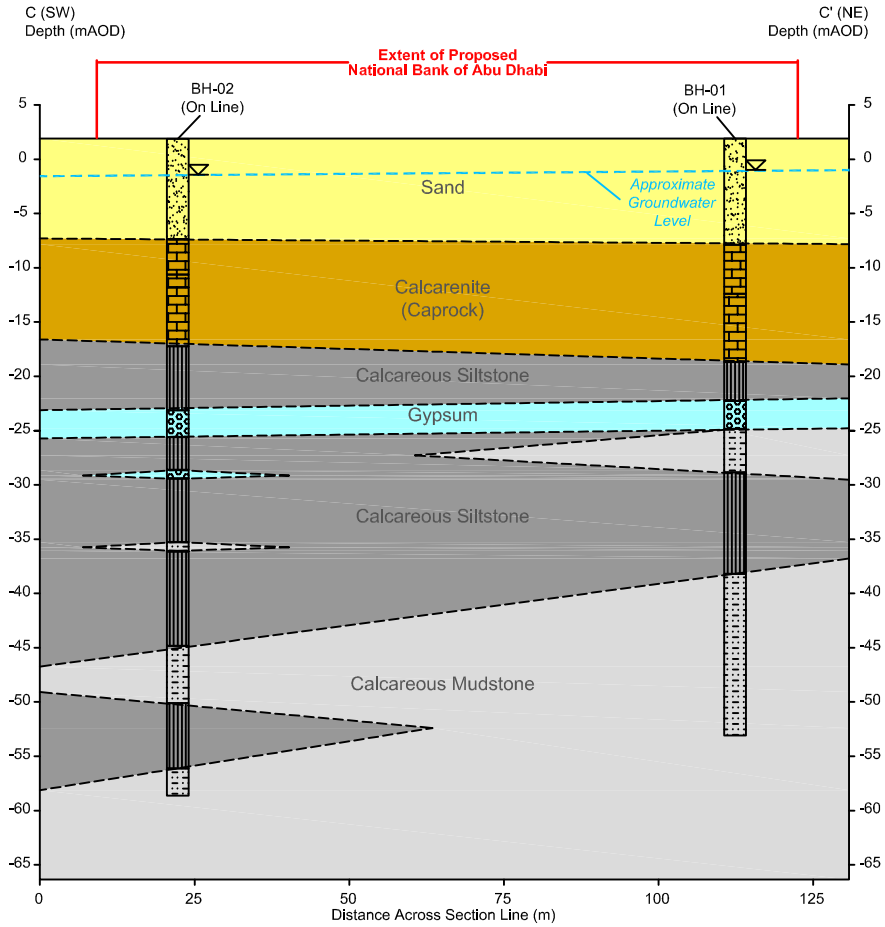

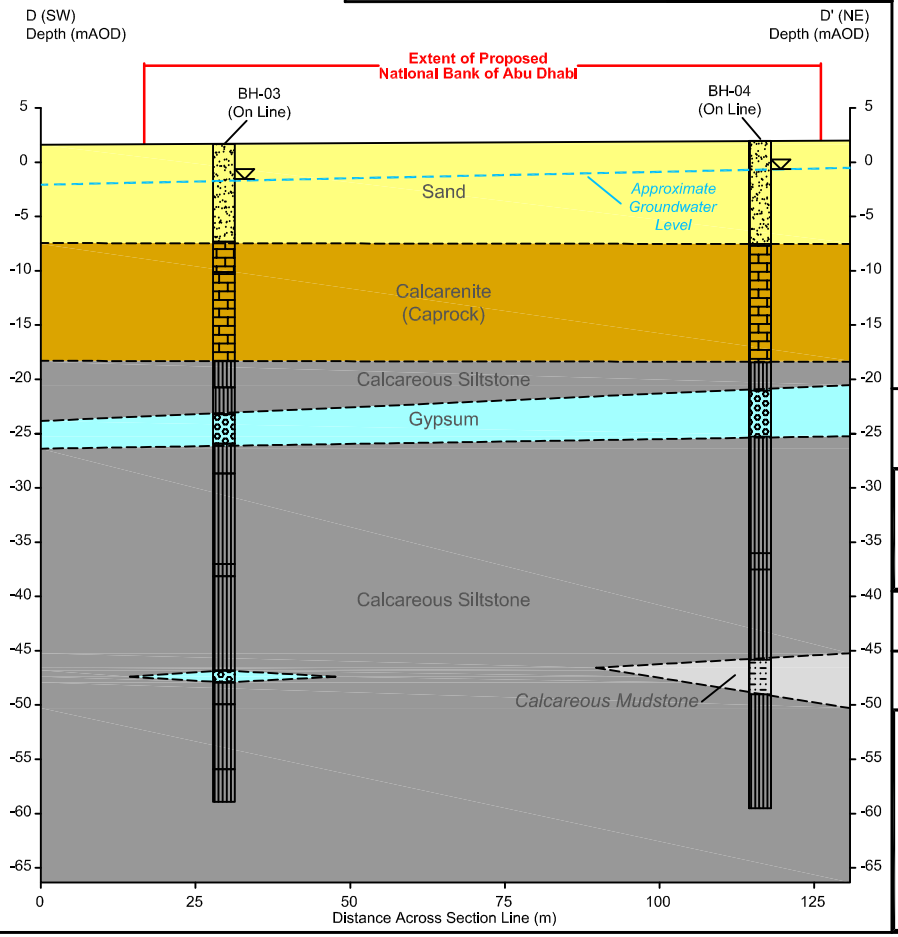

Notes

It should be noted that, whilst presented as separate strata within the NBAD ground investigation borehole logs and interpretative cross sections, the Calcareous Siltstones and Calcareous Mudstones have subsequently been shown (within this thesis) to be of comparable characteristic and mechanical properties to one-another, and to comprise predominantly clay sized particles.

Instances of Calcareous Siltstone noted within the NBAD site investigation / cross sections should therefore be interpreted as being Calcareous Mudstone.

Site:
National Bank of Abu Dhabi (NBAD)

Title:
Interpretative Geological Cross Sections
Cross Section C - C'
&
Cross Section D - D'

Figure Number:
Figure 3.12

Scale:
As Shown

Newcastle University
School of Civil Engineering &Geosciences
School of Civil Engineering and Geosciences,
Newcastle University,
Newcastle,
NE1 7RU

It should be noted at this point that material logged as SILTSTONE in the NBAD site investigation is superficially (and mechanically and characteristically) similar to that of the MUDSTONE layers noted in the Yas-Mina investigation. Indeed particle size distribution tests and plasticity indices (discussed in later chapters) confirm their comparable nature. It is often the case in site investigation that a similar material logged by different people will result in slight variations in descriptions. For the purpose of clarity, the material referred to as MUDSTONE in the Yas-Mina site and the SILTSTONE in the NBAD site will now only be referred to as calcareous mudstone, as this description best describes the material of interest during this thesis.

Boreholes were located at the coordinates provided in Table 3.2.

Table 3.2: Summary of borehole coordinates in both UTM and Latitude and Longitude (NBAD site).

Borehole Number:	Universal Transverse Mercator (UTM) Coordinates:	Latitude and Longitude Coordinates:	Borehole Elevation (masl)	Total Boring Depth (mbgl)	Depth to Groundwater (mbgl)
BH-01	N 2712259.7 E 235754.4	24°30'5.84"N 54°23'32.58"E	1.90	60.00	2.90
BH-02	N 2712198.8 E 235686.9	24°30'3.82"N 54°23'30.22"E	1.88	60.50	3.30
BH-03	N 2712264.4 E 235700.5	24°30'5.95"N 54°23'30.66"E	1.66	51.60	3.20
BH-04	N 2712187.5 E 235743.9	24°30'3.48"N 54°23'32.25"E	1.97	61.50	2.60
BH-05	N 2712221.8 E 235714.2	24°30'4.58"N 54°23'31.18"E	1.85	80.15	3.40

All rotary core boreholes were advanced using a double tube PQ rotary core barrel which produced cores of 83mm diameter (meaning that they require re-cutting to 70mm diameter before being tested within triaxial equipment). Cores were carried out in runs of 1.5m in order to maximise recovery. Water flush was used during the advancement of the boreholes; however its pressure was regulated carefully in order to prioritise good recovery rates. Where necessary, flush was switched to a solution containing a natural starch polymer (guargum) when recovery rates dropped too low (Fugro Middle East, 2013).

In the case of the NBAD site, samples were wrapped in plastic film, tin-foil then placed inside cardboard tube sections with ends sealed with hard setting wax. Cores were then laid horizontally in 2 large metal containers which themselves were filled with polystyrene foam and polystyrene blocks, as seen in Figure 3.13.

Figure 3.13: Sample core packaging and storage from NBAD site investigation as received by Newcastle University.

Unfortunately due to the way in which the cores were sealed and transported, several samples were noted to have split at the joining point between the rigid cardboard tube sections. In addition, several cores from the NBAD site were found to be dry and desiccated at the time of testing due to inadequate sealing techniques and could not be used for mechanical testing. Due to this, samples would be opened and inspected immediately prior to the commencement of testing, and if samples were noted to be visibly cracked or dry to touch would be set aside and used only for characterisation tests that do not rely upon in-situ conditions having been retained.

3.4. CHAPTER SUMMARY

The geology of the area around Abu Dhabi Island is highly variable both laterally and vertically due to the dynamic past and present sedimentary environment. Water salinity is high and average water depth low, producing a system capable of precipitating carbonates and evaporites rapidly within a short geological timescale. This area is being heavily developed with ambitious architectural projects, and yet serious engineering concerns ranging from corrosive and aggressive groundwater, ground dissolution / subsidence and piling through 'Caprock' continue to complicate design (Epps, 2011).

It is noted from a thorough review of literature that little information is published regarding the mechanical behaviour of these coastal deposits. What little data there is arises from a small number of published site investigation reports; however results originate from routine laboratory tests such as UCS testing or else in-situ tests such as SPT's. Specialist testing, for example advanced triaxial testing, has not been carried out within these few published works.

The calcareous mudstone being studied was likely to have been formed in a low energy, hyper saline environment such as the lagoonal terraces. Significant thicknesses of this material are noted in all borehole positions, often inter-bedded with gypsum.

Gypsum and evaporite dissolution in the ground under new buildings (brought about partially by anthropogenic activities including ground-source heating and cooling creating groundwater flow) is a major problem in this part of the world. Whilst no gypsum cores were provided for testing during this project, it seems likely that these young soft rocks will contain a percentage of evaporite minerals within their granular / cement structure that may be susceptible to dissolution over time.

As triaxial tests are typically carried out on fully saturated samples using de-aired water it is important that the minerals making up the samples do not deteriorate as the tests progress as this would skew results and mask the true material behaviour. This dissolution problem is compounded by the fact that advanced triaxial tests often take place over the course of weeks, prolonging the exposure of samples to water.

In order to combat this problem, the sensitivity of these soft rock lithologies to water ingress must first be assessed and the type, quantity and positioning of the dissolvable minerals (as well as non-soluble minerals) within the soft rock structure be understood.

A testing programme including the use of XRD and SEM along with standard soil and rock characterisation tests is carried out in later chapters in order to better understand the degree to which dissolution may be occurring as well as to gain insight into the mineralogy of these soft rocks and their cementing agents.

CHAPTER 4. DEVELOPMENT OF METHOD

4.1. CHAPTER 4 INTRODUCTION

The previous chapters identified a gap in research with regard to soft calcareous mudstone's mechanical behaviour. The strength and stiffness of soft rocks was shown to be influenced by a wide array of factors including confining pressure, mineralogy, degree of saturation, the presence of structure and rate of strain. The wider geological setting of Abu Dhabi was also examined in order to provide context for the project.

This chapter focuses upon the development of advanced triaxial and associated testing methods. Problems such as bedding errors, top-cap tilting and human error needed to be assessed and where practical minimised. Working with a small and variable sample size means that tests must be efficient to ensure the maximum amount of data is drawn from the small amount of available material.

The adaptations to both standard testing apparatus and methods of testing are described and justified based on observations made whilst reviewing published literature, along with the results of several experimental trials. In addition to this, non-standard tests (such as DIC of Brazilian tensile tests) are described.

4.2. LIMITATIONS OF TRADITIONAL TRIAXIAL APPARATUS

The triaxial test in soil mechanics is one of the most important tests available and it has developed over the years into a complex and highly accurate means of assessing a soil's engineering properties and behaviour. By adjusting deviatoric stresses and cell pressures, the triaxial apparatus is able to mimic almost any number of realistic in-situ conditions, causing this piece of equipment to be praised on its ability to provide meaningful and largely representative results (Chiu, et al., 1983).

During traditional triaxial testing of soils at large strains, minor errors such as apparatus compliance, strain of porous disks, added stiffness of filter paper drains and end platen compressibility can be all but ignored, however in the analysis of small strain stiffness these problems become much more pronounced, contributing to large discrepancies between in-situ and laboratory behaviour within this range (Clayton & Khatrush, 1986). Care must be taken during all stages of triaxial testing (saturation, consolidation and

shearing) when assessing the small strain behaviour of soils, for example: sample preparation, chemistry of the pore-fluid, method of saturation, sample-loading ram docking procedure, consolidation method, rates of applied stress or strain, stress path direction and local strain measuring equipment / methods of affixing said equipment must all be considered.

Advancements over the years in the way in which local strains, pore pressures and loads are measured have increased the accuracy of the triaxial test, as have advances in sample preparation and data collection / processing techniques. In soil mechanics the triaxial test may be considered a vital engineering tool with adaptations and augmentations available for almost any conceivable test on either cohesive or non-cohesive soils.

Unfortunately the same cannot be said of its application to rock testing and this statement is especially true where soft rocks are concerned (Chiu, et al., 1983). Testing of rocks in the laboratory often makes use of simple index-tests such as the UCS or the Point-Load which are then linked to real-life performance using highly empirical means. Where more advanced tests are used, such as the triaxial test, little guidance is given on how best to test different lithologies or different strength materials.

The setup of the cell itself, for example, needs to be different for rock testing than it is for soil testing as the pressures and loads required are often significantly higher. Apparatus compliance becomes more pronounced both in the metal elements of the triaxial machine and the interconnecting fluid lines as the stresses involved increase and this can mask true results if not allowed for or avoided (Chiu, et al., 1983). In order to produce the higher radial cell pressures, oil is employed instead of water and the cell itself must be of a thick metal build instead of the plastic and Perspex used in soils testing.

Equipment designed specifically for advanced soft rock testing is scarce. Compounding this problem is the fact that soft rocks are, by their very nature, difficult to recover, prepare and test (Dobereiner & Freitas, 1986).

In addition to this, calcareous soft rocks carry with them their own set of challenges. For example, they have highly variable strength and stiffness properties both inter- and intra-lithology, may contain large void ratios (including large surface voids) and are often highly sensitive to exposure to air and water in unconfined conditions. Several industry standard procedures cannot be used during their examination, such as using

standard temperature oven drying (due to the presence of minerals containing molecular water), and the adoption of local strain gauges raises issues related to the means of affixing gauges to samples without causing unwanted stress concentrations or localised damage to cores. An example of this is in the use of electrical resistance strain gauges, which in hard rock testing in unconfined conditions are adhered to the sides of the sample itself, but when adhered to soft calcareous rock samples, cannot obtain adequate purchase due to the loose, often grainy, friable surfaces to which they must be affixed (Kim, et al., 1994), a problem that increases as the samples begin to dry.

Results from the testing of Glacial Till are briefly presented within this chapter as they were used as a proxy for soft rocks within the early stages of experimentation, from which much was learnt about the practicalities of adopting local strain gauges and measuring small strain stiffness without risk of causing damage to the samples of soft rock available.

4.2.1. *CUTTING AND SHAPING*

Correct preparation of samples for use in triaxial testing is one of the most important steps to ensure results are accurate. This is well known in rock testing, however is equally important in soil and soft rock testing, especially when small strain stiffnesses are being assessed. Great care should be taken to ensure that sample ends are flat and parallel as this will reduce, although not totally remove, the likelihood of bedding errors developing.

Bedding errors are a common problem in the small strain triaxial testing of geomaterials. In routine testing it is generally assumed that the top and bottom testing platens are totally smooth and parallel to the top and bottom of the sample being tested (Bromhead & Patel, 2000), in reality however this is not the case and imperfections can cause the top and bottom of the soil sample to crush and flatten in response to the movement of the loading ram, resulting in bedding errors. These can develop for two reasons:

1. Difficulty in trimming the sample end faces to be parallel with the testing apparatus causing an angular contact between sample and loading ram (potentially allowing rotational strains at the sample ends during shearing), and:
2. Surface imperfections or irregularities of the sample top and bottom due to a loose granular surface (in sands and sandstones) or prominent coarse grains set

within a finer matrix (for example with glacial clays and other heterogeneous materials).

These situations are displayed diagrammatically as Figure 4.1.

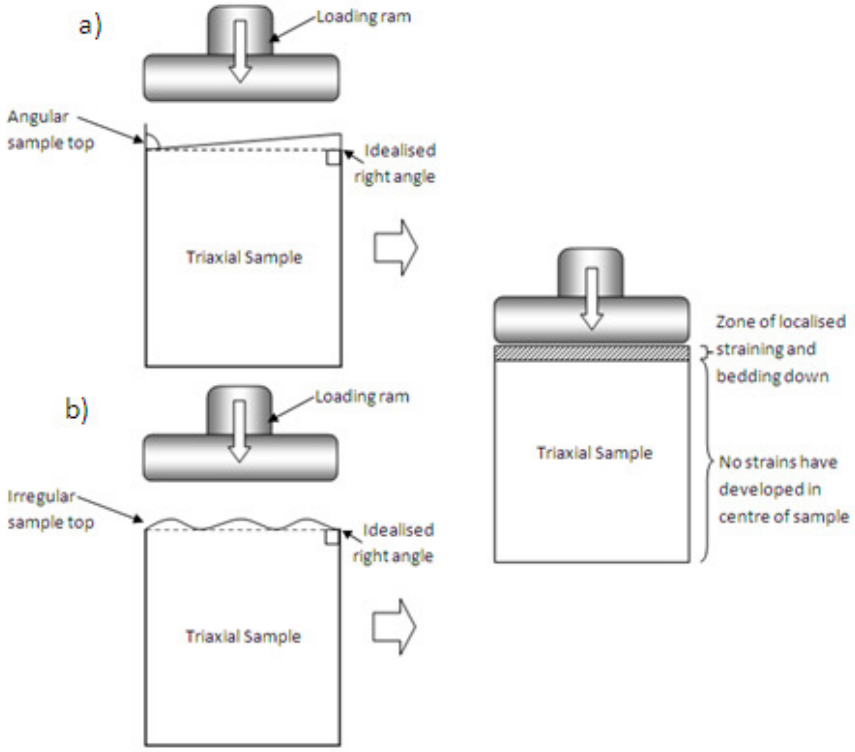

Figure 4.1: Development of bedding errors as a result of; a) angular sample top, and; b) irregular or loose granular sample top.

This initial soil movement in response to loading is not a true strain, but a localised rearranging of grains or a crushing of loose particles. Ultimately, the top and bottom of the sample appear to strain before the sample has truly taken the full intended load, resulting in lower estimations of stiffness and high estimates of strain if the full sample behaviour is taken into account. In the context of small strain stiffness behaviour this phenomenon may have devastating results on the recorded data. This behaviour is also (and especially) true in the testing of soft rocks. Kim et al, (1994) state that externally measured strains taken during the triaxial testing of soft rocks are almost totally unreliable and that the effect of bedding errors increases in severity as the stiffness of the material increases (Ismail, et al., 2001).

The first step in addressing the problem of bedding errors regardless of the type of test is to ensure that all samples are cut and shaped correctly. This can be carried out manually in soils testing, however as the stiffness of the materials increase so does the accuracy required in the cutting and shaping of sample ends.

Several authors have suggested the use of gypsum end-capping in order to provide as flat a contact between the samples of soft rock and the testing platens as possible (Barla, et al., 2000) (Silvestri & d'Onofrio, 2000). This method is attractive as it can be used on uneven or irregular core shapes. Unfortunately, the stiffness of the gypsum end caps are very similar to the soft rock samples themselves and as pore water pressures are to be measured and controlled (and permeabilities estimated) this method was not considered appropriate for use during this research.

This problem can be counteracted to some degree if k_0 consolidation is being carried out, as the bedding errors take place during the anisotropic consolidation following the application of axial stress rather than during shearing. Likewise a cyclic axial load may be applied within the elastic range of the sample to eliminate this bedding problem, however this process can affect subsequent results as well as being very difficult to achieve in practice (due to both inter-sample variability and the restrains of conventional apparatus) and so is undesirable (Ismail, et al., 2001). Also these methods do not aid isotropically consolidated static tests which form the bulk of the testing in this report and indeed the majority of testing in industrial practice.

Instead, the issue of bedding errors would be overcome by using local strain gauges with sample cores cut to approximately 5% greater than their required 140mm length by a clipper saw, then carefully ground flat and parallel by a surface grinder without using oils or water lubrication. This method provides cores cut to a degree of parallelism to within 0.1 degrees or better.

In the case of samples from the Yas Mina site, this could be achieved by simply removing a ridge of cheesecloth wrapping fabric and wax adjacent to the area required for preparation, then cutting and grinding in such a manner as to cause minimal disturbance whilst maintaining the natural water contents.

Samples cores sent from the NBAD site investigation, however, were found to have too great a diameter for use within Newcastle Universities advanced triaxial apparatus without first being manually cut with a soil laithe. Any off cuts would be used to preform moisture content, classification and /or optical analysis testing.

4.2.2. *PREVENTING UNWANTED LEAKAGE AND PUNCTURES*

Cell pressures and pore pressures are separated via a rubber membrane in all standard triaxial apparatus. The unwanted development of a water pathway between the cell

pressures and internal porewater pressures during a test, for example due to an ineffective seal or a puncture, is time consuming to rectify. Should this occur, the whole cell must be drained and deconstructed followed by the removal of all local strain gauges and their subsequent reattachment and calibration on a new membrane. Given that a single test may take up to several weeks to complete, an unscheduled dismantling of all apparatus is clearly best avoided. In the worst case scenario, such as during the testing of sensitive materials prone to deteriorate on unconfined contact with water (such as calcareous mudstone), a leak resulting in a sudden drop in effective stress may irreversibly damage a sample.

The most common cause of a membrane puncture is during the triaxial testing of samples with a high surface porosity. As the membrane is forced into any surface voids due to differential pressures between the cell and the internal water pressure, the membrane will be locally stretched thin and deformed. This localised stretching is apparent at low effective stresses, however becomes increasingly problematic as effective stress rises (Figure 4.2 a) and worse still during shearing (Figure 4.2 b).

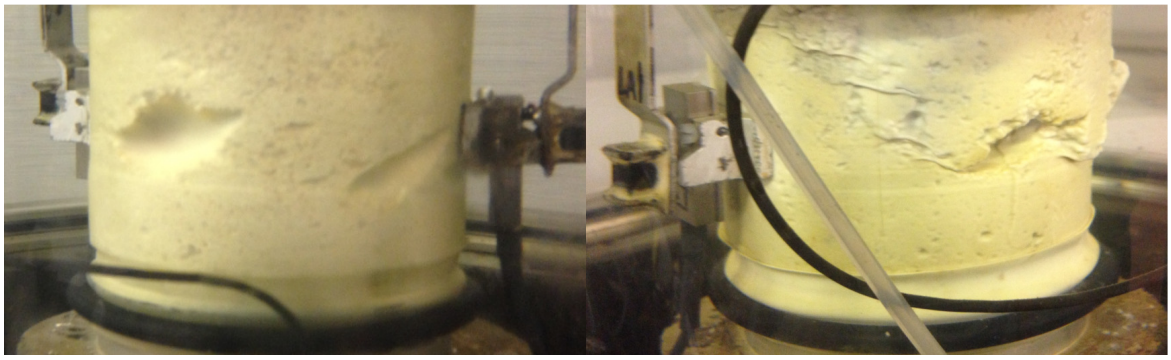

a) b)

Figure 4.2: An example of localised membrane stretching and deformation

An effective solution to this problem is to fill the surface voids. When choosing the 'filling' material it is important not to increase (or reduce) the overall stiffness of the sample, and therefore materials such as Portland cement are not a viable option. It is important not to use impermeable materials as this could alter the way in which excess pore pressures dissipate. Ideally a filler as close to the properties of the sample being tested should be used. Offcuts of the sample itself are ideal and due to the re-mouldable nature of calcareous mudstones, this was the proposed solution whenever this situation was encountered. This filler material was used during tests employing Bender Elements to infill the 'trench' that houses the element and ensures a close contact is achieved.

The next most common cause of a leak forming (other than the pre-existence of an imperfection within a rubber membrane) is an inadequate seal between the membrane and the upper and lower testing platens. This is especially true when testing at high rates of strain or when carrying out extensional tests at low effective stress.

During the testing of glacial tills it was found that the use of three rubber O-rings at both the top and bottom of the sample prevented leaks. As such this simple but effective solution has been incorporated into the testing of soft rocks as demonstrated in Figure 4.3 in steps a) though f).

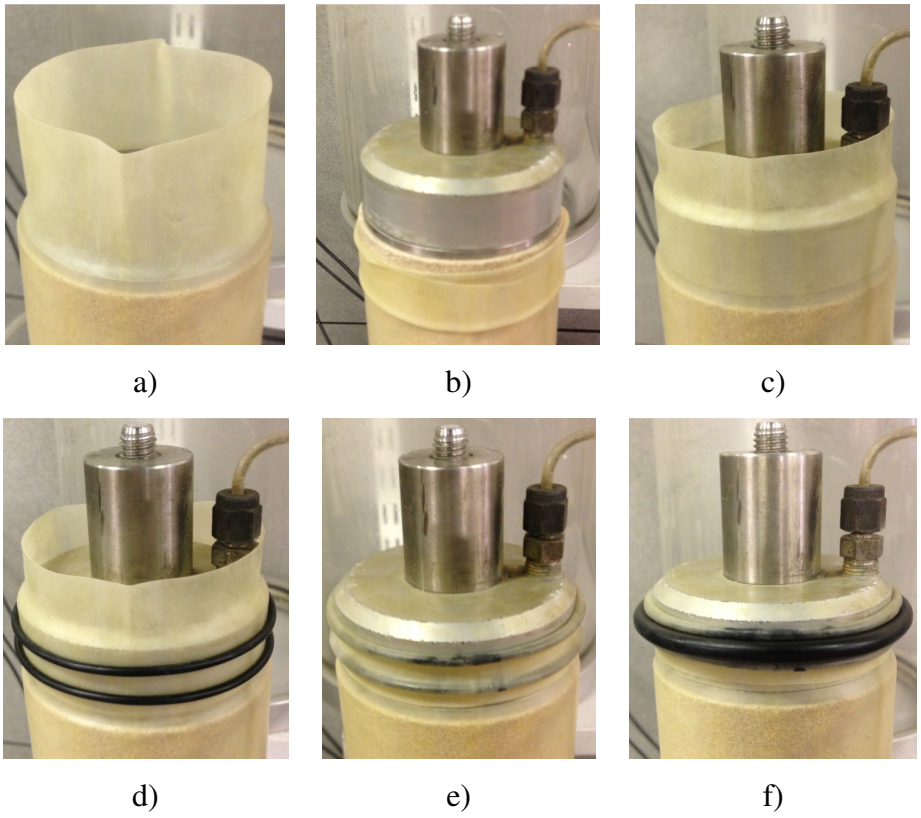

Figure 4.3: Three rubber O-ring membrane sealing method.

4.3. SELECTION OF LOCAL INSTRUMENTATION

One of the most significant advances in the laboratory testing of geomaterials over the last couple of decades has been the development of the local strain gauge (Burland & Symes, 1982); (Clayton & Khatrush, 1986); (Heymann, 1998); (Atkinson, 2000); (Lehane, 2000); (Heymann, et al., 2005). Local strain gauges focus the measurement of displacements to the central third of a triaxial or uniaxial sample (as seen in Figure 4.4), thus avoiding inaccuracies inherent in bedding down of sample ends and those caused by apparatus compliance.

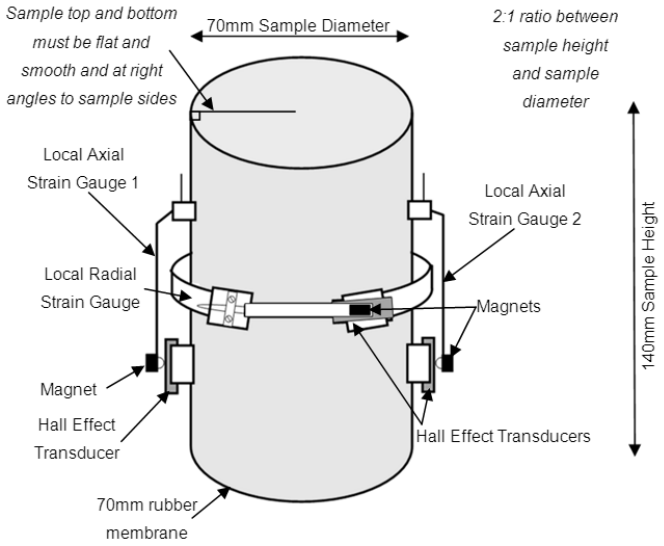

Figure 4.4: Typical layout of local hall effect strain gauges mounted on a triaxial specimen.

Strains measured from gauges fixed to the sample surface are expected to be comparatively lower for a given stress than those measured externally from outside the triaxial apparatus (Burland, 1989), as seen in Figure 4.5 and in practice during the testing of glacial tills in Figure 4.6.

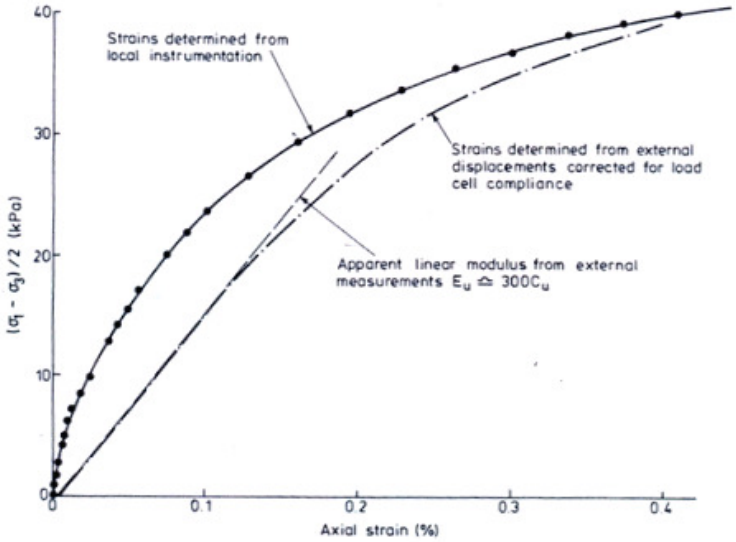

Figure 4.5: Graph showing deviatoric stress verses axial strain, highlighting differences between strain measured externally and locally (taken from (Burland, 1989)).

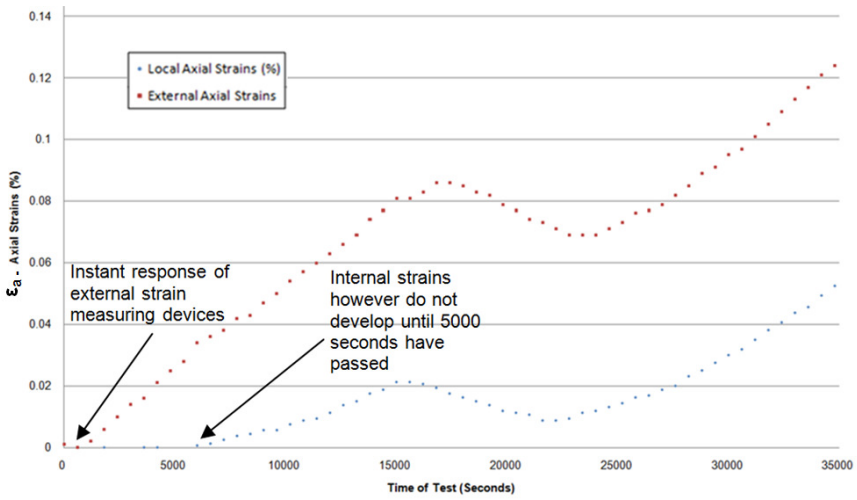

Figure 4.6: Disparity between external and internal measurements of strain at small strains (Simpson, 2010).

Jardine et al, (1984) highlighted the need for a simple and repeatable test for the accurate measurement of stiffness, particularly at small strains and since then a number of solutions have been devised (Heymann, et al., 2005).

Several common direct methods can be employed to measure small strains of soft rocks in a laboratory environment:

1. **Local Displacement Transducers**. Many variants of local displacement transducers exist including electro-level gauges and Hall Effect gauges. Both types of local strain gauges are noted to be highly accurate (with resolutions to <1μm and accuracies of ±2 and 6μm) and capable of measuring the strain behaviour of materials within the small strain range through to the large strain range, thus producing a full non-linear stiffness profile for any sample tested. They are also able to be used in triaxial testing apparatus, but are difficult to attach to the sample surface accurately, and because they measure displacements and not actual strains an element of human error is introduced when measuring the original gauge length by hand prior to testing (Jardine, et al., 1984); (Clayton & Khatrush, 1986); (Heymann, et al., 2005). Hall effect transducers have been used extensively by the author during the testing of Glacial Tills and are noted to be quite reliable, although lack the accuracy of some of the other methods within the very small strain range.
2. **Linear Variable Differential Transformer (LVDTs)**. LVDT's have a longer measuring range than Hall Effect / electro-level strain gauges, and are therefore more suitable to measuring large strains as well as small strains. Their accuracy is also higher than local displacement transducers, however, in order to use them

within triaxial apparatus a nonconductive cell fluid must be used in place of water (Goto, et al., 1991); (Heymann, et al., 2005); (Berre, 2010). LVDT's are often heavier too which is a problem with friable rocks where methods of firmly affixing gauges are limited.

3. **Electrical Resistance Strain Gauges.** This apparatus directly measures strain in the orientation of the long axis. In the testing of hard rocks, these gauges are adhered to the sample in a number of configurations, however, in soft rock testing the friable nature of the rocks may disallow the use of such equipment as they may become dislodged from the sample surface during shearing.
4. **Circumferential Extensometers**. This method of measuring radial strains is usually used on hard rocks and concrete and works via a chain which wraps around the outside of a sample, measuring increase in chain length as sample expands diametrically (epsilontech, 2010). It is considered by many researchers to be the best method of measuring radial strains, as unlike all other methods, the whole circumference of the sample is taken into account as opposed to specific reference points. This device can operate at very high pressures and temperatures and a number of models are available depending upon purpose. Testing on soft rocks may however be more problematic due to the potential for disintegration causing loss of chain grip. Another problem is that only diametric expansion may be measured, meaning that this apparatus may not be used during tensional / extensional triaxial tests and must be paired with another method if axial strains are to be measured.
5. **DIC (Digital Image Correlation).** This method is a modified / more up to date version of that employed by Lehane (2000) during testing of Belfast Soft Clay. Lehane (2000), from Trinity College Durham made use of a videoextensometer to measure strains theoretically as low as 0.0008% within a triaxial environment, although Lehane (2000) reported resolutions being averagely 0.003%. This system, like the DIC, tracks high contrast dots and maps their relative movements which are drawn on to the sample membrane (or sprayed on, as with Newcastle University's DIC) and as such has the benefit that any dimensioned specimens may be used and also no maximum strains limits apply. Samples also undergo little to no disturbance whilst the 'gauges' are applied and the 'gauges' are light weight. Newcastle University's DIC system cannot be used in triaxial apparatus, however may be employed during unconfined testing procedures.

6. **X-ray and Optical Methods**. These have been used by various authors (Roscoe, et al., 1963); (Arthur & Phillips, 1975) and measure strains by tracking the displacement of reference points marked on the sample membrane or within the sample itself using sophisticated cameras, similar to DIC (although DIC is somewhat more recent in design).
7. **Laser Interferometry**. This method, based upon the Fabry-Perot principle, is used by Heymann et al, (2005) and is capable of displacement measurement accuracies of 0.005μm, twelve times more accurate at high resolutions than LVDT's. Downsides to this method, however, include the requirement to accurately measure light wavelengths, laser output stability, mirror tilt, Piezo-actuator drift and changes in the refraction index of the cell fluid making its use within triaxial apparatus difficult.

In-direct methods can also be employed to measure small strain stiffness / small strains of soft rocks in a laboratory environment:

1. **The Resonant Column Apparatus**. This technique, used by Richart et al (1970) involves applying periodic small strain increments on the sample, however it does not provide direct measurements of elemental behaviour of the soil being tested.
2. **Bender Element Testing**. This was used by, amongst other authors, Viggiani & Atkinson (1995) and Heymann (1998) for measuring the maximum shear modulus of a soil of known density by observing the velocity of shear waves through the material, usually in triaxial apparatus. This method has been noted to produce errors of up to 14%, however Atkinson (2000) states the accuracy of this method can be very high. Another advantage is that stiffness at zero strain can be measured, giving the material's maximum shear stiffness (G_0), a very important parameter for many numerical models. This method is becoming increasingly used in both academic and industrial applications (Viggiani & Atkinson, 1995); (Jovicic & Coop, 1996); (Karg & Haegeman, 2005); (Black, 2009); (Yamashita, et al., 2009); (Fonseca, et al., 2009); (Chan, 2010) (Camacho-Tauta, et al., 2012); (Rees, et al., 2013).

The following questions were devised prior to testing to ensure the selected method is able to produce results that are reliable, repeatable and realistic:

- Can the equipment be used within a triaxial cell, or is it better suited to UCS?
- Can the apparatus measure strains in extension as well as compression?
- Does the equipment provide measurements to a high enough degree of accuracy for small strain analysis?
- Can the apparatus be used in conjunction with other small strain measuring equipment such as radial gauges?
- Does the salinity or friability of the samples pose a problem in the use of this equipment?
- Are destructive preparation methods required to affix the gauges to specimens?

Only once these factors have been considered can suitable and 'fit for purpose' apparatus be selected. The finalised methods adopted for measuring the small strain stiffness of soft rocks within this project was a combination of Hall Effect gauges and (to a lesser extent) Bender Elements, as these best fulfilled the role required and fell within the realistic budget of this research project.

4.3.1. *LOCAL STRAIN GAUGE SETUP*

The Hall Effect gauges used (shown in Figure 4.7) are accurate to approximately 0.005% of a mm and have a full range of 10,000 mV, showing maximum noise levels of +/- 0.002mm displacements.

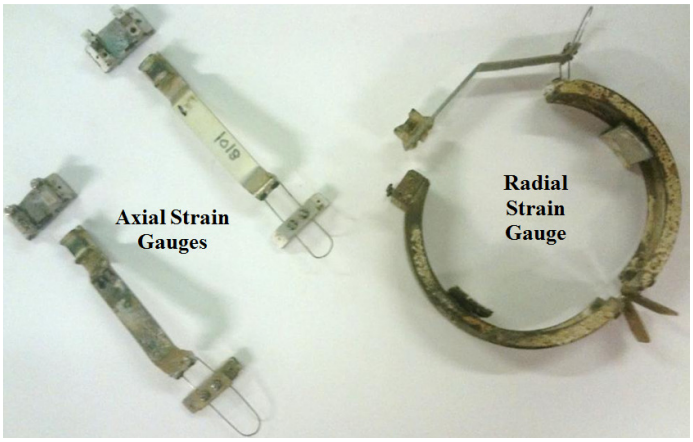

Figure 4.7: Two axial strain gauges and a radial strain gauge. Transducers are not shown in this photo.

These strain gauges were then adhered to triaxial samples in the following manner (Figure 4.8):

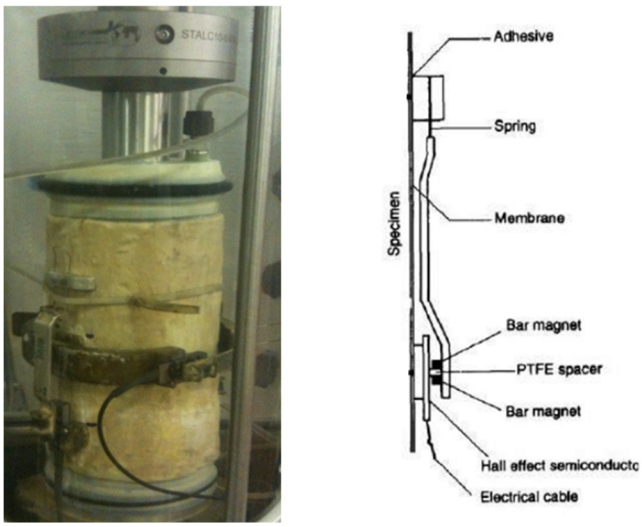

a) b)

Figure 4.8: a) photo showing Hall Effect gauges mounted on soft rock sample. b) diagram showing a single axial Hall Effect gauge mounted on a sample in cross section (adapted from (Bishop & Henkel, 1964)

In order to accurately calculate the development of strains using Hall Effect strain gauges, it is important to know the initial gauge length prior to shearing (L_0). This part of the setup requires a degree of care to eliminate human error.

L_0 is the original gauge length of the strain gauges prior to the shearing stage of the test. As small strain stiffness measurements using Hall Effect gauges rely upon accuracies of 0.005% strains it is vital that displacements are not mis-interpreted.

In order to ensure repeatability between tests the following methodology for measuring the L_0 of the axial and radial Hall Effect strain gauges was devised.

4.3.2. *LOCAL AXIAL STRAIN GAUGE L_0*

Before the strain gauges are adhered to the sample, the membrane is first marked up with permanent marker at the locations the gauges will occupy. This process is aided by a metal ruler marked up with guidelines to act as a template and ensure repeatability between tests (Figure 4.9).

Figure 4.9: Photo showing sample being marked prior to gauges being affixed.

This method provides a rough guide and reduces the sample preparation time, but using the approximate gauge lengths marked out on the ruler with no additional measurements would result in large inaccuracies. An inaccuracy as small as 1mm in L_0 can result in wildly different strain calculations throughout the entire test, especially if an average of both local gauges is to be used in calculations.

For example, a displacement of 0.02mm over a gauge length of 75mm L_0 will equate to a strain of 0.027%. However, if the gauge had been inaccurately measured to be 80mm the equivalent strain for the same displacement would be 0.025%. This difference may appear only minor, but in the context of small strain stiffness behaviour, inaccuracies such as this will dramatically alter the calculated shear strains and therefore ultimately the shear stiffness. If similar errors are also present in the radial strain gauge then the collected results may well be entirely meaningless unless compensated for.

Figure 4.10 shows the effect of miss-measuring L_0 by +/- 5mm using an example of Glacial Till. The figure highlights that these errors scarcely effect the measurement of stiffness and strains within the large strain range as all the data sets converge at approximately 0.2% shear strain. Within the lower end of the small strain range however, inaccuracies as large as +/- 15MPa shear stiffnesses are introduced:

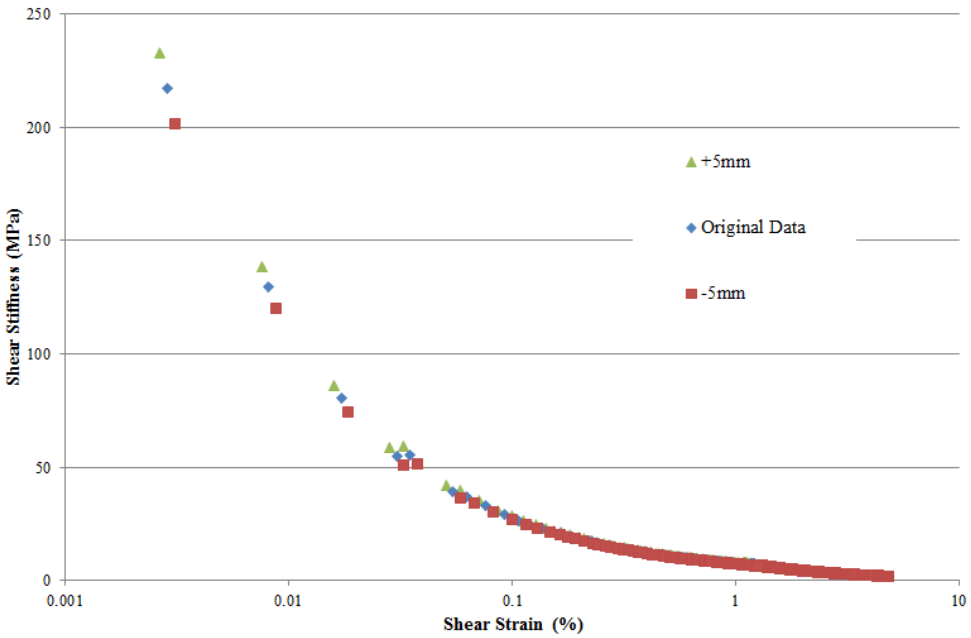

Figure 4.10: The effect on shear strains and shear stiffness of miss-measurement of local axial and radial L_0 on a sample of Glacial Till.

It is therefore important to accurately measure the exact L_0 of strain gauges prior to shearing and track the evolution of the respective gauge lengths through saturation, consolidation and docking.

During the testing of soils, local strain gauges may be pinned into the sample to ensure no 'play' occurs between the sample and the strain gauges during shearing. This allows L_0 to be easily measured as the distance between these pairs of pins (assuming they represent fixed points and strain development occurs between these fixed points), as shown in Figure 4.11.

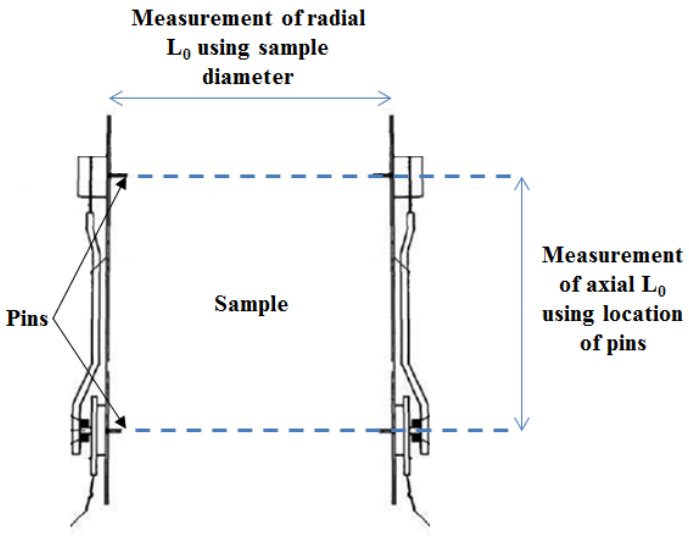

Figure 4.11: Measurement of L_0 when using pinning (adapted from (Bishop & Henkel, 1964))

Unfortunately pinning cannot be used on the soft rocks studied within this thesis. These materials are weak and friable and may even be locally ductile, and as such fixing gauges in place by piercing the membrane and then drilling the sample is not practical due to the generation of local stresses surrounding the pins, the creation of potential water flow pathways (and therefore local softening) and potential sample damage.

Jardine, *et al* (1985) compared the displacements measured via local strain gauges adhered only to the sample membrane against those from foil strain gauges adhered directly to the sample itself. This work showed that providing high cell pressures were used 'play' errors occurring between the two methods was negligible. In order to validate these claims, several tests were carried out on custom rubber samples comparing the simultaneous development of strains from both a 'pinned gauge' and a gauge adhered only to the sample membrane. Results showed that within the small strain range, both methods provided highly comparable stiffnesses and that 'play' only occurred when entering into large strains (3-4%).

However, this method does present the minor issue that; unlike the pinning method, there are no definitive fixed points from which to measure L_0.

An assumption is therefore made that the displacements measured via local axial strain gauges occur about the centre of the apparatus (as would be the case were the samples pinned), as shown in Figure 4.12. This gauge length is therefore measured accurately using digital callipers prior to testing and recorded.

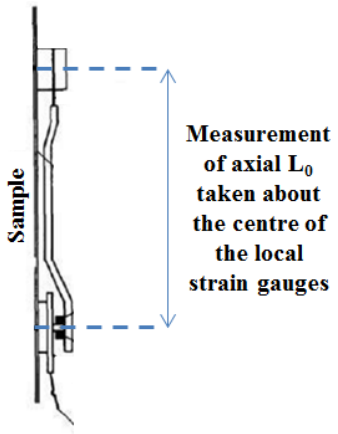

Figure 4.12: Measurement of axial L_0 (adapted from (Bishop & Henkel, 1964))

During the various stages of an advanced triaxial test L changes. L may increase during saturation as the samples swell (although care is taken to minimise this) and likewise L may decrease during consolidation as the sample decreases in size due to water

expulsion. In addition to this, the innate flexibility of the gauges thin wire components and of the membranes themselves means that the gauges are prone to 'settle' into position during the filling of the triaxial cell with water/oil and during the initial application of cell pressure.

Because of these reasons the change in L between the time the initial gauge length is measured manually and the beginning of the shearing stage must be tracked so that it becomes possible to obtain correct results.

By positioning the gauge's magnetic component to their zero gauze position on the Hall Effect transducer during setup, it is ensured that the largest possible measuring range is available for any movement that may take place during filling of the cell, docking, saturation, consolidation and ultimately shearing. Figure 4.13 shows the typical locally measured displacements (and therefore changes in L_0 for the start of shearing) that occur during these steps on a samples of Glacial Till. This test does not use the 'Fixed Topcap' docking method (addressed later in this chapter).

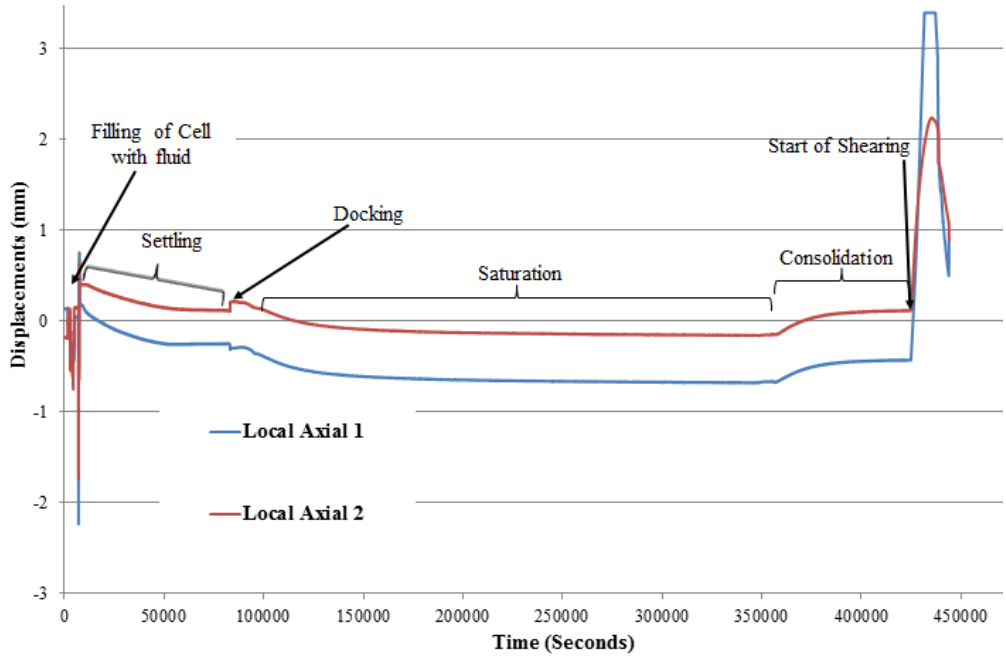

Figure 4.13: Uncorrected 'raw' displacements from local axial strain gauges during the various stages of triaxial testing on Glacial Till.

By accounting for the change in gauge length prior to shearing from the original measured L_0, an accurate gauge length may be found for use in all axial and shear strain calculations. Often this correction appears only minor as every effort has been made to minimise swelling and other unwanted sample disturbances, however by compensating for errors such as these the accuracy of results may be increased.

4.3.3. *LOCAL RADIAL STRAIN GAUGE L_0*

Much that is true for the local axial strain gauges is also true for the radial gauge and so shall not be repeated; however one additional point must be made in the calculation of strains using radial gauges. The L_0 of the radial gauge is simply the diameter of the sample at the point the radial gauge is affixed. Unlike the axial gauges however, any displacements recorded from the Hall Effect transducers must be halved. This is because unlike the axial gauges which are free to move up and down the sample in tandem to the movement of the sample, the radial gauges are fixed at two diametrically opposite points which pivot about a hinge. This hinge is itself diametrically opposite the point at which the Hall Effect transducer and associated magnet touch one another, meaning that all strains experienced at the fixing points are effectively doubled. This can be seen in Figure 4.14, albeit in an exaggerated diagrammatical form.

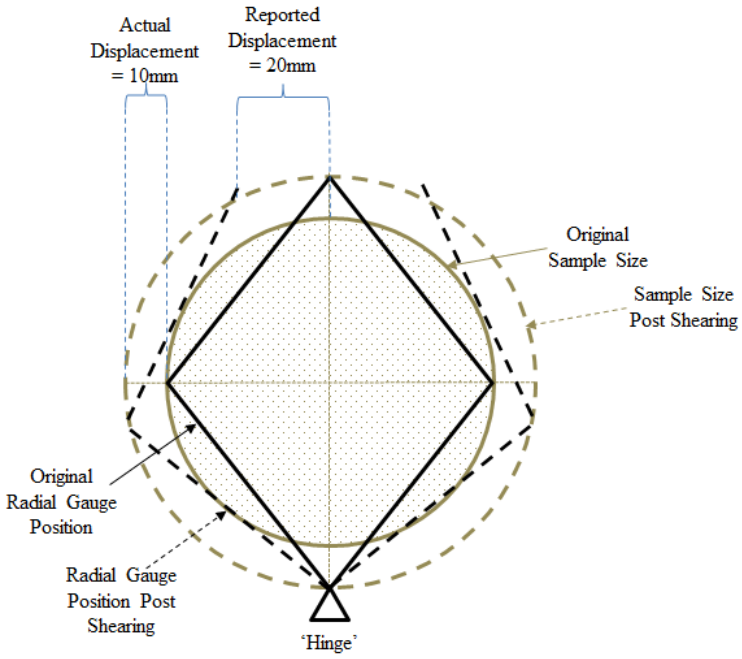

Figure 4.14: Radial gauge opening reporting double the actual displacements.

To compensate for this effect the formula for calculating radial strains must be adjusted (equation 4.1), this is also advised by GDS in their local strain gauge manuals:

$$\varepsilon_r = \left(\frac{[\Delta L/2]}{L_0}\right) \times 100 \qquad 4.1$$

4.3.4. *LOCALLY MEASURED STRAINS AS A SOURCE OF ERROR*

It is generally accepted that locally measured strains are a true reflection of the behaviour of a material during triaxial testing and that measured strains, for example radial strains, are more accurate than calculated and inferred strains using an assumed Poisson's ratio and a known external axial strain.

Whilst this is largely true, one must consider that the optimum positioning location of the gauges (within the central third of the sample) may in itself give rise to incorrect, or at least exaggerated, data.

This is because any localised vertical strains occurring near the sample / platen contacts will be ignored by the local axial gauges (which measure only the centre of the sample) thus providing only the stiffest estimations of axial behaviour, whilst at the same time the maximum (and therefore least stiff) radial strains will be measured by the local radial gauges (as they tend to be positioned over the point of greatest 'barrelling' at the centre of the cylindrical sample, caused by restrained end effects at the sample top and bottom as seen in Figure 4.15 (Grisso, et al., 1984); (Sheng, et al., 1997)).

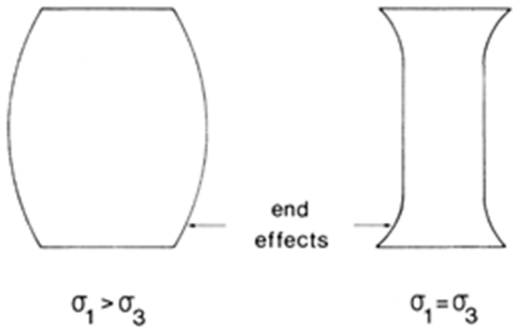

Figure 4.15: Theoretical sample shape after applied stress given end restraint, a) during shearing and b) during isotropic consolidation (Grisso, et al., 1984).

These factors must be taken into account when calculating any composite strains, such as shear strains and volumetric strains, and where possible alternative estimations should be analysed for completion (for example external measurements of axial strain, albeit incorporating bedding errors, and measurements of volume change taken from back volume changes), if only for cautious comparison.

Measurements of volumetric strains via back volume changes are themselves potentially subject to criticism, as a typical triaxial test will only require 95% saturation (a B value of 0.95). This means that whilst water may well be passing into and out of a sample via

a back pressure one can never be entirely confident that the volume changes represent absolute changes in the sample's volume (although they are a very close indicator).

4.4. METHOD OF AFFIXING GAUGES AND THE EXAMINATION OF SAMPLE – MEMBRANE 'PLAY'

When using local strain gauges it is critical that the gauges themselves be fixed firmly to the sample prior to testing. During the testing of soils it is possible to pin the gauges (pinning) by perforating the rubber membrane with metal pins through the gauges and into the soil, maintaining a water tight interface with the use of rubberised sealing glues / adhesives. This provides the user with the confidence that the gauges are only able to strain between the fixed rigid pinning points. Likewise in the testing of hard rocks, electrical resistance strain gauges may be adhered to the sample directly (although considerations need to be made for the stiffness of the glue).

Manual pinning requires the sample to be relatively homogeneous and ideally clayey in nature. Heterogeneities, such as the gravels and cobbles present in Glacial Tills, can prevent a pin from penetrating a sample to the desired depth, or even deflect the pin as it enters (causing the gauge to be misaligned). Once a material stiffness becomes too high for pins to be pressed into the sample manually, holes must be drilled for the pins to occupy before being fixed in place with a suitable filling agent. Pins cannot simply be forced into samples due to the possibility of a sample splitting (particularly true of weak laminated samples). The drilling / filling process is time consuming however, and may damage a delicate sample or allow it to excessively dry out as it is worked upon. Also, the presence of the pins themselves can create localised stress / strain concentrations within weak samples and open up pathways for water ingress (causing localised softening about the pin), altering the reported stiffness results. As the pinning process requires the membrane to be punctured, this too opens up the possibility that a leak between the cell and back pressure may be formed, effectively ruining a test (and the sample in question). Samples that contain large surface and internal voids also present problems when pinning, as the pin may enter the sample at an area occupied by a void, thus obtaining no purchase.

In UCS, gluing gauges directly to a sample surface cannot be carried out if the sample is friable or prone to alteration when drying out (creating a loose sample surface) and in triaxial apparatus gluing gauges to the sample surface may be problematic due to the presence of water, progressively softening a sample or reacting with the adhesive itself.

The soft rocks tested within this report have combinations of several of these issues, which are compounded by the fact that only a small sample set is available (making risky procedures that may damage samples highly undesirable). As such, the use of pinning has been discounted during this research project.

In an attempt to solve this issue, several other methods of affixing local strain gauges have been considered:

Ismail, et al (2001), carried out testing on artificially cemented calcareous soils. Due to the specific preparation method of these artificial samples it was possible to incorporate aluminium footings within the inside of the samples by first adhering them to the interior side of the membranes prior to sample mixing and preparation. This is clearly not an option for the testing of natural rock cores, although the principal of adhering strain gauges to a sample without puncturing the membrane is attractive.

Silvestri & d'Onofrio (2000) agrees that it is neither easy nor desired to perforate the rubber membrane during triaxial testing and suggests an alternative method for affixing strain gauges. By creating a number of grooves filled with gypsum cement (quick-rock) directly beneath the desired points of contact of the gauges and gluing the membrane to the sample themselves, uncertainties surrounding localised sample deterioration and stress / strain localisation can be avoided. This is shown in Figure 4.16.

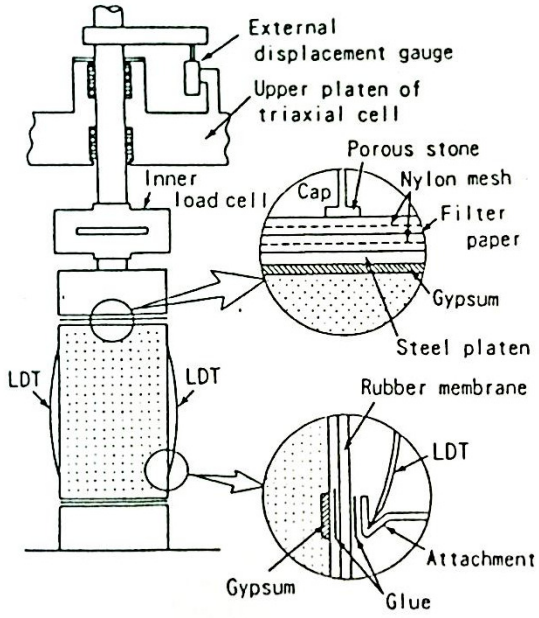

Figure 4.16: Method of affixing local gauge to membrane whilst preventing 'play' as used by (Silvestri & d'Onofrio, 2000) and originally suggested by (Tatsuoka, 1996).

This suggested method is unfortunately even more time consuming than pinning and is considered by the author of this thesis to be potentially destructive to the samples in question. The soft rocks tested within this research rapidly dry when exposed to open air and become friable, a process that is known to take place rapidly and that was raised as a key issue during routine testing. The use of gypsum during testing is discounted, as the materials in the focus of this project are deposited in evaporite rich areas where gypsum is prevalent. This could cause undesired confusion during any post testing optical / chemical analysis of samples and the presence of gypsum may even alter or add to the stiffness of the tested material.

The solution that was initially deemed acceptable was to rely upon the difference between internal pore pressures and outside cell pressures to hold the strain gauges in place, which themselves are adhered to the outside of the membrane. Gauges adhered to the sample in this fashion are referred to as 'loose' gauges. Using 'loose' gauges gives rise to the possibility of 'play' occurring between the membrane and the sample surface, meaning that strains measured may not represent the true strains developed in the sample as the membrane moves relative to the sample (Tatsuoka & Kohata, 1995) (Ismail, et al., 2001). Jardine, et al (1985), however, stated this may not to be the case:

By carrying out a series of experiments comparing displacements measured via local strain gauges adhered only to the sample membrane against those from foil strain gauges fixed to the sample itself, Jardine, *et al* (1985) showed that, providing high cell pressures were used, 'play' errors occurring between the two methods was negligible.

In order to better understand this behaviour, several control tests were carried out upon both a custom rubber sample (that has very smooth sides and is impermeable) and a very stiff sample of Springwell Sandstone (with comparatively rough sides and a high permeability) comparing the simultaneous development of strains from both a fixed gauge and a gauge adhered only to the outside of the sample membrane ('loose'). Data retrieved from those tests carried out on the rubber sample will be examined first.

4.4.1. *RUBBER CONTROL SAMPLE*

The rubber specimen was created to mimic the proportions of the triaxial specimens tested within this report. They were cylindrical, 68.5mm diameter by 133.0mm length (2:1 ratio of length to diameter) with ends cut to be as flat and parallel as possible so as to minimise the occurrence of bedding errors. Testing was carried out within triaxial apparatus using standard setup procedure where applicable (although no saturation was

required and back / pore pressure lines were left open to drain into a constant negative pressure of -10kPa). Photographs detailing the setup of this test are shown as Figure 4.17.

a) b) c) d)

Figure 4.17: Setup of the rubber specimen control tests.

The sample was mounted into the triaxial apparatus in the usual manner with stainless steel drainage discs set both above and below the rubber specimen (Figure 4.17, a)). A small quantity of contact adhesive was then applied to two locations on the sample. These locations would serve as the fixed adhesion points for local axial strain gauge 1. The membrane was then put in place, gluing the rubber control sample to the inside of the membrane in a similar way to that suggested by Silvestri & d'Onofrio (2000), (Figure 4.17, b)). The sample top cap was then put in place and the whole system was sealed from the external cell pressure using the three o-ring method (Figure 4.17, c)). Finally the two Hall Effect strain gauges were fixed to the sample at 90 degrees to one another about the sample's centre, (Figure 4.17, d)). Starting gauge lengths were measured and the Perspex cell assembled ready for testing. Local axial strain gauge 1 (LA1) was considered the 'fixed' control gauge, whilst local axial strain gauge 2 (LA2) was adhered only to the outside of the sample membrane in order to assess the amount of 'play' occurring.

The control testing programme was as follows:

Stress controlled tests, (starting at 50kpa deviator stress then increased to 100kpa then 150kpa over the course of two 5 minute stages), were carried out at cell pressures of 0,

100, 300 and 600kPa in order to measure the amount of 'play' occurring and also quantify how this changed with increasing mean effective stress (as Jardine, *et al* (1985) indicated any 'play' would decrease with increasing confinement). Displacements were also measured during the 'isotropic consolidation' stages (moving from 0 to 100 kpa confining etc). Finally a strain controlled test was carried out which was allowed to run for several days to address the possibility of any progressive slippage between the sample and the membrane during a representative shearing stage.

Results from a representative stress controlled compression test can be seen as Figure 4.18.

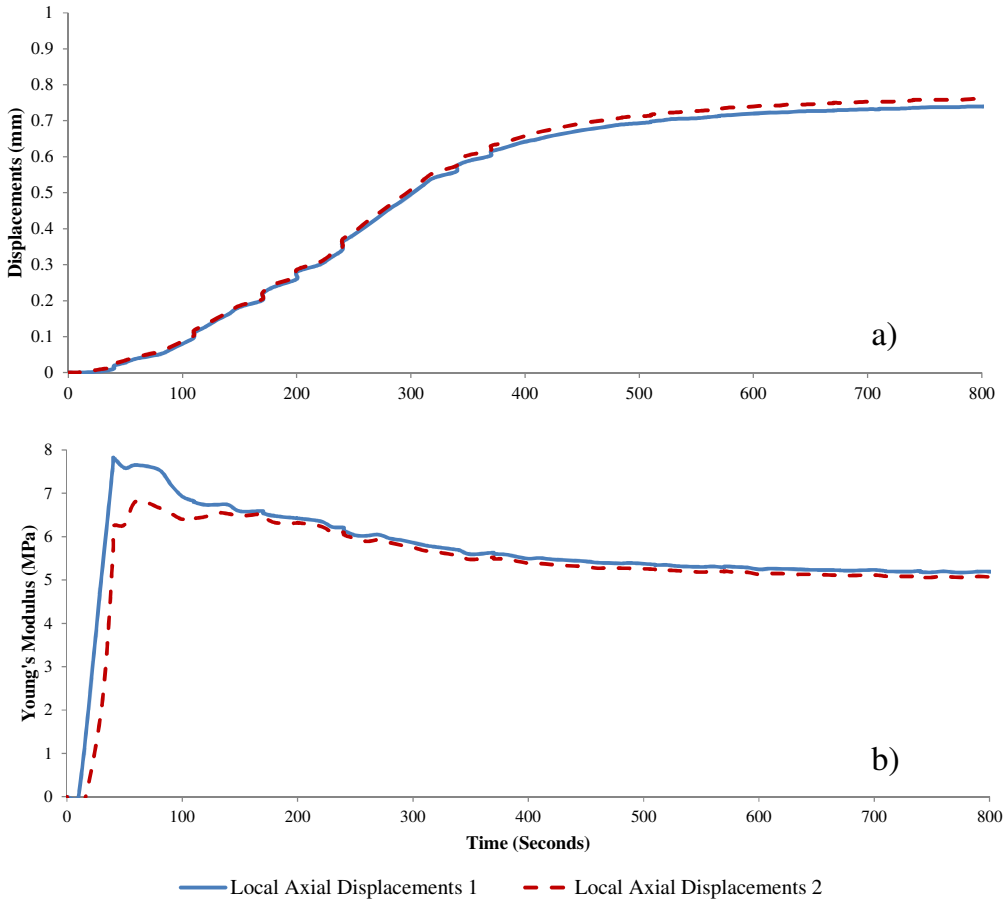

Figure 4.18: Comparison between fixed gauge (LA1) and lose gauge (LA2) during increase in *q* from 50 to 100kPa on a rubber specimen held at σ_3 = 0kPa. a) shows displacements, b) shows Young's Modulus.

Displacements during the initial application of load were repeatedly comparable between the fixed and loose local axial strain gauges (as seen in Figure 4.18 a)), providing similar stiffness behaviour throughout the full strain range. Minor deviations were noted on all tests (for example during the first 100 seconds of Figure 4.18 b)),

however neither the fixed nor the loose method consistently indicated the higher stiffness meaning that a certain amount of variability exists due to factors such as human error in the measurement of initial gauge lengths or due to minor imperfections in the sample itself and the adopted loading geometry (this too has been noted on tests where both gauges were firmly affixed and in practice obtaining identical displacements from two separate gauges is very unlikely, especially on a natural soil / soft rock with an inherently anisotropic structure).

In order to identify a strain range where the two affixing methods provide the best comparable results a single strain rate test was carried out. This test was conducted at a mean effective stress of 600kPa and the sample was sheared at 0.001% per minute. Results are presented as Figure 4.19.

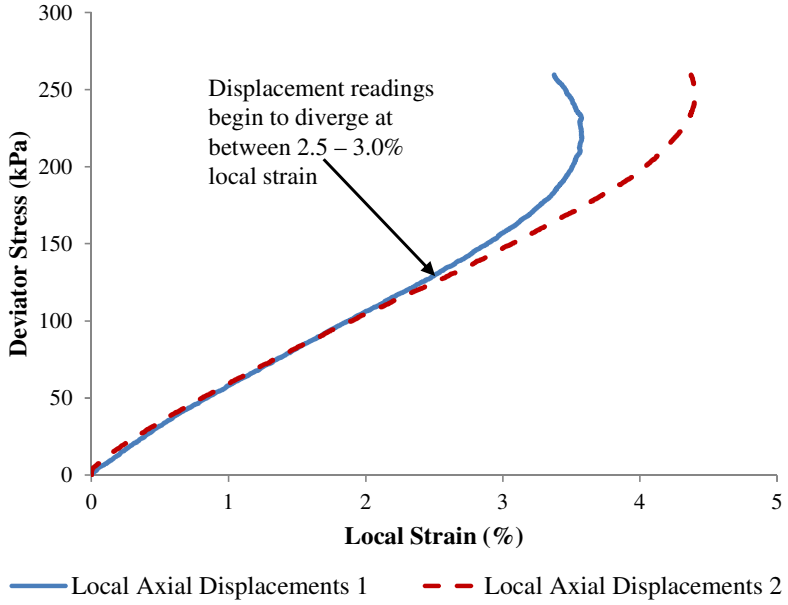

Figure 4.19: Comparison between fixed gauge (LA1) and lose gauge (LA2) during shearing of a rubber control specimen at p'_0 = 600kPa and shearing rate of 0.001%/min^{-1}.

Results of Figure 4.19 showed that within the small strain range through to the lower end of the large strain range, both methods provided highly comparable strains (and therefore ultimately, stiffnesses). 'Play' only begins to occur upon entering into large strains of 2.5 – 3.0% and greater. Local strains of this magnitude fall outside of the optimum operational range of the Hall Effect strain gauges themselves (also the majority of rocks, even soft rocks, are likely to fail before large strains are generated).

Throughout the whole testing programme carried out on the rubber control samples the largest amount of observed 'play' occurred during the interval stages where cell

pressure was increased independent of deviator stress (analogous to isotropic consolidation). Figure 4.20 a) shows a comparison between local displacements during 'consolidation' from 0 to 100kPa whereas Figure 4.20 b) shows displacements associated with an increase from 300 to 600 kPa. The large displacements present in the local axial displacement 2 data (loose) of Figure 4.20 a) occurring as a series of steps or 'jumps' should be noted.

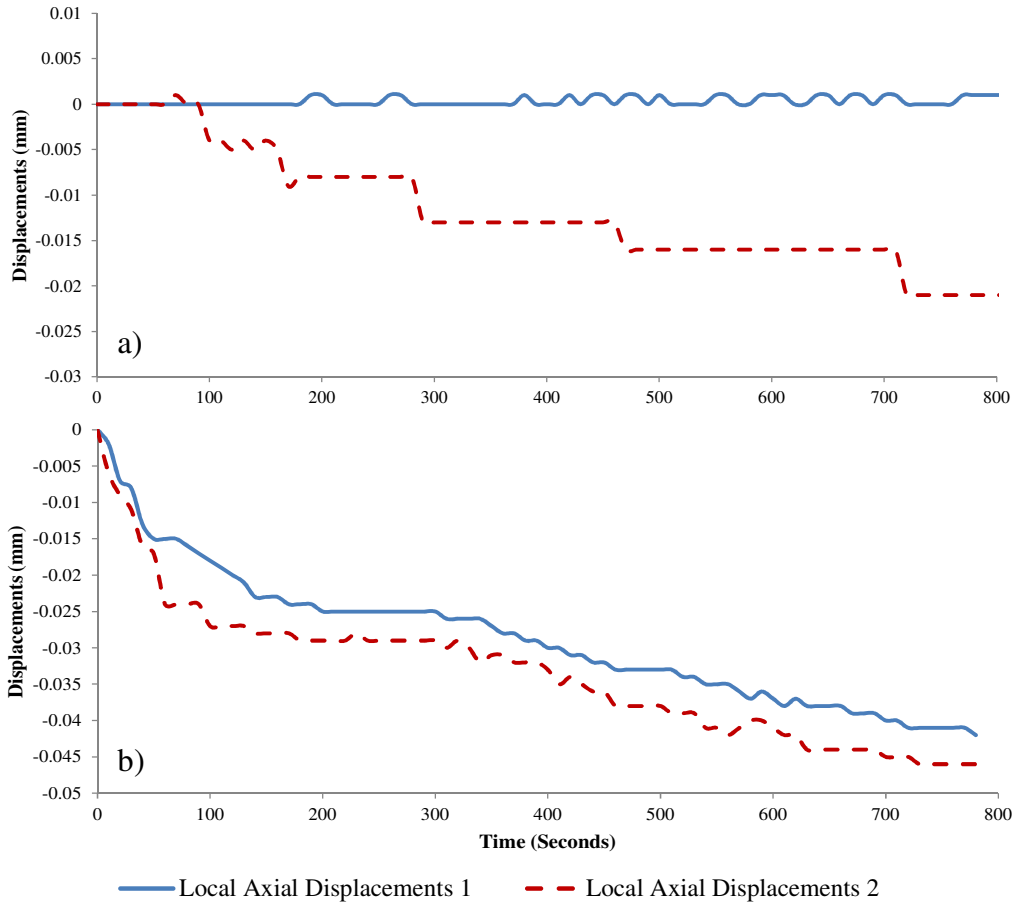

Figure 4.20: Comparison between fixed gauge (LA1) and lose gauge (LA2) during isotropic consolidation of a rubber sample from a) 0 to 100kPa *p'*, and b) 300 to 600kPa *p'*.

The sudden 'jumps' noted during the 0 to 100 kPa isotropic consolidation stress state changes (Figure 4.20 a)) were not observed during any shearing stage carried out on the rubber control specimens and were initially thought to be linked to the impermeable nature of the rubber along with its very smooth surfaces. It was assumed that as the rubber sample attempted to isotropically contract, the elasticated 70mm diameter membrane becomes comparatively too large for the <68.5mm diameter sample, and with a mean effective stress of only between 0 to 100kPa (which, due to the impermeable nature of the rubber, may not be acting evenly over the whole specimen), the membrane may have been temporarily able to slide relative to the sample

circumference. This does not occur once mean effective stresses of between 200 to 300kPa have been achieved, when both the fixed and loose gauge show similar displacements, for example those within Figure 4.20 b).

4.4.2. *SPRINGWELL SANDSTONE CONTROL SAMPLE*

A series of control tests similar to those undertaken on the rubber sample were carried out on a sample of Springwell Sandstone. This was done in order to observe how permeability aids in the adhering of triaxial testing membranes, held in place using only the differential pressure across the membrane, and also to assess a potential minimum strain range where 'loose' local strain gauges may become unreliable. Springwell Sandstone samples have a higher surface roughness than the rubber control samples, although do not display any macro-void or surface imperfections of any kind and are very uniform in shape from top to bottom. It should be noted at this point that, unlike the rubber control sample which was created to be as homogeneous as possible, the Springwell Sandstone has pre-existing heterogeneities (as they are taken from natural block sub-samples) that may introduce a degree of natural variability between the behaviour of the material directly underlying the two gauge locations, making precise comparisons more difficult.

The sandstone specimen was cylindrical, 73.9mm diameter by 140.2mm length (2:1 ratio of length to diameter) with ends cut to be flat and parallel. Photographs detailing the setup of this test are shown as Figure 4.21.

a) b) c) d)

Figure 4.21: Setup of the Springwell Sandstone specimen control tests.

Testing was carried out dry within triaxial apparatus using the same setup procedure as that of the rubber control tests. The testing programme was entirely stress controlled, due to the significantly higher stiffnesses of the samples tested. Tests started at 50kpa deviator stress then increased to 500kPa, 2000kpa then ultimately to 5000kpa over the course of three 10 minute stages. Again, these stress controlled test stages were carried out at a variety of cell pressures, namely; 0, 300, 400, 600, 800 and 900kPa. Displacements were also measured during the 'isotropic consolidation' stages in order to better understand the development of relative sample-membrane movements, as was carried out on the rubber control samples.

Figure 4.22 displays a representative comparison between the behaviour of the fixed local strain gauge 1 and the loose local strain gauge 2 during triaxial compression. Figure 4.22 a) shows a close relationship between the two gauges displacements verses time and Figure 4.22 b) shows an equally good match between the two plots of calculated Young's Modulus verses time.

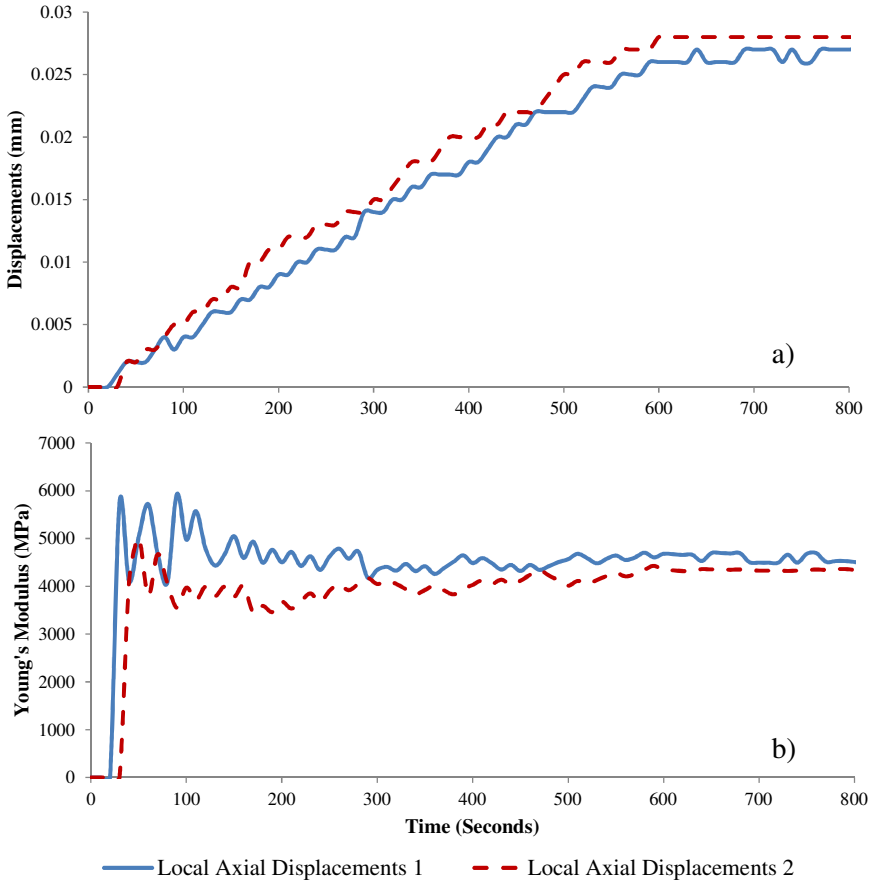

Figure 4.22: Fixed gauge (LA1) and loose gauge (LA2) during increase in *q* from 500 to 2000kPa on Springwell Sandstone held at σ_3 = 800kPa. a) shows displacements, b) shows Young's Modulus.

Results during stress controlled compression tests were consistently comparable between the fixed and loose local axial strain gauges, even at low confining pressures (as seen in Figure 4.23 which demonstrates the development of local displacements at two low confining pressures namely a) 300kPa and b) 400kPa). Minor discrepancies were again noted during all tests, as with the rubber control samples, with no test displaying perfectly identical behaviour between LA1 and LA2. However neither the fixed nor the loose gauges showed consistent, repeatable errors indicating a certain degree of natural variability is controlling the local straining behaviour of this sample.

During all compression stages carried out on the Springwell Sandstone very good comparisons could be made between the fixed and loose local axial strain gauges, even during stages with short stress probes, where the maximum axial strains generated equated to only 0.015%. This indicates that there is not a minimum strain range during compression where a loose gauge may start to be considered as unreliable and that the small strain range may still be measured to a high degree of accuracy using this method.

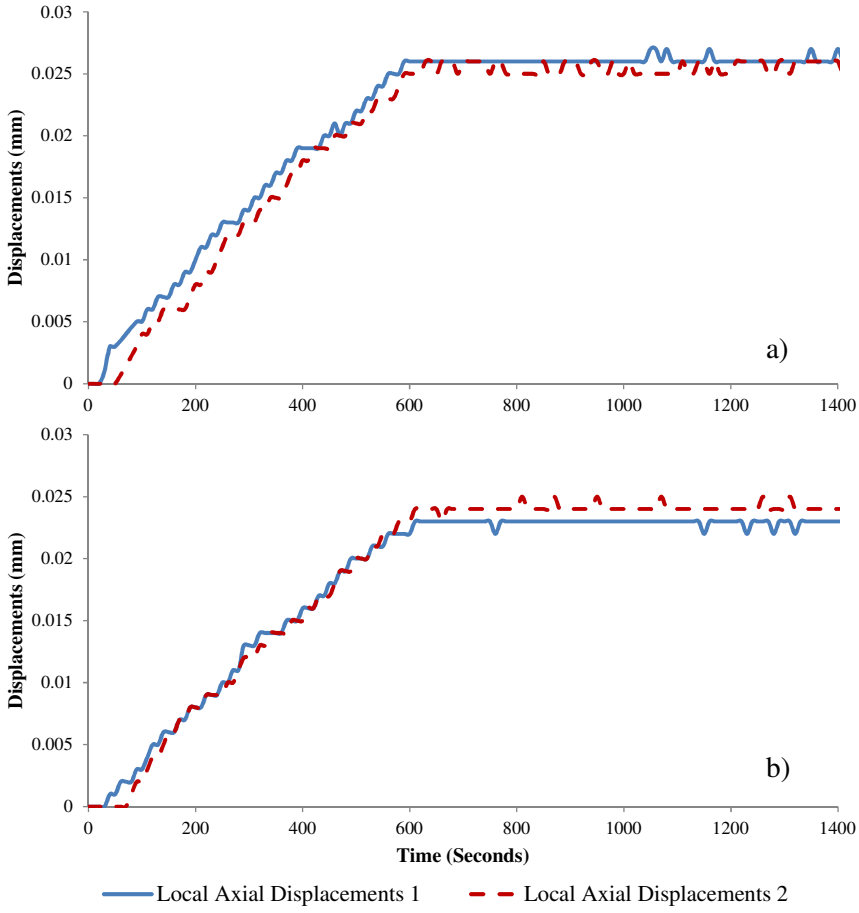

Figure 4.23: Fixed gauge (LA1) and loose gauge (LA2) during compression from 50 – 2000kPa deviator stress of Springwell Sandstone at confining pressures a) σ_3 = 300kPa, and b) σ_3 = 400kPa.

Isotropic compression stages once again displayed the greatest amount of 'play' occurring, manifesting as large local axial 2 displacements. This was particularly frequent during initial consolidation stages, moving from a *p'* of 0 to 100kPa, 100 to 200kPa and from 300 to 400kPa, although the large displacement steps (jumps) were observed in isolated incidents during consolidation to *p'* as high as 800kPa.

σ_3 was incrementally raised from 0 to 900kPa over numerous stages before decreasing in stages to 0kPa. It was repeatedly noted that the amount of 'play' decreases as mean effective stress conditions rose, however upon the removal of high cell pressures into low cell pressure, equivalent amounts of error were not encountered. Figure 4.24 a) shows the displacements occurring during isotropic consolidation from 300 to 400kPa (a small, but important difference between the fixed and loose gauge movements is noted) and Figure 4.28 b) shows the displacements occurring during the associated swelling stage at the same pressure range (where near identical movements develop between the fixed and loose gauges). Discrete steps shown on all portions of the data (Figure 4.24) are due to the Hall Effect gauges operating near their minimum capacity.

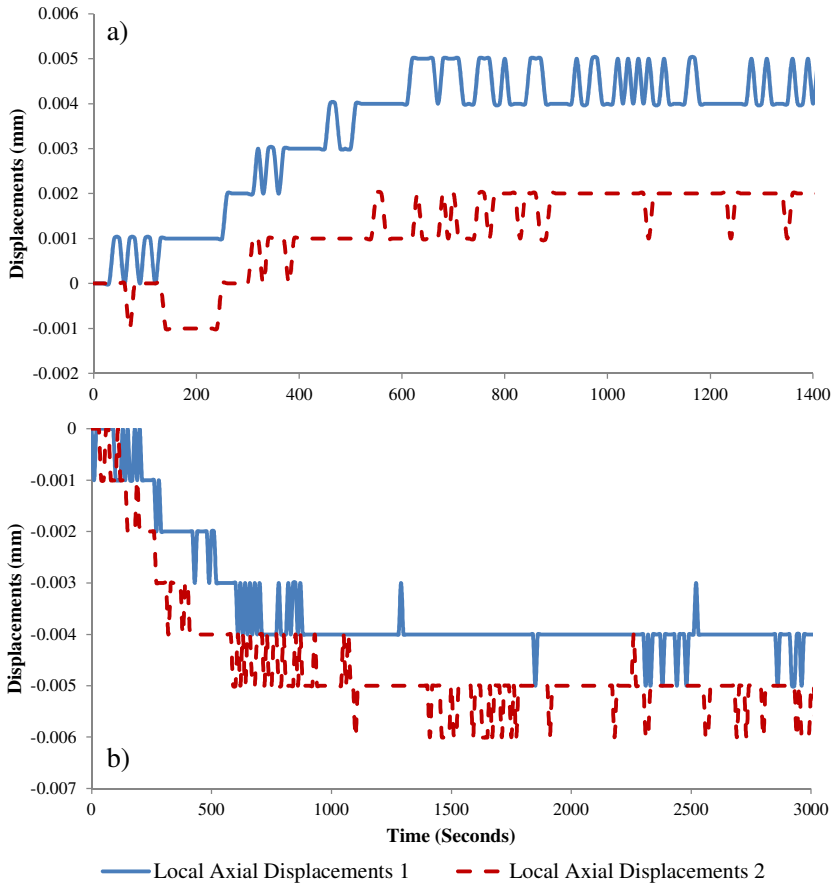

Figure 4.24: Comparison between fixed gauge (LA1) and lose gauge (LA2) during isotropic consolidation / swelling of Springwell Sandstone from a) 300 to 400kPa *p'*, and b) 400 to 300kPa *p'*.

When radial stress is re-applied to the sample the gauges have been noted to move in synchronisation, at both low and high radial stress states. This behaviour was noted repeatedly and suggests that a key factor controlling how well a 'loose' gauge will be adhered to a sample is not just a function of the magnitude of mean effective stress, but also a function of time. The membrane will, over time, settle into position and effectively mould itself more closely to the sample surface making it more likely to move with the sample, as opposed to generating errors in the form of slips and jumps. As such, later isotropic consolidation stages display less 'play' for any given effective radial stress state.

The 'play' between sample and membrane during the early isotropic consolidation stages occurs, in part, as a product of the perfectly cylindrical nature of both the rubber and sandstone samples used and the characteristic 'jumps' become less likely to occur as the surface roughness of the specimen increases. Tests carried out by the author of this thesis on natural samples of Glacial Till using only the 'loose' method, for example, have not displayed such behaviour during any phase of testing nor have tests upon highly porous calcarenite samples. Further-more, once samples have been allowed time to 'settle', the membrane appears to mould more closely to the sample circumference, thus reducing the likelihood of 'play'.

In order to minimise errors, any changes to the initial gauge length of local gauges during docking, saturation and consolidation should be tracked and accounted for prior to shearing.

Once accounted for, the errors associated with 'play' occurring during initial consolidation stages can be all but negated and these errors do not appear to greatly affect the results of shearing in compression at any mean effective stress level providing the strains generated are less than 2.5%.

Using the 'loose' gauge method is attractive for several reasons, especially when the availability of samples is limited. The 'loose' method is quicker during assembly of the cell and sample (therefore incurring less sample drying), it causes less damage to samples than pinning or creating gypsum footings, no local stresses accumulate around any pins or footings, and no accidental water ingress is generated by leakage through pinned holes. However, whilst the minor variations noted between affixing methods during compression stages is believed to be acceptably small, the preferred method is clearly to firmly fix strain gauges in place on the sample.

An acceptable compromise to the Silvestri & d'Onofrio (2000) method is to fix local strain gauges in place using an adhesive between the membrane and the sample at the points of contact. Gauges, both axial and radial, will be firmly adhered to all samples prior to testing in order to minimise the development of minor variations.

However, due to the clay-like nature of the tested calcareous mudstones upon exposure to water, there exists the potential for glued gauges to progressively lose their firm bond with the sample surface and become 'loose', held in place only by the differential pressure between the outside and inside of the membrane. Whilst this situation is sub-optimal, results from control testing on the rubber and sandstone samples indicate that reliable results may still be obtained providing a settling time of not less than 2 days is allowed, that local strains of 2.5% are not exceeded and that mean effective stresses greater than 200kPa are used during shearing stages.

When testing natural samples of soils and rocks it is highly unlikely that two axial gauges placed diametrically opposite one-another will produce identical strain data. Both local axial and local radial gauges are bound by the limitations stated previously.

4.5. LOADING GEOMETRY 'DOCKING' METHOD

Bedding errors are a problem in UCS and triaxial tests and the use of local strain gauges are therefore crucial in the acquisition of accurate strain data.

Externally measured strains will always show some evidence of bedding. However, by carefully ensuring the sample ends are flat and parallel, much can be done to limit (although never remove) the occurrence of this issue. It should be noted, however, that whilst unrealistically high compressional strains at the top and bottom of the sample during bedding may be ignored when adopting local strain gauges measurements, any rotation or tilting of the sample during the initial contact between the loading ram and the top platen (docking) may still generate inaccuracies within the central third of the sample.

'Docking', that is to say the connection between the loading ram and the sample top, during a standard triaxial test will typically occur following the consolidation stage of testing according to standard procedure. During assembly, filling of the cell, saturation and consolidation, the loading ram usually remains a certain distance above the sample top until the end of consolidation when the cell is raised and the ram and the sample top platen will come into contact immediately prior to shearing. Older, non-computerised

systems have to obey this procedure, for if the sample 'docking' was to take place prior to the other steps, any volumetric changes occurring within the sample would impose anisotropic stresses on the sample (as the rigid loading ram resisted the swelling of the sample during saturation, for example, and whilst this could be manually corrected it would have required full time supervision and constant adjustments. Due to the development of computer controlled systems, this is fortunately no longer the case).

4.5.1. *CONICAL / CONCAVE GEOMETRY*

Standard triaxial top platens have a concave shaped indentation, or conical seat, set into them to allow the loading ram to align itself with the centre of the sample during 'docking'. This can be seen in Figure 4.25.

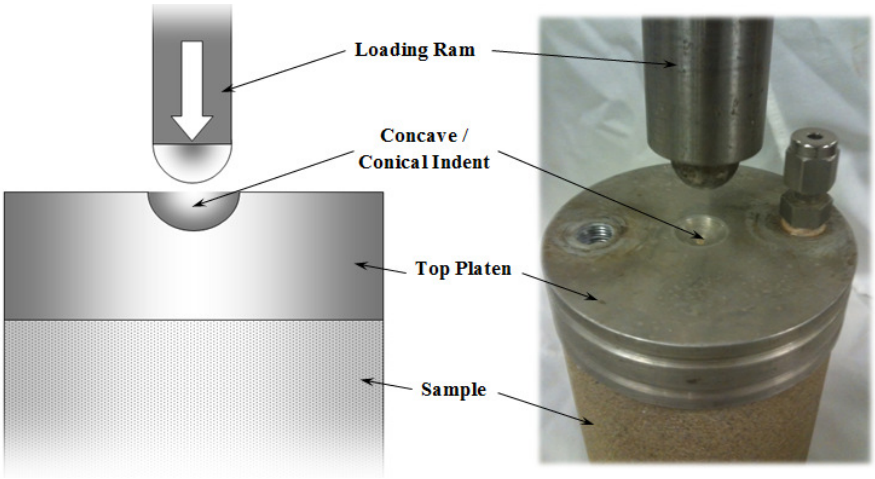

Figure 4.25: Conical seat / concave indent within triaxial top platen.

This method, whilst perfectly adequate for use during the examination of large strains, has been observed to cause rotational straining of the sample during 'docking' if the ram and platen are even marginally misaligned. As the loading ram lowers relative to the sample (as the triaxial cell rises) the edge of the rounded loading ram end often does not make a flush and even contact with the conical indent, which causes the top platen to tilt. This titling is only measurable if local strain gauges are being used and manifests itself by the development of compressional strains on one side of the sample and extensional strains diametrically opposite, as seen in Figure 4.27 and Figure 4.27. This continues until the loading ram is correctly seated and docked (Baldi, et al., 1988); (Heymann, 1998); (Silvestri & d'Onofrio, 2000); (Clayton & Heymann, 2001); (Gasparre, 2005); (Heymann, et al., 2005).

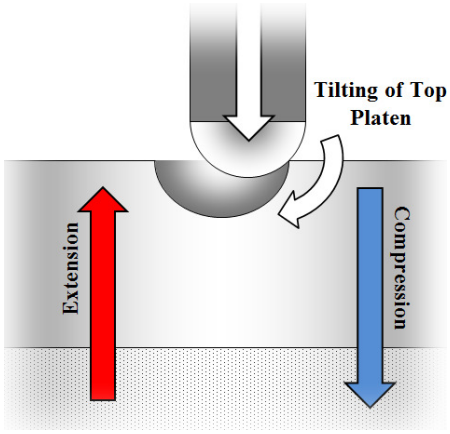

Figure 4.26: Development of both extensional and compressional strains during docking procedure using a concave / conical seat.

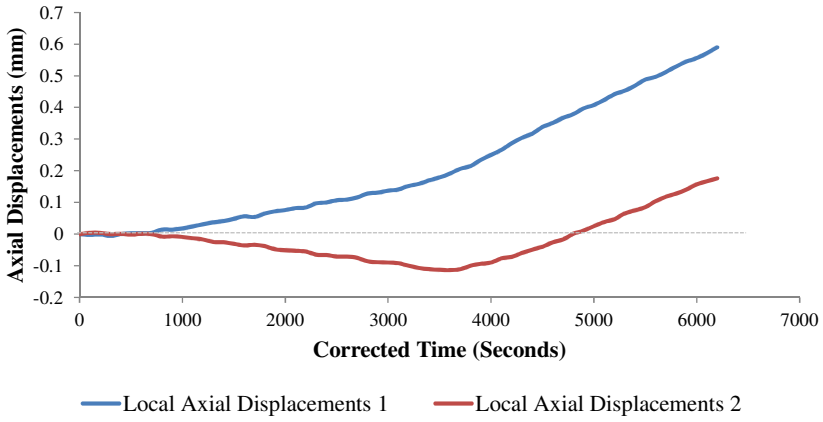

Figure 4.27: Extensional and compressional displacements observed during docking procedure using a concave / conical seat during the testing of Glacial Till.

Tilting has the overall effect of masking true stiffness within the initial very small and small strain range. The full load imposed by the ram is also not transferred evenly into the sample until this seating is complete; this can be seen in Figure 4.28 and in turn causes errors in the calculation of axial / deviatoric stress.

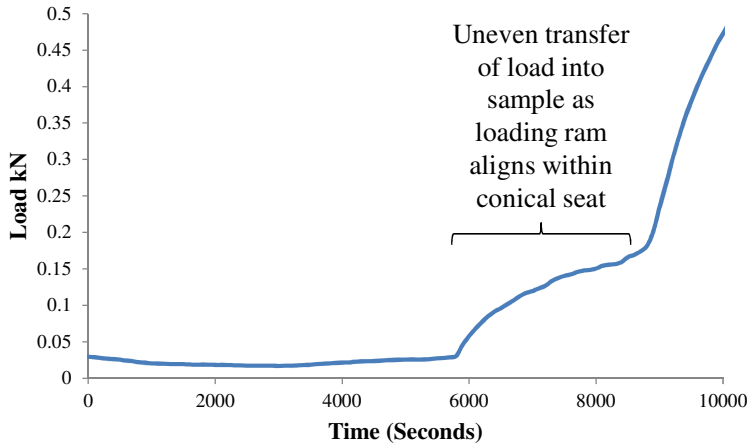

Figure 4.28: Gradual onset of load during docking when concave platens used.

The degree to which the loading ram and top platen need be misaligned in order to observe such behaviour is very small, raising questions about the necessity of the concave indentation in all but those tests examining large strains. The amount to which a sample's top cap may initially be misaligned with the loading ram may be small or insignificant during the setup of the sample within the cell, however tilting may progressively develop during the saturation and consolidation of a sample, particularly if heterogeneities exist. Errors in the measurement of stress during docking at the start of shearing are damaging to results when trying to understand non-linear stiffness behaviour, particularly within the small strain range (where the errors will be greatest).

4.5.2. *FLATTENED GEOMETRY*

In order to overcome this problem an alternative approach is required. Several docking methods exist (including the 'half ball' method proposed by Gasparre (2005)) and the effect that each has upon the measurement of initial stiffness has been examined within this section of the report in the context of small strain stiffness. This experimental testing was carried out on samples of undisturbed Glacial Till. Assumptions are made that this behaviour would also translate to the testing of soft rocks.

Firstly a flat platen method was adopted. This was achieved by covering the conical seat by a firmly adhered flat brass cylinder, as seen in Figure 4.29.

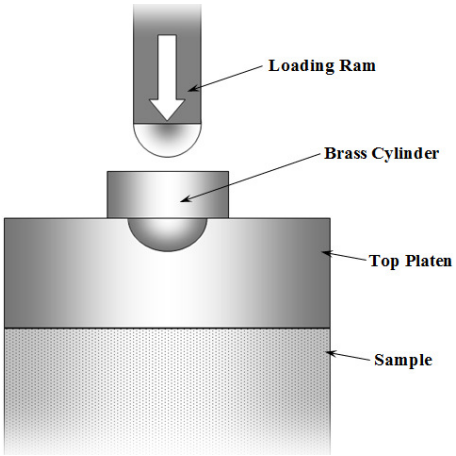

Figure 4.29: The use of a brass cylinder to create a flat platen contact.

By using a flat top platen, load is instantly transferred from the loading ram into the sample prompting axial stress and strain to develop immediately and allowing high stiffnesses to be observed. This method was considered adequate by Clayton & Haymann (2001) when testing clay and chalk.

During the examination of the small strain stiffness of Glacial Till, both the traditional conical indentation method and the flat platen method were compared. Figure 4.30 shows the shear stiffnesses calculated from the moment the loading ram made contact with the top platen. The flat platen method shows the expected high initial stiffness's which degrade with strain, whereas the sample which was 'docked' using the concave / conical seat, displays a scatter of results until 0.06% shear strains where stiffness gradually rises (coinciding with the ram connecting firmly with the base of the seat) until large strains develop.

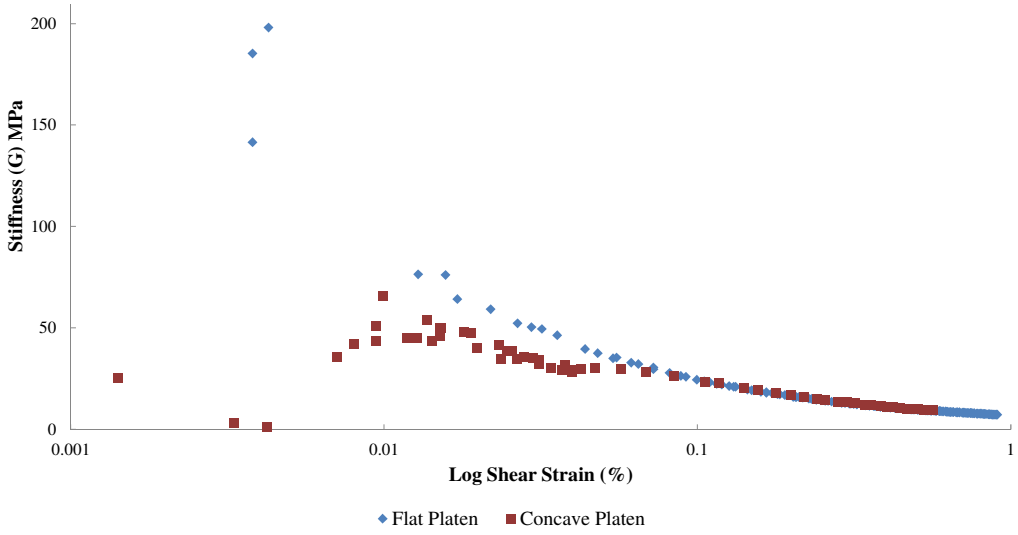

Figure 4.30: Docking procedure errors causing initial shear stiffness of sample of Glacial Till to be masked using the concave platen.

It is clear from these results that the use of a conical seat within a top platen masks measured stiffnesses during the docking procedure compared to that of the flat platen method. As the loading ram attempts to align itself within the conical seat, one local axial gauge will typically display exaggerated compressional strains whilst the diametrically opposite gauge shows extension. This causes averaged strains to provide meaningless stiffness estimates, especially when considering the errors associated with the loading of the sample too. This effect is not seen in the flat platen method.

If a conical seat must be used then it is suggested that readings only be taken after docking movement is completed, however this will ultimately underestimate the shear stiffnesses calculated as the highest stiffness is always observed at lower strains and it is unlikely a shearing stage using this setup would be able to begin from q = 0kPa due to the stresses involved in fully seating the loading ram.

Unfortunately, when using a method without the concave seating (such as a flat platen) there is no guarantee that the load is being transferred from the loading ram directly through the centre of the top platen, nor is there any means of correcting any mal-alignment or angular contact between the ram and the sample, as shown in Figure 4.31.

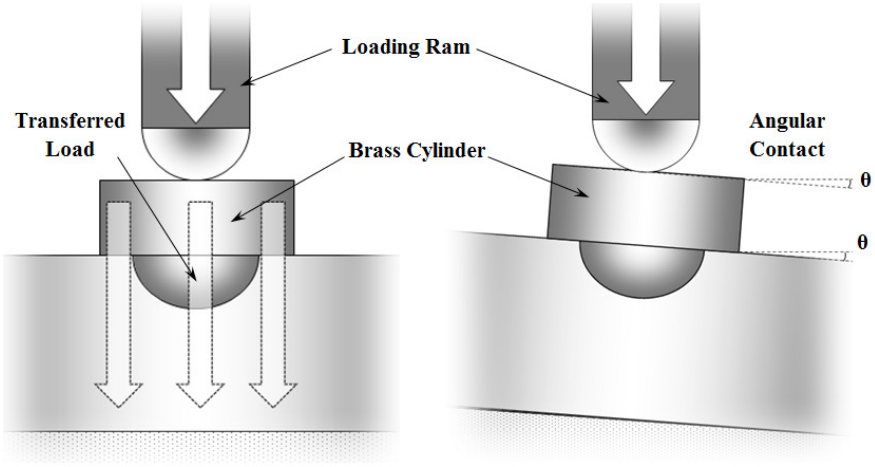

Figure 4.31: Development of angular stress component using flat platen top.

The introduction of this angular component adds complexity to the calculation of stresses and so in order to use a flat top platen during testing, an assumption must be made that the applied load translates only into the axial stress (σ_a).

4.5.3. *HALF BALL GEOMETRY*

Acknowledging these limitations, Gasparre (2005) created an alternative method that acts a compromise between the flat platen top and the conical indented platen top. This method allows the loading ram to transfer load centrally whilst preventing the development of excessive rotational strains. By placing a lubricated 'half ball' within the concave indent prior to testing, a flat loading ram can connect to the platen with the minimum of disturbance. This arrangement is shown as Figure 4.32.

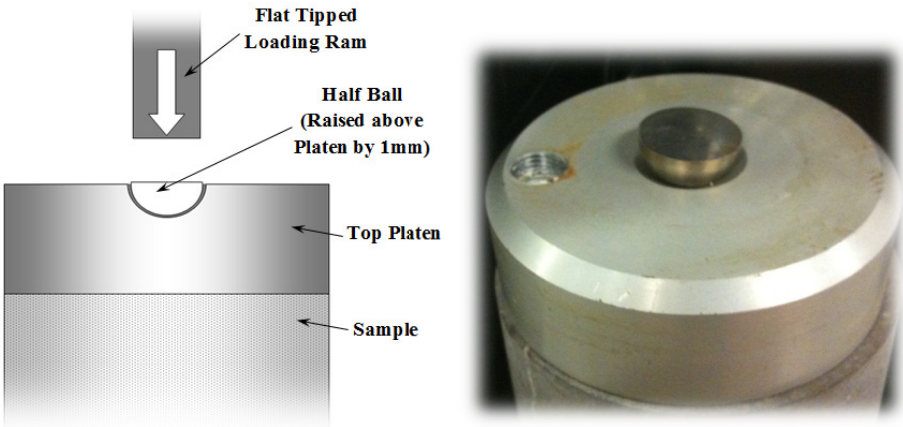

Figure 4.32: 'Half Ball' method, as used by Gasparre (2005)

When tested by the author on Glacial Till specimens this method was found to produce mixed results. Some tests recorded this method negating the tilting issue, whilst others showed that the amount of tilt could be quite pronounced (although never to the same degree as the concave testing platens). Examples of these mixed findings are presented as Figure 4.33 a) and b) which show the axial displacements of local strain gauges during docking procedure applying this method. Of all the tests carried out upon Glacial Till using this 'Half Ball' method, nearly 50% have shown some evidence of tilting within the early stages of shearing.

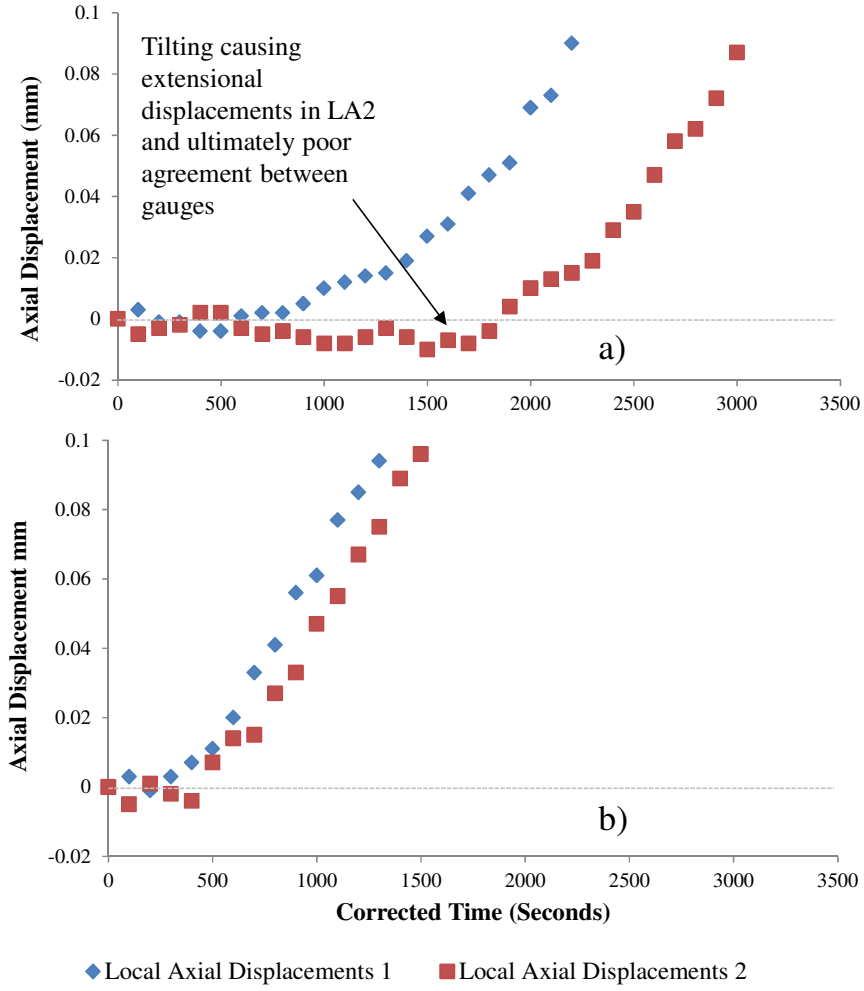

Figure 4.33: Local axial displacements during docking using Gasparre (2005) 'Half Ball' method. a) shows pronounced tilting and poor agreement between LA1 and LA2, b) shows negligible tilting.

This series of experiments were repeated on several samples of reconstituted Glacial Till in order to assess the effect of the different docking methods using near identical samples (to limit inter-sample variability affecting the results of testing). The samples were pre-consolidated to a high effective stress within consolidometer then cut and prepared to be approximately 140mm x 70mm height to diameter ratio. The samples were then saturated and isotropically consolidated to between 180-200 kPa mean

effective stress prior to shearing. 2No. samples were docked using the concave method, 2No. samples using the flat method and 2No. using the Half Ball method. Samples were not sheared to failure, as the purpose of the tests was purely to observe docking/seating error development.

Identical strain rates were used and samples were saturated (to B values in excess of 0.95) and consolidated for similar periods of time. All samples were fitted with local strain gauges so that their small strain stiffness behaviour could be observed. The resulting stiffness degradation profiles are presented as Figure 4.34.

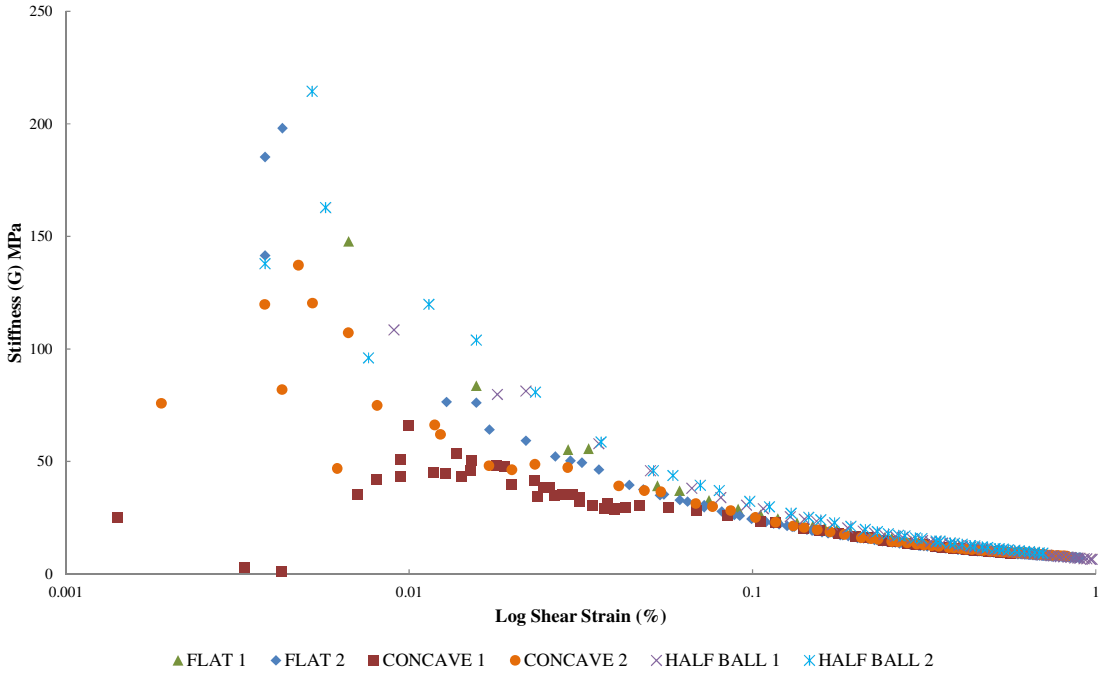

Figure 4.34: Effect of changing 'docking' method on the undrained shear stiffness of reconstituted Glacial Till using identical setup and shearing rates

The samples docked using the flat and half ball method generally show a good agreement in their shear stiffness degradation, starting high (in the case of these tests between 150 and 200 MPa) then degrading to a low value at around 1% shear strain. The concave platen tests however show a much greater spread of data, crucially within the small strain range, and it is not until 0.2% strain that the concave results join the overall curve.

4.5.4. *FIXED / RIGID GEOMETRY*

All three 'docking' methods covered have one large disadvantage, the inability to put a sample into relative tension. The three methods of 'docking' using a; concave top platen, flat top platen and a half-ball top platen, all allow the sample to be compressed at

a steady rate of strain / stress, however all rely upon the natural properties of the subject sample to swell or re-bound following the removal of stress and none of the systems allow negative deviatoric stress levels to be achieved. They all also allow the sample to tilt / rotate to some degree as the top platen is free to move. In order to carry out tensile testing a fixed / rigid contact is required between the ram and the sample top platen.

Whilst the testing of soft rocks under tension / extension within triaxial apparatus is not within the scope of this research project, several other benefits are gained through the use of a fixed / rigid loading ram – top platen contact:

1. This method disallows any occurrence of sample tilting as the orientation of the platen is perfectly at right angles to the orientation of the loading ram and perfectly parallel to the base pedestal.
2. Because 'docking' using this method is carried out at the beginning of the test (providing an automated system capable of maintaining q = 0kPa conditions is used), any change in shape / volume of a sample during saturation and consolidation does not manifest itself in the form of an angular displacement, meaning that the sample is kept centralised relative to the base pedestal and loading ram.
3. Whilst a state of q = 0kPa is being maintained, this setup can accurately measure the amount of strain occurring between the sample top and bottom due to swelling / consolidation using the external axial LVDT (and local gauges), as bedding errors take place (and are recorded and accounted for) during the initial setup of the sample. Also due to bedding errors occurring at a very early stage they do not mask true stiffness development during the later shearing stage.
4. This method indirectly encourages precise sample preparation. Unlike the other methods, which allow for a certain margin of error in the degree of parallelism between the sample top and bottom and the amount of misalignment in the location of the sample on the base pedestal, the fixed / rigid 'docking' method requires that the sample be perfectly parallel and central (as the fixing bolts will not align otherwise). As the 'docking' stage takes place so early into the test using this method, any misalignment can be quickly identified and fixed.

The fixed / rigid method of 'docking' (shown in Figure 4.35) is carried out manually once the cell is placed over the sample to be tested (with local strain gauges logging so that any displacements may be recorded and later allowed for). The loading ram is lowered through the cell by hand until the load cell comes into contact with the raised

bolt on top of the steel spacer. The ram is then manually screwed firmly into place (a few turns in the opposite direction prior to assembly will avoid tangled wires). The cell would then be filled and testing would proceed as normal.

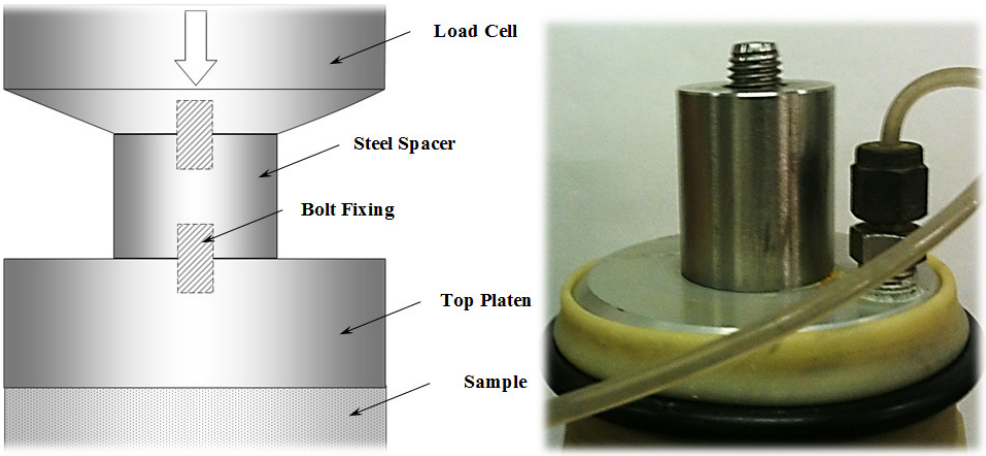

Figure 4.35: Fixed / rigid loading ram to top platen 'docking' method

It should be reiterated that this fixed / rigid 'docking' method requires a triaxial setup that allows stages to automatically retain set deviatoric stresses. If this is not the case then this method cannot be adopted as the sample would undergo unwanted stresses during the saturation and consolidation stages of testing (assuming the loading ram remains rigid and resists sample expansion / contraction).

Observation of the diametric local axial displacements during the initial stages of shearing using this method provide very strong agreements between Local Axial 1 and Local Axial 2, as seen in Figure 4.36.

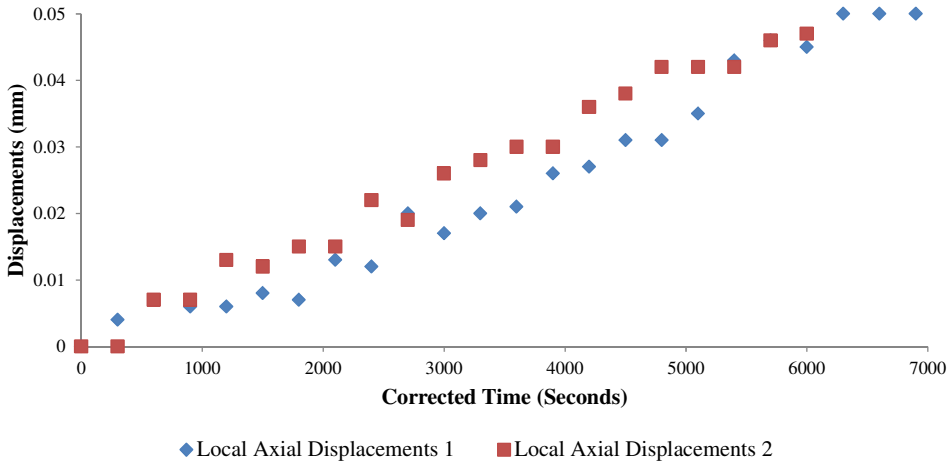

Figure 4.36: Local axial straining during docking using 'fixed / rigid' method at start of shearing

This method proved to be reliable and repeatable during initial experimentation on Glacial Till samples and is therefore employed throughout all testing carried out within

this thesis on calcareous soft rocks. Due to the strong agreement between the two gauges using this method, closer fitting individual small strain shear stiffness degradation curves are also obtained (increasing ones confidence in employing an average value). It should be noted that natural samples will almost always display slightly different strain behaviour when measured from diametrically opposite locations.

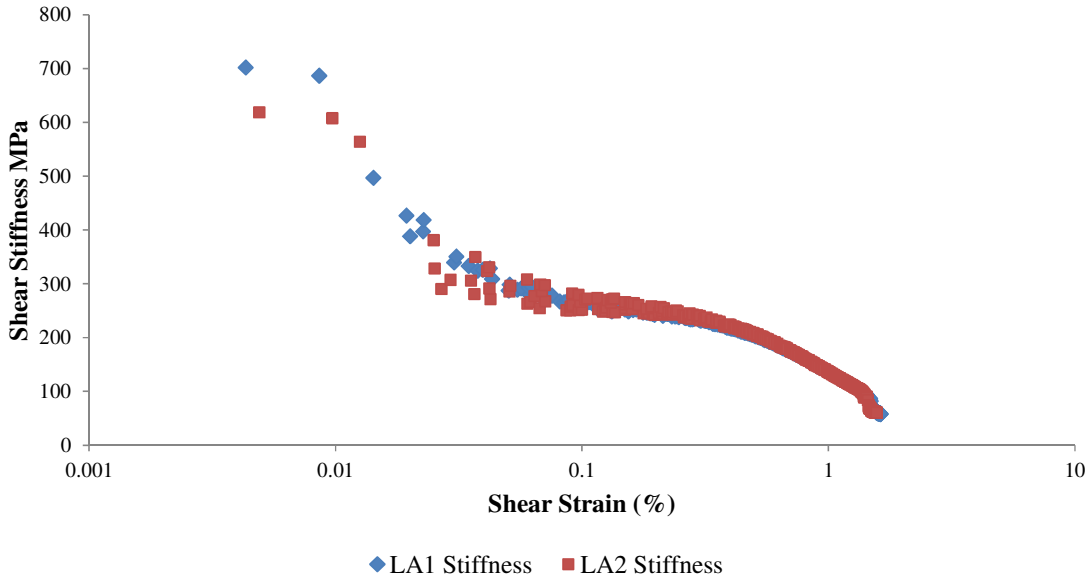

Figure 4.37: Good correlation between LA1 and LA2 derived shear stiffness vs shear strain data using fixed / rigid method.

4.6. CALCULATION OF CHANGING CROSS SECTIONAL AREA

Knowing the cross sectional area of a sample throughout a triaxial test is very important as it is required in order to calculate axial stress. During the course of a triaxial test the cross sectional area of a sample changes in response to the stress state under which it is subjected. During saturation the area will increase as the sample swells and during consolidation the opposite will occur. During a compressional shearing stage the cross sectional area of a sample will increase, although the amount by which it appears to do so is largely dictated by the method used (either by direct or indirect measurements or via simple calculations). It has been noted, however, that all these methods carry potential sources for error / limitations.

BS1377-8:1990 requires a known initial sample area (A_0), which is then modified during consolidation using equation 4.2 to find the area at the end of consolidation (A_c).

$$A_c = A_0 \times \left(1 - \frac{2}{3} \times \frac{\Delta V_c}{V_0}\right) \qquad 4.2$$

Where (ΔV_c) is the change in volume of a sample during consolidation (measured from back volume change). This method makes the assumption that a specimen will deform as a right cylinder, and that there is a known relationship between axial and radial strains, as shown in equation 4.3:

$$L_c = L_0 \times \left(1 - \frac{1}{3} \times \frac{\Delta V_c}{V_0}\right) \qquad 4.3$$

Where L_0 is the original sample length and L_c is the modified length following consolidation. It should also be noted that the BS1377-8:1990 does not recognise sample area changes to occur during saturation, as all water introduced to the sample is assumed (wrongly) to be displacing air, making little allowance for swelling.

During undrained compressional shearing the BS1377-8:1990 uses an assumed relationship between the known, measured axial strains (ε_a) and the calculated radial strains (assuming a poisons ratio of 0.5) to provide a modified area (A_s), as shown in equation 4.4:

$$A_s = \frac{A_c}{1 - \varepsilon_a} \qquad 4.4$$

This method assumes the sample deforms as a right cylinder and does not take into consideration the existence of bedding errors (exaggerating axial strains), end effects (and barrelling), or the possibility of materials to behave in a non-uniform way (such as heterogeneous materials or materials prone to dilation).

During drained compressional shearing (with measurement of volume change) the BS1377-8:1990 incorporates measurements of back volume change, however makes similar assumptions to those stated in the undrained test, as shown in equation 4.5:

$$A_s = \frac{1 - \varepsilon_v}{1 - \varepsilon_a} \times A_c \qquad 4.5$$

Likewise, the GDS programme used during all tests makes similar assumptions when calculating a changing area. Due to the way in which both the axial strains and volumetric strains are linked to the indirect measurement of cross sectional area, any excessive bedding errors or excessive movement of the external axial LVDT during docking or assembly will manifest itself as large changes in cross sectional area.

An example of this can be seen in Figure 4.38 where the actual cross sectional area of the sample at the beginning (and indeed end) of docking is around 4800mm^2, however

due to apparent axial displacements of 14mm whilst the cell was being assembled, the calculated area according to the GDS software is 5200 mm^2 by the end of assembly.

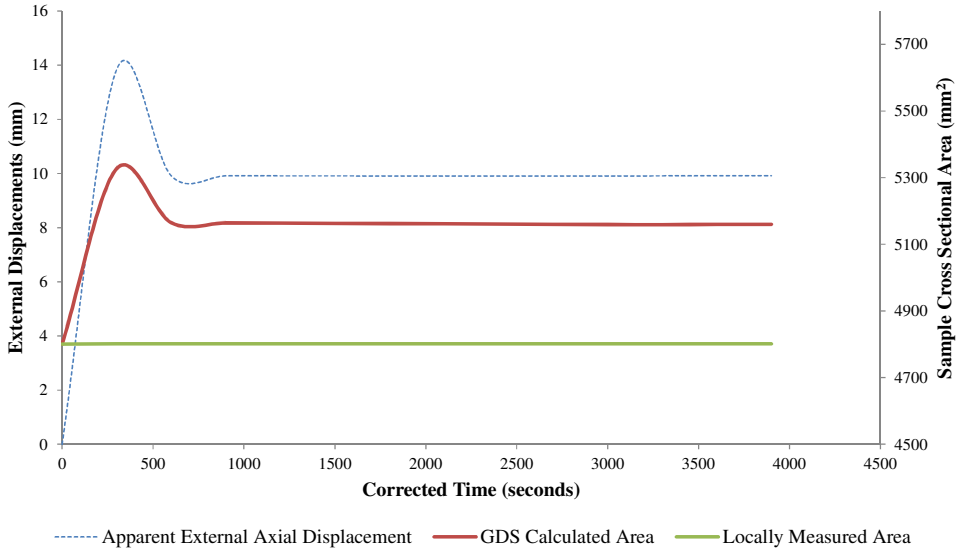

Figure 4.38: Errors in the automated calculation of cross sectional area introduced during cell assembly and docking.

Also shown on Figure 4.38 is the cross sectional area calculated using the locally measured radial displacements. These show that during assembly there is no change to the area of the sample.

It is possible to avoid this miscalculation of area using the GDS software by starting the logging process after the cell is fully assembled and once docking has been carried out. Whilst this would appear to provide more accurate estimates of cross sectional area it is not advised. Logging during the initial stages of assembly and docking is essential, as any real strains that are generated (and recorded by the local gauges for example), no matter how minor, would risk going un-recorded, skewing all results thereafter.

One way to overcome this problem is during post processing, by introducing an offset to the GDS data, putting calculations closer in line with those measured directly on the sample via local strain gauges. Once this is carried out, the calculated areas between the two methods fall into good agreement for the majority of the test duration (although all stresses need to be manually recalculated to incorporate these adjusted areas). This can be seen in Figure 4.39.

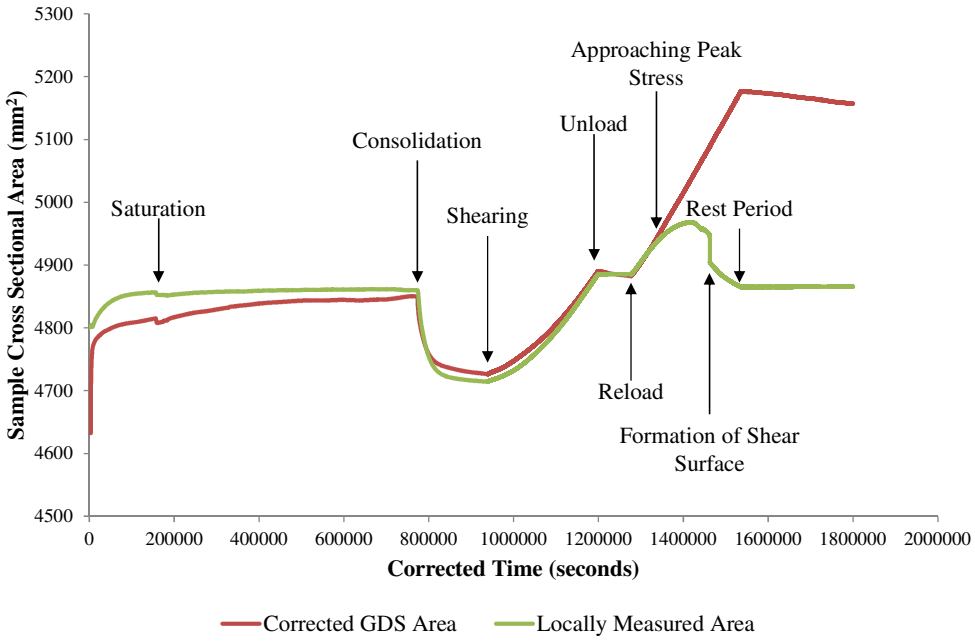

Figure 4.39: Automated calculation of area with offset (corrected GDS area) compared with calculation of area using local direct measurements.

Relying exclusively on the measurements of diametric displacements provided by the local gauges is tempting, as this would result in all calculations of stresses and strains to have originated from 'local' apparatus, minimising the effect of bedding and allowing other common sources of error (including accurately measuring cross sectional area increase of samples during saturation) to be monitored throughout a test. Unfortunately this method has the limitation that the radial strain gauge is located at the centre of the sample at the point most affected by end effects (barrelling).

A more significant problem is that of the behaviour of the sample once shearing begins, as peak stresses are approached and yielding begins, large radial displacements may be measured. This is particularly true of materials displaying a degree of brittle behaviour, and as a good shear surface develops the accurate measurement of cross sectional area becomes very difficult (as shown in Figure 4.39 post failure). It is also possible for the Hall Effect Gauges to 'dislocate' if the strains developed are very high (although this is generally not seen and results should be discounted following the point of dislocation in both the radial and axial gauges).

Figure 4.40 a) shows comparisons between the three methods of calculating area (namely using the raw GDS calculations, the corrected GDS calculations and finally those employing only local direct measurements) in terms of calculated deviator stress vs time and Figure 4.40 b) shows the equivalent shear stiffness vs shear strains from the

same test. The two figures demonstrate well the variations caused by adopting different methods of calculating sample cross sectional area.

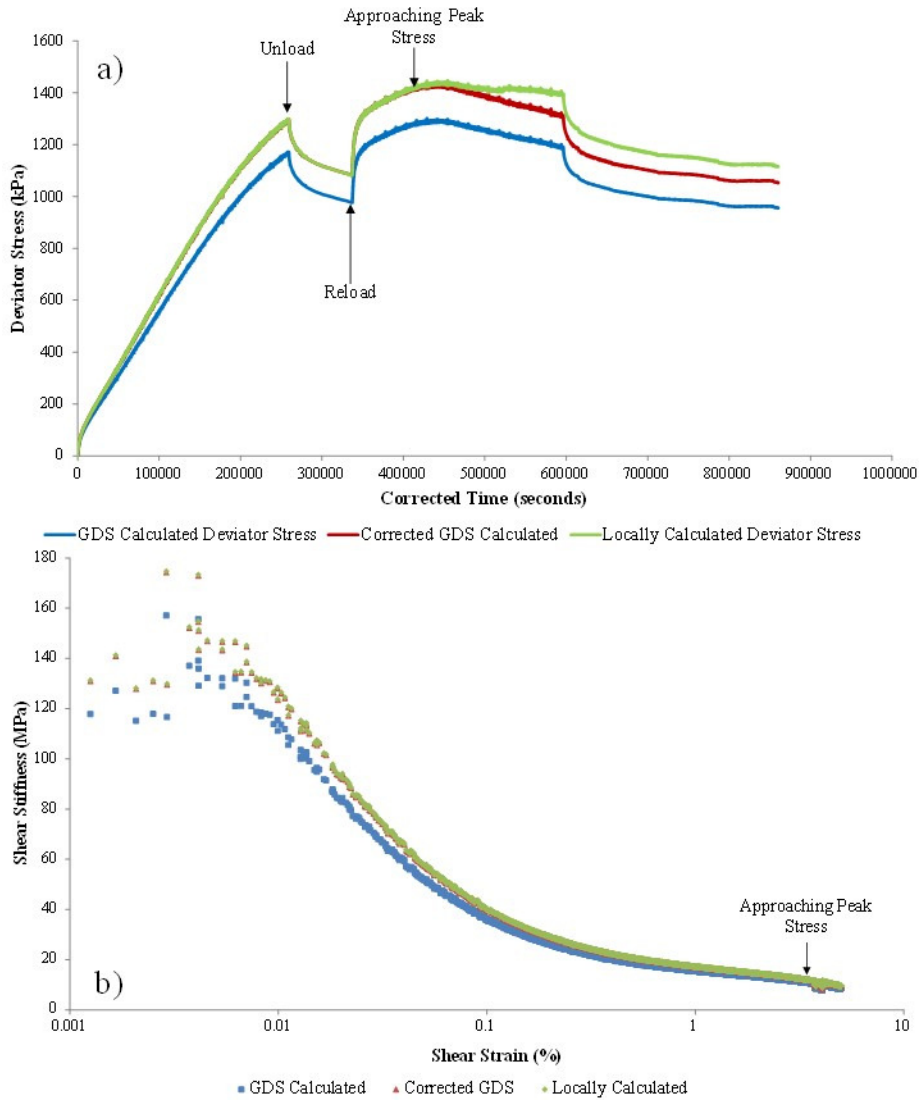

Figure 4.40: Comparison between a) Deviator stress and b) Shear Stiffness using the three methods of calculating area.

Using the raw GDS calculations without making corrections will underestimate both stiffness and strength for the duration of the test, as errors brought about during setup will manifest as increased cross sectional area. It is therefore important that post processing is carried out so that more realistic mechanical properties may be recovered.

The corrected GDS data and the data employing direct local displacement measurements show a very good correlation up until the point of yielding as the peak stress is approached where upon the two methods provide higher (corrected GDS) and lower (locally measured) estimates of deviator stress respectively. In terms of small

strain shear stiffness degradation, these two methods provide highly comparable results, even on the approach to peak stress.

In the interests of repeatability along with reducing time spent in post-processing, the direct method (using local radial measurements) is suggested for the calculation of changing area during triaxial testing. As small strain stiffness is the key concern of the triaxial tests, the minor variations to the post-failure stresses that this method introduces are considered to be negligible. In addition to this, shear strain (and therefore shear stiffness) calculations within this thesis are based upon the data recorded from local measurements and so using this information to calculate area changes and deviator stresses provides good continuity. Direct measurements of radial displacements are therefore adopted for the calculation of cross sectional area throughout this thesis.

Using local strain measurements in the calculation of stresses must be carried out in post processing, as the GDS software available at Newcastle University is not set up in such a way as to override the GDS calculations. This means that during saturation / consolidation stages where the Advanced Loading module is set to maintain q = 0kPa conditions, there may be minor discrepancies brought about by the incorrect calculation of area that cannot be corrected in real time. Figure 4.41 shows a comparison between the raw GDS recordings of deviator stress during saturation / consolidation and those calculated during post processing using local strain measurements.

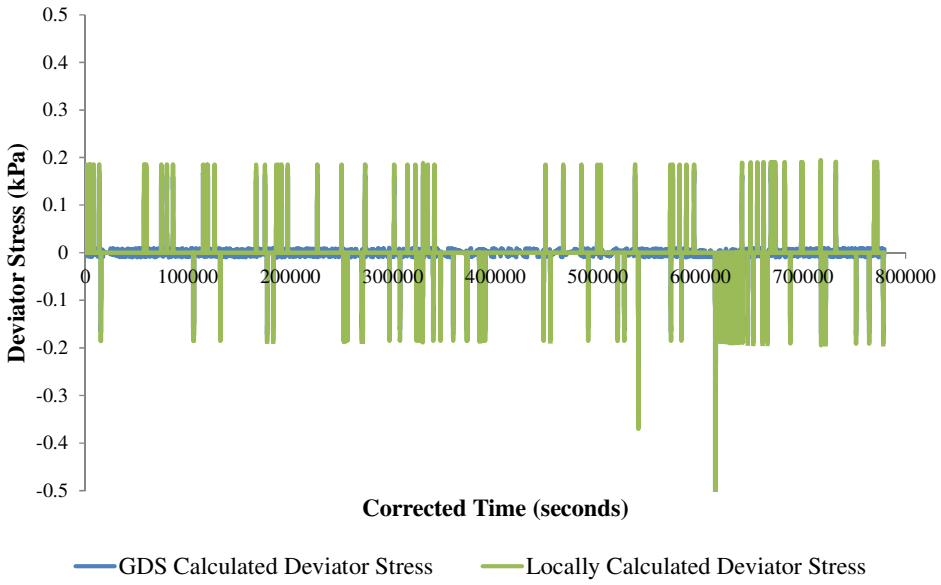

Figure 4.41: Comparison between automated calculation (GDS) of deviator stress during saturation / consolidation and those calculated using local displacements.

Whilst the GDS raw data maintains a state of q = 0kPa throughout both saturation and consolidation, by recalculating area using local displacement measurements fluctuations in deviator stress do occur. However, these fluctuations are within a very small range (±0.2kPa and a maximum fluctuation of -0.5kPa) and are therefore considered negligible for the purposes of the majority of testing carried out within this thesis. These fluctuations are likely to be associated with the noise of the Hall Effect transducers.

4.7. INSTALLATION / INTERPRETATION OF BENDER ELEMENTS

In order to carry out Bender Element tests upon a sample in triaxial apparatus, the apparatus itself must first be modified. This included the installation of a custom base pedestal and top cap along with modified cindered brass porous disks (as shown in Figure 4.42)

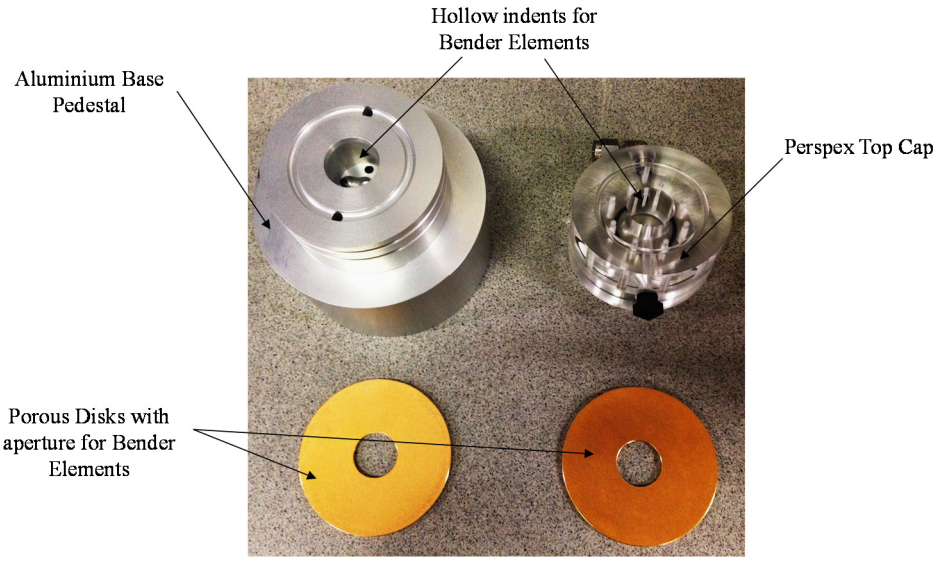

Figure 4.42: Photograph showing modified base pedestal, top cap and porous disks to allow installation of Bender Elements.

The top cap was created in such a way as to allow the 'fixed' docking method to be used in conjunction with Bender Element tests, as shown in Figure 4.43.

Figure 4.43: Photograph showing screw thread on the top cap used in Bender Element tests.

The Bender Elements ultimately feed into a unique serial pad which is then connected to a control computer installed with the latest GDS Bender Element Software (GDSBES) Package (version BENDERS 2.2.4). It should be noted that this is controlled manually and is not a part of the GDS Triaxial package. Because of this, any data gathered via the GDSBES needs to be manually checked in post processing in order to 'sink' the triaxial data and Bender Element data to the same time intervals.

To prepare a sample for testing, first a groove must be made into the sample to accommodate the Bender Elements. This is not generally required on samples of clay, however due to the stiffer nature of soft rocks; this was needed as the Elements could not be pushed into the sample without breaking. A 3mm deep, 15mm long and 5mm wide groove was cut using a fine chisel. It is important that the orientation of these grooves is the same on both the top and bottom end of the sample so that they will align with the installed Bender Elements. This groove is created by hand using slow movements (with no percussive element that could fracture the sample). The groove is shown schematically in Figure 4.44.

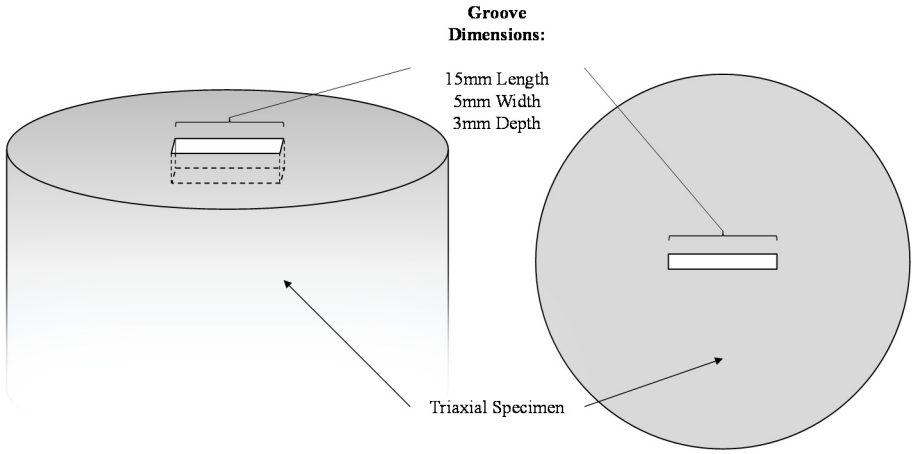

Figure 4.44: Diagram showing the location and dimensions of 'groove' to house Bender Elements, a) isometric and b) plan view. Diagram NTS

These grooves are then filled with a paste comprising of the wetted offcuts of the specimen itself, then the sample is placed upon the pedestals in a careful manner ensuring the Bender Elements fit firmly into the grooves.

Once the sample is installed into the triaxial apparatus and the GDS software set to 'just log', the GDSBES specific information can be inputted including specifying the height of the sample in question (in mm), followed by inputting the desired frequency of sampling and sample time. These were set to 2000ksamp/sec and 5ms respectively and

an automatic gain option selected (in which the GDS software selects the most appropriate level of gain). For the test carried out within this thesis a sinusoidal source wave with a period of 0.2ms and an amplitude of 14V was used. Samples may then be periodically subjected to an induced source wave throughout testing, with both source and received wave results being automatically stored within the GDS BES system ready for saving as .bes files.

To assist in the interpretation of results a number of methods are available, namely the Time Domain, Frequency Domain or cross correlation (Fonseca, et al., 2009); (Chan, 2010). Rees, et al (2013) suggest using the Time Domain method, and have provided a piece of software (the GDS Bender Element Analytical Tool, or BEAT) which works in conjunction with the data obtained using GDS BES. This is also the method used most frequently by a number of other authors, although specifics regarding the interpretation of findings varies between authors (Viggiani & Atkinson, 1995); (Jovicic & Coop, 1996); (Karg & Haegeman, 2005); (Black, 2009); (Yamashita, et al., 2009); (Fonseca, et al., 2009); (Chan, 2010) (Camacho-Tauta, et al., 2012); (Rees, et al., 2013). The Time Domain method is used within this thesis.

The GDSBEAT is an 'Add In' for Excel, and processes saved .bes files, attempting to locate four points within the morphology of the received waveform in order to calculate travel times (in ms). These four points are shown in Figure 4.45 and are termed the first deflection (A), first 'bump' (B), zero crossing (C) and first major peak (D), all representing increasingly large travel times.

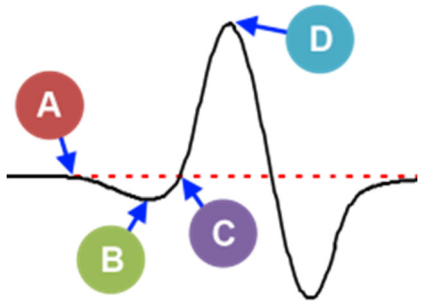

Figure 4.45: Idealised morphology of received waveform showing points A – first deflection, B – first 'bump', C – zero crossing and D – first major peak. (Rees, et al., 2013)

Whilst the BEAT is generally good at locating these points, received waveforms that do not broadly conform to the idealised morphology can sometimes be misinterpreted, as shown in Figure 4.46 a). This can often be remediated by inverting the sign of the

output and re-running the analysis (as this does not affect the travel times) as shown in Figure 4.46 b), creating a much more 'idealised' pattern.

a)

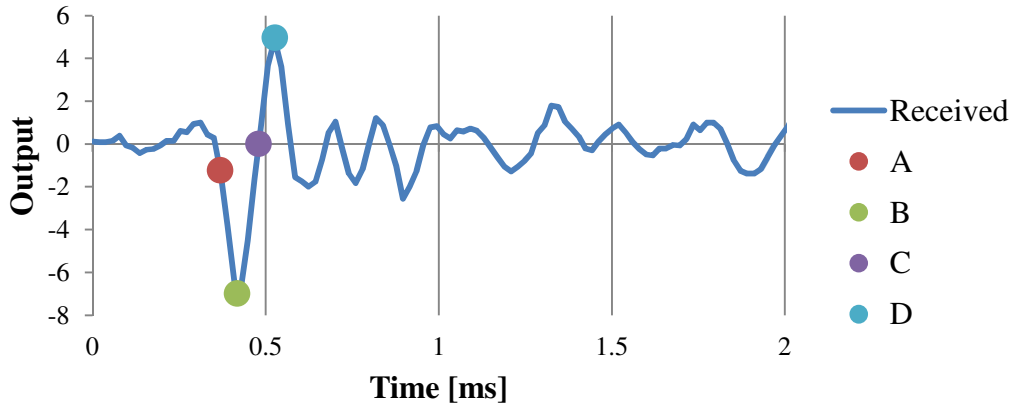

b)

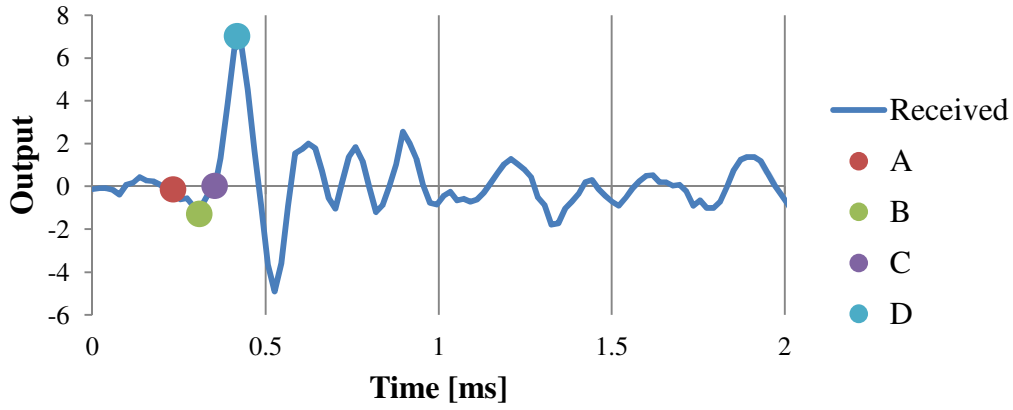

Figure 4.46: Diagram showing a) received waveform with incorrectly located points A-D and b) reversed waveform with correctly located points A-D using BEAT.

A degree of engineering judgement is also required, particularly with locating the first deviation point as the iterative calculation used by BEAT struggles to cope with noise in the received waveform.

Once a given waveform is interpreted, a seismic wave velocity (Vs) may be calculated. This uses the following formula (Ferreira, et al., 2014):

$$V_s = \frac{L}{Ts} \qquad 4.6$$

Where L is the length of the sample at the time of testing (distance between Bender Elements) and Ts is the travel time from a given point on the waveform. To accurately obtain the sample length at any given time during a test it is crucial that axial deformations be measured and 'sinked' with the sampling times of the Bender Elements. This was done be triggering a new testing stage with a unique number at the moment of sampling using the Bender Elements.

Ultimately shear stiffness at zero strain (G_0) may be determined using the following formula (Ferreira, et al., 2014):

$$G_0 = \rho \times V_s^2 \qquad 4.7$$

Where (ρ) is the bulk density at the time of sampling with Bender Elements. In order to calculate this accurately it is important that the amount of water entering the sample during saturation is known, as well as any water mass leaving the sample during the various consolidation stages. In addition, the radius of the sample is measured using Hall Effect local strain gauges, which when coupled with axial deformations allow accurate volume changes to be calculated, and therefore bulk density.

This procedure allows the estimation of G_0 to be calculated for all four points (A-D) using the Time Domain method.

4.8. APPLICATION OF DIC TO THE INDIRECT TENSILE STRENGTH TEST

This sub-chapter presents results from two experimental studies aimed to demonstrate the benefits of using Digital Image Correlation (DIC) as a substitute to traditional local strain gauges during Brazilian testing, as well as making recommendations for its application to soft rocks. All tests in this chapter are carried out on samples of Springwell Sandstone, however findings were pivotal in shaping the finalised soft rock tensile strength testing methodology. The first study applies the DIC technique to qualitatively and quantitatively assess the influence of different loading geometries on strain localisation across the surface of a sample via comparisons between ASTM, ISRM and flattened disk loading methods (Wang & Xing, 1999). The second study assesses the optimum thickness (t) to diameter (D) ratio via assessments of out-of-plane displacements.

It is not the aim of this thesis to provide exhaustive descriptions of either the current understanding of the Brazilian in-direct tensile test theory, or the development of DIC, however brief backgrounds are presented in order to add context to the two studies.

Findings from this study are published in a journal article entitled ‘The application of digital image correlation to Brazilian testing of sandstone’ (Stirling, et al., 2013).

4.8.1. *BRAZILIAN TEST AND DIC BACKGROUND*

The Brazilian test is an indirect tensile strength test most commonly used on rock samples (although has been known to be applied to soils) via the application of load across the diameter of a disk shaped specimen. In theory (assuming 2D biaxial linear elasticity.), the sample will fail in a brittle manner according to Griffith failure criterion at or around the centre of the disk where tangential stresses ($\sigma_{\theta y}$) overcome the material's uniaxial tensile strength and where radial compressive stress (σ_{ry}) is approximately three times greater as shown in Figure 4.47, where, r = radial distance, R = disc radius and P = the applied load (Yu, et al., 2009).

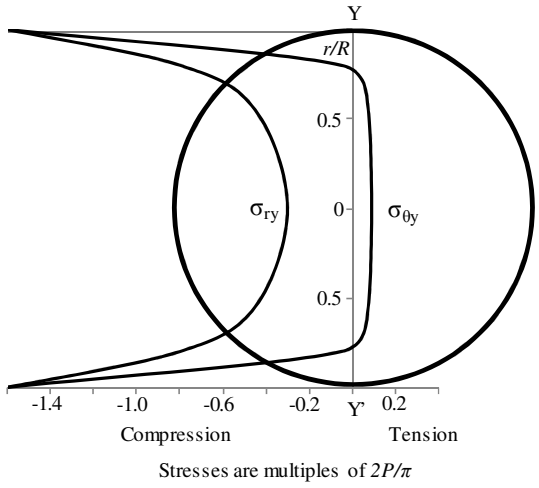

Figure 4.47: Stress distribution along line YY' in the Brazilian test (Fairhurst, 1964)

It should be noted that a failure of the disk within the sample centre is vital in ensuring a valid test, and that failure did not initiate from unwanted crushing at the sample ends.

In order to measure the development of local strains during Brazilian in-direct tensile testing, several authors have attempted affixing strain gauges to the surface of specimens in both horizontal and vertical orientations (Hondros, 1959); (Yanagidani, et al., 1978); (Jianhong, et al., 2009); (Dave, et al., 2011). This technique provides accurate results over a localised area, however is both time consuming and difficult to prepare. In addition, this method is unsuitable for use with weak, friable lithologies, as the strains measured may affected by the stiffness of the gauge and adhesive.

DIC is a means of measuring and recording the development of deformations across a sample surface in three dimensions (without the need for direct contact with the sample) via the capture of successive images, which can then later be calculated into strains via

the use of computer based cross correlation. The use of computer assisted image analysis tools for use in the measurement of deformations during material testing was first being used during the 1980s (Peters & Ranson, 1982); (Sutton, 1983); (Stirling, 2014)and is used in a form similar to that of its modern day equivalent by Chu, et al (1985). This method has since been applied to many areas of material testing, although its use in geotechnical engineering is a recent development (Sutton, et al., 2000).

This method uses two (or more) calibrated parallax cameras to obtain high-resolution images which, via comparison between initial and deformed states, may be used to calculate strains. By first coating a sample in a random, high contrast speckle pattern, displacements may be tracked by the cameras on the basis of pixel distortion. The apparatus can measure, to a high degree of accuracy, the development of strains in both the vertical and horizontal directions whilst also allowing out-of-plane displacements to be assessed.

Since the correlation of individual pixel distortions is difficult, a small area of approximately 2-30 pixels square is used instead. This area is referred to as the subset, within which light intensity distribution or the 'grey level' is assumed not to change during a given test. An example of a subset deformation is given as Figure 4.48, which shows the undeformed reference image a) followed by images b) and c) which depict incremental deformation. This changing subset can then be identified as the test progresses using its unique 'grey level', as defined in the reference image a). The displacement of the initial image may then be determined, from which strains may be calculated (Stirling, 2014).

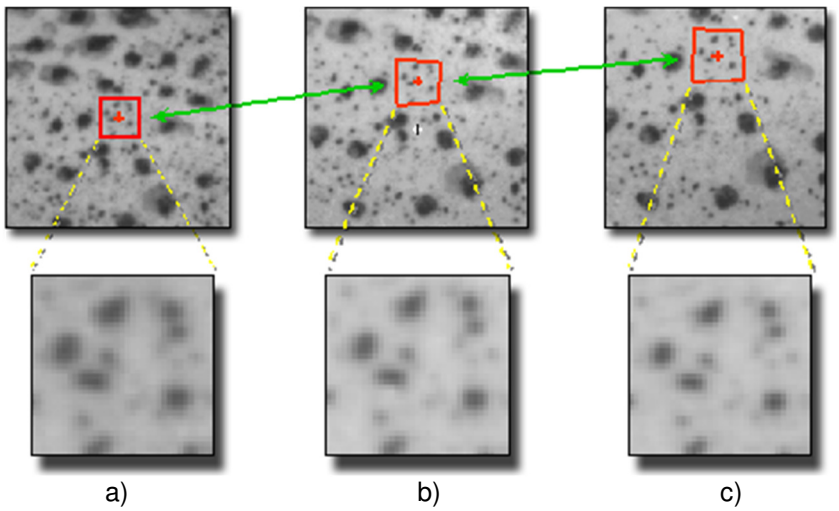

Figure 4.48: Example of a progressively deforming subset (Correlated Solutions, 2010); (Stirling, 2014)

The function used to match the deforming subset is based on cross-correlation, show by the following formula:

$$C(x, y, x^*, y^*) = \frac{\sum F(x,y)G(x^*,y^*)}{\sqrt{\sum F\,(x,y)^2 \sum G(x^*,y^*)^2}} \qquad 4.8$$

Where F(x, y) represents the 'grey level' at the point (x, y) in the reference image and G(x*, y*) represents the 'grey level' at point (x*, y*) in the deforming image. The coordinate change from (x, y) to (x*, y*) represents the deformation that has occurred between the two images (Correlated Solutions, 2010); (Stirling, 2014).

Cross correlation is started at a user defined 'seed point', from which the results obtained are used by the algorithm to form the analysis at the second point and so on in an iterative manner until the entire sample area is analysed (Stirling, 2014).

DIC has several advantages over traditional strain gauges. These include; its relative ease of use following setup, its ability to measure the full strain field rather than discrete lengths/sections and (most importantly for this thesis) its compatibility with soft and friable sample surfaces, as traditional local strain gauges are difficult to adhere.

4.8.1. *TESTING METHOD*

All testing was conducted using an Instron 5585H universal testing machine. This device is able to apply either a constant loading rate or rate of displacement. Both the ISRM and ASTM standards recommend stress controlled testing, applying a constant rate of load such that samples will fail within a reasonable timeframe. In order to achieve failure in accordance with these standards, a loading rate of 3.225kN/min was back-calculated from the average tensile strength of Springwell sandstone (3.725 MPa) as observed by Alsayed (2002) with a desired time to failure of approximately 5 minutes. This rate was used during all stage 1 tests. Rates used during stage 2 tests are derived with respect to the thickness of the samples tested.

Two cameras were mounted on a tripod and profile bar then centred symmetrically about the sample position. The cameras were fitted with telephoto lenses of 28mm focal length. A camera to sample distance of approximately 0.50m was used and cameras formed approximately a 30° angle of incidence, providing the desired degree of out-of-plane resolution as set out in the user guide (Correlated Solutions, 2010). The DIC setup is shown in Figure 4.49.

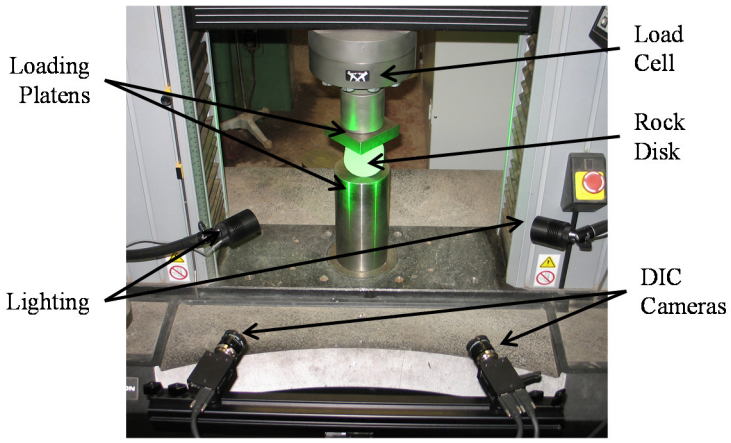

Figure 4.49: DIC and testing rig setup

Before testing of the sandstone samples, the DIC setup was checked to confirm it correctly interpreted displacements by cross checking it with the Instron 5585H built in displacement transducers. Markers were placed on the front edge of both the upper and lower loading platen that could be tracked using the VIC-3D inspection tool in post processing. A rubber sample was mounted between the two platens and a constant load applied whilst recording with the DIC. The measurements from both methods are plotted against each other in in Figure 4.50 and it can be seen that they correlate well.

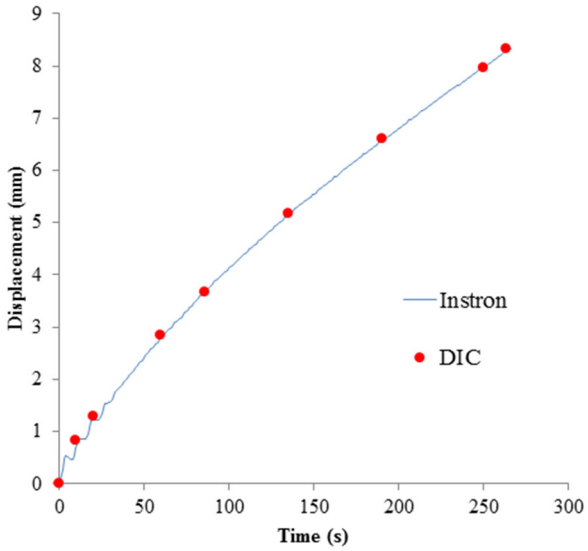

Figure 4.50: Calibration of the DIC against Instron external strains using a rubber sample.

In preparing the samples for DIC, a black-on-white speckle pattern was applied to the prepared face using fine aerosol paint to achieve a 50:50 coating that is both non-repetitive and anisotropic (Figure 4.51) (Correlated Solutions, 2010). The Vic-Snap DIC software was used to monitor samples throughout testing (Correlated Solutions, 2010) and used to confirm the 2-30 pixels per speckle requirement. Additional lighting was

used in order to maintain sufficient contrast of the pattern. Image capture was conducted at intervals of 50ms (20fps). This was deemed more than sufficient to record sample deformation. A reference image was captured prior to application of load in order that subsequent relative sample deformation could be computed.

Following compilation of test images, an area-of-interest (AOI) was marked on the reference image consisting of the speckled face of the sample (Figure 4.51). An analysis grid and two analysis seed points, from which analysis begins, were marked in the AOI where least deformation was expected i.e. away from loading contacts and the disc centre. Two seed points were used to ensure the continuation of analysis on either sides of the potential fracture. Due to the prescription of this grid (and only complete squares being analysed (Figure 4.51)), a varying area around the circumference of the AOI is lost despite a fine grid spacing being set. This resulted in the flattened geometry of W0.5_ samples not being apparent in the post-processed output.

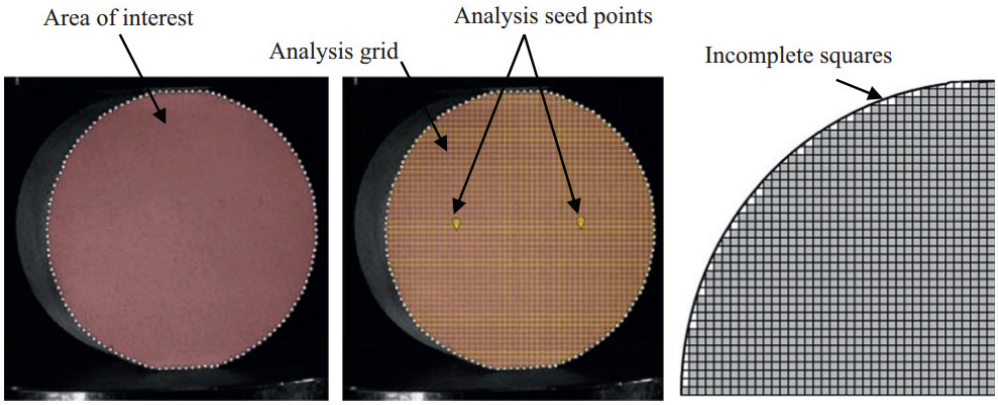

Figure 4.51: Reference image and analysis area selection

A single level of grid discretisation was used for all analyses as this relates to the use of a consistent speckle pattern. Once the analysis specification was made using the reference image, all subsequent deformation of the speckle pattern in the test images was then tracked using the system software, Vic-3D (Correlated Solutions, 2010). Minor flaws in the contoured output may result from the accumulation of paint, highlighting the importance of an even speckle pattern.

4.8.2. *STUDY 1 - LOADING GEOMETRIES*

Fairhurst (1964) stated that tensile strengths calculated from Brazilian testing on rocks are highly dependent upon the method of loading. Three of the most common loading methods are shown as Figure 4.52. Load is denoted with a (P) and the area over which the load is applied is depicted by black bold arrows.

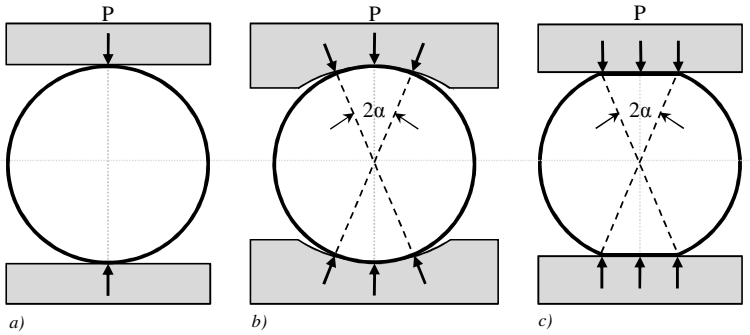

Figure 4.52: Loading methods a) Flat-point (ASTM, 1984), b) Arch-arch (ISRM, 1978) and c) Flat-flat (Wang & Xing, 1999)

ASTM standards suggest the use of flat platens, applying load to the samples at diametrically opposite ends (Figure 4.52a), and recommends t/D ratios of between 0.2 – 0.75 as being valid (ASTM, 1984). This method has been criticised within the literature as crushing at the loading points causes failure to occur distal to the disk centre (Hudson, et al., 1972); (Wang, et al., 2004). Andreev (1991) and Yu, et al. (2009) attempted to minimise the point load crushing of the sample ends by use of 'cushions' made from materials of a range of stiffnesses to decrease localised stress concentrations. Whilst this succeeded in reducing crushing, it introduces additional uncertainties in calculating the stresses and strains during testing along with increasing sample preparation time. Work conducted by Andreev (1991) highlighted the inaccuracy in the application of cushions with respect to the transfer of load to the disc itself. The suggested use of cardboard and plywood in the ASTM standard is arbitrarily defined and in the interest of consistency between methods, no cushioning is used.

The ISRM standard recommends the use of a curved platen, with a radius 1.5 times greater than the sample, as shown in Figure 4.52b. It also suggests using a t/D ratio of 0.5 (ISRM, 1978). The ISRM method requires loading platens of varying curvature depending upon the sample being tested to ensure a repeatable 2α angle of loading is achieved across the sample's circumference. This will often mean manufacturing bespoke platens, or else risking tests being criticised as invalid.

To address these concerns, Wang & Xing (1999) suggested a modified Brazilian disk geometry, with flattened, parallel surfaces on the top and bottom of the disk that create a good contact between sample ends and loading platens without generating point loads and associated crushing, as shown in Figure 4.52c. Wang & Xing (1999) suggested that the flattened surfaces form an angle of 2α angle of approximately 20°, assisting in the initiation of fracturing at the disk centre (Wang, et al., 2004); (Yu, et al., 2009).

The ISRM and Wang & Xing (1999) methods share a common 2α angle, defining the boundary of the loaded area as shown in Figure 4.52b and c. The area subject to loading in the ISRM method is noted to be comparatively greater than that of the Wang & Xing (1999) as it is applied over a curved surface.

In order to compare these loading geometries, samples of Springwell Sandstone were cored from a block sample using an 81.5mm external diameter diamond core barrel. The discs were finished on a surface grinder to ensure their faces were flat and that the t/D ratio was accurate to within 0.01. Both the ASTM and ISRM methods require the use of circular discs, samples that required a flattened disc geometry were cut to the specification of Wang & Xing (1999) as shown in Figure 4.53.

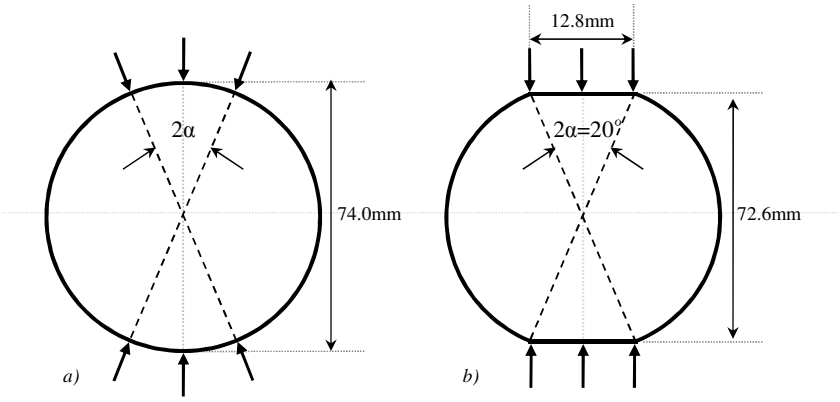

Figure 4.53: Rock disc geometries; a) ISRM and ASTM and b) Flattened (Wang & Xing, 1999).

The rock disks were oven dried for a period of 48 hours in 105ºC ovens. A t/D ratio of 0.5 was maintained for the purpose of comparison between tests and a loading rate of 3.225kN/min was used. Table 4.1 details the testing programme used during study 1.

Table 4.1: Sample geometries during study 1.

Test ID	t/D Ratio	Testing Method	No. of Samples Tested	Loading Rates (kN/min)
I0.5_	0.5	ISRM (1978)	3	3.225
A0.5_		ASTM (1984)	3	
W0.5_		Wang & Xing (1999)	4	

All samples were loaded until failure, following which tensile strengths (σ_t) were calculated using equation 4.9. This assumes materials display linear elasticity until failure and that maximum tensile stresses are induced normal to the loaded diameter such that failure occurs at the disk centre. The tensile strength of samples cut with the flat loading geometry is calculated using equation 4.10, with the introduction of

coefficient, *k,* which is related to the α angle (Figure 4.53b). When $2\alpha=20°$, as it does in all flattened tests within this thesis, k=0.9644 (Wang, et al., 2004).

$$\sigma_t = \frac{2P}{\pi Dt} \qquad 4.9$$

$$\sigma_t = k \times \frac{2P}{\pi Dt} \qquad 4.10$$

Table 4.2 shows the calculated tensile strengths of all samples tested during study 1.

Table 4.2: Tensile strength of samples during study 1.

Test	Testing Method	Failure Load, *P* (kN)	Tensile Strength, σ_t (MPa)
A0.5_A	ASTM (1984)	14.30	3.32
A0.5_B		14.99	3.49
A0.5_C		13.77	3.20
I0.5_A	ISRM (1978)	14.71	3.42
I0.5_B		13.93	3.24
I0.5_C		10.10	2.35
W0.5_A	Wang & Xing (1999)	17.92	4.02
W0.5_B		18.49	4.15
W0.5_C		15.16	3.40
W0.5_D		18.54	4.16

Tensile strengths were derived from the load corresponding to failure as observed from the externally measured load-strain relationship (Figure 4.54). Failure is defined by an abrupt loss of stiffness often accompanied by a fracture (although not necessarily visually apparent) and where a constant loading rate may no longer be maintained. Prior to the failure load, no factures have developed and samples are assumed to behave in a linear elastic manner.

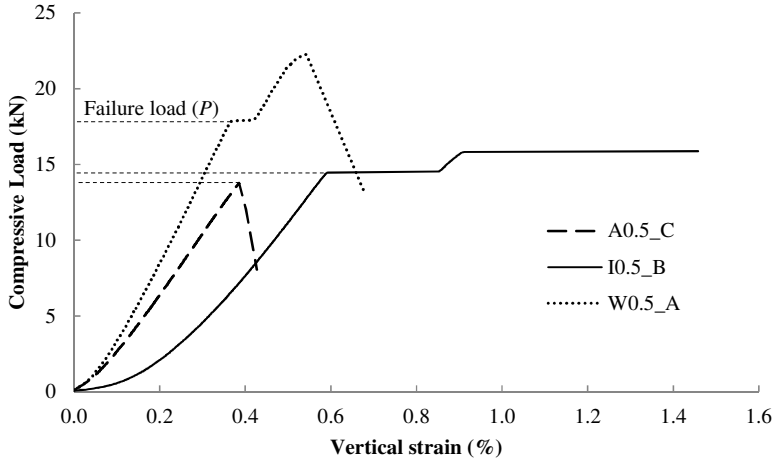

Figure 4.54: Representative load-strain results

Sample failure marked the end of tests carried out in accordance with ASTM standards, as samples fractured, rendering them unable to carry more load. The load-strain behaviour of samples tested following ISRM guidance and Wang & Xing, (1999) flattened geometry typically showed a temporary plateau following failure where load remained approximately constant and rapid vertical compressive straining was observed as the Instron attempted to maintain a constant loading rate. In these cases, the load imposed upon the sample continued to rise following this plateau until testing was stopped manually. This is due to the sample being constrained by the testing platens and beginning to shear. Omitting post-failure behaviour (caused by sample constraint), load-strain relationships are presented for each test in Figure 4.55.

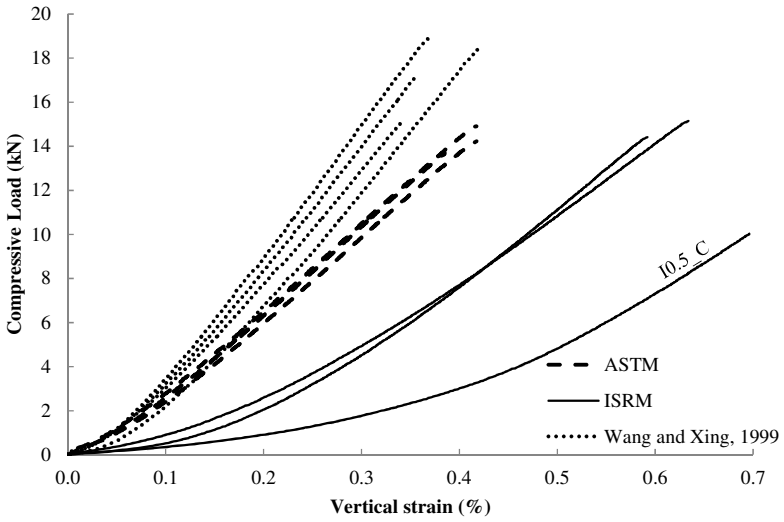

Figure 4.55: Compressive load - vertical strain data for study 1.

Results showed a high level of consistency in both stiffness and failure load within each testing method, with the exception of test I0.5_C, likely to be due to an unforeseen flaw within the sample. Samples tested using the flattened geometry showed the stiffest response to loading, failing at higher loads whilst undergoing less vertical strain than the ASTM and ISRM specifications. Tensile strengths of the ASTM and ISRM tests were similar. Externally measured strain behaviour of samples upon initial loading, however, differed greatly, with significantly higher vertical strains being observed using the ISRM setup. This is likely to be due to total displacements incorporating the additional compliance of the curved platens. Bedding effects are seen in the externally measured displacements of all three methods, manifesting as an initial soft response to load.

Vertical strain between the top and bottom of the disk were measured both locally (using DIC) and externally (using the Instron). By comparing representative tests from

each loading method, higher stiffnesses are captured using the DIC (which ignores bedding errors and localised sample crushing) than are seen when using only external vertical strains, as shown in Figure 4.56. By using these locally measured strains, comparable stiffness and failure strains are found for all loading methods, as would be expected for tests on the same rock. This is not seen when using external strain data.

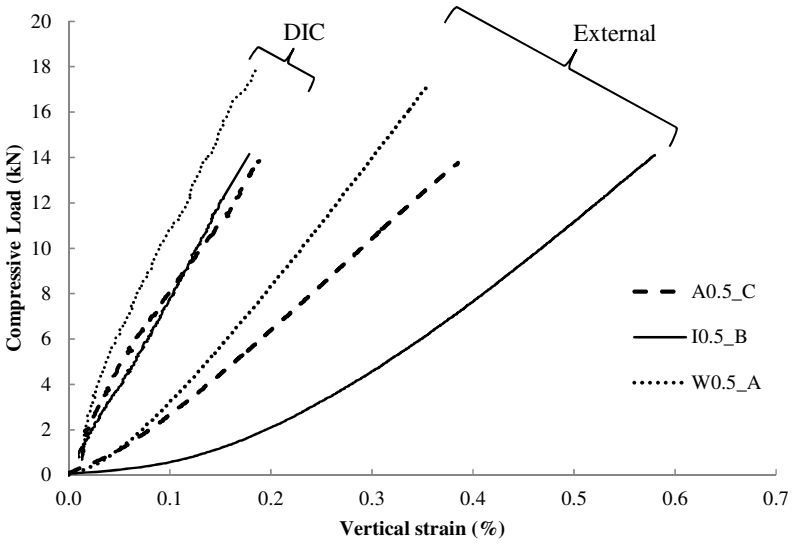

Figure 4.56: Load-corrected displacements recorded internally (DIC) and externally for representative samples

Post-fracture images from the three loading methods are shown in Figure 4.57. A representative ASTM sample (after reassembly) shows asymmetrical notches at the top and bottom of the sample as a result of crushing brought about by point loading (Figure 4.57a). The ISRM test shows the central fracture is typically accompanied by secondary fractures that open from the circumference at the outer points of contact with the curved platens, as shown in Figure 4.57b.

The growth of fractures during tests using the flattened geometry was easily captured due to their relatively slow stepwise propagation, as shown in Figure 4.57c-f. Figure 4.57c shows the flattened sample immediately prior to failure with no fracture visible. Subsequent images, taken at the times shown, depict the propagation of the fracture, which notably originates from the centre of the disk, as shown in Figure 4.57d. The final fractured state is presented as Figure 4.57f and shows the stepped geometry of the central fracture. Failure load (P) was taken at the instant the initial central fracture opened according to the load-displacement data, however it should be noted that the load continued to increase as the fracture propagated steadily through the sample until it spanned the whole diameter.

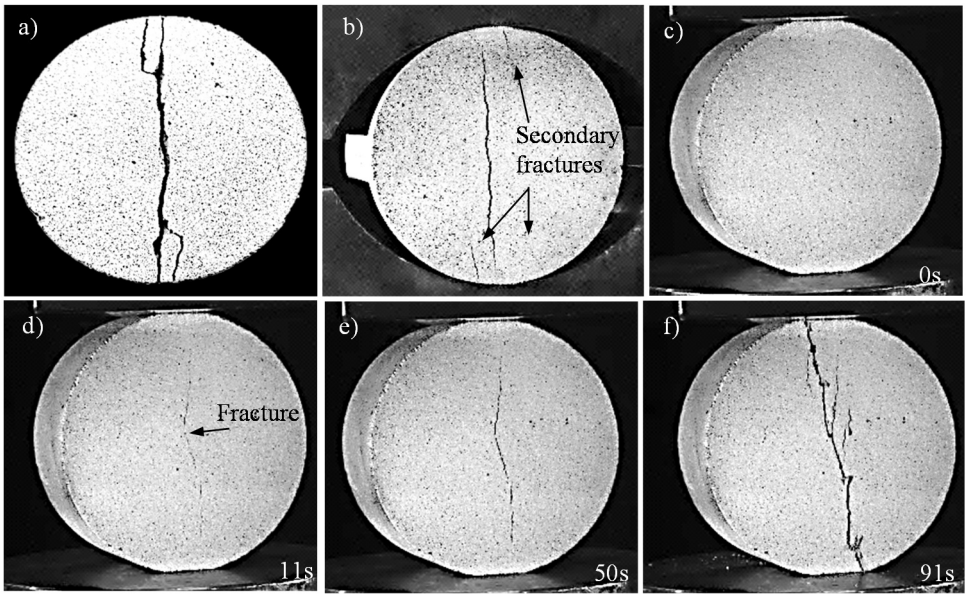

Figure 4.57: Samples during and post-failure a) Sample A0.5_A post failure, b) I0.5_B at onset of fracture and c-f) W0.5_A fracture growth post-failure

By examining the development strains locally using DIC, it is possible to compare the locations of strain concentrations between loading methods. For comparison, representative contour plots both horizontal and vertical strains are presented as Figure 4.58. Plots represent the sample state immediately prior to failure.

Qualitative assessment of Figure 4.58a (ASTM), highlights two distinct regions of horizontal extension located near the top and bottom of the disk. Compressive strains caused by loading can be clearly seen in Figure 4.58b with the greatest vertical compressive strains occurs at the edge of the disk. These regions of high vertical compression are accompanied by areas of maximum horizontal compression located at [A] in Figure 4.58a. This is interpreted as evidence of crushing, as the greatest compression is shown here in both orientations, corresponding well with the observed fracture pattern in Figure 4.57a.

Results from the ISRM loading method are shown in Figure 4.58c & d. Again, the areas of greatest compression are seen to be located to the top and bottom of the sample, however, due to the use of the curved-platens, these areas are not perfectly diametrically opposite. This eccentric behaviour has been observed by several authors and is due to the imperfect interface between the sample curvature and that of the loading platens (Hondros, 1959); (Jianhong, et al., 2009); (Wang & Xing, 1999); (Wang, et al., 2004). The lateral extent of the sub-vertical strains are shown to be comparable to that of the ASTM testing method despite a (theoretically) greater contact area, suggesting a degree of point loading.

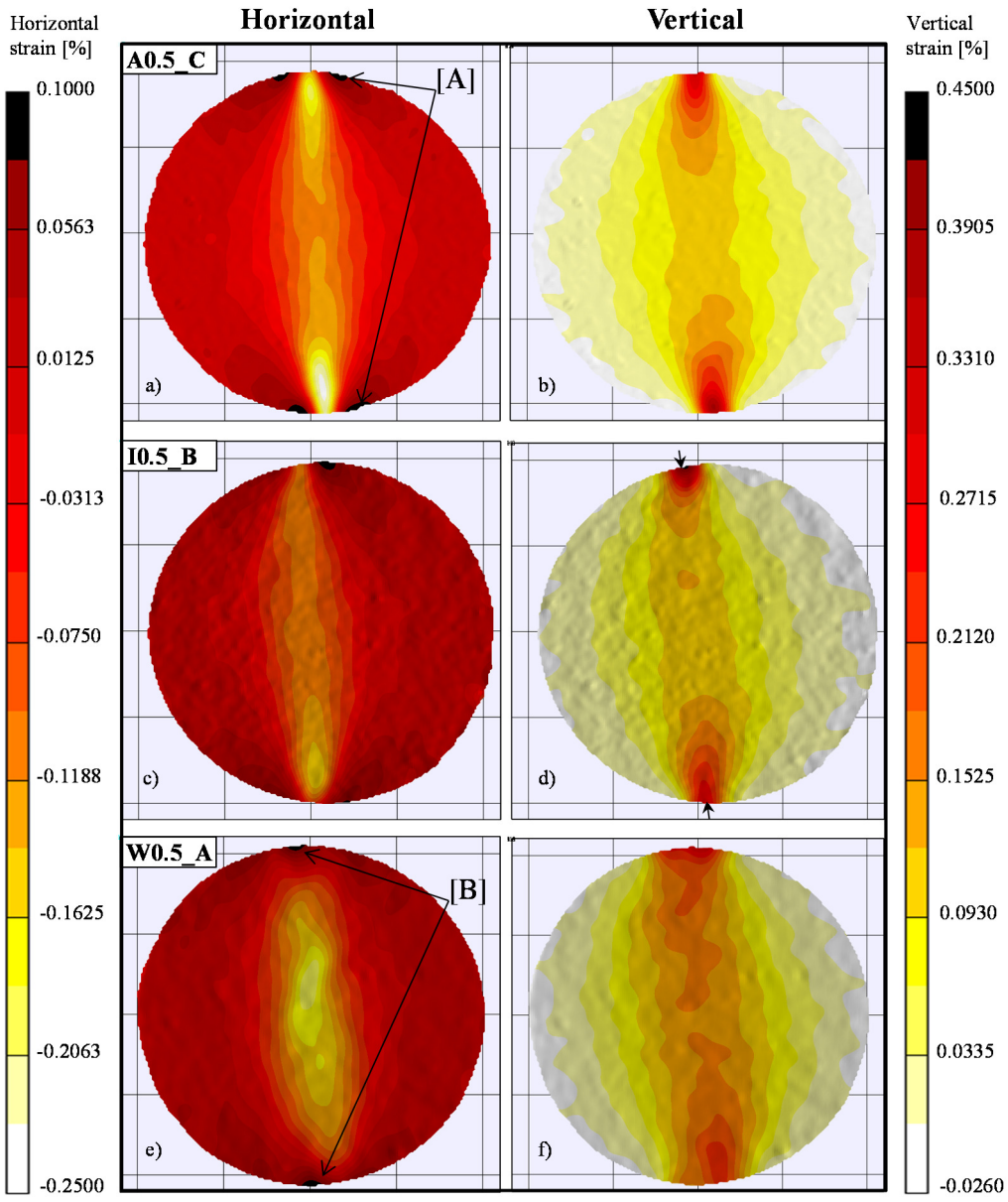

Figure 4.58: Horizontal and vertical strain distributions immediately prior to failure a-b) ASTM, c-d) ISRM and e-f) Flattened

Using the flattened disks, maximum horizontal compression is located at the loading ends of the disk (at [B] in Figure 4.58e) and is not associated with the extensional maximum strains. The dominant region of horizontal extension is observed to have formed at the centre of the disk, representing the greatest compliance with idealised theoretical failure criteria. In contrast to the ASTM and ISRM methods, the flattened disks display a broader distribution of vertical compressive strains along with lower overall magnitudes, as seen in Figure 4.58f. This is due to load being applied over a greater area of the disk circumference to that of the ASTM method, although the contact area should theoretically be similar to that of the ISRM loading method.

In order to quantitatively compare the development of tensile strains (and hence comment upon the likely associated generation of tensile stress across the loaded diameter), strain profiles have been produced as Figure 4.59.

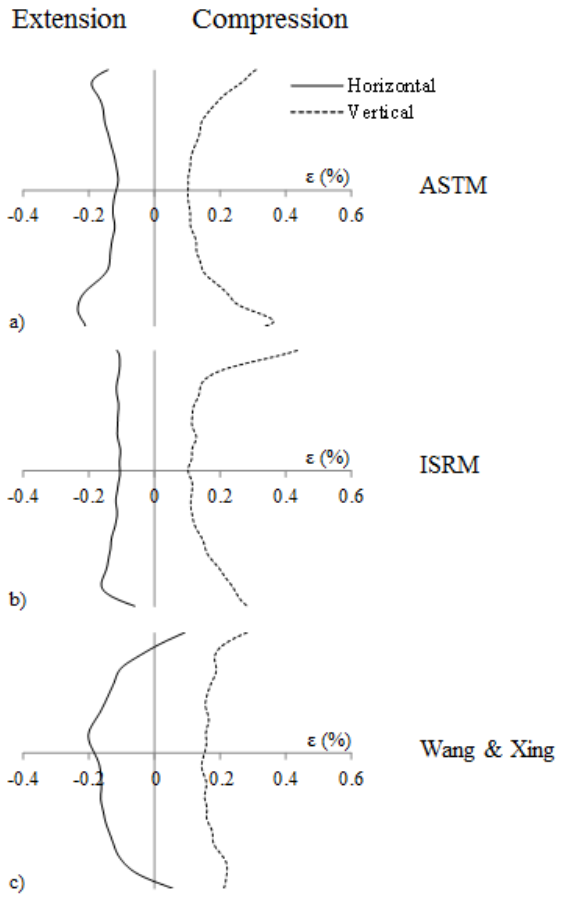

Figure 4.59: Strain profiles across loaded diameter immediately prior to failure

In Figure 4.59a) the ASTM method shows only compressive vertical strains to have developed across the sample, with a maximum of 0.36% at the loading points. Horizontal strain is entirely extensional across the disk in the vertical orientation. Along this vertical profile, two regions of high extensional horizontal strain are visible, correlating with the areas of maximum compressive vertical strain. The minimum horizontal strain, -0.11% is found to be located at the centre of the disc. Assuming linear elasticity, the areas of maximum tensile stress are found to be located approximately 5mm inward from each loading point, suggesting that fractures initiate from these regions. This is counter to the observations made by Yanagidani, et al. (1978), using more traditional local strain gauges and is counter to the Brazilian test theory.

A similar vertical compressive trend may be seen in Figure 4.59b) where curved-platens were used during ISRM testing. Maximum vertical compressive strains, and therefore

assumed compressive vertical stresses, are found at the loading points, with a maximum of 0.44% strain at the top of the disk. The distribution of horizontal strain is found to be more even across the disk diameter than that of the ASTM method, with an average of -0.1%. Greatest horizontal extension is measured in the lower half of the disk with a maximum of -0.16%. This suggests failure initiated around the lower contact point.

The maximum horizontal extension found using the flattened disk method is located at the disk centre (Figure 4.59c). Vertical strain is found to be greatest towards the points of loading (maximum of 0.28%) although is more evenly distributed across the sample than the other methods owing to the larger area over which the load is imposed. Horizontal strains are seen to be compressive at these points, possibly brought about by the additional restraint offered by the large contact area.

Although samples tested with the curved platens and with flattened geometries share a similar (theoretical) loading area, the two methods produce different results. Several authors including Wang, et al., (2004) and Jianhong, et al., (2009) have stated that although the purpose of the curved loading platens is to distribute load over a known area, in practice confidence in the ability to maintain this area throughout testing is limited, as shown in Figure 4.58c and d. The flattened method reduces this uncertainty as sample ends can be cut to be parallel with a high degree of accuracy, all but removing 'bedding-in' errors, as seen in Figure 4.55.

The DIC was also able to calculate of out-of-plane displacements. Figure 4.60 displays the vertical surface profiles taken immediately prior to failure. It can be seen in ASTM tests that an outward protruding region at the sample top and bottom exists. As this is in the area proximal to loading it is likely to be related to crushing. ISRM tests exhibit similar behaviour. Surface profiles for tests conducted on flattened disks show a more level face, indicating that less sample crushing was occurring due to the load being applied over flat and parallel surfaces.

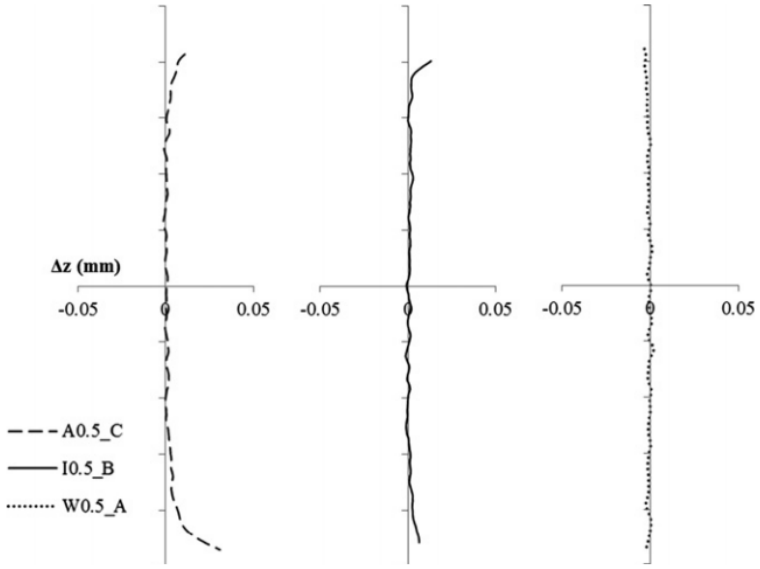

Figure 4.60: Out of plane vertical surface profiles immediately prior to failure.

4.8.3. *STUDY 2 – EFFECT OF DISK THICKNESS*

The second study aimed to investigate the effect of sample thickness with reference to the ASTM recommended t/D ratio range to better prescribe a methodology for the testing of soft rocks in Brazilian tensile testing. Test ratios are provided in Table 4.3.

Table 4.3: Sample geometries during study 2.

Test ID	*t/D* Ratio	Testing Method	No. of Samples Tested	Loading Rates (kN/min)
A0.1_	0.1	ASTM (ASTM, 1984)	3	0.645
A0.2_	0.2		3	1.290
A0.5_	0.5		3	3.225
A0.75_	0.75		3	4.839

The ASTM standard suggests a ratio range of between 0.2-0.75 and these extremes were tested in addition to the 0.5 ratio used in study 1. To investigate the ability of the DIC system to measure out-of-plane displacement on the disk face, a ratio of 0.1 was also tested as this was anticipated to exhibit the greatest displacement. Loading rates were based upon sample thicknesses, calculated to induce failure at an approximately consistent time (around 4 minutes), as shown in Table 4.3 and tensile strengths is presented in Table 4.4. It can be seen that a broadly constant tensile strength are obtained, although the magnitude of load at failure is proportional to disk thickness.

Table 4.4: Tensile strength of Springwell sandstone during study 2.

t/D ratio	Test	Failure Load, *P* (kN)	Tensile Strength, σ_t (MPa)
0.1	A0.1_A	2.71	3.15
	A0.1_B	2.55	2.97
	A0.1_C	2.72	3.16
0.2	A0.2_A	5.76	3.35
	A0.2_B	5.37	3.12
	A0.2_C	6.45	3.75
0.5	A0.5_A	14.30	3.32
	A0.5_B	14.99	3.49
	A0.5_C	13.77	3.20
0.75	A0.75_A	18.02	2.79
	A0.75_B	19.70	3.05
	A0.75_C	19.60	3.04

Representative tests have again been selected to demonstrate the effect of t/D ratio on out-of-plane displacements. The DIC is capable of resolving z-displacements to an accuracy of ±0.001 mm. Surface profiles taken vertically are provided as Figure 4.61.

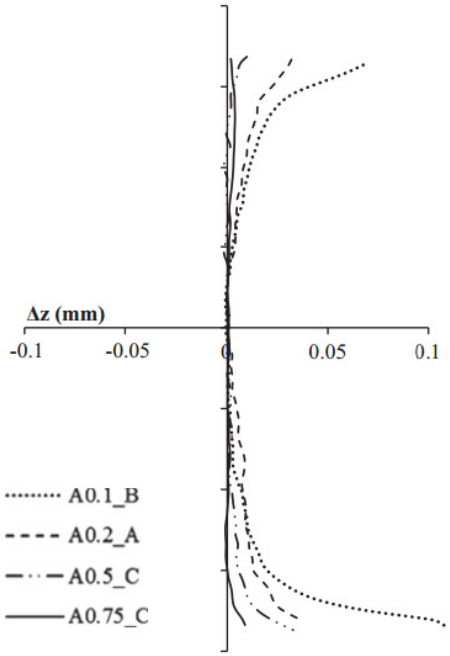

Figure 4.61: Vertical surface profiles of representative samples immediately prior to failure

Samples prepared to a ratio of 0.75 exhibited the smallest degree of out-of-plane displacements except at the bottom of the disk where minor deflections are seen. As the t/D ratio is reduced, the degree of z-plane deformation increases, particularly towards the top and bottom of the disks near the loading points. Samples cut to a 0.1 ratio display the greatest out-of-plane displacements of between 0.02mm and 0.06mm.

The location of the maximum z-displacements of all samples corresponds with the position of the maximum vertical compressive strains as seen in Figure 4.62. This is likely to be in part a result of Poisson's effect along with evidence of crushing.

Total vertical strains increase as t/D ratios reduce, meaning that thinner samples undergo greater vertical strains than thicker ones, despite all samples failing at comparable tensile stresses. The greatest horizontal compression measured for each sample is once again seen to be adjacent to the loading points. Figure 4.62 shows that the intensity of horizontal extensional strain increases with reducing t/D ratio.

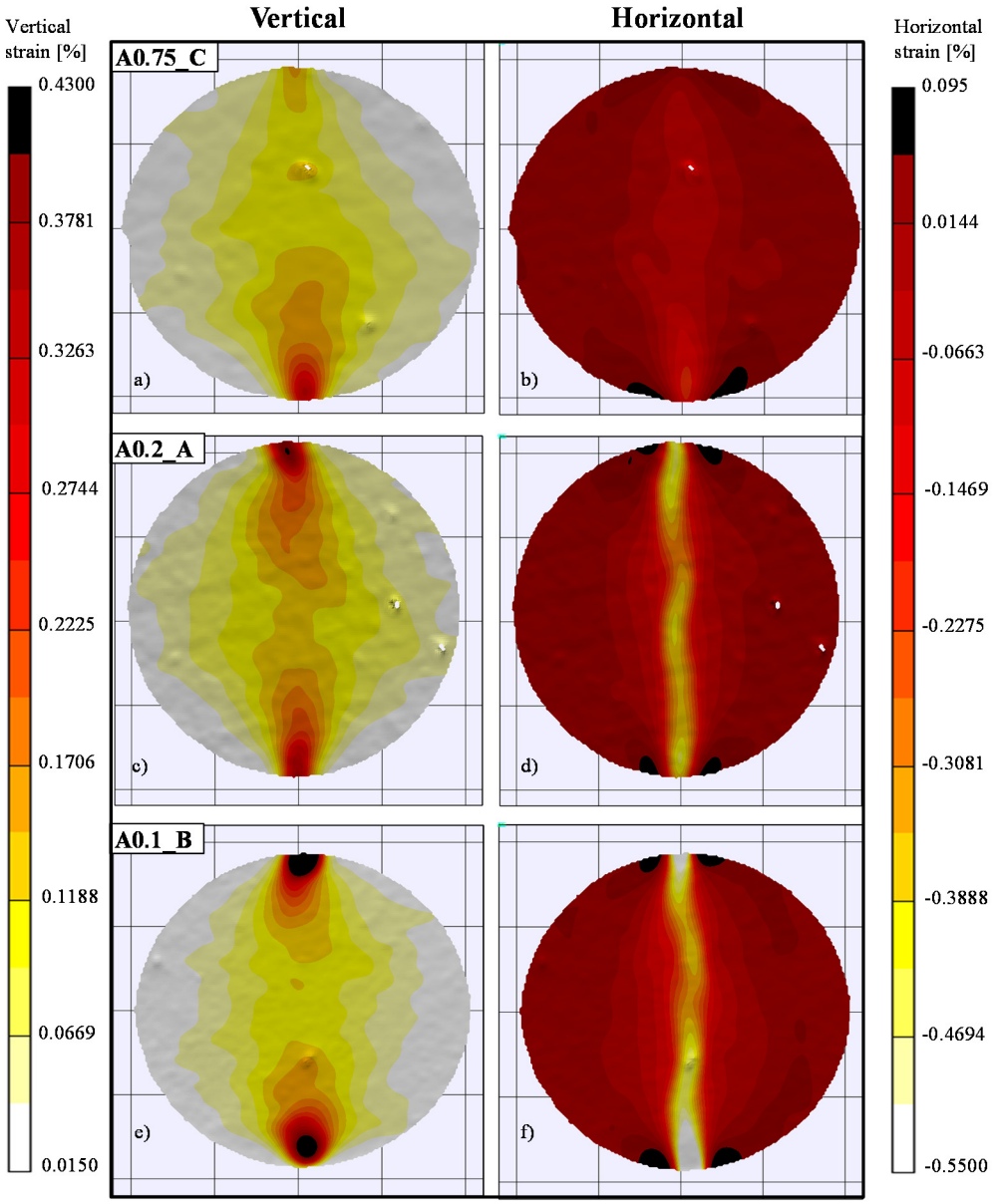

Figure 4.62: Strain distributions immediately prior to failure for samples of t/D ratios a-b) 0.75, c-d) 0.2 and e-f) 0.1

4.8.4. *CONCLUSIONS OF STUDY 1 AND 2*

By comparing the effect of varying sample geometry and loading techniques on surface strains and out-of-plane deformations in study 1, DIC has allowed several conclusions and recommendations to be drawn:

- The ASTM and ISRM tests show the greatest tensile strain concentrations close to the loaded ends, (along with regions of highest compressive strains), implying fracture initiation occurs in these regions as opposed to the disk centre. Crushing was also noted at the sample ends, further evidenced by out-of-plane strains.
- Flattened disks showed consistently centralised extensional horizontal strain maximums along with centralised failure origins and minimal z-strains.
- Flattening of sample ends to a 2α angle of 20^{o} will be applied to the testing of soft rocks in order to increase the likelihood of centralised failure origins.

In study 2 out-of-plane displacements were measured with varying sample thickness. General findings and recommendations were as follows:

- As disk thickness decreased, increased out-of-plane displacements were measured, coincident with regions of largest vertical compressive strains.
- Calculated tensile strengths were unaffected; however findings are counter to the solely 2D deformation assumption inherent in Brazilian testing.
- Ideally, large t/D ratios would be recommended during testing of soft rocks, as this promotes the 2D assumption by minimising out-of-plane movements, however due to the limited quantity of sample cores available a t/D ratio of 0.5 is considered appropriate.

By using DIC to measure small-scale displacements, not only are more realistic strain behaviours observed than would be captured externally, this measurement is made throughout the full strain field in 3D which would be impossible to replicate with strain gauges.

Traditional local strain gauges require sample contact along with knowledge of the relative stiffness of the gauges themselves, they are also limited in the sense that they may not be used with friable or soft materials. The DIC system is contactless and the stiffness of the paint is considered to be negligible making it perfect for use with soft rocks such as those tested within this thesis.

4.9. ARTIFICIAL GROUNDWATER SOLUTION

There is known to exist dissolvable minerals both inter- and intra-bedded within the soft calcareous mudstone of this research. The superficial effect of dissolution on the mineralogy of samples is examined on a qualitative level later within this thesis via the use of methods such as SEM and XRD.

Oedometer tests (and to a far lesser degree, dispersivity and durability tests) are employed within this research to understand the mechanical effect of the calcareous mudstone dissolution on a quantitative level. Whilst the triaxial tests carried out during this report used only de-aired water as a pore fluid (as is standard practice), the oedometer, dispersivity and durability tests were carried out using both de-ionised water and a synthetic groundwater of similar salinity and pH to that of natural groundwater samples from this area.

Several bottled samples of groundwater taken from boreholes at the Yas Mina site investigation were supplied at the start of this project, however was too small in volume to allow repeatable tests with it serving as a pore fluid to be performed. To combat this, Ion Chromatography (IC) and Inductively Coupled Plasma (ICP) analysis were carried out on the water samples in order to better understand their chemical makeup and ultimately allow synthetic replication for use as a reproducible porefluid where required.

Both samples tested showed similar quantities of anions and cations and results of the IC and ICP analysis is presented as Table 4.5.

Table 4.5: IC and ICP quantitative analysis of GW1 and GW2.

Anions Detected by IC	Anions PPM	Cations Detected by ICP	Cations mg/l
Groundwater Sample 1			
Chloride	13271	Calcium	684
Nitrite	5115	Magnesium	1871
Phosphate	41	Sodium	14438
Sulphate	5227	Potassium	664
Groundwater Sample 2			
Chloride	13778	Calcium	1023
Nitrite	4529	Magnesium	1866
Nitrate	3	Sodium	14671
Phosphate	7	Potassium	669
Sulphate	6383		

These results, coupled with a knowledge of the local calcareous and evaporitic geology of the area, indicates dissolved salts to include CaCo3, MgSO4, NaCl and KCl, with NaCl displaying the highest abundance. Unfortunately closer examination of results

revealed a charge imbalance, which was ultimately compensated for by including more carbonate.

The most convenient salts which would fulfil the detected anion and cation requirements and that are easily dissolvable are as follows, for dissolving within one litre of water:

- Magnesium chloride hexahydrate ($MgCl_2.6H_2O$) – 15.609 g
- Calcium chloride dihydrate ($CaCl_2.2H_2O$) – 3.753 g
- Sodium chloride (NaCl) – 10.754 g
- Sodium sulphate anhydrous (Na_2SO_4) – 9.438 g
- Sodium nitrite ($NaNO_2$) – 6.792 g
- Sodium hydrogencarbonate ($NaHCO_3$) – 18.716 g
- Potassium hydrogencarbonate ($KHCO_3$) – 1.705 g
- Sodium nitrate ($NaNO_3$) – 0.0041 g (4.1 mg)
- Potassium dihydrogen orthophosphate (KH_2PO_4) – 0.0100g (10.0 mg)

Unfortunately in practice mixing this fluid together as one batch causes a degree of 'blocking', whereby not all the salts may enter solution. In particular calcium sulphate is precipitated out of the solution and the mixture remains clouded.

In the interests of creating a readily repeatable solution, a simpler mixture of chemicals was proposed:

- Magnesium chloride hexahydrate ($MgCl_2.6H_2O$) – 15.6g
- Sodium chloride (NaCl) – 10.74g
- Sodium nitrite ($NaNO_2$) – 6.79g
- Potassium hydrogencarbonate ($KHCO_3$) – 1.7g

When mixed into 1 litre of deionised water, this simplified solution fully dissolves as well as providing the correct pH (7.4) along with the major salts found within the natural groundwater.

4.10. CHAPTER SUMMARY

This chapter aimed at tailoring a number of existing tests to better suit an application with soft rocks, as well as developing synthetic pore water that better represented in-situ ground water chemistry than deionised water. It also addressed some limitations of the standard triaxial tests with a particular focus on sample preparation and the measurement of strain using locally emplaced Hall Effect gauges.

Some simple suggestions were made regarding the cutting and shaping of samples in triaxial apparatus in order to avoid bedding errors and unwanted punctures and leakages.

A rational was presented for the selection of Hall Effect gauges as local strain measuring tools and some common limitations were addressed. A repeatable method of measuring initial gauge lengths prior to testing was stated as well as a means of tracking any changes to gauge length throughout saturation and consolidation, phases of testing that are frequently overlooked with regard to the development of strains.

An alternate method of affixing local strain gauges was suggested whereby the membrane is adhered to the sample surface at the locations the local gauges will occupy, negating the need to 'pin' or otherwise penetrate the membrane or sample. This method was proven to provide good results during testing on both a rubber and sandstone control sample. Furthermore, the effect of differential pressures during testing in avoiding sample to membrane 'play' was also shown through the use of local strain gauges, increasing confidence in the decision not to use sample penetrating pins on the sensitive and limited number of samples within this thesis.

The loading geometry of the triaxial top cap and loading ram was also assessed, showing that standard concave docking mechanisms generated unwanted rotational strains within a triaxial sample and ultimately suggestions of a 'fixed' or 'rigid' setup were made.

The validity of the assumption that disk shaped samples fail in tension at their centre during Brazilian testing using ASTM and ISRM standards was examined through the use of DIC. Results showed that more consistent centralised failures occurred in samples that adopted flattened surfaces at the loading locations and an examination of out of plane (z-axis) strains indicated that samples should be prepared with a 2:1 diameter to thickness ratio in order to avoid excessive bending.

Findings from this chapter informed the finalised methodology presented in the following chapter.

CHAPTER 5. FINALISED METHODOLOGY

5.1. CHAPTER 5 INTRODUCTION

The previous chapter described the developments undertaken by the author in order to arrive at a finalised testing method for the multi-scale characterisation of soft calcareous mudstones. These developments included determining a standard to: prepare samples, overcome bedding and seating errors, accurately calculate changing cross sectional area and assessing the reliability of local strain measurements with respect to affixing methods. In addition, an examination of a novel full field strain measuring tool (DIC) is carried out in order to assess the most appropriate sample thickness and loading geometry. Many of the findings were specific to the testing of calcareous soft rocks, however several are applicable to soil and general rock testing too.

This chapter states the adopted apparatus and methods used by the author during the mechanical testing phase of this thesis along with non-standard optical characterisation methods. The first half of this chapter details methods used to find general index properties, then focuses on the advanced triaxial testing method. The adopted method used during other mechanical tests, such as the Brazilian Tensile Test and One-Dimensional Consolidation Test is then covered, with any deviations from the relevant standards (British Standards / ISRM / ASTM) stated where applicable. Finally, this chapter states the apparatus and methods used in the non-standard optical characterisation phase of this thesis.

5.2. GENERAL / INDEX PROPERTIES

The following sections detail methods used to obtain general index properties. These methods are applicable to several later tests and are often carried out in conjunction with mechanical testing.

5.2.1. *MOISTURE CONTENT*

Due to the presence of salts such as halite and gypsum, it is important to keep the maximum temperature of the ovens to 40^{o}C so as not to drive off any moisture retained within these mineral's molecular structure as opposed to the 105^{o}C recommended in BS1377-2:1990. This reduced heat means an extended period of time is required for

drying, as typical time periods of 48 hours do not suffice. It has been found that 5 days is sufficient to obtain consistent measurements of moisture for small fragmented samples and a period of not less than 10 days for whole triaxial samples following the completion of testing.

Moisture content (w) can be found using equation 5.1:

$$w = \left(\frac{M_w}{M_s}\right) \times 100 \qquad 5.1$$

Where M_w is the mass of the water, (measured in grams and found by difference between the oven dried mass and the mass of the original wet material mass), and M_s is the mass of the solids (in grams). Convention dictates this value is expressed as a percentage.

Two moisture contents are taken from all samples prior to testing and are of as great a mass as possible to increase the reliability and accuracy of the findings. As samples are weighed both before (wet) and after testing (both wet and dry), initial and final moisture contents may be found retroactively.

5.2.2. *BULK DENSITY AND DRY DENSITY*

The bulk density of all samples is obtained from initial measurements BS1377-2:1990. Bulk density (ρ) is calculated using equation 5.2:

$$\rho = \frac{M}{V} \qquad 5.2$$

Where M is the initial mass of the triaxial sample (measured in grams) and V is the initial volume (measured in cm^3). This provides bulk densities equivalent to Mg/m^3.

It is convenient to use samples prepared for triaxial experimentation for the calculation of bulk densities. As the sample is uniformly cylindrical in shape and of a reasonably large mass it is easier to obtain a bulk density from an intact core sample than it is from rough fragments.

Once initial moisture contents are known dry densities (ρ_d) can be calculated using their relationship to bulk density (equation 5.3), again expressed at Mg/m^3 in accordance with BS1377-2:1990:

$$\rho_d = \frac{\rho}{1 + \left(\frac{w}{100}\right)} \qquad 5.3$$

5.2.3. *VOID RATIO AND POROSITY*

Initial void ratio (e_0) can be inferred from the relationship between dry density, the density of water (ρ_w) and particle density / specific gravity (Gs) as noted in BS1377-2:1990. Initial void ratio is calculated using equation 5.4:

$$e_0 = \left[\frac{Gs}{(\rho_d/\rho_w)}\right] - 1 \qquad 5.4$$

Void ratio is unitless. Porosity (n) is expressed as a percentage and may then be obtained using equation 5.5:

$$n = \left(\frac{e}{1+e}\right) \times 100 \qquad 5.5$$

5.3. ADVANCED TRIAXIAL TESTING METHODOLOGY

5.3.1. *RECOVERY AND TRANSPORTATION OF SAMPLES*

This stage of the methodology was unfortunately outside of the author's control, as samples were recovered and prepared for transport outside of the author's presence. Details pertaining to the recovery, transportation and storage of samples (specific to each site) are covered in Chapter 3.

5.3.2. *TRIAXIAL TESTING SETUP*

Triaxial tests within this thesis were carried out using a setup similar to that of an advanced soils test (with minor adaptations), as detailed in Figure 5.1.

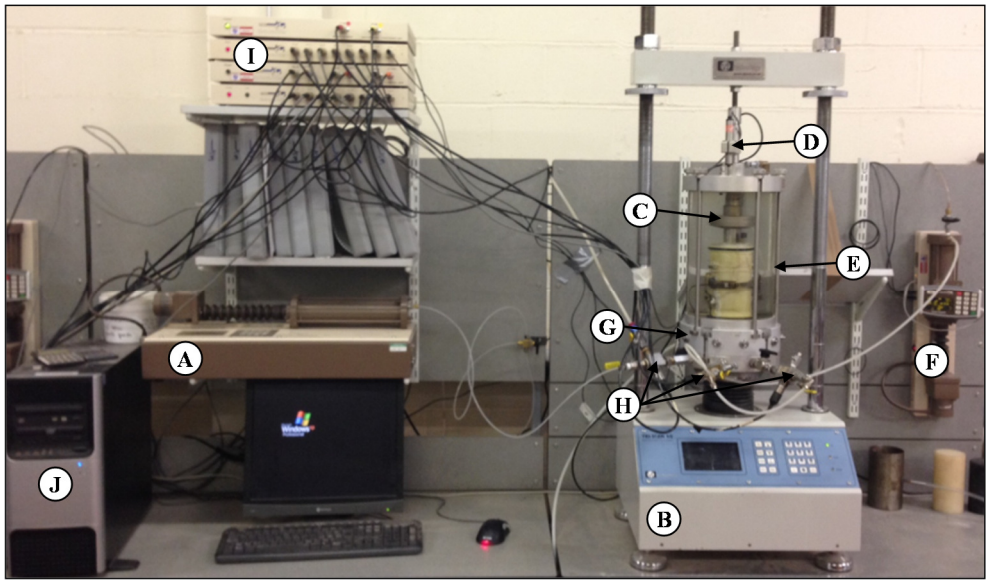

Figure 5.1: Triaxial testing setup.

The hardware shown in Figure 5.1 is as follows:

A. GDS 3MPa water/oil/air pressure controller. Used for supplying and regulating cell pressures and monitoring cell volume change, this may be programmed manually or via the GDS software.
B. VJ Technology Advanced Digital Triaxial System. This can be programmed manually or can be controlled via the GDS software to raise the testing cell at a precise rate of strain (in conjunction with the external LVDTs) or stress (in conjunction with the load cell).
C. GDS 64 kN internal load cell.
D. External LVDT for recording / measuring external ram displacements.
E. The Perspex cell itself has a maximum allowable internal pressure of 1.7MPa and so all tests are limited to 1.6MPa within this low pressure setup.
F. GDS 1MPa water/oil/air pressure controller. Used for supplying and regulating back pressures and monitoring volume change, this may also be programmed manually or via the GDS software. Also capable of generating negative pressures to assist with saturation of samples (manual only).
G. Custom made access ring. This ring can support 10No. local instruments.
H. Druck pressure transducers of 2000kPa capacity and resolution of 0.01kPa.
I. GDS Serial Pads for the collection and processing of raw data.
J. Desktop computer installed with GDS software.

A detailed schematic of the triaxial cell itself is shown as Figure 5.2.

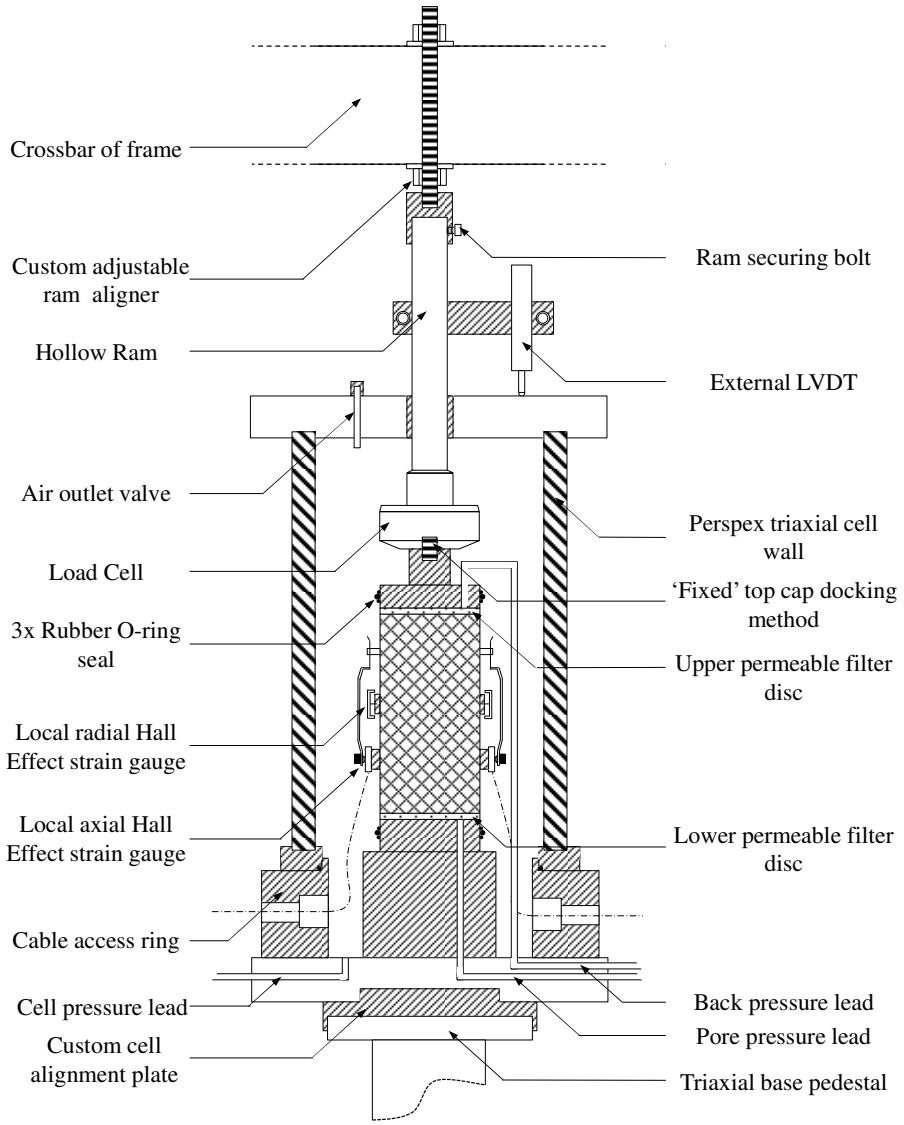

Figure 5.2: Advanced Triaxial Testing Cell and Local Instrumentation Setup

The final setup of the testing apparatus including loggers and desktop computer can be seen diagrammatically as Figure 5.3.

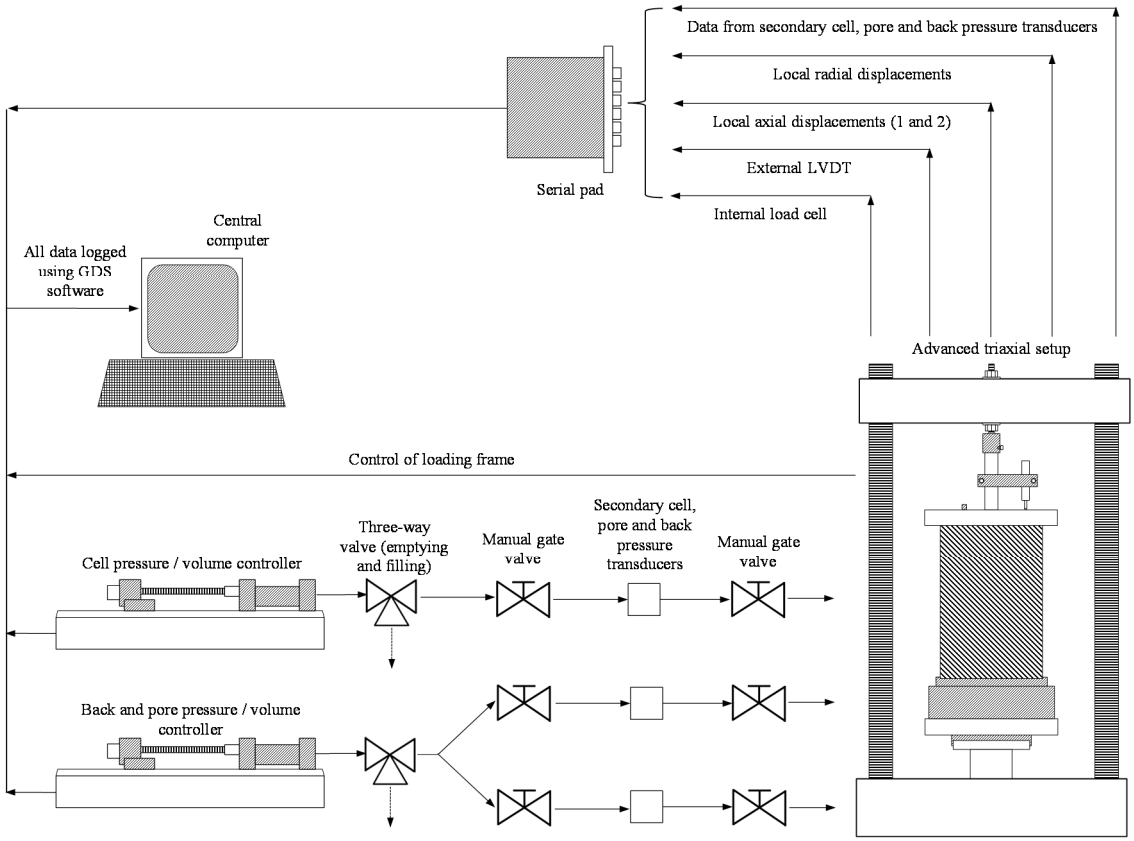

Figure 5.3: Schematic diagram of triaxial testing setup

The control system is that of GDS – GDSLAB version 2.3.6 with the following modules:

- **AdvancedLoading** – This is the most flexible of the modules as it is fully programmable and thus capable of following many desired stress paths. Used during all tests utilising the 'fixed cap' top platen as deviatoric stress may be controlled.
- **Satcon** – For saturation, B-test and consolidation of samples. Not used in conjunction with fixed top cap as unwanted deviatoric stresses are generated as samples attempt to shrink or swell against the static loading ram.
- **TriaxialAcquisition** – A simple module which 'just logs'. Useful during manual control tests and whilst initial sample setup is being performed (for example during the filling of the triaxial cell with fluid in order to measure any changes in local instrumentation readings).

In addition to the apparatus shown previous, rubber O-rings, standard rubber membranes and sintered steel porous disks were used in all experiments.

5.3.3. *CALIBRATION OF EQUIPMENT*

The apparatus used in the triaxial tests includes a number of components that require regular calibration in order to insure they are maintained. This includes the:

- Internal Load Cell;
- External LVDT;
- Cell, Pore and Back Pressure Transducers, and;
- Hall Effect Transducers.

The GDS software includes an equipment management window where all data being received from the connected hardware may be monitored and controlled in real time. Within this window there are a number of advanced options including calibrations, the ability to set 'soft' zero's and manual adjustments to the PID's.

The internal load cell was calibrated against a standard reference load cell (to UCAS requirements) and the external LVDT against a precision micrometre. The cell, pore and back pressure secondary transducers were all calibrated against a GDS pressure / volume controller and the Hall Effect Transducers against a set of digital callipers.

The calibration wizard (Figure 5.4) allows manual input of readings (in kPa or mm) that correlate to the hardware's output (in mV), in order to form a best fit line, which may be further adjusted if necessary. As a general rule, three readings are taken per increment in order to allow for noise and a mean value taken.

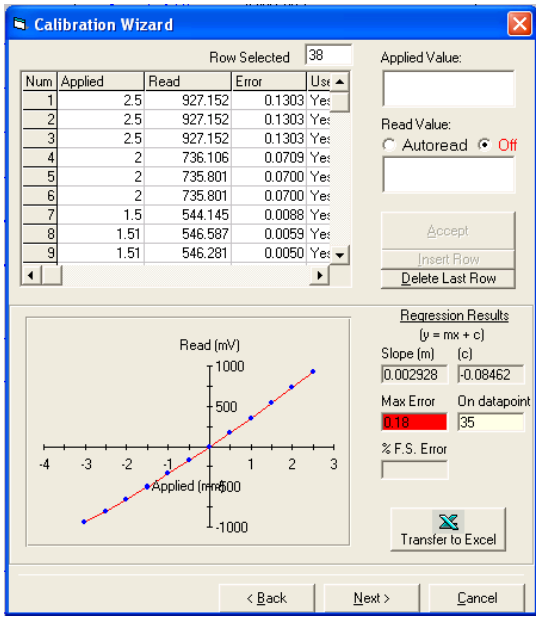

Figure 5.4: Example of best fit line method showing a degree of noise using GDS calibration wizard.

This calibration process was undertaken before the testing program and every three months thereafter to insure all devices continued to be accurate and reliable.

5.3.4. *SAMPLE PREPERATION / INSTALLATION INTO CELL*

Samples were carefully unwrapped and cut to length with ends ground parallel as described in the previous chapter. Off cuts are re-wrapped using clingfilm and re-sealable plastic bags and stored within a core-box for further use (for example carrying out tensile or particle density tests) or else used to immediately assess moisture contents.

Prior to the samples being placed into triaxial apparatus their dimensions are taken using a set of digital callipers. Only one length is recorded per sample as the cutting / shaping process it relatively accurate and parallel to within a high tolerance, however multiple readings of lengths are checked around the sample circumference to ensure this assumption is correct. The diameter of samples are taken from at least three points (top, centre and bottom) so that an average diameter may be obtained. Any obvious imperfections are noted and a brief description made (in accordance with BS5930).

The back / pore pressure lines are flushed with de-aired water and all air is removed from the system where possible. Water is ensured to be present on the top and bottom platens and pre-soaked porus disks put in place.

Samples are weighed on a digital scale and their mass recorded. Samples are photographed before being placed upon the saturated filter discs and adhesive applied to the location of the sample the local strain gauges will ultimately make contact before being covered by the sample membrane. All procedure prior to this point is carried out as rapidly as possible so as to preserve the natural moisture content of the samples tested. Once the membrane is in place and the rubber O-rings applied to the top and bottom platens, a seal is assumed to have been formed and the sample is considered to be in a less time critical state with regard to beginning testing proper.

A positive p’ is created by applying a -10kPa negative back pressure.

The local strain gauges are adhered and adjusted such that the magnetic component rests as close to the transducer’s zero gause position. The gauge’s initial length is noted.

5.3.5. *TRIAXIAL ASSEMBLY / TEST START*

Sample information is entered into the GDS program, a 'new test' started and the 'TriaxialAquisition' module selected in order to 'just log' the incoming information.

The internal load cell is lowered and screwed onto the sample's top cap in order to complete the 'fixed docking' procedure. If any mal-alignment exists, the sample is deemed to be inadequately parallel and further sample preparation is required.

Once these conditions are satisfied, the cell may be fully assembled and filled with water as detailed in BS1377-8:1990. Any changes to local strain gauge length that occur as a result of the cell filling process and docking will also be recorded and can later be incorporated / removed from final calculations of strain during post processing where applicable.

5.3.6. *SATURATION STAGE*

The adopted method of saturating samples is an adaptation the BS1377-8:1990 'saturation by increments of cell pressure and back pressure' with additional elements proposed in Silvestri & d'Onofrio's (2000) 'wet setting method'. This uses progressive steps of pore pressure equalisation (following manually increased back pressures) alongside successive B-tests (achieved by increasing radial pressures in an undrained manner and measuring pore pressure response). B-values are found using equation 5.6:

$$B = \frac{\Delta u}{\Delta \sigma_3} \qquad 5.6$$

This process is repeated until a B-value of 0.95 or greater is achieved. Because of the use of a fixed top cap, the 'AdvancedLoading' module is used as opposed to 'TriaxialAcquisition' or 'SatCon'. This allows q to be maintained at 0kPa regardless of sample swelling.

These steps are carried out with minimum differential pressures between the cell and pore pressures. A general guideline proposed is that differential pressures be not less than 50kPa once saturation has started (in order to minimise swelling) and not greater than the in-situ p' of the sample. Numerous steps of between 50-100kPa are carried out.

An adaptation to this method sees an initially imposed negative back pressure of -10kPa to assist in the speed of the subsequent saturation and decrease the likelihood of damage during this initial stage, followed by a steady single rise of cell and back pressures until a back pressure of 300kPa is achieved without changing p'. Any sample swelling will

be recoded via the GDS programme in conjunction with the local strain gauges and can then be accounted for and minimised where possible and incorporated into post processing.

5.3.7. *CONSOLIDATION STAGE*

Consolidation of samples was carried out in an isotropic manner, largely in accordance with BS1377-8:1990. Following saturation, cell pressures are raised whilst allowing pore pressures to drain against a constant back pressure in such a way that the desired p' is achieved.

Back pressures should not be lower than that of the final stage of saturation, as this would risk air coming out of solution and potentially lowering B-values to less than 0.95. In addition, the target p' shall be reached at as high cell and back pressures as possible, within the restrictions of the available apparatus, to reduce any remaining errors occurring due to partial saturation. For example, a p' of 300kPa achieved by cell pressures of 1300kPa, deviator stresses of 0kPa and pore pressures of 1000kPa is preferable to the same p' achieved via cell pressures of 600kPa, deviator stresses of 0kPa and pore pressures of 300kPa.

Again, due to the use of a 'fixed top cap', consolidation is carried out using 'AdvancedLoading' in the GDS software to ensure no unwanted deviator stresses are introduced.

Consolidation is assumed to be complete when back volume change has reduced to negligible levels (95% of excess pore water dissipation or better) and on-sample local strains having also reduced to negligible (creep) levels.

Tests are carried out on separate samples at 235kPa, 470kPa, 940kPa and 1300kPa p'. No multi-stage tests were carried out. This represents the approximate in-situ stress of many of the samples tested (235kPa) as most were obtained between 15 – 20mbgl with varying groundwater depths, followed by an investigation into the effect of increased mean effective stress (by doubling p'). 1300kPa p' represents the safe limit of the apparatus used, achieved via cell pressures of 1700kPa and pore pressures of 400kPa.

5.3.8. *SHEARING STAGE*

All tests carried out within this thesis are drained. Tests are sheared over the course of a week (approximating 10% external strains, therefore smaller internal strains). The initial small strain stiffness degradation is the primary focus of this phase of testing.

It is inadvisable to have highly variable strain rates between tests as the results will be incomparable (as strain rate is known to affect stiffness measured (Silvestri & d'Onofrio, 2000)). As such, it is important to arrive at a repeatable reference rate which will then be adopted for all tests to be compared.

BS1377-8:1990 uses an assumed 'significant strain interval' in conjunction with back volume change vs square root time relationships obtained during consolidation to calculate a maximum rate of axial displacement for shearing. All tests carried out in this thesis are sheared at rates at least an order of magnitude slower than these guideline rates and so the significant strain interval method has not been adopted.

Instead, tests within this thesis are carried out at rates equivalent to external strains of 0.001%/min^{-1} unless otherwise stated. This is input manually into the GDS system using the AdvancedLoading module whilst simultaneously programing the desired cell and back pressures to 'hold'.

All external and internal stresses, strains, loads and pressure are recorded at regular intervals by the GDS software, typically every 10 seconds for the duration of the test and raw data can be plotted graphically in real time.

5.3.9. *TEST END AND DISMANTLING*

Shearing is assumed to have completed when either a large drop in deviator stress is noted; a visible and distinct shearing plane has developed on sample that can be traced through the sample's diameter, or; the maximum deformation of both the Hall Effect local gauges has been reached, whichever comes first.

Deviator stress is then set to return to 0kPa, pressures are lowered simultaneously (whilst maintaining positive p') and the cell is emptied. The sample is removed from the membrane and photographed before being weighed and transferred to the 40ºC oven.

5.3.10. *BENDER ELEMENT (G_0) TEST - PREAMBLE*

One sample tested was used to find the G_0 profile of the calcareous mudstone with increasing confining pressure. The saturation and consolidation stages were as described in the preceding sub-chapters, as was the method of assembling and dismantling the triaxial apparatus. The main deviations from the previously stated methodology were in the sample preparation (as grooves in the sample must be made at the centre of the specimen ends to house the bender elements as shown in the previous chapter) and in the layout of the apparatus / local instrumentation setup.

The following sub-chapters detail the specific methodology for the setup of samples tested using Bender Elements

5.3.11. *BENDER ELEMENT (G_0) TEST – INSTRUMENT SETUP*

Broadly the setup of the tests utilising Bender Elements is the same as those detailed previously in the advanced triaxial programme. The only physical modifications to the apparatus are to the sample top cap and base platen. These modified additions are tailor made by GDS along with cindered brass porous disks that have an aperture to accommodate the Bender Elements. The top cap also allowed the 'fixed' docking method to be used in conjunction with any tests using Bender Elements, as shown in the previous chapter.

The cables associated with the Bender Elements exited the triaxial cell via the cable access ring and into a unique serial pad, external to the other serial pads used in the previously explained layout. This serial pad is then connected to the control computer which is installed with the latest GDS Bender Element Software (GDSBES) Package (version BENDERS 2.2.4).

5.3.12. *BENDER ELEMENT (G_0) TEST – SAMPLE PREPARATION*

Samples are prepared in the same manner as those stated in section 'sample preparation and installation into triaxial cell', however immediately before being placed within the cell, a groove is cut within the centre of the sample ends as detailed in the previous chapter. These grooves are then infilled with a thick paste comprised of a remoulded slurry of calcareous mudstone.

5.3.13. *BENDER ELEMENT (G_0) TEST – SOFTWARE PREPERATION*

Once the sample is installed into the triaxial apparatus and the GDS software set to 'just log', the GDSBES specific information could be inputted. This requires specifying the height of the sample in question (in mm), followed by inputting the desired frequency of sampling and sample time. These were set to 2000ksamp/sec and 5ms respectively and an automatic gain option selected (in which the GDS software selects the most appropriate level of gain).

The shape of the waveform and its properties must then be input. For the test carried out within this thesis a sinusoidal source wave with a period of 0.2ms and an amplitude of 14V was used. These features can be seen schematically on Figure 5.5.

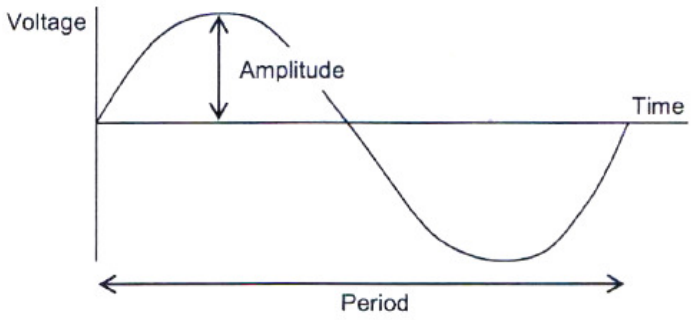

Figure 5.5: Sinusoidal Waveform

5.3.14. *BENDER ELEMENT (G_0) TEST – DATA ACQUISITION*

Data acquisition needed to be carried out at discrete times throughout the consolidation phase of the test, reflecting the incremental increases in the mean effective isotropic consolidation stress state of the sample being tested. As the properties of the material being tested dictated the rate at which consolidation would occur, it was deemed that manual (as opposed to automatic) sample points would be selected for the GDSBES.

These data points (triggered manually over the course of the three week long test) were taken in sets of three, so that averages may be drawn and erroneous data identified and omitted without sacrificing information. They were carried out at approximately 100kPa increases in isotropic mean effective stress states up to a mean effective stress of 1250kPa.

5.3.15. *BENDER ELEMENT (G_0) TEST – POST-PROCESSING*

Once all information is gathered and sufficient data points tested (3No. per consolidation stage), the raw data from the GDSBES must be analysed so that S-wave travel times (seismic wave velocities, Vs) may be calculated, and ultimately shear stiffness at zero strain (G_0) determined.

This was achieved chiefly by exporting the raw data (in .bes file format) to Microsoft excel, then identifying the source and reflected wave forms via a bespoke Excel 'Add In' called GDSBEAT (Bender Element Analytical Tool (Rees, et al., 2013)). The data was then interpreted using the Time Domain method, which assesses the time difference between source and received waves with respect to several points on the received wave morphology (first deviation, first 'bump', zero crossing and first major peak). The samples bulk characteristics including its density, length, radius and mass are also back calculated using a combination of locally emplaced Hall Effect gauges and volume

controllers in order to calculated both Vs and G_0 using formula 4.6 and 4.7 in the previous chapter.

5.4. STANDARD MECHANICAL / CHARACTERISATION TESTS

Whilst the main focus of the project is on the small strain stiffness properties of soft calcareous mudstone within triaxial apparatus, several other tests will also be carried out in order to better understand the behaviour of these complex materials. This includes several tests from BS1377:1990, ASTM and the ISRM standards, with varying degrees of adaptation to better suit the material in question.

Testing methods covered in this section include those of:

- Atterberg Limit Tests;
- Dispersivity Tests;
- Durability Tests;
- Particle Density Tests;
- Particle Size Distribution Tests (including both sedimentation by pipette and hydrometer);
- One Dimensional Consolidation Tests (both undisturbed and remoulded intrinsic using deionised and saline pore water), and;
- Brazilian Tensile Tests (with DIC to examine the effect of different loading geometries).

5.4.1. *ATTERBERG LIMITS*

Atterberg limits and particle size distribution tests will be carried out on samples to assist the overall characterisation of the materials in accordance with BS1377-2:1990. The only deviation from standard procedure is that sample drying will occur at 40ºC.

A sub-set of samples will also be characterised with respect to the effect of salinity within the pore-water. The saline fluid used will be as specified in the previous chapter.

5.4.2. *DISPERSIVITY*

Dispersivity tests were carried out on several samples of calcareous mudstone in accordance with BS1377-5:1990 ‘Crumb Tests’, with modifications to the standard procedure being the testing of samples submerged in a saline solution, representative of the groundwater of Abu Dhabi island. Methodology covering the production of the synthetic groundwater solution is described in the previous chapter.

5.4.3. *DURABILITY*

Slake durability tests were carried out on several sample off cuts and were prepared and tested in accordance with ISRM: (Brown, 1981). The only significant deviation from standard procedure was that samples were dried at 40ºC instead of the recommended 105ºC. Two cycles of wetting and drying were carried out, providing results in terms of both first cycle (I_{d1}) and second cycle (I_{d2}) durability.

5.4.4. *PARTICLE DENSITY*

Particle density was found for all samples using the 'glass jar method' as detailed by BS1377-2:1990. Deviations from standard procedure included that drying was carried out at 40ºC and that samples were crushed mechanically within a Siebtechnik disk mill (Figure 5.6) as opposed to manually.

a) b)

Figure 5.6: a) Siebtechnik disk mill, and b) milling rings.

Crushed and dried samples of this material are noted to be highly hydrophilic, and as such require rapid transportation between ovens and weighing apparatus, or else risk inaccurate mass measurements being taken as atmospheric moisture is absorbed into the powdered sample.

5.4.5. *PARTICLE SIZE DISTRIBUTION AND SEDIMENTATION*

This test was possible due to the cementation of the calcareous mudstone being weak and deteriorating readily with prolonged exposure to water and gentle agitation.

Tests were carried out using the 'wet sieving' method detailed in BS1377-2:1990.

The clay / silt fraction (the majority of the sample by weight) was then subject to further testing (sedimentation) via both pipette and hydrometer methods in accordance with BS1377-2:1990. A particle density of 2.70Mg/m^3 was assumed where applicable.

Samples were oven dried at temperatures of 40^{o}C.

Following the generation of results from Atterberg Limits and PSDs, the activity of samples is also calculated.

5.4.6. *ONE DIMENSIONAL CONSOLIDATION*

One dimensional consolidation testing was carried out in accordance with BS1377-5:1990. Two types of apparatus were used during this study, a high pressure oedometer (capable of achieving a maximum vertical stresses of 7.8MPa) and a low pressure oedometer (maximum vertical stresses of 1.6MPa).

Deviations from the BS1377-5:1990 arose during sample preparation and later during sample drying (as a 40^{o}C oven was used). During preparation, sharpened oedometer rings were pushed into pre-prepared thin disks of undisturbed sample (2mm thicker than the thickness of the ring) at a constant loading rate. Any samples damaged during this process were discarded.

Once samples were successfully located within the oedometer ring with (no macro voids noted between the ring and the sample), the top and bottom of the samples were cut to be flat and parallel with the ring itself using a sharp knife. This was carried out as rapidly as possible so as not to allow samples to dry.

At the start of testing, swelling pressure was measured in all undisturbed samples tested using the BS1377-5:1990 suggested method of maintaining zero displacement (within a tolerance) whilst adjusting loads to compensate for swelling related vertical strains.

In addition to the tests carried out on undisturbed samples, several remoulded samples were created from slurries. These were formed in order to assess the ICL (intrinsic compression line) and were created by forming slurries of soft rock and water to greater than the material's liquid limit. These were then tested within the oedometer in the usual manner, being cautious not to overload the samples too quickly as this may result in loss of sample solids.

The effect of introducing saline pore-waters (the chemistry of which is specified in section 4.9 of this thesis) is also measured on both remoulded and undisturbed samples.

5.5. BRAZILIAN TENSILE TESTING USING DIC

This phase of testing builds on the methodology and preliminary results obtained in Chapter 4 during the testing of Springwell Sandstone using DIC (Stirling, et al., 2013). DIC was selected as a means of measuring the development of local strains on-sample during the indirect tensile (Brazilian) test due to the difficulty in adhering traditional strain gauges to loose and friable materials.

5.5.1. *SAMPLE PREPARATION*

A variety of core samples were selected from those remaining following the triaxial testing programme. Cores displaying excessive moisture loss or containing pre-existing weaknesses (such as cracks and fissures) were discarded, insuring only intact samples were subject to testing.

Sample cores showed a range of diameters, however were all cut to have a 2:1 diameter to thickness ratio (to within 0.15) so as to limit the out of plane bending occurring (as per the findings of Stirling, et al (2013), summarized in Chapter 4. In addition to this, samples were prepared to have both arched and flattened loading contact points, for later comparison of the localisation of strains when loading using flat platens. Flattened samples used a 2α angle of 20^{o} (Wang & Xing, 1999); (Wang, et al., 2004), carried out using a surface grinder to within a high degree of parallelism.

The sample discs were then spray painted with a coating of matt white acrylic paint, before being covered by an even, non-repetitive, isotropic and high contrast speckle pattern of matt black acrylic spray paint in accordance with the Correlated Solutions (2010) suggested practice (Figure 5.7).

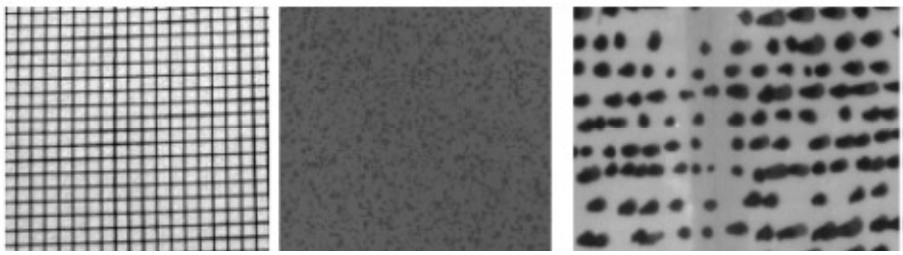

Figure 5.7: Examples of inappropriate speckle patterns (Correlated Solutions, 2010).

Inter-sample variation was avoided by painting the samples in batches. This had the additional benefit of speeding up the process when compared to the affixing of more traditional local strain gauges.

Once the thin layer of paint was dry, samples were weighed and dimensions recorded.

5.5.2. *CAMERA SETUP AND CALIBRATION*

Two high resolution cameras were mounted on a tripod across a profile bar, centred symmetrically about the sample to ensure a fair visual coverage, as seen in Figure 5.8. The cameras employed a focal length of 28mm with 2.0mm relative aperture, with an angle of incidence of between 30^{o} and 50^{o}. The sample was placed approximately 500mm away from the centre of the tripod setup.

Additional cold source lighting (Figure 5.8) ensures an even coverage of light as well as maintaining a high contrast between the speckles and the white undercoat. Care was taken to ensure the sample was not overly lit, as this can cause errors in post processing.

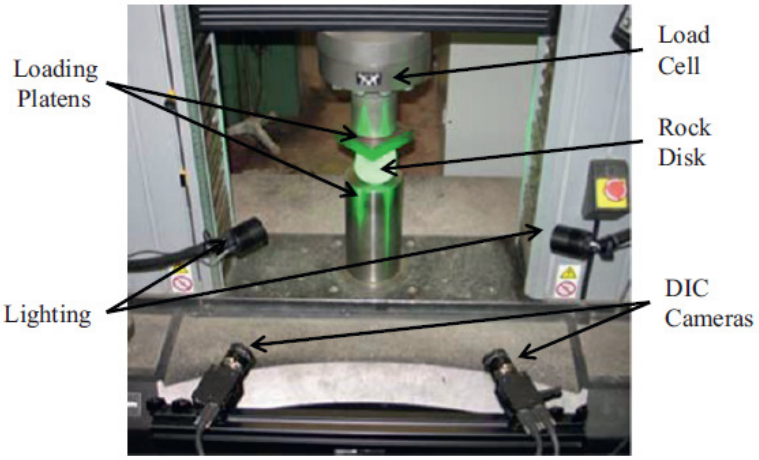

Figure 5.8: DIC camera and lighting setup.

The cameras are manually focused individually with the assistance of the VIC-Snap software's digital zoom function to ensure the highest degree of focus was attained on the pixel level. This is carried out on a sample with a representative speckle pattern to check that individual speckles make up ≈30 pixels.

The setup is then calibrated using an appropriate calibration plate in conjunction with the VIC-Snap and VIC-3D software's calibration module, and carried out in accordance with the Correlated Solutions (2010) suggested practice.

5.5.3. *TENSILE TESTING AND IMAGE CAPTURE METHOD*

Tests were carried out using an Instron 5585H universal testing machine, which is capable of applying a constant loading rate or a set rate of displacement during compression or extension. This ensured that ISRM and ASTM standards were able to be

followed where applicable. The system has an in-built load cell and all displacements and loads are output to a bespoke piece of software, and ultimately transferred to Excel.

Samples were installed between the two flat loading platens and which were then manually lowered until nearly touching the sample. A loading rate of 200N/min was set for all tests, as this allowed samples to fail within the ISRM and ASTM standard time frames with few exceptions.

The VIC-Snap software was set to capture images at a frequency of 500ms, and following the manual capture of an initial reference image the Instron 5585H and the VIC-Snap software were started simultaneously.

Tests were considered complete when the sample visible fractured. At that point the load would be manually removed and the fragmented sample taken, weighed and placed within a 40^{o}C oven for the measurement of moisture contents. Moisture contents were measured after 7 and 28 days.

5.5.4. *POST PROCESSING*

Images recorded using the VIC-Snap software were imported into VIC-3D along with calibration images.

An area of interest (correlation window) was then manually traced around each sample's initial reference image taken at zero time (Figure 5.9a), and two seed points (nodes) manually positioned within the left and right sides of the sample at points likely to undergo relatively small displacements (Figure 5.9a). The VIC-3D software will then superimpose an analysis grid (subset grid), with a subset size deemed appropriate for each specific sample, controlled by the coarseness of the speckle pattern (Figure 5.9b).

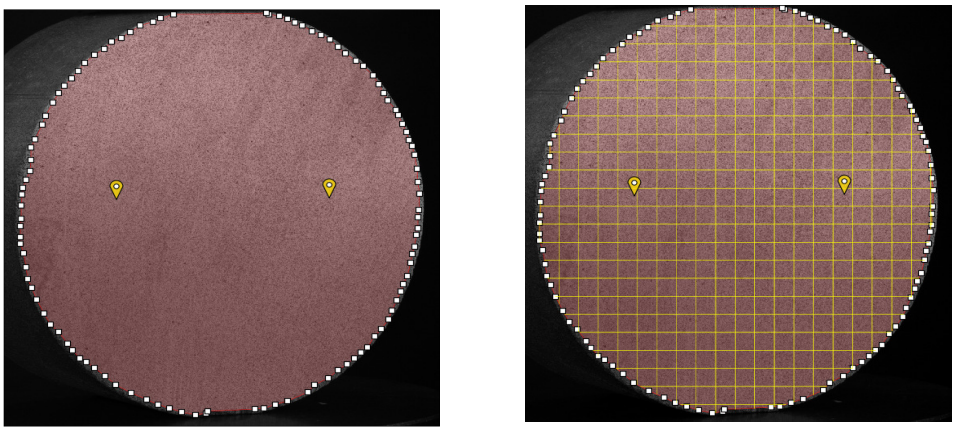

a) b)

Figure 5.9: Outputs from VIC-3D Software of sample NB03 35.8C (F) showing a) Correlation Window and seed points, and b) Subset grid.

By using the software's in-built analysis modules the images from the two cameras were compiled into 3D displacement contour data at each time interval. This data could then be viewed as 2D strain data in both the x- (Exx) and y- (Eyy) axis, with reference to the initial images taken at zero time, and individual images extracted as .tif files.

5.6. NON-STANDARD OPTICAL CHARACTERISATION METHODS

5.6.1. *X-RAY DIFFRACTION*

Qualitative XRD testing was carried out on several samples of calcareous mudstone to characterise the range of minerals present as well as to highlight any potentially problematic minerals that may degrade upon being saturated with water (as this has implication for long triaxial tests).

As samples are destroyed during the testing process, their degree of prior disturbance is irrelevant. Fragments sourced from the outside of the cores would likely have been sufficient to fulfil this role, however so as not to accidentally have results affected by cross contamination from the drilling flush, samples were instead taken from the core centres.

A range of samples were prepared for XRD by first drying 100g of calcareous mudstone in a 40^{o}C oven before crushing using a Siebtechnik disk mill until the powder would pass through a 63µm sieve. Selection of samples for XRD analysis was random.

Samples were then further sub-divided in order to assess their compositional change when introduced to water. Each sample chosen was split in two; a 'dry' half that would be set aside in its powdered form and a 'washed' half that would first be placed within a cone of 11µm filter paper and be allowed to have deionised water flow through it for several hours. Once this process was complete, the 'washed' sample would be oven dried and crushed once more as previously described.

A PANalytical X'Pert Pro Multipurpose Diffractometer (fitted with an X'Celerator and secondary monochromator) was used to identify likely mineral phases present within the calcareous mudstone samples. Samples were scanned in 'continuous mode' using the X'Celerator RTMS detector.

Data was analysed using the PANalytical X'Pert Data Viewer software as well as being transferred to Excel for ease of subsequent comparisons between 'Dry' and 'Washed' states as well as inter-sample comparisons / validation with SEM results.

5.6.2. *SCANNING ELECTRON MICROSCOPY*

Two phases of qualitative SEM tests were carried out:

- Phase 1 was carried out to assess the range of minerals present both pre and post 'washing' with deionised water, and;
- Phase 2 was carried out to obtain high resolution, high magnification images of the minerals present to assess their relative abundances and observe their 3D micro-structure.

Both phases of the study required the preparation of small broken fragments, approximately $1cm^3$ in size and displaying at least one fresh rough surface. Samples were selected, where possible, from cores also subject to XRD analysis. It should be noted that all SEM tests are carried out on samples pre-shearing, and that the effect of shearing on the micro-structure of samples is not assessed.

Phase 1

Small broken fragments of calcareous mudstone were first oven dried at 40°C for 48 hours before being sub-sampled in such a way that at least two good $1cm^3$ sized pieces were available from each core to be tested.

One specimen from each core would be briefly submerged in deionised water in order to remove any dissolvable minerals on their surface. These samples were known as the 'washed' samples, and the samples allowed to dry without being submerged in deionised water were known as the 'dry' samples. The washed samples would then once again be allowed to dry in a 40°C oven, as moisture present in the samples prohibits use within the various SEM machines.

Once dry, all samples would be mounted onto aluminium stubs (Figure 5.10) using Achesons Silver ElectroDag 1415 and allowed to dry overnight (as the more frequently used sticky carbon discs could not be used due to the dry surfaces of the mudstones being friable).

Figure 5.10: Calcareous Mudstone mounted onto aluminium stubs in preparation for SEM.

The ESEM machine used was a Philips XL 30 FEG SEM fitted with an EDX system to allow the semi-quantitive detection of elements with an atomic mass equal to or greater that 12(carbon).

The ESEM was used to record high resolution images of samples at up to 5000x magnification without needing to coat specimens in gold or carbon (as this would have disallowed the use of the 'elemental point analyses'). Testing was carried out at a low vacuum (≈1.3 x10^{-7} mbar) and elemental point analysis was undertaken at several locations on both the 'dry' and 'washed' samples for comparisons against one another, but also for comparison with XRD analysis.

Phase 2

This phase of the SEM testing aimed to qualitatively assess the micro-structure of a range of dry specimens. These samples were prepared in the same manner as those of phase 1 with the exception that no 'washed' samples were produced.

Once samples were affixed to their aluminium subs and allowed to dry they were coated in a thin layer (a standard 15µm thickness) of gold using a Polaron SEM coating unit.

Specimens were then examined using a Stereoscan 240 SEM again using a low vacuum (≈1.3 x10^{-7} mbar) and digital images were taken at a range of magnifications, collected using Orion6.60.6 software.

CHAPTER 6. CHARACTERISATION / PETROGRAPHIC STUDY

6.1. CHAPTER 6 INTRODUCTION

The previous chapter stated the finalised methodology adopted for all tests within this thesis, which was itself informed (in part) from the developmental aspects present in Chapter 4. Tests presented and discussed in this and the following chapter (Chapter 7) were carried out according the methodologies discussed in Chapter 5.

This chapter presents and discusses the results of the various characterisation and petrographic tests carried out on samples of Calcareous Mudstone, with the following chapter covering results from the mechanical testing programme.

Results within this chapter are ordered in terms of scale from micro to macro. Optical techniques such as XRD and SEM are presented first, as they focus on very small scale (micro) features such as particle-to-particle contacts and composition, followed by results of tests such as Atterberg limits and PSD's depicting increasingly bulk characteristics.

It should be noted that, whilst results are ordered from micro to macro scale for clarity of presentation, due to the practical and temporal restrictions surrounding the availability of apparatus and raw materials, in practice several tests were carried out parallel to each other. Findings from preliminary triaxial tests, for example, helped inform the overall testing programme in an iterative manner and as such results from different tests feedback into one another, particularly during their discussion. The author would attest that micro to macro scale characteristics of soft calcareous mudstones are inherently linked and due to this there is much unavoidable cross over between this chapter and the chapter directly succeeding it (results of mechanical study).

Samples within this thesis are sub-divided into Type A and Type B based upon observed differences in their mineralogy, micro-structure and mechanical behaviour. This chapter, along with the following chapter, define what is meant by these terms and provides comparisons between these two 'Types' of Calcareous Mudstone.

6.2. PETROGRAPHIC STUDY

The natural cores sourced from the Yas Mina site originated from two layers of calcareous mudstone occurring within close vertical proximity to one another separated by a thin laterally discontinuous gypsum bed. Specific depths and borehole numbers are noted on all samples tested and graphics accordingly and samples from the Yas Mina site are denoted with the prefix *YM*. A small degree of unavoidable natural variability existed between cores; however overall specimens were superficially similar to one another, allowing for direct comparison. Samples sourced from the NBAD site were similar to those from Yas Mina, however originated from greater depths, again from two layers of calcareous mudstone separated by a gypsum bed. Samples from NBAD are prefixed *NB*. A typical sample from either site could be described:

Very weak, thinly laminated, light grey, argillaceous, CALCAREOUS MUDSTONE.

Initial average bulk densities (ρ) of 2.02Mg/m^3 were measured along with average natural moisture contents of 21%. Average dry densities of 1.69 Mg/m^3 and void ratios of 0.59 could then be calculated, and whilst these values can be taken as largely representative of the bulk material, several important (albeit small) inter-sample differences were noted that affected their properties in profound ways.

Preliminary mechanical testing (Figure 6.1) revealed samples could be divided into two distinct behavioural types, despite their superficial similarities. Some samples failed following a high peak stress with a high stiffness (from here onwards denoted as 'Type A') whilst others failed at larger strains and lower stresses (denoted by 'Type B') making the development of a conceptual behaviour model for these apparently similar samples challenging if based purely upon macro-scale, mechanical characteristics.

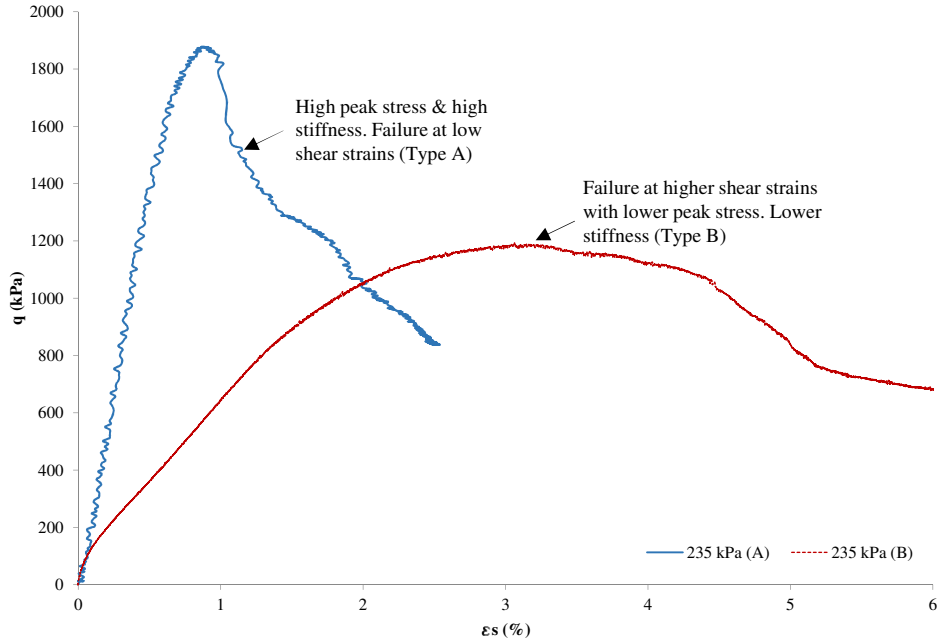

Figure 6.1: Preliminary triaxial testing results on two samples consolidated to 235kPa p'$_0$.

A full review of all mechanical tests carried out in this thesis, including Brazilian indirect tensile tests and triaxial tests, is examined in the following chapter. Table 6.1 summarises the schedule of tests carried out within this chapter exploring the micro-scale, optical and index characteristics of the calcareous mudstone.

Table 6.1: Summary of tests carried out upon calcareous mudstone samples

Sample Code	Borehole No.	Sample Depth (mbgl)	XRD	SEM	Atterberg Limits	Particle Density	PSD	Dispersivity	Durability
YM5-18.40	5	18.40	X	X	X	X	X	X	X
YM8-17.85	8	17.85			X	X	X	X	
YM38-19.20	38	19.20		X	X	X	X		
YM39-19.20	39	19.20	X		X	X	X	X	
YM38-15.40	38	15.40		X	X	X	X	X	
YM38-16.30	38	16.30	X	X	X	X	X	X	X
YM39-14.40	39	14.40	X		X	X	X	X	
YM39-15.10	39	15.10	X		X	X	X		
NB01-33.10	01	33.10			X	X	X	X	
NB02-23.50	02	23.50	X		X	X			
NB02-40.00	02	40.00		X	X	X	X	X	X
NB03-29.00	03	29.00			X	X	X	X	
NB03-45.50	03	45.50	X	X	X	X	X		
NB01-44.75	01	44.80	X		X	X	X	X	
NB02-39.90	02	39.90	X	X	X	X	X		
NB03-35.80	03	35.80	X	X	X	X	X	X	X

6.3. X-RAY DIFFRACTION ANALYSIS

XRD analysis was carried out in two phases. Phase 1 examined the bulk mineralogy of calcareous mudstones from the Yas Mina site and also assessed the effect dissolution had on mineralogy in a qualitative manner. Phase 2 also examined the bulk mineralogy of samples of calcareous mudstone; however did so in a quantitative manner, this time on samples from the NBAD site (the exception being sample YM39-15.10).

6.3.1. *PHASE 1 – QUALITATIVE XRD ANALYSIS*

Two sets of qualitative XRD tests on powdered bulk samples were carried out in order to characterise both mineralogy and the potential effect of dissolution. Samples were selected from the 'Type A' (namely YM5-18.40 and YM39-19.20) and 'Type B' (namely YM39-14.40 and YM38-16.30) specimens to see if a mineralogical discrepancy might account for the mechanical differences. Samples were taken only from the Yas Mina site, due to availability of NBAD samples at the time of testing.

In addition, sub-samples of all specimens were prepared by exposing them first to flowing deionised water, in order to assess the effect of dissolution. In total 4No. samples from the Yas Mina site were analysed using XRD, both before exposure to flowing water (named 'Dry' samples) and after (named 'washed' samples).

All 'Dry' samples tested are compared against one another in Figure 6.2, with notable mineral phases highlighted.

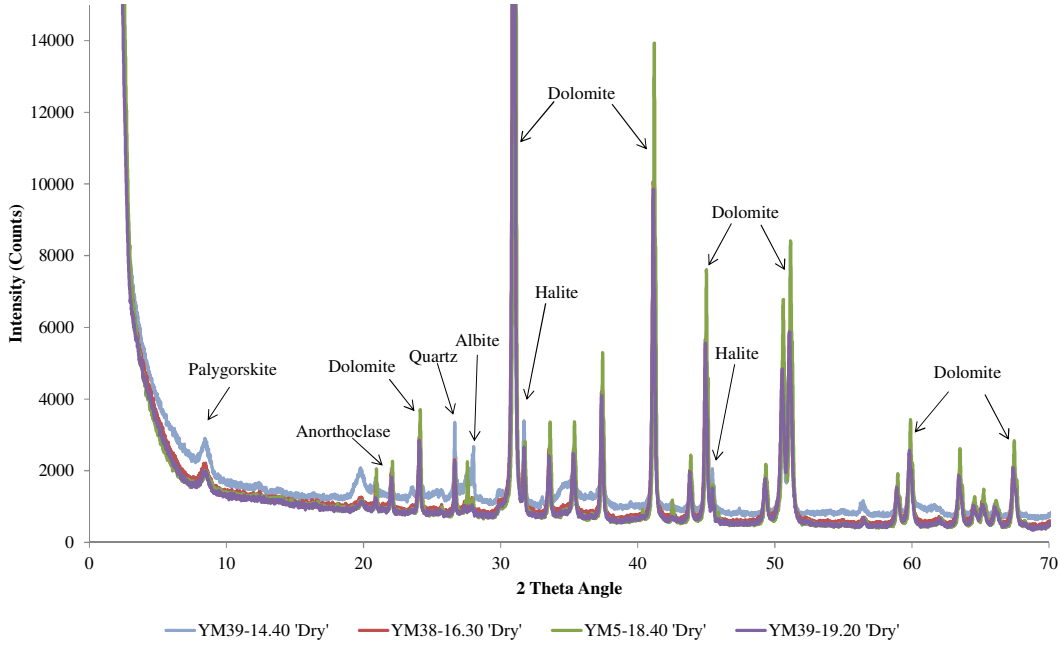

Figure 6.2: XRD comparison of all 'Dry' samples of calcareous mudstone.

All samples are noted to show similar peak angles and peak heights, indicating that they are comprised of very similar minerals qualitatively. Figure 6.2 is scaled to enable better comparisons between minor constituents, revealing the presence of Albite, Anorthoclase, Quartz, Halite and the clay mineral Palygorskite in all samples; however Dolomite is clearly the prevailing mineral type (as shown in Figure 6.3) with very high intensity counts. Interestingly, no Calcite was noted in any of the samples tested.

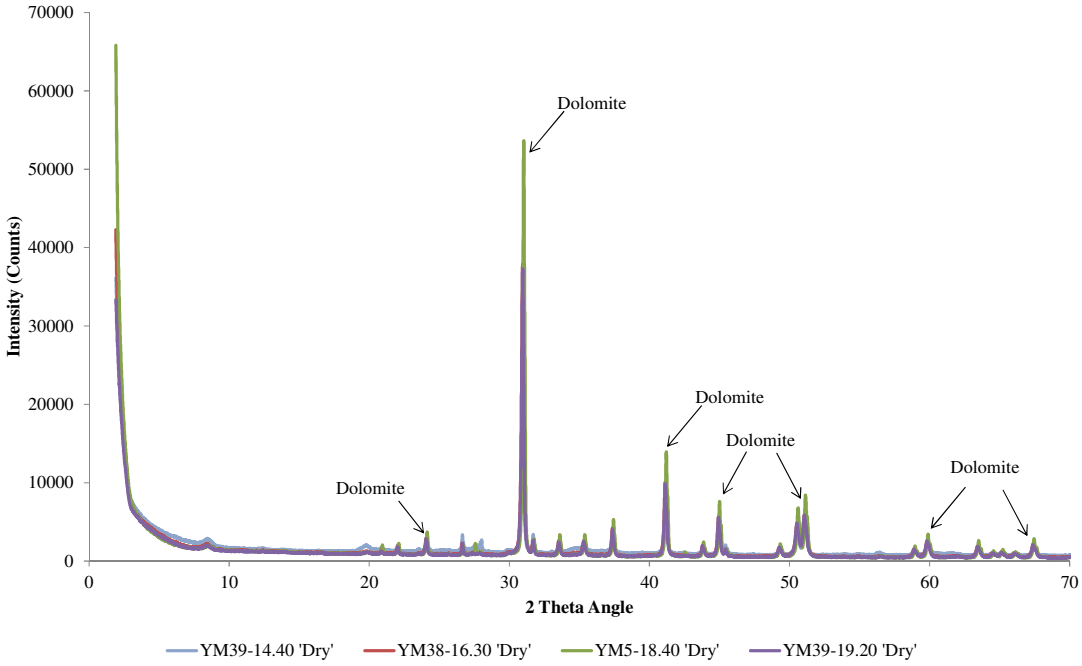

Figure 6.3: XRD comparison of all 'Dry' samples, without re-scaling.

Dolomite is a common mineral to be found associated with sediments and rocks formed in hyper-saline water bodies, however its method of formation is a great source of controversy within the literature, as Dolomite is not forming today at the earth's surface except within extreme environments such as hot springs (Eugster & Hardie, 1978); (Last, 1990); (Sanz-Montero, et al., 2006). The geological history of this area (see Chapter 3) describes repeated cycles of marine transgressions and the formation of lagoons, lagoonal channels, sabkhat, backwater reefs and other sub-environments that are still seen today along the coast of Abu Dhabi, however applying the notion of uniformitarianism to compare the modern surface and older buried deposits is not possible, as all modern calcareous sediments precipitating within this area are composed of Calcite and/or Aragonite (Evans , et al., 1973); (Scherf & Rullkotter, 2009). And yet all sample cores from depth tested within this thesis are shown to be predominantly Dolomite, and indeed this is the case in many hyper-saline lakes the world over (Sanz-Montero, et al., 2006). This is a reoccurring issue within the geological community and is given the name 'The Dolomite Problem'. Even attempts to reconstruct conditions to

allow its precipitation within the laboratory are largely unsuccessful, unless carried out at very low temperatures with high pH (>9.5) that are generally unrepresentative of in-situ conditions (Krauskopf & Bird, 1995).

It is not the aim of this thesis to answer the question as to the origin of the Dolomite deposits at the study sites; however it is interesting to note the variety of processes and theories that might be responsible for its presence, ranging from the replacement of Calcite of Aragonite by Dolomite and the replacement of Gypsum by Dolomite to the microbially mediated precipitation of Dolomite by algae and sulphate-reducing bacteria (Pierre & Rouchy, 1988); (Machel, 2001); (Sanz-Montero, et al., 2006).

The minor quantities of Quartz and Feldspars present in the XRD analysis (with low intensity counts) are likely to be due to occasional grains of detrital debris, transported from an adjacent high energy sub-environment into the low energy sub-environment that allowed the carbonate muds to form. These occasional grains of quartz and feldspar are coarser than the mudstone matrix, and as such are easily identified during SEM and PSD analysis.

Halite in these samples is probably present due to the recent precipitation of remnant saline pore-water from the sample drying during preparation for testing, although the potential for crystalline Halite existing within the mudstone structure is not ruled out.

One mineral of significant interest is Palygorskite, which occurred in all samples. This was originally misidentified as Muscovite Mica in sample YM5-18.40'Dry', however the reoccurrence of Palygorskite in the other 'Dry' samples tested along with the presence of Palygorskite in YM5-18.40'Washed' (and no Muscovite) led to the sample being re-tested and Palygorskite being positively identified.

Palygorskite is a hydrous magnesium alumina (and iron) silicate, a fibrous clay mineral, the origin of which is debated at length within the literature (Haydn, et al., 2005). Palygorskite, sometimes known as Attapulgite, is a member of the Hormite family of clays, along with Sepiolite, (although Hormite is now considered an antiquated term), and has many industrial uses due to its sorptive capacity including lubricants, adhesives, paints and pharmaceuticals (Haydn, et al., 2005); (Benaissa, et al., 2013). It tends to be found in carbonate sedimentary rocks and sediments deposited in high temperature / salinity marine / lagoonal waters (Isphording, 1973); (Rodriguez-Navarro, et al., 1998); (Haydn, et al., 2005); (Macklin, et al., 2011); (Benaissa, et al., 2013) as well as forming in peri-marine and non-marine environments by detrital sedimentation under varying

salinity conditions. Stagnation of the source water, along with its alkalinity, the presence of Si- and Mg-rich fluids and intense evaporation are all considered to be critical to its formation (Inglès & Anadón, 1991); (Haydn, et al., 2005).

The modern day lagoons around the Abu-Dhabi coast fluctuate in temperature and salinity throughout the year. Some are well connected to the main body of the Arabian Gulf, whilst others are more isolated allowing them to become hyper-saline. It is likely that these conditions were also present in the older, buried, soft rocks potentially giving rise to the ideal environment for localised high concentrations of Palygorskite to form within the carbonate mudstones (Haydn, et al., 2005).

The highest peak indicating Palygorskite during XRD analysis, like many clay minerals, occurs at a low 2 Theta angle (with 2 Theta being defined as the angle between the incident x-ray beam and the diffracted beam received by the detector). Within this region there is much noise associated with the limitations of the test itself, making Palygorskite difficult to quantitatively measure.

A selection of sub-samples were exposed to flowing deionised water in order to qualitatively assess their susceptibility to dissolution on a mineralogical scale. These 'Washed' samples provide results that are highly comparable with one another (as shown in Figure 6.4).

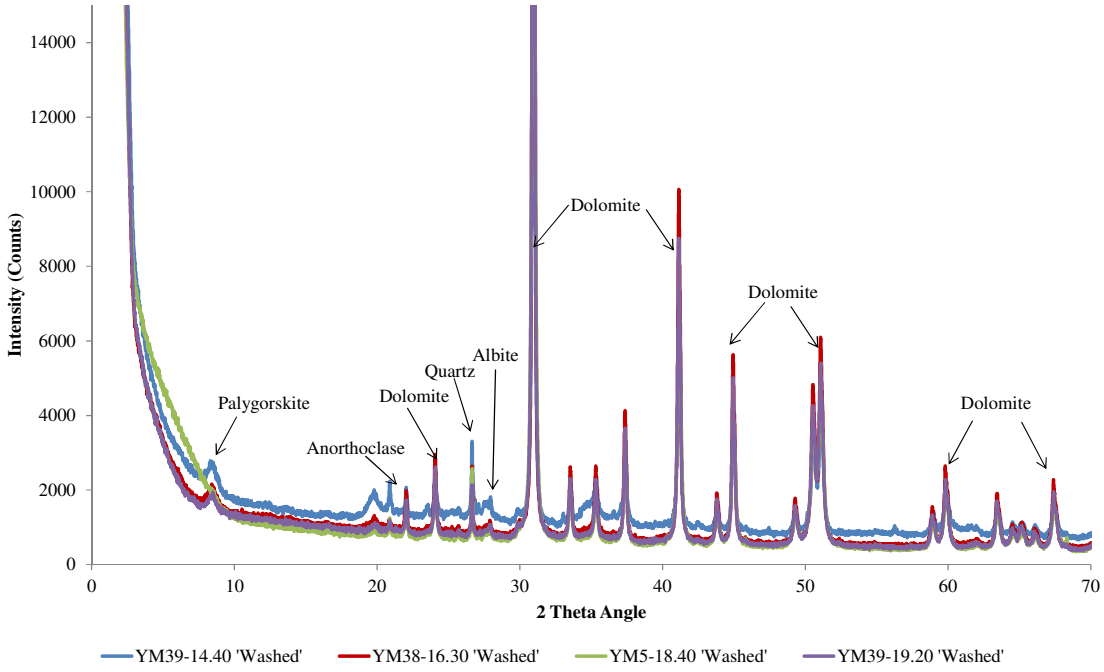

Figure 6.4: XRD comparison of all 'Washed' samples of calcareous mudstone

Aside from showing minor changes to the peak height of the dolomite intensity counts and minor reductions in the low angle mineral intensity counts, (which are both thought

to be related to the method of filtering the 'Washed' samples), the only mineralogical change following exposure to deionised water is in the total loss of Halite. This is most easily demonstrated using a direct comparison (Figure 6.5):

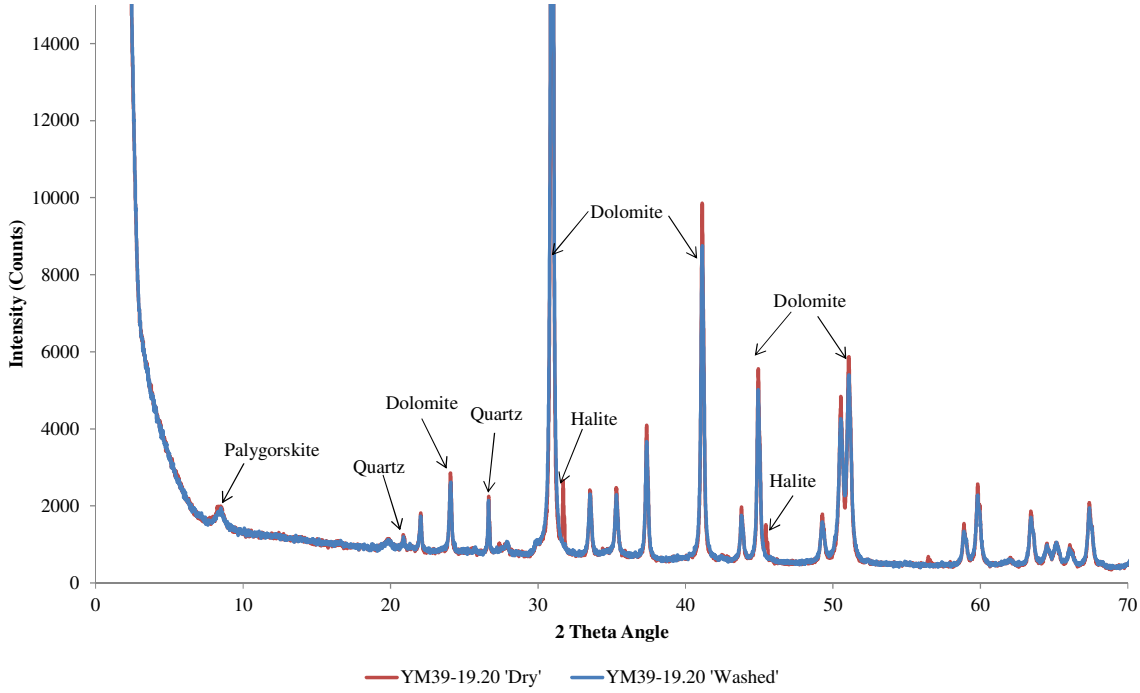

Figure 6.5: XRD analysis of a representative calcareous mudstone sample both before and after exposure to deionised water.

As Halite is so easily removed during exposure to flowing water, there exists a possibility of the integrity of the calcareous mudstone to be damaged by the loss of this mineral, or by other dispersible or soluble components. This could potentially create problems when testing samples in triaxial apparatus (or any laboratory test that typically uses pore fluids), and may also go some way towards explaining the observed pattern of this lithology becoming decreasingly competent with prolonged exposure to fresh water. As a minimum concern, any low saline pore fluid passing through these materials will increase in salinity as the Halite is dissolved, possibly altering the shrink / swell characteristics of any clay minerals with which it interacts as a given test goes on.

XRD analysis revealed no gypsum or anhydrite within any of the samples tested, despite the in-situ proximity of the sample cores to known gypsum beds. A comparison of pure, 'star quality' gypsum is shown next to a representative sample in Figure 6.6, it can be seen that no peaks are familiar to both data sets.

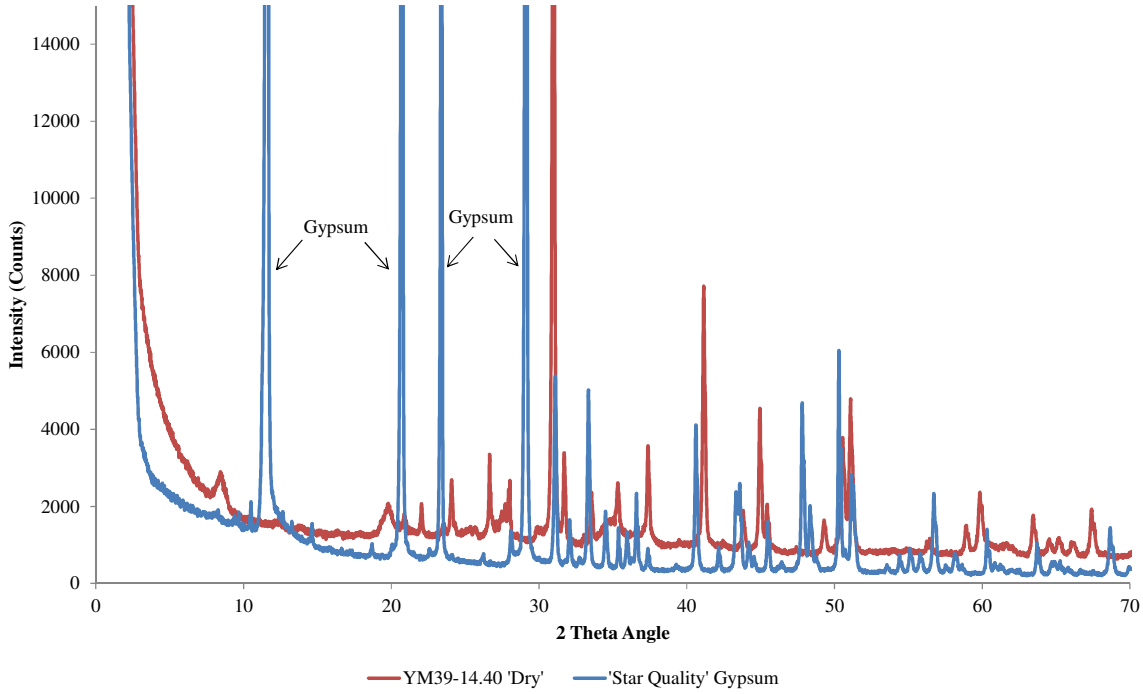

Figure 6.6: Comparison between star quality gypsum and representative 'Dry' sample using XRD.

This allows gypsum to be excluded as a candidate for dissolution within the samples tested, however may be present in small quantities within some of the untested samples (no macro scale crystals were noted during examination of any of the sample cores).

It is important to note that qualitative XRD analysis was unable to highlight any mineralogical difference between the 'Type A' and 'Type B' materials noted during mechanical testing, meaning that any differences must be due to the relative abundances of minerals present and not due solely to the presence of specific minerals.

6.3.2. *PHASE 2 – QUANTITATIVE XRD ANALYSIS*

Quantitative (or semi-quantitative) XRD tests on powdered bulk samples were carried out in order to characterise samples' mineralogy. No sub-samples were taken or tested during this second phase of XRD analysis and so the effect of dissolution is not assessed. Samples were again selected from the 'Type A' specimens (namely NB02-23.50 and NB03-45.50) and 'Type B' specimens (namely NB01-44.75, NB02-39.90 and NB03-35.80), along with sample YM39-15.10, to see if differences in the relative abundance of minerals present might account for the mechanical differences noted.

Once again, all tests showed samples to comprise Dolomite, Quartz, Halite and Palygorskite regardless of depth or strength, and XRD plots of intensity counts against 2-Theta angle shows very similar inter-sample patterns as well as showing patterns similar to those from the Yas Mina site.

Rietveld refinement is a method of quantifying relative abundances of powdered bulk crystalline materials by examination of the peak shape and size during XRD analysis (Rietveld, 1969). This analysis is considered semi-quantitative, as inherent limitations of the powdered XRD method (for example reduced ability to identify minerals with low 2 Theta angle crystal phases and minerals with poorly formed crystalline forms) can prevent absolute quantities being reported. This method revealed the following percentages of minerals to be present (Table 6.2):

Table 6.2: Summary of Rietveld analysis on calcareous mudstone samples

Sample Code	Borehole No.	Sample Depth (mbgl)	Dolomite (%)	Quartz (%)	Halite (%)	Palygorskite (%)	Strength Designation*
NB02-23.50	02	23.50	88.0	1.0	1.8	9.2	'Type A'
NB03-45.50	03	45.50	89.0	4.0	2.5	4.5	'Type A'
YM39-15.10	39	15.10	73.0	1.1	2.9	23.0	'Type B'
NB01-44.75	01	44.80	73	6.9	2.4	17.7	'Type B'
NB02-39.90	02	39.90	84	3.6	2.0	10.4	'Type B'
NB03-35.80	03	35.80	82	2.0	2.0	14.0	'Type B'

*from correlations with mechanical data

From these results is can be seen that the 'Type A' samples have overall higher percentage fractions of Dolomite (average of 88.5%) and lower percentages of Palygorskite (average of 6.9%) whilst having similar amounts of Quartz and Halite to the 'Type B' samples. The 'Type B' samples, by contrast, have significantly lower percentages of Dolomite (average of 78.0%) whilst also having higher amounts of Palygorskite (average of 16.3%).

These trends correspond well to the findings of the PSD analysis where upon 'Type B' samples have a greater percentage of clay sized grains than 'Type A' specimens.

6.4. SCANNING ELECTRON MICROSCOPY (SEM)

This section of the thesis, like the XRD analysis before it, is broken into two studies. Firstly, SEM is used to assess the mineralogy of a suite of samples in order to corroborate the findings of the XRD analysis. This study also examines the effect of exposure of samples to deionised water to assess any dissolution that occurs.

The second study is purely optical/observational, using high resolution images of samples for comparison in order to observe the microscopic 3D particle organisation / orientation of the calcareous mudstones constituents.

In both cases, several 'broken sections' (approximately 6mm^3 in size and displaying at least one fresh rough surface) were prepared in order to assess initial micro-structure. The evolution of micro-structure with shear strain is not examined within this thesis.

6.4.1. *MINERALOGICAL AND DISSOLUTION ESEM ANALYSIS*

A total of 4No. samples are assessed during this first study, all originating from the Yas Mina site. Samples used in this first study include both those representing 'Type A' specimens (YM5-18.40 and YM38-19.20) and those representing 'Type B' specimens (YM38-15.40 and YM38-16.40).

Initial low magnification (x350) images show a relatively homogenous clay to silt sized rock that is broadly mono-mineralic except for the occasional fine sand sized grains that are set within the overall fine groundmass along with localised high contrast areas (for example as seen in Figure 6.7).

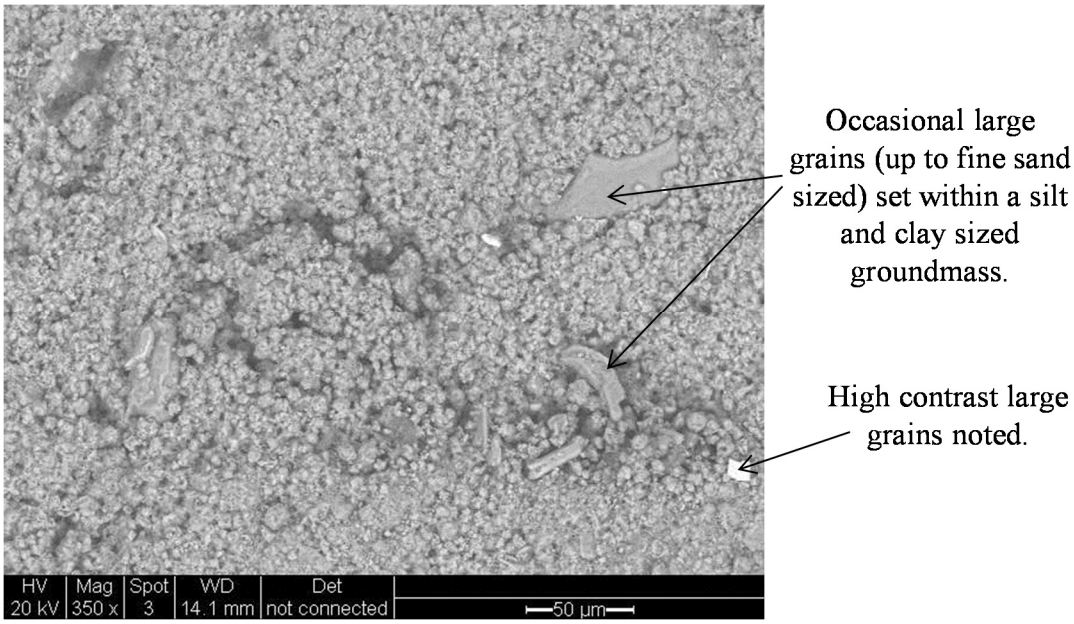

Figure 6.7: Example of low magnification ESEM image of calcareous mudstone, taken from sample YM5-18.40.

Elemental point analysis of the specimens carried out at higher magnifications (x2000) revealed the makeup of the groundmass to be predominantly calcium, magnesium, carbon and oxygen with traces of aluminium and potassium (as shown at point 0 in Figure 6.8 and Figure 6.9).

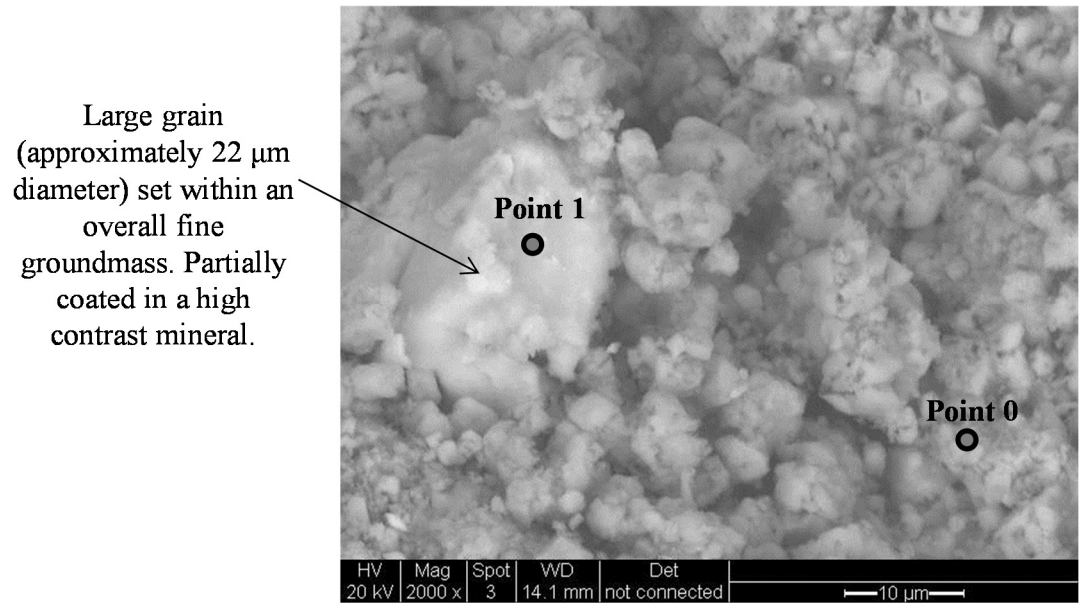

Figure 6.8: ESEM image of sample YM5-18.40 with elemental point analysis locations annotated.

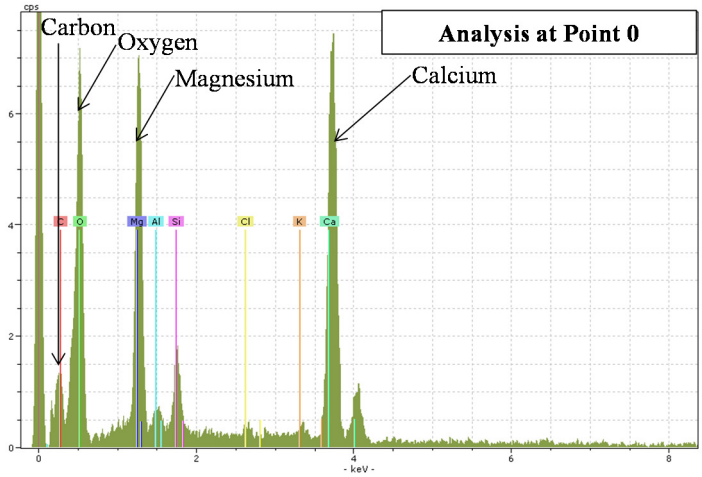

Figure 6.9: Elemental analysis of sampleYM5-18.40 at point 0.

These findings support the XRD mineralogical interpretation that Dolomite is the prevailing composition of this lithology. Bench tests using dilute (10%) hydrochloric acid (HCL) also support the dolomite rich nature of all samples tested (Burnett & Epps, 1979); (Macklin, et al., 2011), as cold HCL provokes no reaction whilst warm HCL causes effervescing. The groundmass appears tightly compact, predominantly fine (micritic) rounded grains, with multiple grain to grain contact points. What is more, the composition of the groundmass particles is the same as that of the contact points between the particles. This indicates that the cementing agent is of the same mineralogy as that of the groundmass particulate. High magnification (x5000) show grains to be fused to one another, and there to be thin needle form minerals present (Figure 6.10). These needle like minerals may be the Palygorskite identified during XRD analysis, however image resolution is too low without the benefit of gold plating and the elemental point analysis could not capture reliable information given their small size.

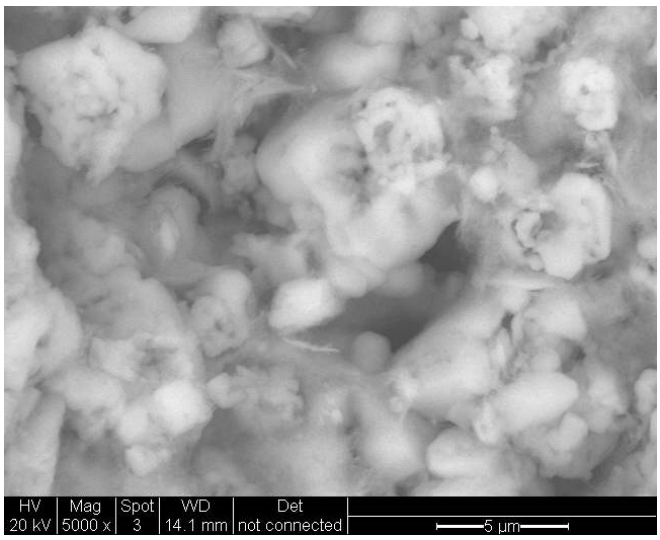

Figure 6.10: 5000x magnification of sample YM5-18.40 showing grains to be fused to one another. Minerals with needle forms are also present within voids.

The rare fine sand sized grains were also analysed using the ESEM point analysis (for example at point 1 in Figure 6.8 and Figure 6.11) and were found to comprise silica, oxygen, aluminium and magnesium along with sodium and chlorine.

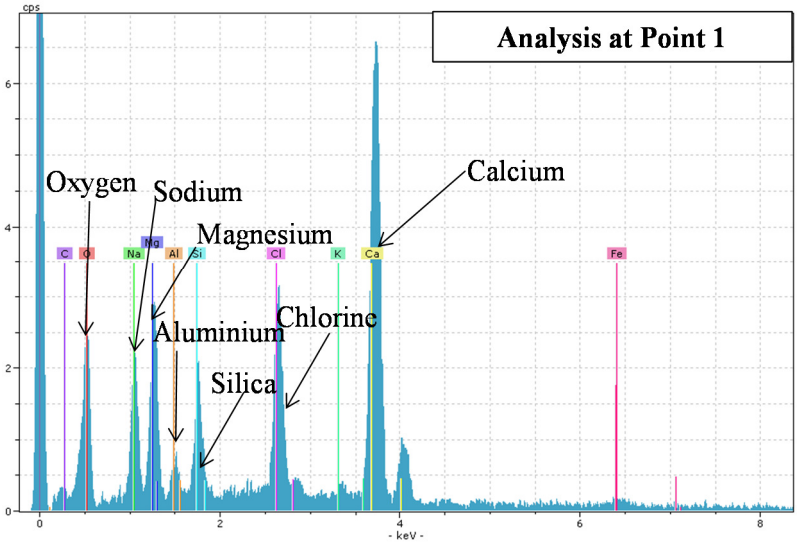

Figure 6.11: Elemental analysis of sampleYM5-18.40 at point 1.

With respect to the findings of the XRD analysis, along with knowledge of relative mineral harnesses, the elemental data gathered at the locations of the sand sized grains noted in all samples are interpreted as being quartz and feldspar.

Halite, being composed of sodium and chlorine, is also thought to be present. Most locations analysed in samples YM38-15.40, YM38-16.40, YM5-18.40 and YM19.20 showed the presence of sodium and chlorine, particularly in high contrast regions. It is thought that this mineral is precipitating during the drying phase of sample preparation,

from the existing saline pore-waters, creating a thin coating on the walls of voids, as opposed to there being crystalline halite existing within the lithologies structure.

In order to assess the effect of dissolution on sample structure and mineralogy, samples were submersed in deionised water for a short period of time before being re-dried and analysed using ESEM. Analysis of a representative sample is shown as Figure 6.12.

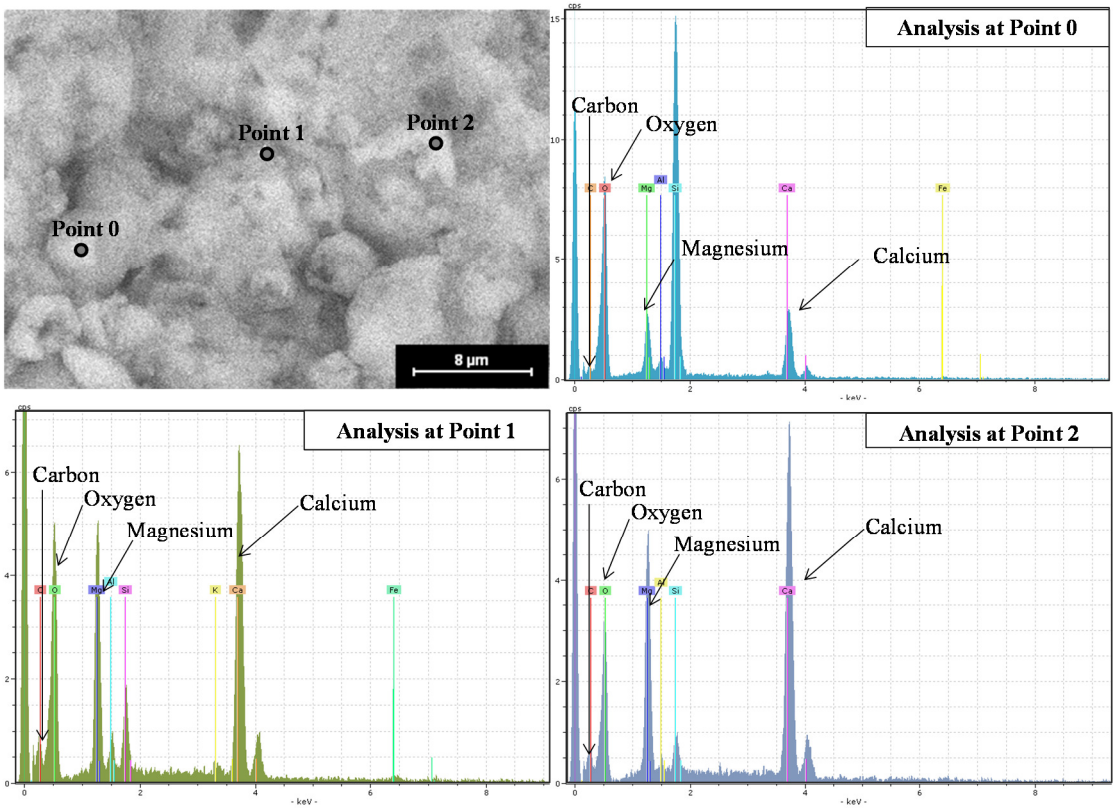

Figure 6.12: ESEM analysis of sampleYM5-18.40 following submersion in deionised water.

Superficially the 'Washed' calcareous mudstone samples were noted to become very weak and clay-like prior to being re-dried. Once dry however, the macro and micro scale SEM analysis showed little change from their 'Dry' state.

Point analysis of the 'Washed' samples differed from their 'Dry' state only in that they showed no (or very minor) traces of sodium and chloride, indicating that any Halite present had been removed during the exposure to deionised water.

The ESEM analysis revealed little mineralogical difference between 'Type A' and 'Type B' samples.

6.4.2. *OPTICAL SEM ANALYSIS*

Several samples were also selected to be coated in gold to a thickness of 15nm to achieve higher SEM resolutions for imaging purposes in the second stage of this study.

This study included samples from both the Yas Mina and NBAD sites, again with specimens representing both the 'Type A' (YM5-18.40, YM38-19.20, NB02-40.00 and NB03-45.50) and 'Type B' (YM38-15.40, YM38-16.40, NB02-39.90 and NB03-35.80) mechanical behaviours.

By coating samples in gold, a significant increase in image clarity and resolution is gained, at the expense of the elemental analysis tool (EDX). Reanalysing samples looked at in study one (YM5-18.40, YM19.20, YM38-15.40 and YM38-16.40) has allowed the micro-structure of the calcareous mudstone to be better understood. The rounded (peloidal), fused dolomite grains can be clearly seen, for example in sample YM5-18.40 (Figure 6.13) along with occasional rhombic grains.

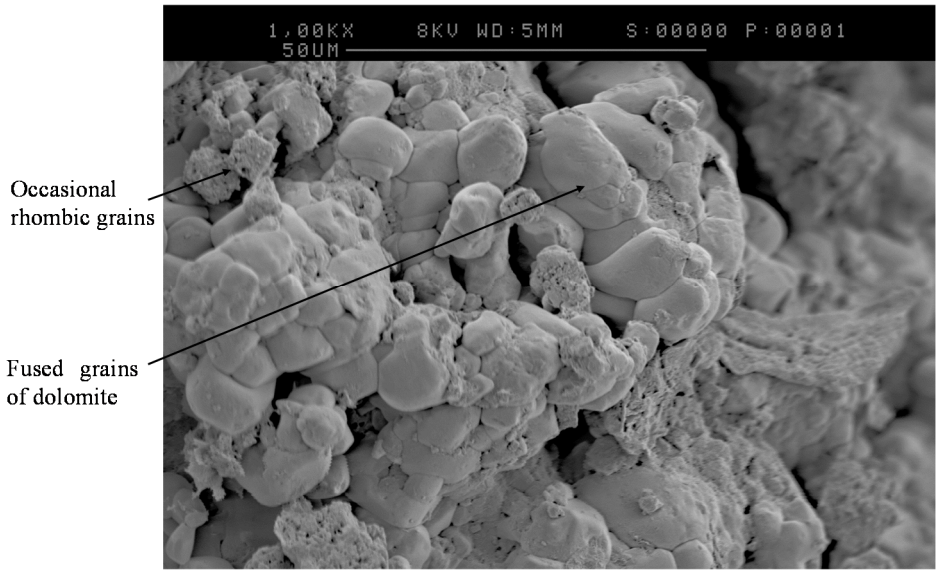

Figure 6.13: SEM analysis of sampleYM5-18.40.

It is likely that the tightly bonded subhedral peloids (rounded, fused grains) are in fact the remains of a partially dissolved interlocking mosaic, a common feature in carbonate digenesis caused by neomorphism (a process of continual localised precipitation and dissolution of grains and grain contact points during digenesis) (Mazzullo, 1992); (Jameson, 2009).

The rhombic shaped grains (rhombs) were initially thought to be calcite; however no calcite was shown to be present during XRD analysis. These grains are now interpreted as being partially dissolved Dolomite, as rhomboid shapes are also a common form of Dolomite crystals (Sanz-Montero, et al., 2006).

SEM images highlight great differences between 'Type A' and 'Type B' samples in terms of both their structure and the presence (or lack) of the inter-clast clay mineral

Palygorskite, that was not observable when using the lower resolution ESEM setup in the previous study. A clear example of this is by comparison of a 'Type A' sample (YM5-18.40) and a 'Type B' sample (YM38-16.40) in Figure 6.14.

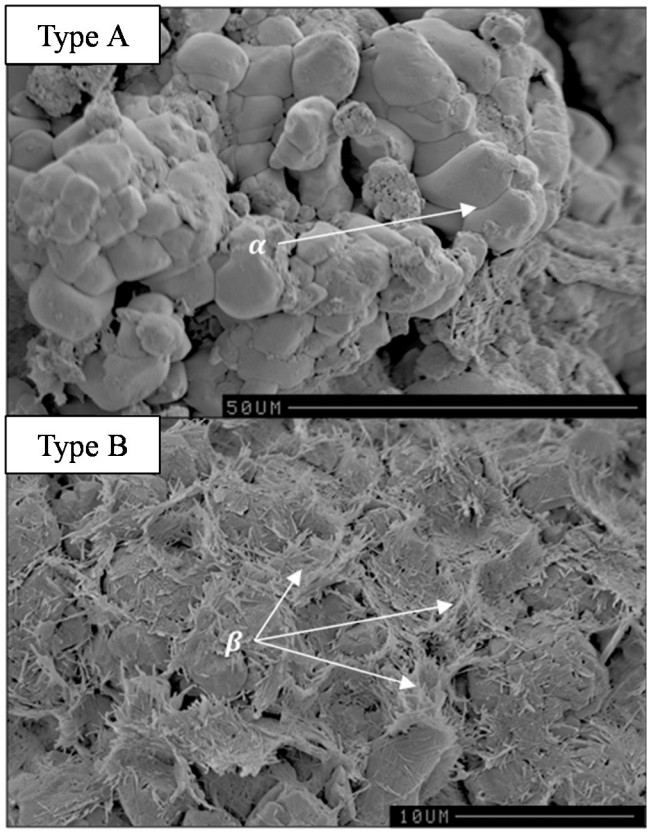

Figure 6.14: Type A sample displaying inter-clast fusing of dolomite with low amounts of Palygorskite, and Type B sample showing a high percentage of inter-clast fibrous Palygorskite and an overall smaller grain size.

Figure 6.14 Type A shows clasts of Dolomite fused tightly together with very little or no inter-clast minerals present (for example at point α), whereas Figure 6.14 Type B contains high quantities of a clay mineral with a micro fibrous morphology located both on and between clasts (for example at points β). These trends are broadly representative of the 'Type A' and 'Type B' samples.

The fibrous clay mineral in question is believed to be Palygorskite (as indicated in the XRD analysis) and due to its superficial morphology being markedly similar to that of the Palygorskite tested by Neaman & Singer, (2000) and Benaissa, et al, (2013). It appears as mono-mineralic assemblages of straight fibres at random orientations to one-another within void spaces and between larger grains, a common textural form when associated with Dolomite or Marls and is thought to be formed via its precipitation from solution (Singer, 1981). Merkl, (1989), identified that Palygorskite may appear as short length (<10µm) and long length (>10µm), signifying low magnesium and high

magnesium respectively (Haydn, et al., 2005). Based on the size of the Palygorskite fibres found in all SEM images, it can be deduced that the low magnesium short-length form is more common in the samples studied in this thesis, as the Palygorskite tended to be present as assemblages of numerous 2-8µm long fibres.

Interestingly, the previously mentioned process of neomorphism that is thought to be responsible for the tightly bonded mosaics, is believed to be inhibited by the presence of clay minerals. This perhaps explains why samples displaying more Palygorskite (Type B) are significantly weaker mechanically than those with relatively less (Type A), as will be shown in the following chapter.

Several 'Dry' samples tested displayed areas that appeared to be fully fused, to the point that individual grains seemed amorphous, such as those seen in YM38-19.20 (Figure 6.15).

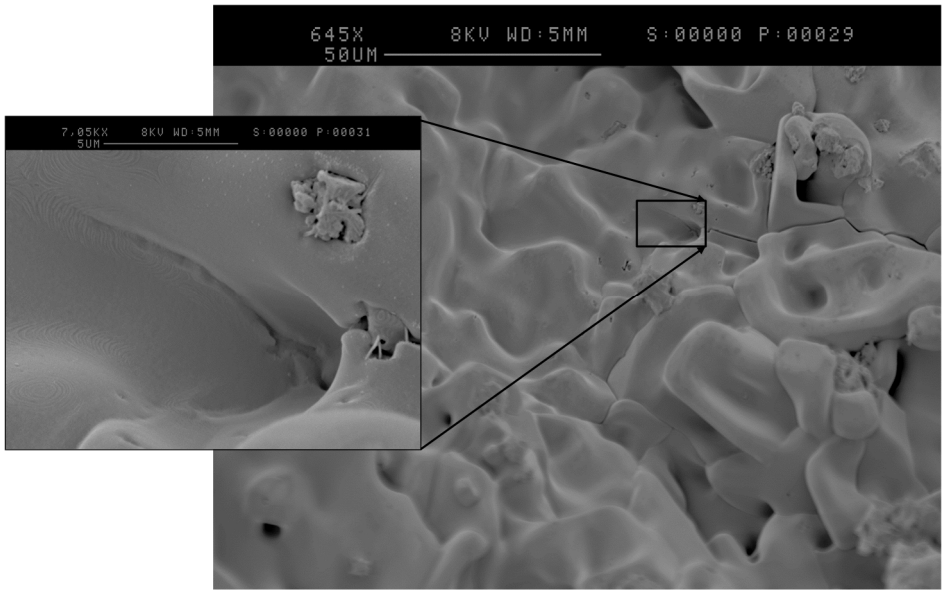

Figure 6.15: Sample YM38-19.20 displaying a highly amorphous texture.

Initially this feature was interpreted as an advanced stage of neomorphism, particularly as it appeared more commonly in the 'Type A' samples tested. However when seen at high magnifications (such as that of the inset picture in Figure 6.15) a very smooth texture is noted, unlike that seen at high magnifications around fused Dolomite grains (as shown in Figure 6.16).

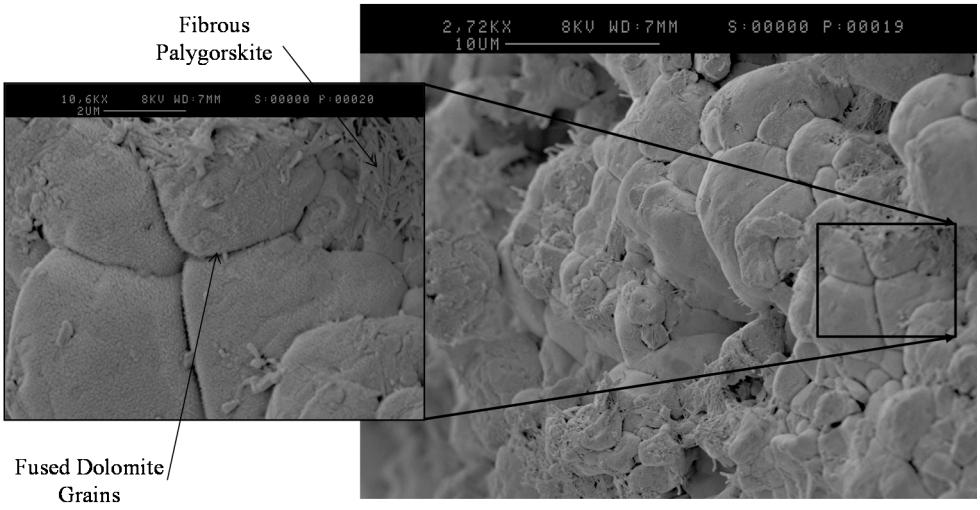

Figure 6.16: Sample YM5-18.40 showing a high magnification image of a set of fused Dolomite grains.

This common amorphous feature is now believed to be a thin layer of Halite, effectively coating both the Dolomite groundmass and the inter-granular Palygorskite as it precipitates and is frequently noted in the Yas Mina samples.

Samples from the NBAD site displayed features similar to the fused grains noted in Figure 6.16, particularly within Type A specimens, however they are noted to appear to be significantly smoother in appearance, superficially similar to the Halite coatings noted earlier in Figure 6.15. At high magnifications, for example Figure 6.17 (and inset), these features are noted to contain areas covered in frequent hollows, through which the underlying fibrous Palygorskite may be seen and the grains themselves are texturally rough, as opposed to amorphous.

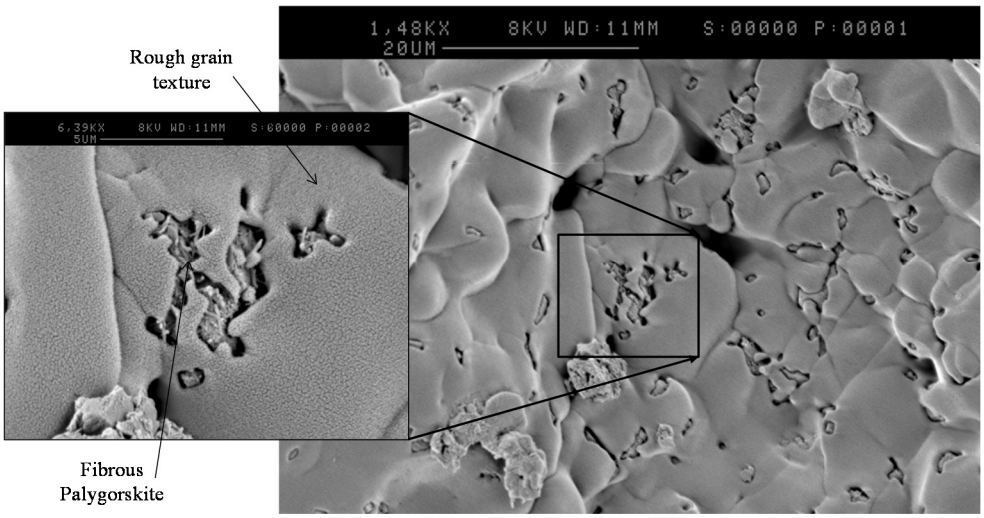

Figure 6.17: Sample NB2-40.00 showing a high magnification image of Palygorskite within Dolomite.

These high resolution images are captured using gold coated samples in SEM, allowing detailed features to be clearly observed. Unfortunately it is not possible to verify the mineralogical makeup of these features using EDX, as these techniques are mutually exclusive to one another, and preparing a single sample for analyses using both techniques consecutively is practically very difficult to achieve. As such, interpretation of features such as those shown in Figure 6.17 is problematic. It is believed that, due to the rough texture noted, this feature is indeed an example of fused Dolomite grains, albeit at a later stage than that shown in Figure 6.13 and Figure 6.16 (possibly owing to the greater depth of origin, and therefore age, of the materials in question).

The Dolomite appears to have grown over the Palygorskite fibres (overgrowths) to a degree, again likely due to processes of neomorphism (Jameson, 2009), however the existence of Palygorskite filled hollows perhaps supports the previous hypothesis that the clay mineral is stopping the Dolomite grains from fusing fully.

A final observation was made in sample NB01-44.75 where the fibrous mineral present was taking on a 'mesh-like' appearance unlike the more acicular form of the Palygorskite in the shallower samples (Figure 6.18).

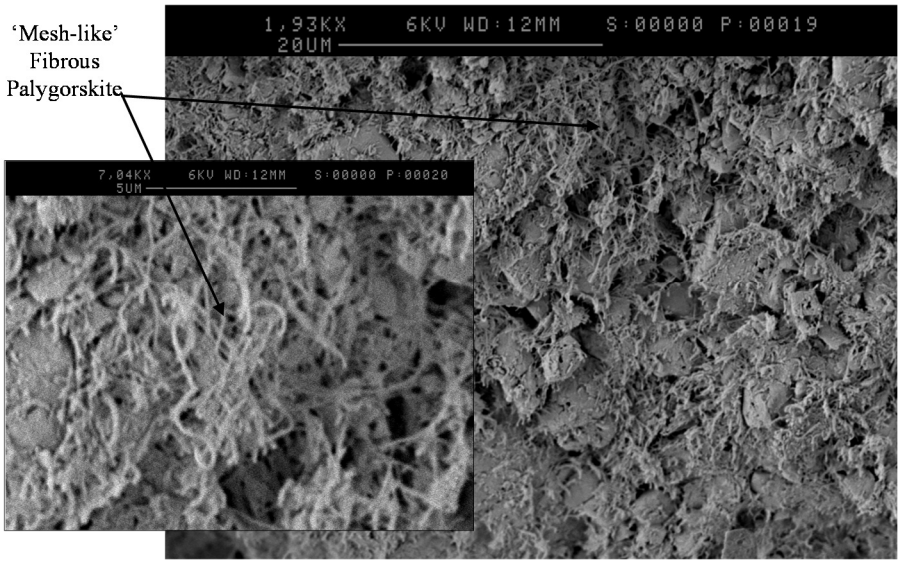

Figure 6.18: Sample NB01-44.75 showing 'mesh-like' Palygorskite form within Dolomite.

This was initially interpreted as a change to Illite in the clay fraction, however XRD analysis (and indeed findings of Atterberg and activity levels) indicate this not to be the case. It is possible that this 'mesh-like' appearance is a different phase of Palygorskite, however once again XRD analysis carried out on bulk samples shows no detectible evidence of multiple phases of this clay mineral. This 'mesh-like' configuration is also noted to be superficially similar to samples analysed as part of Bontognali, et al (2010)

research on similar materials sourced from microbial mats in Abu Dhabi, although no organic matter was detected within this specific sample to verify its origin as such.

Based on the preliminary triaxial tests along with both the XRD / SEM testing it is believed that the presence (or absence) of large quantities of inter-clast Palygorskite within samples is responsible for the significant differences in mechanical behaviour during physical testing. The mechanism responsible for the decrease in material strength with increased clay content is thought to be related to a combination of the swelling properties of Palygorskite (during shearing when fully saturated, for example), along with earlier digenetic processes having been inhibited (resulting in weaker bonded Dolomite grains).

6.5. ATTERBERG LIMITS

Atterberg limits were carried out primarily to classify whether the remoulded calcareous mudstones behave as a clay-like or silt-like material, and secondarily to attempt to distinguish between the 'Type A' and 'Type B' specimen types using an inexpensive and repeatable standard test. Results within this section are presented site specifically before being directly compared and discussed and finally the effect of changing salinity of the pore-water (to better represent the in-situ chemical conditions is explored).

6.5.1. *YAS MINA ATTERBERG LIMITS*

Sample results of Atterberg limits from the Yas Mina site are averaged and summarised in Table 6.3. Multiple repeat tests were carried out on each core in order to provide more reliable mean results from a broader data set.

Table 6.3: Summary of Yas Mina samples Atterberg Limits

Sample Code	Borehole No.	Sample Depth (mbgl)	Plastic Limit (%)	Liquid Limit (%)	Plasticity Index	Plasticity Designation	Strength Designation*
YM5-18.40	5	18.40	24.0	42.9	18.9	CI	'Type A'
YM8-17.85	8	17.85	20.8	32.6	11.8	CL	'Type A'
YM38-19.20	38	19.20	28.2	46.4	18.2	CI	'Type A'
YM39-19.20	39	19.20	21.7	37.9	16.3	CI	'Type A'
YM38-15.40	38	15.40	26.6	54.4	27.8	CH	'Type B'
YM38-16.30	38	16.30	26.3	45.1	18.8	CI	'Type B'
YM39-14.40	39	14.40	29.7	50.5	20.8	CH	'Type B'
YM39-15.10	39	15.10	26.6	66.2	39.6	CH	'Type B'

*from correlations with mechanical data

Results are plotted graphically in Figure 6.19. It should be noted that the strength designations are derived from physical mechanical performance (triaxial data and Brazilian tensile strength data), which will be discussed in the following chapter.

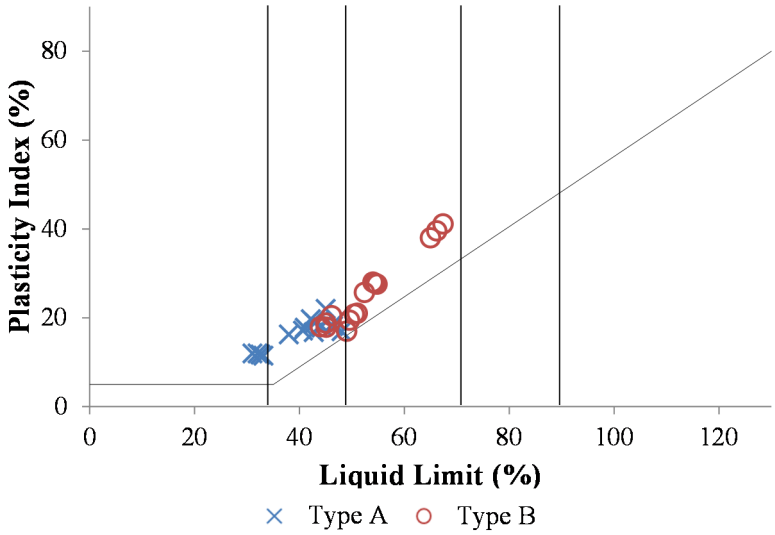

Figure 6.19: Cassegrande classification showing both 'Type A' and 'Type B' samples from the Yas Mina site.

Samples initially appeared to show a wide spread of results, however once grouped into those which showed mechanically strong and stiff behaviour ('Type A') and those prone to relatively weaker, more ductile mechanical behaviour ('Type B'), a clear pattern emerged.

It should be noted that all results plot above the A-line, immediately categorising the remoulded calcareous mudstones as having clay-like behaviour. Average 'Type A' samples have plastic limits of 23.9%, liquid limits of 40.4% and plasticity index of 16.6%, designating them as being of intermediate to low plasticity (some samples were noted as being non-plastic, these do not appear in Figure 6.19). The 'Type B' samples had mean values of 27.6%, 53.0% and 25.4% respectively and were designated as being of intermediate to high plasticity.

6.5.2. *NBAD ATTERBERG LIMITS*

Samples tested from the NBAD investigation are also averaged, summarised and presented in Table 6.4 and are plotted graphically in Figure 6.20. Multiple sub-samples were again taken from each core. Strength designations are derived from triaxial and Brazilian tensile strength data.

Table 6.4: Summary of NBAD samples Atterberg Limits

Sample Code	Borehole No.	Sample Depth (mbgl)	Plastic Limit (%)	Liquid Limit (%)	Plasticity Index	Plasticity Designation	Strength Designation*
NB01-33.10	01	33.1	23.0	43.5	20.5	CI	'Type A'
NB02-23.50	02	23.5	23.3	42.3	19.1	CI	'Type A'
NB02-40.00	02	40.0	27.8	44.0	16.3	CI	'Type A'
NB03-29.00	03	29.0	21.1	37.8	16.7	CL	'Type A'
NB03-45.50	03	45.5	23.3	36.0	12.8	CL	'Type A'
NB01-44.75	01	44.8	26.2	53.1	26.9	CH	'Type B'
NB02-39.90	02	39.9	29.5	52.3	22.8	CH	'Type B'
NB03-35.80	03	35.8	28.5	48.5	20.0	CI	'Type B'

*from correlations with mechanical data

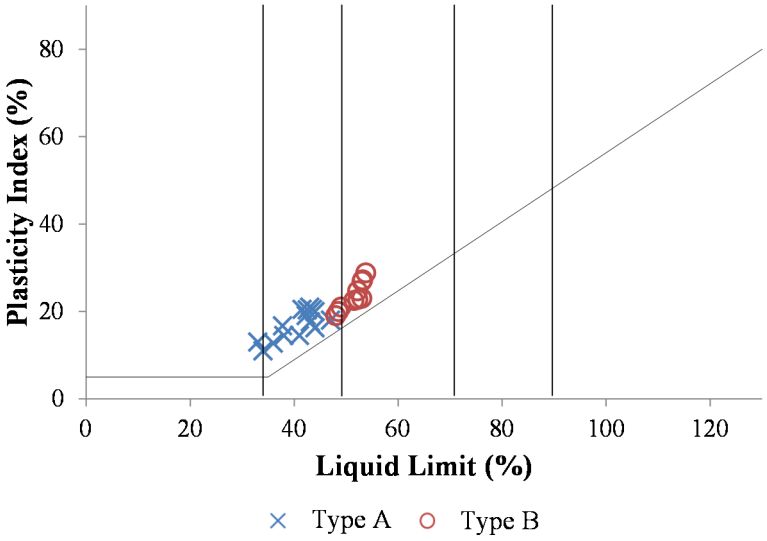

Figure 6.20: Cassegrande classification showing both 'Type A' and 'Type B' samples from the NBAD site.

As with the Yas Mina site, all results plot above the A-line categorising the remoulded material as having clay-like behaviour. Average 'Type A' samples have plastic limits of 23.7%, liquid limits of 40.7% and plasticity index of 17.1%, designating them as being of intermediate to low plasticity whilst 'Type B' samples had mean values of 27.9%, 51.5% and 23.6% respectively, being designated as intermediate to high plasticity.

By merging the data from both the NBAD and Yas Mina sites, Figure 6.21 can be plotted.

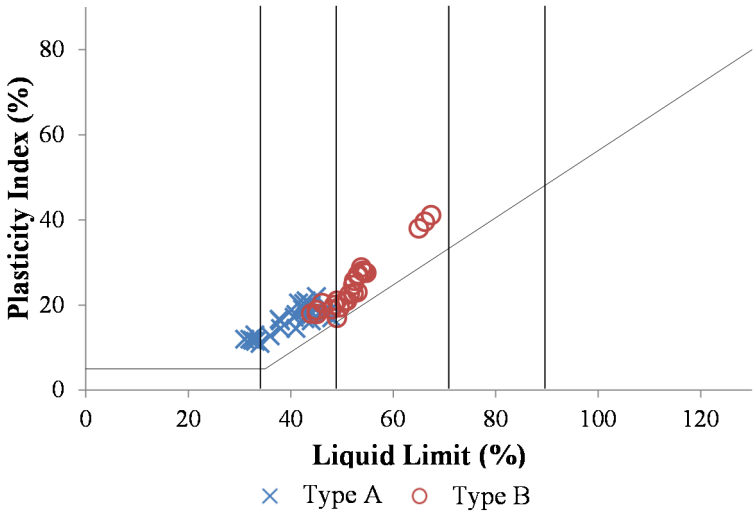

Figure 6.21: Cassegrande classification showing both 'Type A' and 'Type B' samples from both sites.

The liquid and plastic limits show that the calcareous mudstones encountered in both sites are highly comparable. Furthermore the 'Type A' and 'Type B' behaviours noted during mechanical examination can be seen to form tight clusters of data points, irrespective of sample depth or borehole number (and location) with only a few examples of outliers. Average 'Type A' samples have plastic limits of 23.8%, liquid limits of 40.6% and a plasticity index of 16.8, whilst 'Type B' samples have higher values of 27.7%, 52.4% and 24.7% respectively. This increase in plasticity is interpreted to be a result of higher concentrations of Palygorskite in the 'Type B' samples, which is concordant with the findings of the SEM and XRD analysis.

As such, Atterberg limits may be used as an inexpensive and rapid (albeit, cautious) means of determining the likelihood of this lithology displaying relatively strong or weak mechanical characteristics.

It should be noted that this method could be used only as an initial estimate of physical behaviour, particularly if the calcareous mudstone's remoulded liquid limits fall within the range of 44 and 48%, as there is a region of overlap between the 'Type A' and 'Type B' data clusters.

Vardanega & Bolton (2011) attempted to link the plasticity index and liquid limit of natural clays to their stiffness degradation curves. Whilst a simple approach such as this is practical and attractive, results from such empirical correlations were shown to be highly inaccurate, as the design charts produced were subject to errors of ±50%. It is suggested that instead, Atterberg limits be carried out in order to predict the likely

behaviour of samples of calcareous mudstone (Type A or B) in order to better inform further tests.

6.5.3. *EFFECT OF SALINITY – 'TYPE A' MATERIAL*

Four sets of samples were taken from both the Yas Mina and NBAD sites from depths that correspond to 'Type A' mechanical behaviour. These sample sets comprised of four or more sub-samples to allow Atterberg limit tests carried out using both deionised and synthetic saline water, and average trends to be observed. It is known that the rheological properties of Palygorskite change with pH (and indeed the length to width ratio of the Palygorskite fibres, although all Palygorskite in this thesis are classified as 'short-length' with similar ratios noted between samples in SEM analysis) (Neaman & Singer, 2000); (Haydn, et al., 2005), however little is published about its change in behaviour with increased salinity in a geotechnical context. Table 6.5 presents the results of this study numerically whilst Figure 6.22 presents findings graphically.

Table 6.5: Summary Atterberg Limit tests carried out upon 'Type A' samples using both deionised and saline water.

Sample Code	Borehole No.	Sample Depth (mbgl)	Plastic Limit (%)	Liquid Limit (%)	Plasticity Index	Plasticity Designation	Water Chemistry
YM5-18.40	5	18.40	24.0	42.9	18.9	CI	Deionised
YM8-17.85	8	17.85	20.8	32.6	11.8	CL	Deionised
NB02-23.50	02	23.50	23.3	42.3	19.1	CI	Deionised
NB03-29.00	03	29.00	22.4	39.5	17.1	CL	Deionised
YM5-18.40	5	18.40	21.7	41.3	19.6	CI	Saline
YM8-17.85	8	17.85	19.4	31.5	12.1	CL	Saline
NB02-23.50	02	23.50	19.1	40.9	21.8	CI	Saline
NB03-29.00	03	29.00	19.6	41.0	21.4	CL	Saline

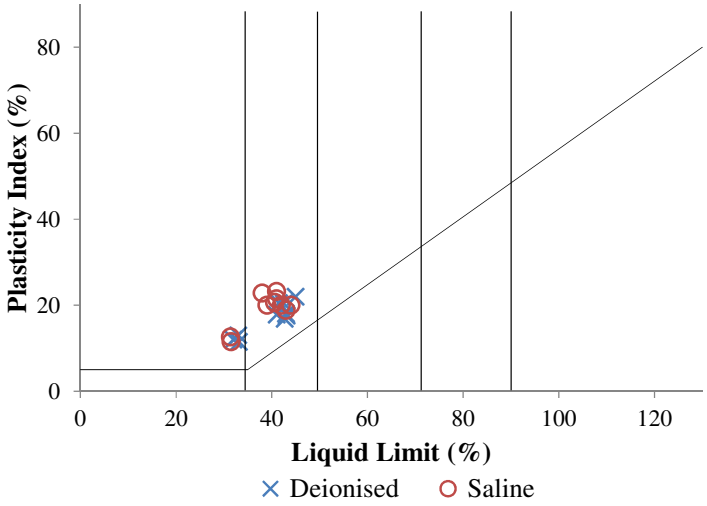

Figure 6.22: Cassegrande classification showing the effect of salinity on 'Type A' samples.

On average, 'Type A' samples tested using saline water have a reduced plastic limit (reduced by 2.7%), slightly reduced liquid limit (reduced by 0.5%) and therefore a raised plasticity index (increased by 2.1%), although any given sample is not effected enough to change its plasticity designation and in the case of sample NB03-29.00, liquid limits were noted to marginally increase.

6.5.1. *EFFECT OF SALINITY – 'TYPE B' MATERIAL*

As with the 'Type A' specimens, four sets of samples were taken from both the Yas Mina and NBAD sites that represent samples displaying 'Type B' mechanical behaviour. Sub-samples were again taken and average trends recorded. Table 6.6 presents results numerically and Figure 6.23 graphically.

Table 6.6: Summary Atterberg Limit tests carried out upon 'Type B' samples using both deionised and saline water.

Sample Code	Borehole No.	Sample Depth (mbgl)	Plastic Limit (%)	Liquid Limit (%)	Plasticity Index	Plasticity Designation	Water Chemistry
YM38-15.40	38	15.40	28.8	54.3	25.5	CH	Deionised
YM39-14.40	39	14.40	26.6	66.2	39.6	CH	Deionised
NB01-44.75	01	44.75	26.2	53.1	26.9	CH	Deionised
NB03-35.80	03	35.80	28.5	48.5	20.0	CI	Deionised
YM38-15.40	38	15.40	28.0	50.0	22.0	CI/CH	Saline
YM39-14.40	39	14.40	26.0	62.3	36.3	CH	Saline
NB01-44.75	01	44.75	24.8	51.4	26.6	CH	Saline
NB03-35.80	03	35.80	26.8	48.0	21.2	CI	Saline

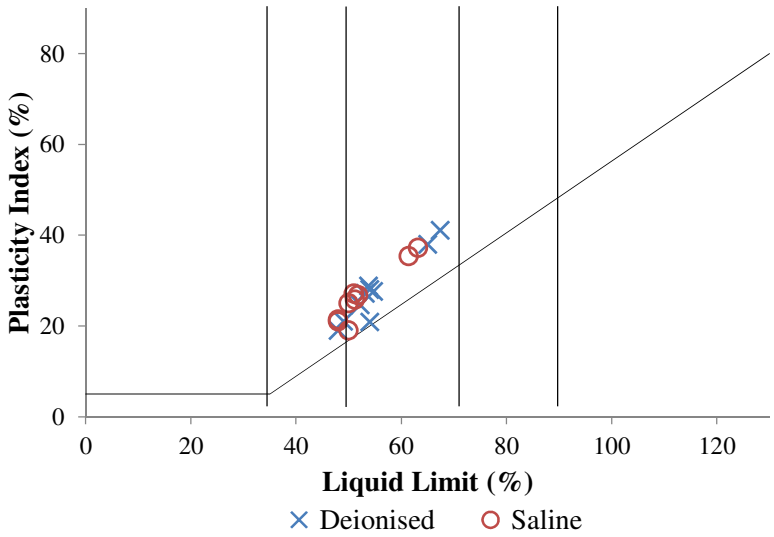

Figure 6.23: Cassegrande classification showing the effect of salinity on 'Type B' samples.

Figure 6.23 shows the 'Type B' samples tested using saline water to have a more notable reduction in their Atterberg limits than the 'Type A' samples in the previous section. Average plastic limits are reduced by 1.3%, liquid limits by 2.4% and an average plasticity index decrease of 1.1% is noted. In the case of sample YM38-15.40, this overall lowering of plasticity limits was enough to reduce its plasticity designation from clay of high plasticity (CH) down to that of intermediate plasticity (CI). These findings are contrary to findings within the literature that suggest Palygorksite to be insensitive to the presence of dissolvable salts (Galan, 1996); (Neaman & Singer, 2000)

It is likely that the calcareous mudstone studied will display a greater susceptibility to changes in pore water salinity as the percentage of clay minerals present increases, explaining why the 'Type B' samples, (which quantitative XRD analysis indicated to have greater percentages of Palygorskite), show a more pronounced and repeatable difference between saline and deionised result sets than those of the relatively clay depleted 'Type A' samples.

The effect of salinity is explored further in the following chapter with respect to the calcareous mudstone's one-dimensional compression characteristics.

6.6. PARTICLE DENSITY

Several particle density tests were carried out on samples from both study sites and from a variety of depths. Results are averaged from two tests per sample and materials displaying 'Type A' and 'Type B' behaviours are again annotated. Results are shown as Table 6.7.

Table 6.7: Summary of Particle Density tests on Calcareous Mudstone

Sample Code	Borehole No.	Sample Depth (mbgl)	Particle Density (Mg/m^3)	Strength Designation*
YM5-18.40	5	18.40	2.58	'Type A'
YM8-17.85	8	17.85	2.76	'Type A'
YM38-19.20	38	19.20	2.75	'Type A'
YM39-19.20	39	19.20	2.70	'Type A'
YM38-15.40	38	15.40	2.60	'Type B'
YM38-16.30	38	16.30	2.55	'Type B'
YM39-14.40	39	14.40	2.61	'Type B'
YM39-15.10	39	15.10	2.65	'Type B'
NB01-33.10	01	33.1	2.73	'Type A'
NB02-23.50	02	23.5	2.78	'Type A'
NB02-40.00	02	40.0	2.77	'Type A'
NB03-29.00	03	29.0	2.75	'Type A'
NB03-45.50	03	45.5	2.70	'Type A'
NB01-44.75	01	44.8	2.73	'Type B'
NB02-39.90	02	39.9	2.52	'Type B'
NB03-35.80	03	35.8	2.64	'Type B'

*from correlations with mechanical data

Bulk particle density results varied between 2.52 Mg/m^3 to 2.78 Mg/m^3 with the magnitude of values at the lower end of the results range being lower than expected for a calcareous mudstone. Calcite has a particle density of 2.71 Mg/m^3 (however has not been shown to be present during XRD analysis) whilst Dolomite has a particle density of 2.87 Mg/m^3 (Huat, et al., 2012); (Kogel, et al., 2006); (Reeves , et al., 2006); (Venkatramaiah, 2006); (Fang , 2002). Quartz has a particle density of 2.65 Mg/m^3 and is known to be present in small quantities within all samples tested along with traces of various feldspars (with particle densities ranging between 2.50 Mg/m^3 and 2.80 Mg/m^3).

In order for bulk particle densities as low as 2.52 Mg/m^3 to be measured, the average particle density would have to be lowered by a significant quantity of minerals with lower densities being present.

Halite has a particle densities of 2.17-2.20 Mg/m^3 and Palygorskite's particle density is between 2.10 Mg/m^3 and 2.20 Mg/m^3 (Kogel, et al., 2006); (Fang , 2002); (Haydn, et al., 2005). It is hypothesised that locally high concentrations of these minerals produced the decreased particle density results shown in samples YM5-18.40, YM38-16.30 and NB02-39.90.

A mean value of 'Type A' sample's particle density is 2.73 Mg/m^3 whilst 'Type B' specimens average 2.63 Mg/m^3, however a wide degree of variability in results was noted and tests were difficult to replicate successfully from within a given core sample. Whilst 'Type B' samples have a marginally lower particle density than 'Type A' samples, and incorrect assumptions of particle density can inadvertently affect the

outcome of other characterisation tests (such as PSDs), due to the superficial similarities of samples displaying the two behavioural types it is difficult to estimate what particle density value to assume prior to testing (as it is through the use of tests such as PSDs that the 'Type A' and 'Type B' behaviours may be identified before undergoing mechanical experimentation).

This problem is compounded due to the lateral and vertical variability of the composition of this lithology (seemingly variable even within a single core sample) along with limited quantities of raw materials (as particle density tests require a significant weight of powdered rock, and an iterative testing programme would require considerably more).

In order to overcome this issue, a particle density of 2.70 Mg/m^3 is assumed for all calculations (with the true average being 2.68 Mg/m^3).

A note of caution when measuring this property in practice, however, as powdered samples of this lithology have been observed to be highly hydrophilic, readily absorbing ambient moisture from the atmosphere (as shown in Figure 6.24, when 3.88g of calcareous mudstone was noted to rapidly increase in mass over time), and this needed to be accounted for when obtaining sensitive moisture mass measurements.

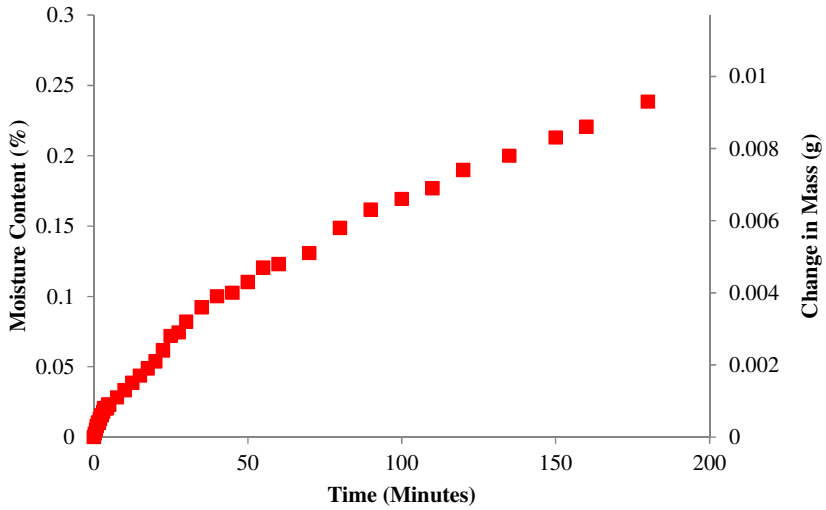

Figure 6.24: Hydrophilic nature of dry powdered calcareous mudstone.

This effect is likely to be associated with both the Halite and Palygorskite content, as both of these minerals will readily intake atmospheric moisture. It is recommended that samples be transferred directly from oven drying to weighing using containers with air tight seals.

6.7. PARTICLE SIZE DISTRIBUTION

PSD tests were carried out in accordance with BS1377 through a combination of wet sieving followed by sedimentation by both pipette and hydrometer methods. By immersing samples in a weak dilution of de-flocculent and subjecting to mild agitation samples would readily disintegrate, allowing standard soil PSD tests to be carried out.

Samples from both the Yas Mina and NBAD sites were tested. Results are again presented site specifically throughout the following section before being discussed together.

6.7.1. *YAS MINA PSDS*

All samples tested showed broadly similar PSD curves, being made up of between 97.9% and 100% fine particles (less than 63µm in diameter), with the majority of the grains being of fine to coarse silt size (despite behaving as a clay in terms of plasticity) with rare sand sized particles.

The largest variability in grain size fractions occurs in the clay sized particle range, where percentage of particles smaller than 2µm diameter constituted a range of between 14.5 up to 43.4%, depending upon sample.

When results are colourised to represent the 'Type B' (red) and 'Type A' (blue) relative strengths noted during mechanical testing, a pattern emerges (as seen in Figure 6.25).

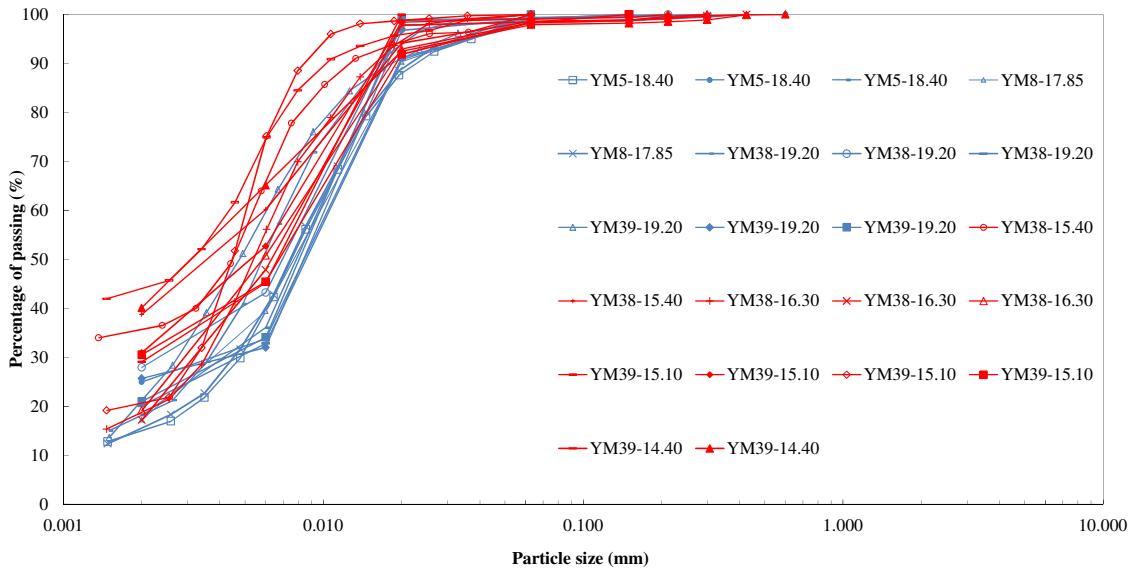

Figure 6.25: Full PSD curves for all Yas Mina calcareous mudstone samples tested.

PSD curves are shown separated into 'Type B' and 'Type A' in Figure 6.26.

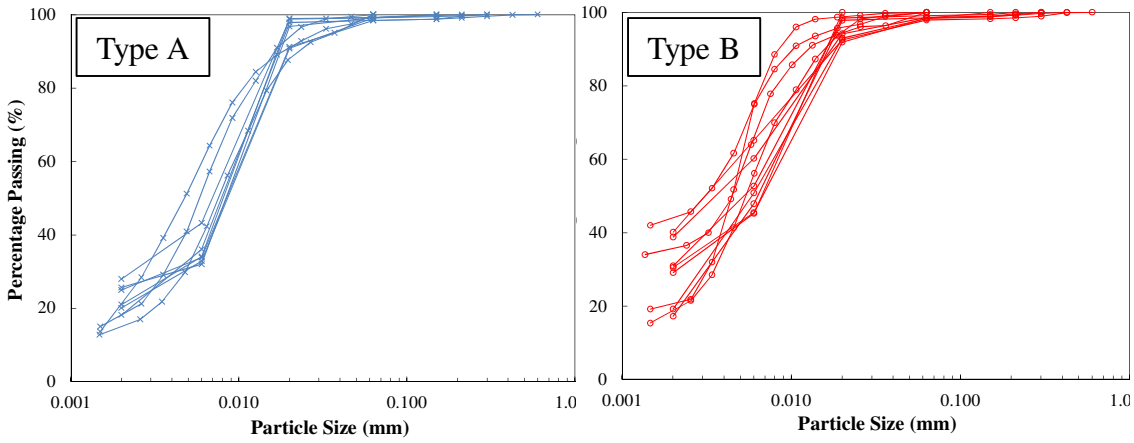

Figure 6.26: PSD curves for Yas Mina separated into 'Type A' and 'Type B' variants.

Results, shown in Figure 6.26, indicate that 'Type B' samples have, on average, 9.1% more grains passing the 0.002mm particle size (clay) than those of the 'Type A' samples.

It should be noted, however, that whilst samples YM38-15.40 and YM39-15.10 have a significantly greater fraction of clay sized particles, the remaining 'Type B' samples (YM38-16.30 and YM39-14-40) have similar percentages of grains less than 2µm in diameter (between 17 and 30%) to the majority of the 'Type A' samples. The 'Type B' specimens are noted to also have less coarse silt sized particles than the 'Type A' samples.

Samples YM5-18.40 and YM8-17.85 have the smallest fraction of grains less than 2µm diameter (14.5 and 15% respectively). Furthermore the overall grain size of the 'Type B' samples is marginally finer than that of the 'Type A' type samples.

6.7.2. *NBAD PSDS*

PSD curves from NBAD samples were largely similar to those from the Yas Mina site. Particles of less than 63µm in diameter made up of between 97.3% and 100% of the samples, again with the majority of the grains being of fine to coarse silt size. Clay sized particles made up between 16.0 and 39.0% of the sample mass, again depending upon the individual sample. By colourising the results to represent the 'Type B' (red) and 'Type A' (blue) relative strengths observed during mechanical testing, Figure 6.27 may be plotted.

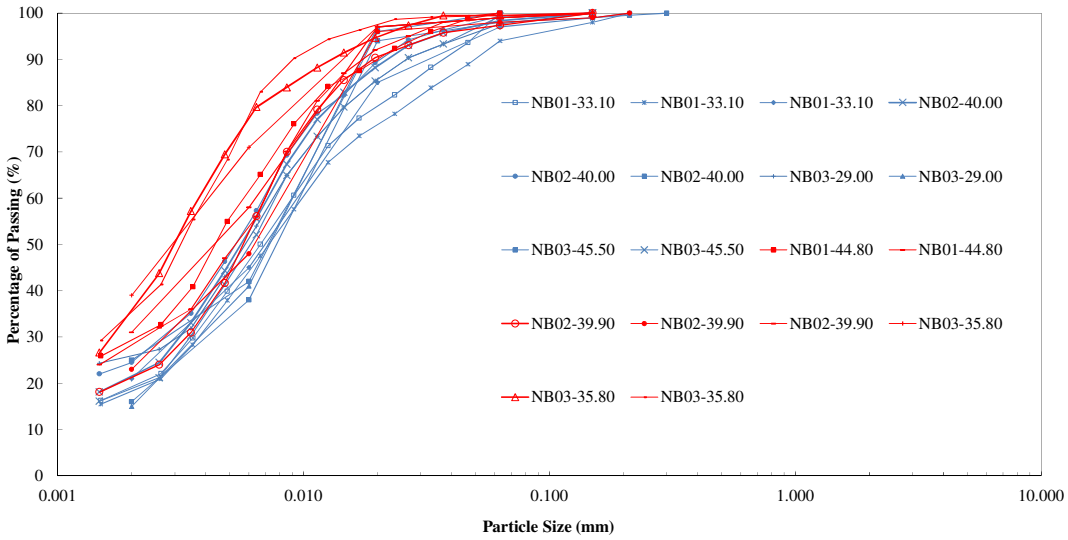

Figure 6.27: Full PSD curves for all NBAD calcareous mudstone samples tested.

As with the Yas Mina samples, the 'Type B' specimens have a greater percentage of grains passing the clay size fraction (9.2% more) than 'Type A' samples, with average 'Type B' samples having 29.7%, and 'Type A' samples showing only 20.5% clay particle sizes. Again, 'Type B' specimens are noted to have less coarse silt sized particles.

Whilst a range of curve shapes are observed, it is noteworthy that both the Yas Mina and NBAD samples show a similar discrepancy between the 'Type B' and 'Type A' material in terms of the average percentage of grains making up the clay sized fraction.

Results from both sites indicate that, whilst the 'Type A' and 'Type B' samples are superficially very similar, there is a discrete difference in the shape of their respective PSD curves in that samples with greater percentages of grains passing 2µm diameter are noted to be mechanically weaker than those with a smaller clay size fraction.

This finding, along with the trends noted in during the plasticity test analysis, could indicate greater amounts of Palygorskite in the weaker samples, although it should be noted that not all grains passing 2µm diameter will be clay. SEM images also note a greater occurrence of Dolomite grains less than 2µm in diameter, which would be misinterpreted as clay if PSDs (including sedimentation by pipette and hydrometer) were used in isolation.

6.7.3. *ACTIVITY OF CLAY FRACTION*

Within a given stratum of clay bearing material there may exist considerable variation in both the PSD curves and the PI if multiple samples are tested (Skempton, 1953), as

has been seen with samples within this thesis. Assuming that the types of minerals present are not changing, these variations must be due to the relative abundances of the minerals being locally different, or appear to be so due to sampling bias.

However, if plasticity is plotted against clay fraction it can be seen that results typically plot on a straight line which intersects the origin, with the amount of scatter being an indication of inter-sample variability in clay mineralogy. In addition to this, it is possible to obtain the activity of the clay fraction of a clay bearing material, allowing it to be categorised as either active, normal or inactive (Table 6.8).

Table 6.8: Skempton, (1953) activity of clay classification.

Classification	Activity
Inactive Clay	<0.75
Normal Clay	0.75-1.25
Active Clay	>1.25

Once a clay's activity is found, estimates can be made as to that material's composition and even geological origin. This is particularly useful where tests such as XRD analysis are not possible, however will be covered within this thesis for completeness.

The activity (Ac), or colloidal activity of a clay can be found by comparing its plasticity index (PI) with its percentage of grains finer than 2µm using formula 6.1 (Skempton, 1953):

$$Ac = \frac{PI}{\% < 2\mu m} \qquad 6.1$$

Mean Ac values gathered from this thesis are shown in Table 6.9.

Table 6.9: Activity of calcareous mudstone clay classification.

Site	Strength Designation*	Classification	Activity
Yas Mina	'Type A'	Normal Clay	0.82
Yas Mina	'Type B'	Normal Clay	0.87
NBAD	'Type A'	Normal Clay	0.85
NBAD	Type B'	Normal Clay	0.83

*from correlations with mechanical data

The clay fraction of the calcareous mudstones is classified as being of 'normal' activity, with an overall average Ac of 84. This indicates that although a small discrepancy between the PI and PSDs exists (particularly between 'Type A' and 'Type B' specimens), that the governing clay mineral present is likely to be the same mineral across samples (although present in differing relative abundances).

Figure 6.28 shows the relationship between PI and percentage clay fraction for both the 'Type A' and 'Type B' materials tested from a) Yas Mina and b) NBAD site investigations.

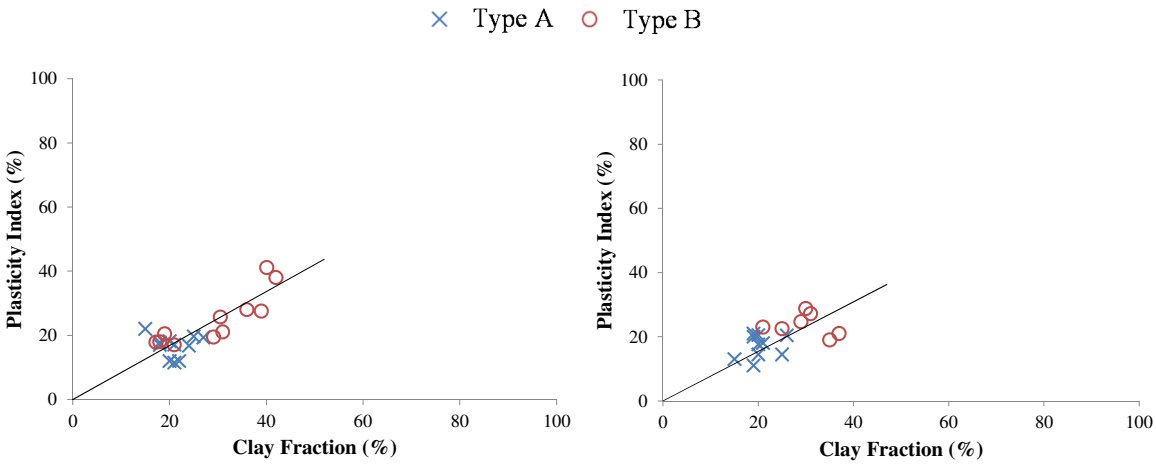

Figure 6.28: Relationship between PI and PSD percentage <2µm. a) Yas Mina and b) NBAD

Relationships from both sites plot in a largely linear manner with a low degree of data scatter indicating that the clay mineral present in all samples, regardless of strength, is likely the same type (i.e. Palygorskite). The gradient of the line of best fit from both sites is also very similar, possibly indicating that Palygorskite is the prevalent clay mineral in the calcareous mudstones of the Abu Dhabi coastal area both laterally and vertically within the local geological succession. This has been proven via XRD and SEM analysis within this thesis, however assessments of activity levels could provide reasonable estimates of clay mineral composition were such tests not available.

It should be noted that several sample's activities, such as YM38-16.30 and NB02-39.90, were approaching being classified as active, having average Ac values of 1.06 and 1.10 respectively (both of these samples were of the 'Type B' type). Palygorskite, in its pure form, has an activity of around 1.2 (Mitchell, 1976); (Wissa, et al., 1982); (Mitchell, 1993), as shown in Figure 6.29 with the dashed line representing a typical activity relationship of pure Palygorskite, although Neaman & Singer, (2000) urge caution when attempting to relate the behaviour of Palygorskite to models made for platy minerals, due to the differences in their particle morphology and surface structure.

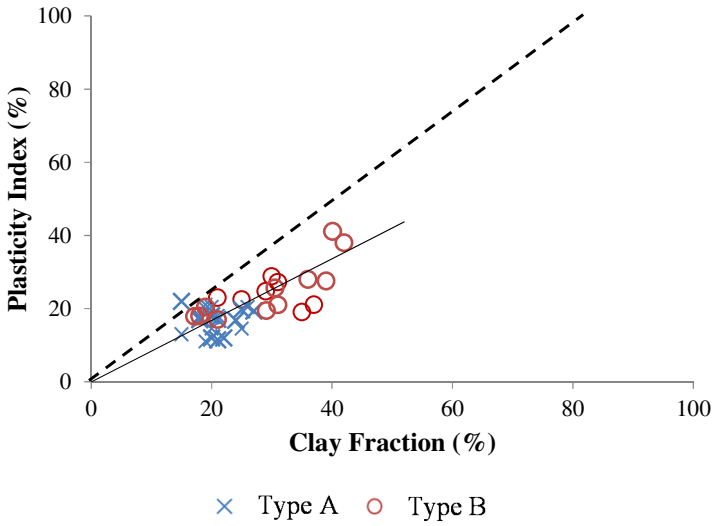

Figure 6.29: Relationship between PI and PSD percentage of both sites compared with that of pure Palygorskite.

Pure Palygorskite's activity is borderline between 'normal' and 'active', meaning that there is a discrepancy between the average values of Ac found in this study (of 0.84) and those expected from the literature. Even in the 'Type B' type samples, where the clay fraction was of a higher proportion of the PSD, Ac values were still lower than that of pure Palygorskite specimens.

This can be explained via examination with the findings of the quantitative XRD analysis. Whilst the PSD analysis shows that a large proportion of the calcareous mudstone is made up of clay sized particles, XRD analysis (and indeed SEM images) show that not all of the grains passing the <2µm fraction are clay minerals. It is often the case that over half of the clay fraction's grains are made up of clay sized particles of dolomite, as opposed to the assumed Palygorskite. This is a known limitation in the assessment of activity (Skempton, 1953). Once this is allowed for (for example using the percentages of Palygorskite found in the quantitative XRD analysis) average Ac levels rise to around 1.3.

6.8. DISPERSIVITY OF CALCAREOUS MUDSTONE

It was known that the calcareous mudstone studied within this thesis displayed a high susceptibility to moisture, rapidly losing cohesion and degrading within minutes of submersion in unconfined conditions. This tendency for samples to deteriorate had been noted anecdotally during routine construction where apparently strong bases of excavations softened rapidly following stress release and a brief rainfall event (Cook, 1999). This behaviour was initially thought to be related to dissolvable minerals such as gypsum or halite going into solution, thereby destroying inter-granular bonds and

allowing the material to disintegrate, however analysis of SEM and XRD indicates that this is unlikely.

The 'Crumb Test' attempts to qualify if a material is susceptible to dissolution and / or dispersion. The test is purely observational, meaning that no quantitative assessments are made. It is generally carried out on soils, however due to the nature of the soft calcareous rocks being sensitive to water; it is thought this test may provide some degree of insight into the behaviour of these weak mudstones. Three sets of 'Crumb' tests are carried out; firstly a series of tests using deionised water, secondly tests following British Standard practices by using a weak sodium hydroxide solution (a mild deflocculant) and thirdly tests using saline water of the approximate chemistry of the groundwater of the site in question, in order to examine the effect of placing samples in an approximate chemical equilibrium to that which they experience in-situ.

6.8.1. *'CRUMB' TESTS – DEIONISED WATER*

Representative samples from both sites (and those representing 'Type B' and 'Type A' variants) were broken into 5 – 6 'Crumbs' of approximately 6mm – 10mm diameter, as specified in BS1377. A total of 4No. tests were carried out on Yas Mina samples and also 4No. on NBAD samples.

These 'Crumbs' were then placed into beakers filled with 50 ml of deionised water and observed over the course of 24 hours in order to identify any dissolution / dispersion taking place.

All samples tested using deionised water were noted to disintegrate and lose their structure to some degree, loose particles detaching from the side of the 'crumbs' and a soap-like layer formed around their exposed surface.

After the full 24 hours, all samples had degraded into very soft clay / silt mounds displaying a high susceptibility to moisture regardless of the site or depth of origin.

All samples tested showed the presence of colloids (grade 2), and all samples tested appeared to behave in a very similar manner and were noted to break down within similar timeframes.

6.8.2. *'CRUMB' TESTS – SODIUM HYDROXIDE*

Once again representative samples from both sites at various depths were prepared in the manner specified by the BS1377. These 'Crumbs' were then placed into beakers

filled with 50 ml of dilute sodium hydroxide (0.001 Mole solution, 0.04g dissolved within 1 litre of deionised water) and observed over the course of 24 hours in order to identify any dissolution / dispersion taking place.

Overall, similar results were found to those observed during testing of samples within deionised water.

Colloids were again noted only to be present in all samples (grade 2) and samples totally disintegrated after the 24 hour mark.

No apparent difference was noted between Yas Mina or NBAD sites and 'Type A' and 'Type B' samples behaved in a very similar way.

6.8.3. *'CRUMB' TESTS – SALINE SOLUTION*

Once again representative samples from both sites (and again at various depths) were prepared for testing. These 'Crumbs' were then placed into beakers filled with 50 ml of saline solution (of a similar chemistry to the groundwater on-site) and observed over the course of 24 hours.

These samples, as with the deionised water and sodium hydroxide solutions, showed evidence of colloids (grade 2) and samples disintegrated in their entirety after 24 hours leaving behind a clay / silt residue.

No apparent difference was noted between the Yas Mina or NBAD samples, nor between the 'Type A' and 'Type B' samples when using saline water.

Results from the 23No. 'crumb' tests carried out are summarised in Table 6.10:

Table 6.10: Summary of 'crumb' tests on Calcareous Mudstone

Sample Code	Deionised Water*		Sodium Hydroxide Solution*		Saline Solution	
	Dispersed*	Colloids Grade †	Dispersed*	Colloids Grade †	Dispersed*	Colloids Grade †
YM5-18.40	Yes	Grade 2	Yes	Grade 2	Yes	Grade 2
YM8-17.85	Yes	Grade 2	Yes	Grade 2	-	-
YM39-19.20	-	-	Yes	Grade 2	Yes	Grade 2
YM38-15.40	Yes	Grade 2	-	-	-	-
YM38-16.30	Yes	Grade 2	Yes	Grade 2	Yes	Grade 2
YM39-14.40	-	-	-	-	Yes	Grade 2
NB01-33.10	Yes	Grade 2	Yes	Grade 2	-	-
NB02-40.00	Yes	Grade 2	Yes	Grade 2	Yes	Grade 2
NB03-29.00	-	-	Yes	Grade 2	Yes	Grade 2
NB01-44.75	Yes	Grade 2	Yes	Grade 2	Yes	Grade 2
NB03-35.80	Yes	Grade 2	-	-	-	-

* a 'Yes' indicates sample crumbs deteriorated significantly during the testing period.
a 'No' indicates samples remained mainly unchanged during the testing period.
a '-' indicates that no samples were tested.
† if present.

An obvious, though noteworthy conclusion from these tests is that samples of this material should under no circumstances be saturated prior to triaxial testing using a vacuum chamber.

6.9. DURABILITY TESTING

This previously noted susceptibility to moisture can be quantified using slake durability tests. Extremely low second cycle durability indices (Id_2) of between 1-5% and first cycle indices (Id_1) of 32-38% are found (following testing methods proposed by Franklin & Chandra (1972), recommended by the International Society for Rock Mechanics (ISRM) (Brown, 1986) and standardised by the American Society for Testing and Materials (ASTM) (ASTM, 1990)). These ranges hold true for both samples from the Yas Mina site and the NBAD site. No significant differences were noted between samples tested of the 'Type A' material or those tested of the 'Type B', nor was there any correlation with depth, or those tested using saline water.

Whilst this occurs within samples under zero confining pressure, it had not been observed on a macro scale during preliminary triaxial testing under confining stress, despite samples being fully saturated.

It is thought that the swelling of clay minerals forcing de-structuration / breakage of bonding to occur is a more likely candidate for an explanation as to why these materials break down in zero confining pressure, saturated environments. Once under low positive effective confining stresses, this degradation is not noted to occur (at least not within the 20 to 40 day time periods that the triaxial tests were carried out in).

It is possible that minor differences in material behaviour may have been observed if the method of sample preparation for the test was more uniform and carried out on only the highest quality samples (ones not displaying any mottling or discoloration), however, due to the simplistic nature of the slake durability test and the random way in which the rock specimens interact with one another during as the test proceeds, conditions such as precise preparation and sample quality are not specified.

6.10. CHAPTER SUMMARY

This chapter has attempted to apply several standard (Atterberg limits, PSD, particle density, dispersivity and durability), and non-standard geotechnical tests (XRD and SEM) to assist in the overall characterisation and sub-categorisation of a soft calcareous mudstone.

XRD and ESEM analysis showed the material in question to comprise predominantly of fine grained Dolomite with minor constituents of Quartz, Feldspar, Halite (being noted to rapidly enter solution in the presence of deionised water), and notably Palygorskite. This assemblage of minerals are quite common for hyper-saline, warm environments (Sanz-Montero, et al., 2006) and indicate that the present day setting of the area is likely to be highly analogous to the conditions that allowed the older soft rocks to deposit (albeit with dolomite instead of calcite).

The effect of clay minerals such as Smectite or Illite on the mechanical and characteristic behaviour of soils and low strength rocks is quite well understood, however little published information relating to Palygorskite specifically is available within the literature (Dixon & Weed, 1989); (Neaman & Singer, 2000). Whilst qualitative XRD analysis showed no mineralogical difference between the phases present in the 'Type A' and 'Type B' material types, quantitative XRD suggested that 'Type B' samples contained a higher percentage of Palygorskite within their clay fraction along with lower quantities of Dolomite.

SEM using gold plated samples showed that the grain to grain contacts of the 'Type A' samples were often tightly bonded or even fused, likely due to the repeated precipitation and dissolution of the Dolomite grains over time. 'Type B' type samples were less well fused and displayed an abundance of fibrous Palygorskite within void spaces, as well as having a finer overall grain size as shown diagrammatically in Figure 6.30.

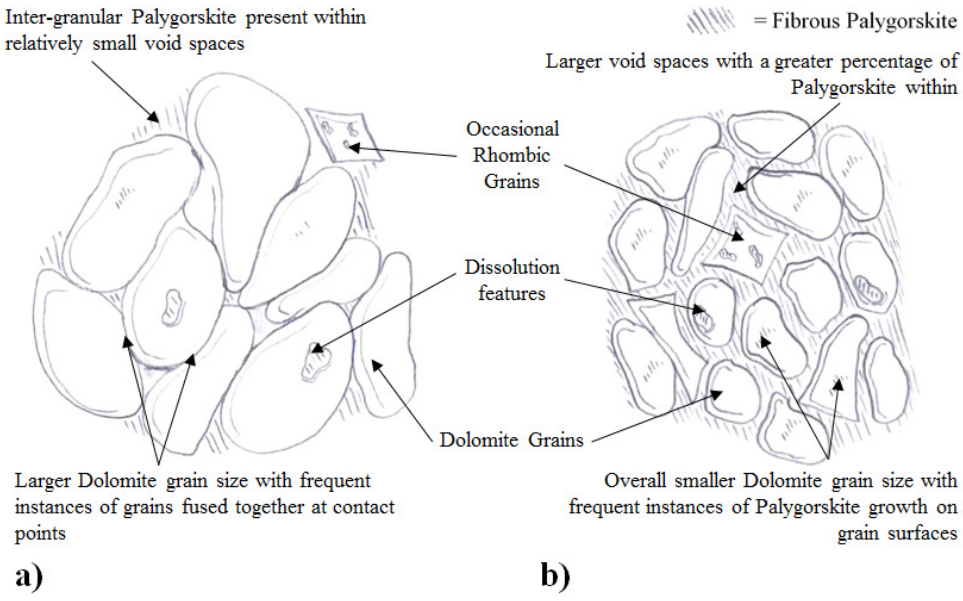

Figure 6.30: Simplified sketches showing the initial micro-structural configuration of typical a) Type A and b) Type B samples.

Atterberg limit tests also highlighted differences in the characteristics of 'Type A' and 'Type B' material types, whereby they had low-intermediate and intermediate-high plasticity respectively. This was interpreted as being due to the presence of a higher quantity of Palygorskite in the 'Type B' samples. The introduction of a saline solution, similar to that of the native in-situ pore-water chemistry, lowered plasticity by a small degree.

PSD corroborated the findings of the SEM analysis in that 'Type B' samples had a significantly higher fraction of grains smaller than 2µm than those of the 'Type A' samples. Comparisons with quantitative XRD results indicate that the <2µm fraction is only made up of around 50% Palygorskite, with the rest being very fine grained Dolomite grains, and calculated activities of the clay size fraction were noted to be lower than that of published values for pure Palygorskite for this reason.

Dispersivity tests showed the material to be highly sensitive to the presence of water in unconfined conditions, breaking down almost entirely with a short time period and producing colloids, and this characteristic was confirmed via durability testing that showed both very low first and second cycle durability.

Finally, results from the petrographic characterisation study of this thesis (in particular PSD results) were used to help calibrate a Distinct Element Method (DEM) simulation of brittle soft rock behaviour carried out by Barreto, et al, (2014). The simulation used a new contact model that included particle bonding and Hertzian-type non-linear behaviour in order to demonstrate that macro-scale behaviours obtained through modelling are not as observed in experimental testing, if realistic PSDs are used as opposed to the more typically assumed PSD input parameters.

Scholtes & Donze, (2013) stated that there are difficulties in determining the values of DEM input parameters that replicate the low UCS / tensile strength ratios representative of brittle rocks. In order to reduce computational cost of simulations, an unrepresentative PSD is often applied, hence the results of existing DEM models, in particular the micro-scale observations which are supposed to explain the unique features of the mechanical behaviour of structured soils and soft rocks, may be questionable. This is an important observation, because micro-structural approaches that incorporate interactions observed in DEM simulations are frequently used to support the development of soil models for structured soils (Yin, et al., 2010).

Whilst the Barreto, et al, (2014) model is still in its infancy, it has highlighted that the complex underlying mechanics of soft rocks during shearing (particularly brittle behaviour) cannot be modelled successfully using existing contact models without making unrepresentative assumptions about material properties.

CHAPTER 7. RESULTS OF MECHANICAL STUDY

7.1. INTRODUCTION

The previous chapter summarised the results of the petrographic / mineralogical and characterisation tests undertaken within this thesis, with reference being made to the mechanical data presented within this chapter. Through the use of standard characterisation tests (such as Atterberg Limits and PSDs) alongside non-standard tests (such as XRD and SEM) it was shown that the calcareous mudstones tested, whilst superficially similar, could be broadly categorised as either displaying 'Type A', or 'Type B' properties.

Type A samples were typically less plastic, have a lower percentage of material passing the 2µm grain size fraction and have lower percentages of Palygorskite. Type A materials were also noted to be better bonded, with lower void ratios and are mechanically stronger (as this chapter will describe) than their Type B counterparts.

Conversely, correlations were drawn between samples displaying the weaker 'Type B' behaviour with having a greater proportion of Palygorskite, poorer bonding, higher plasticity and a greater percentage of fines. Both Type A and B samples were also noted to disintegrate rapidly when exposed to water within unconfined conditions via durability and dispersibility tests.

This chapter will examine in detail the mechanical performance of the soft calcareous mudstones using advanced triaxial testing methods, one dimensional consolidation tests (using both saline and deionised pore fluids) and Brazilian tensile strength tests in conjunction with a novel local strain measuring tool, namely DIC, making reference where appropriate to the findings of the previous chapter.

Results in this chapter ordered in terms of the magnitude of shear strain induced in the sample by a given test, with the triaxial results being presented first (as these chiefly assess the very small and small strain properties of the soft rocks), followed by Brazilian tensile tests (as DIC also addresses local scale strains) and finally presenting the oedometric results.

Once again, it should be noted that whilst results are ordered in this manner for the clarity of their presentation, due to several practical and temporal restrictions

surrounding the availability of apparatus and raw materials, in practice tests were often carried out parallel to one-another. Findings from the previous chapter helped inform the mechanical testing programme which then fed-back into the previous chapter in an iterative manner, again, particularly during their discussion. The author would like to reiterate that the petrographic and mineralogical characteristics highlighted in the previous chapter are inherently linked to the material's mechanical performance, and so there is much unavoidable cross over between this chapter and the chapter directly preceding it.

7.1. MECHANICAL TESTING PROGRAMME

The mechanical testing phase of this thesis utilises triaxial, odometer and tensile tests to characterise the behaviour of the soft calcareous mudstones. Sample cores are given a code with the site name abbreviated as either YM (Yas Mina) or NB (NBAD) followed by the borehole number and depth (e.g. YM5-18.40) from which they arose.

Some core samples were large enough that several subsamples could be taken for additional tests, where this occurs samples receive an additional letter at the end of their code (e.g. YM5-18.40A, YM5-18.40B). Oedometer and Brazilian disk samples were always sourced as multiples from any given core, as the amount of sample required for these tests is significantly smaller than that required during triaxial testing, allowing a single short run of core to provide for multiple test samples. Generally, only one triaxial test sized sample could be retrieved from any given length of core, however a single exception to this is in core YM39-15.10, where two samples were retrieved (denoted A and B).

In total, eleven (11no.) drained triaxial tests, forty-two (42no.) Brazilian tensile strength tests and fifteen (15no.) one dimensional consolidation tests were carried out as part of the mechanical characterisation phase of this thesis.

Samples analysed included those from both the 'Type A' and 'Type B' specimen types in all three mechanical tests, and the relative strength and stiffness's of these types are discussed at length within this chapter. In addition to these tests, a single triaxial test was carried out on a Type A sample (NB02-40.00) which utilised Bender Elements in order to assess the role of mean effective stress on G_0.

More details on the specifics of each testing programme are given in the following sections, however are summarised on Table 7.1.

Table 7.1: Summary of mechanical tests carried out upon calcareous mudstone samples

Sample Code	Borehole No.	Sample Depth (mbgl)	Drained Triaxial Initial Mean Effective Stress p'_0 (kPa)	Drained Triaxial Shear Rate (mm/min)	Brazilian Tensile with DIC	Oedometer (undisturbed)	Oedometer (Remoulded)	Material 'Type' Designation
YM5-18.40 (A-E)*	5	18.40	235	0.0014	A-E	-	-	A
YM8-17.85	8	17.85	470	0.0014	-	-	-	A
YM38-19.20	38	19.20	940	0.0014	-	-	-	A
YM39-19.20	39	19.20	1300	0.0014	-	-	-	A
YM38-15.40	38	15.40	235	0.0014	-	-	-	B
YM38-16.30 (A-C)*	38	16.30	470	0.0014	A-C	-	-	B
YM39-15.10 (A,B)*	39	15.10	940 (A), 1300 (B)	0.0014	-	-	-	B
YM39-14.40	39	14.40	-	-	-	A-B	-	B
NB01-33.10	01	33.10	-	-	-	A-D	A-F	A
NB02-23.50 (A-H)*	02	23.50	-	-	A-H	-	-	A
NB02-40.00 (A-D)*†	02	40.00	-	-	A-D	-	-	A
NB03-29.00 (A-G)*	03	29.00	-	-	A-G	-	-	A
NB03-45.50	03	45.50	-	-	-	A-D	-	A
NB01-44.75 (A-F)*	01	44.80	940	0.014	A-F	-	-	B
NB02-39.90 (A-E)*	02	39.90	940	0.0014	A-E	-	-	B
NB03-35.80 (A-E)*	03	35.80	940	0.00014	A-E	-	-	B

* If sample core dimensions permitted, several sub-samples were prepared for additional tests, denoted by the addition of a letter to the end of the sample code (e.g. YM5-18.40 (A-E)* comprises one drained triaxial and five Brazilian tests)
† G_0 was examined on this sample using Bender Elements.

7.2. ADVANCED TRIAXIAL TESTING PROGRAMME

This section of the thesis explores the effect of both changing mean effective isotropic confining stress (study 1) and rate of strain (study 2) on samples of calcareous mudstone in triaxial compression under drained conditions. The section is broken into two sub-sections accordingly, with the first study including analysis using Bender Elements. A detailed methodology relating to this section is presented within chapter 5.

7.2.1. *STUDY 1 - THE ROLE OF MEAN EFFECTIVE STRESS*

Whilst sample cores of the calcareous mudstone appear superficially similar, displaying similar initial bulk traits and a similar array of minerals, petrographic characterisation tests alongside various mechanical tests have identified two distinct categories of

behaviour, namely ‘Type A’ and ‘Type B’. The previous chapter described, using a suite of standard and non-standard tests, how it is thought that these behavioural differences may be as a result of the amount of inter-clast Palygorskite being present, both currently and during the material’s digenesis.

A suite of triaxial tests were undertaken in order to observe the effect of increasing mean effective stress (p’) conditions on the two material ‘Types’ in order to assess the role that varying mean effective stress has on sample stiffness and failure mechanisms. p’ in triaxial testing is calculated as follows:

$$p' = \frac{\sigma'_1 + 2\sigma'_3}{3} \qquad 7.1$$

Where σ'_1 is the effective vertical stress and σ'_3 is the effective confining stress.

As all samples showed a tendency to rapidly deteriorate in water (during dispersibility and durability testing), saturation using a vacuum chamber, (as per ISRM (Brown, 1986)), could not be used. And due to the low permeability of the calcareous mudstone, coupled with the high percentage of carbonate minerals, saturation using a pressurised carbon dioxide flush preceding the application of de-aired water also could not be used. Instead, the BS1377-8 (BSI, 1990) stepped saturation method with successive B testing was used, with the minor amendment that a minimum p’ of 50kPa be adopted in order to minimise swelling (as measured swelling pressures during one-dimensional consolidation ranged from 12-35kPa). This amendment slowed the saturation process, however increased confidence in the results obtained as swelling was kept to a minimum.

Prior to consolidation, Skempton pore pressure B values of 0.95 were successfully achieved in all tests, typically taking between 5 to 14 days. Back calculated saturation ratio’s (Sr) also supported the assumption that a B value exceeding 0.95 was representative of the sample being 95% saturated or better.

Samples of both ‘Type A’ and ‘Type B’ specimens were then isotropically consolidated to the desired initial mean effective stresses (p'_0) of 235, 470, 940 and 1300kPa and allowed to rest for 48 hours prior to shearing at a set rate of deformation (around 0.0014mm/min equating to 0.001% axial strain (ε_a) per minute) under drained conditions. This rate was selected as it was observed not to be so fast as to generate unwanted excessive pore water pressures, however not so slow that the developing strains be disguised by the sample creeping. It also allowed a good data set to be

obtained within the small strain range during shearing using a reasonable data collection frequency of 10 second intervals for the test duration. The isotropic stresses used (235, 470, 940 and 1300kPa) were selected as 235kPa represented the mean isotropic in-situ stress of specimens, with the following isotropic stresses being doubled up to the maximum safe capacity of the apparatus used.

Reiterating from Chapter 2 of this thesis, deviator stress is calculated using:

$$q = \sigma^1 - \sigma^3 \qquad 2.9$$

And shear strains (ε_s) in triaxial apparatus are found using:

$$\varepsilon_s = \left(\frac{2}{3}\right) \times (\varepsilon_a - \varepsilon_r) \qquad 2.8$$

Where (ε_r) is the radial strain.

Table 7.2 shows the initial properties of the eight (8no.) samples used within this phase of the testing programme along with the conditions under which they were consolidated and sheared.

Table 7.2: Summary of sample properties used during drained mean effective stress tests

Strength Designation	Type A				Type B			
Sample Reference	YM5-18.40	YM8-17.85	YM38-19.20	YM39-19.20	YM38-15.40	YM38-16.30	YM39-15.10A	YM39-15.10B
Site Name	Yas Mina				Yas Mina			
Borehole No.	BH5	BH8	BH38	BH39	BH38	BH38	BH39	BH39
Depth Sample Taken (mbgl)	18.40	17.85	19.20	19.20	15.40	16.30	15.10	15.10
Initial Moisture Content (%)	20.1	20.3	17.80	20.1	20.0	20.1	20.5	21.5
Initial Bulk Density (Mg/m^3)	2.03	2.02	2.02	2.03	2.02	2.02	2.01	2.01
Initial Dry Density (Mg/m^3)	1.69	1.68	1.71	1.69	1.68	1.68	1.67	1.67
Initial Void Ratio	0.59	0.60	0.60	0.59	0.60	0.60	0.61	0.61
Initial Porosity (%)	37.3	37.5	37.7	37.2	37.6	37.6	38.2	38.1
Initial Degree of Saturation	91.1	91.35	81.04	91.3	89.8	90.0	89.5	94.1
Isotropic Mean Effective Stress (kPa)	235	470	940	1300	235	470	940	1300
Shearing Rate (mm/min)	0.0014				0.0014			

Type A samples are shown to have average bulk densities of 2.025 Mg/m^3, average dry densities of 1.69 Mg/m^3 and average initial void ratios of 0.595, whilst the Type B samples had slightly lower bulk densities averaging 2.015 Mg/m^3, average dry densities

of 1.675Mg/m^3 and slightly higher void ratios averaging 0.605. The reasons behind these variations are discussed at length in the preceding chapter.

An initial observation is that densities broadly appear to increase with depth whilst void ratios decrease. This is an expected trend in most deposits of sedimentary origin and is likely to account for a small part of the increased strengths of the deeper, denser Type A specimens tested during this phase of the mechanical programme. However, the differences in mechanical performance of Type A and Type B deposits is too pronounced to be due entirely to depth of origin. Stress strain plots of all eight samples can be seen as Figure 7.1.

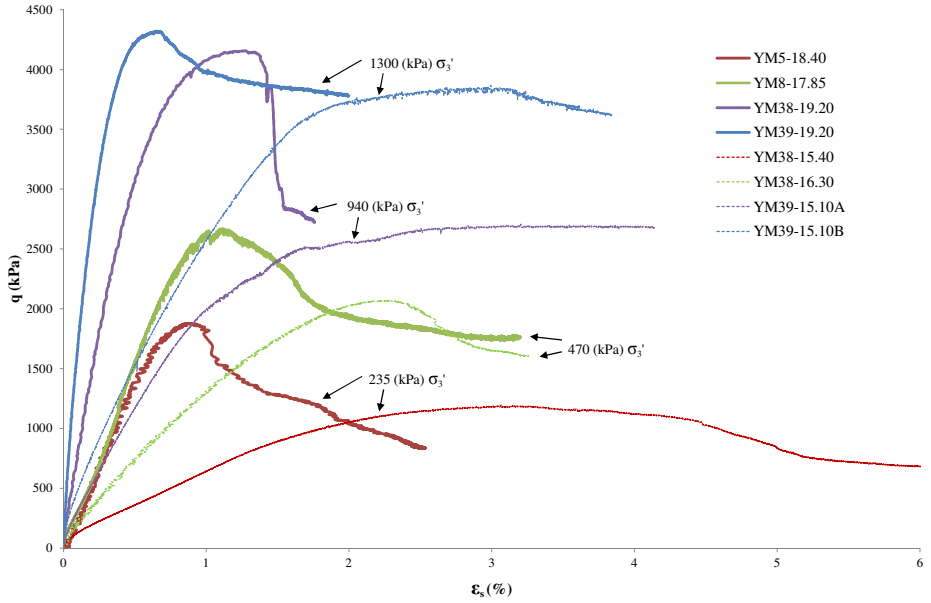

Figure 7.1: Stress – strain relationships with changing p' in calcareous mudstone.

The deviator stress (q) versus shear strain (ε_s) relationships clearly show an increase in maximum deviator stress (q_{max}) with increasing p'_0 along with an overall stiffer response to shear strains on all sample types. All tests on Type A samples display peak behaviour, with visual inspection of samples post failure revealing well defined shear planes, occurring at ε_s of no greater than 1.5% (although the strength loss between peak and residual on sample YM39-19.20 consolidated to 1300kPa perhaps indicates that a process of de-bonding is beginning to occur). Type A samples also have significantly higher q_{max} than any of the Type B samples tested from any given initial stress state.

Type B specimens stop displaying peak behaviour between the 470 - 940kPa p'_0 tests and instead show some degree of strain hardening. Post failure; these samples also have pronounced shear planes, although are they have a marginally more pronounced

'barrelling' at the sample centre (only observable via local strain measurements). This perhaps indicates the degradation of cementicious bonds as isotropic mean effective consolidation states are increased beyond 470kPa. Failure occurs in Type B samples at much greater shear strains of between 2.2 – 4.5%, more than double the shear strains of the Type A samples at failure at any given initial stress state.

It can also be seen within Figure 7.1 that the post failure, residual deviator stress of any given Type A sample is similar to that of the residual Type B sample for a given initial stress state.

The role of increasing initial mean effective stress conditions on the strength of the two material types is more easily seen once sample sets are separated into Type A (Figure 7.2) and Type B (Figure 7.3) behaviours (with both graphics plotted on the same scale for comparison purposes).

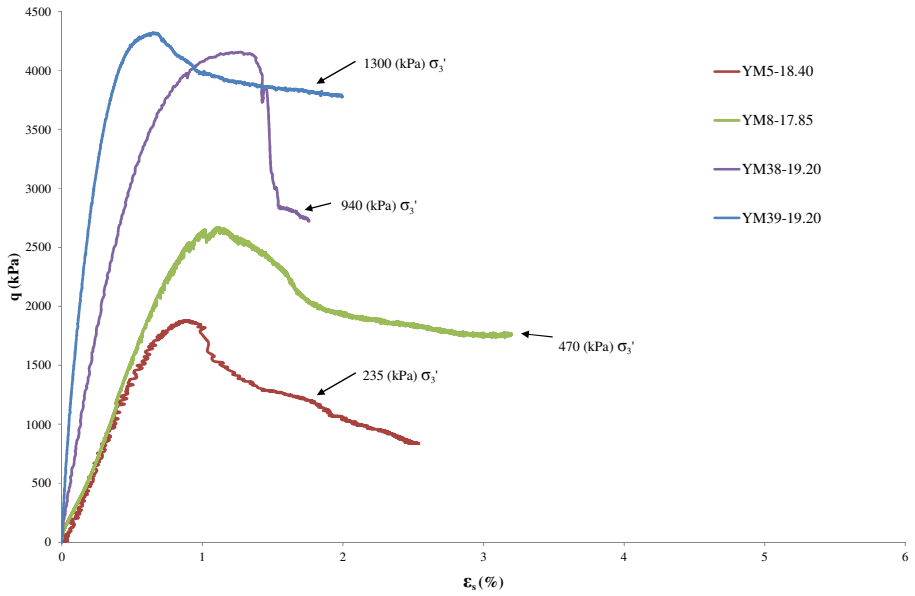

Figure 7.2: Stress – strain relationships with changing p' in Type A calcareous mudstone.

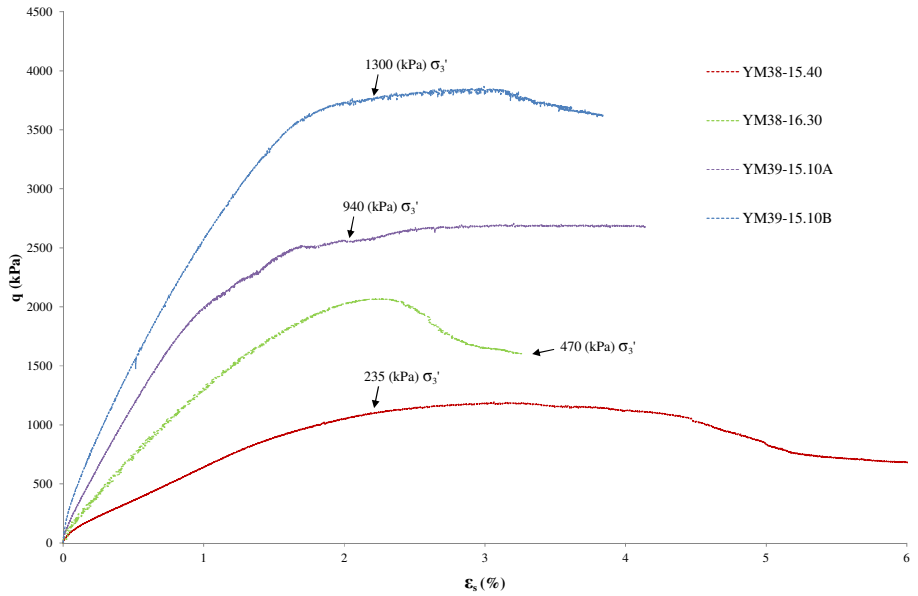

Figure 7.3: Stress – strain relationships with changing p' in Type B calcareous mudstone.

Mean effective stress conditions clearly play a crucial role in governing the mechanical performance characteristics of these deposits, however it is equally important to know what 'Type' the mudstone is before attempting to make predictions as to their strength.

The volumetric strain behaviour of samples is also assessed as samples are sheared, where (ε_v) is calculated using:

$$\varepsilon_v = \varepsilon_a + (2 \times \varepsilon_r) \qquad 2.3$$

Type A volumetric strain behaviour with increasing mean effective confining stress is shown in Figure 7.4 and Type B behaviour in Figure 7.5.

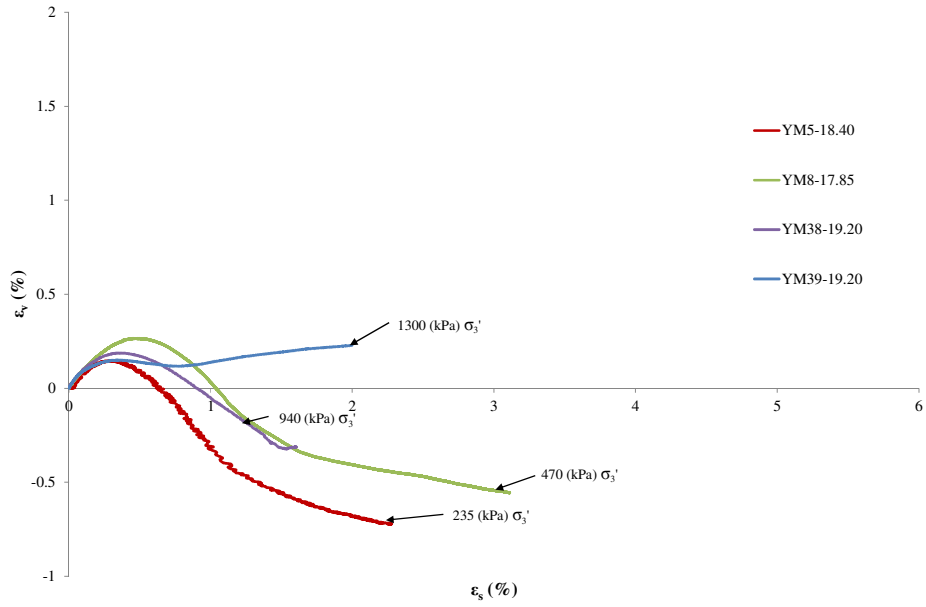

Figure 7.4: Volumetric strain behaviour with changing p' in Type A samples.

Total volumetric strains in Figure 7.4 are noted to be much smaller in comparison to those shown in Type B samples (Figure 7.5), with maximum positive ε_v not exceeding 0.3% and negative ε_v not exceeding -0.7% (as opposed to the 1.7 to -0.8% range noted in Type B samples).

The (ε_v) behaviour in Type A samples is seen to shift from being initially contractant to shear strains of between 0.3-0.5% in all samples tested. This contractant behaviour then shifts to dilatant in the 235, 470 and 940 kPa Type A tests as shear strains increase. Sample YM39-19.20 (consolidated to 1300kPa) is noted to be purely contractant throughout the test, supporting the observations made within the stress-strain analysis of the same sample in the hypothesis that mean effective confining stresses of 1300kPa (or greater than 940kPa) may have caused a degradation to the material's bonding, resulting in a less brittle, more ductile response to stress.

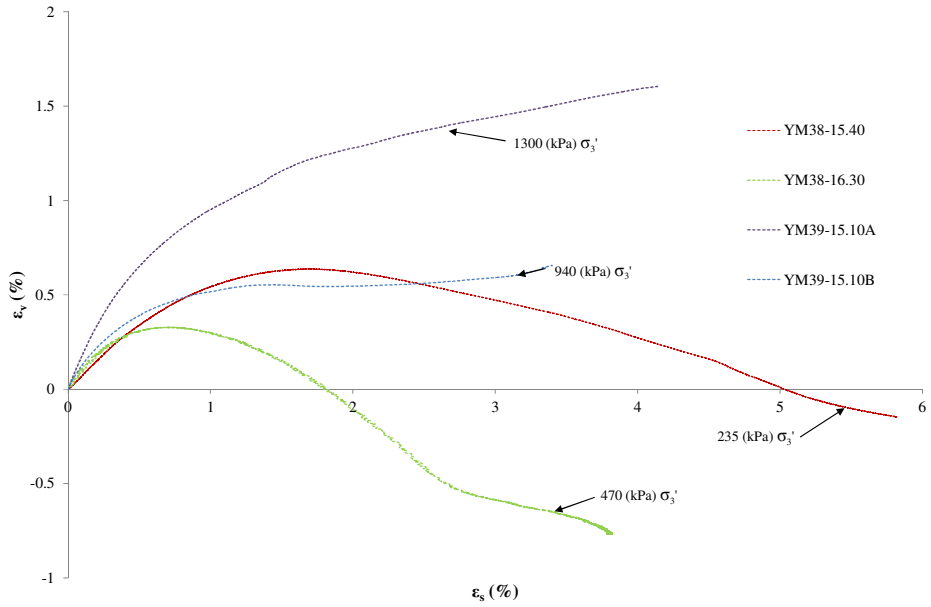

Figure 7.5: Volumetric strain behaviour with changing p' in Type B samples.

A similar shift from dilatant to contractant behaviour is also seen in Type B samples (Figure 7.5), however this occurs only within the samples consolidated to the lower stresses of between 470 – 940 kPa p'_0.

The (ε_v) behaviour in the Type B samples also indicates a shift from 'brittle' behaviour to plastic behaviour as the higher mean effective stress states are reached, likely related to the cementicious bonds contributing to the structure of the material breaking down. This brittle – ductile transition zone is seen to occur at significantly lower values of

(p'_0) in Type B samples, again corresponding well to similar observations noted in the stress-strain analysis covered earlier.

Secant shear stiffness (G) measured is significantly greater within the small strain range for any given sample, as would be expected, deteriorating to a nominal value upon entering large strains. (G) is calculated using:

$$G = \frac{\Delta q}{(3 \times \Delta \varepsilon_s)} \qquad 2.10$$

All samples maximum shear stiffness (G_{max}) are noted to increase with increasing p'_0 conditions within either material 'Type', once again results are presented on two graphs of equal scale for ease of comparison (Figure 7.6 and Figure 7.7).

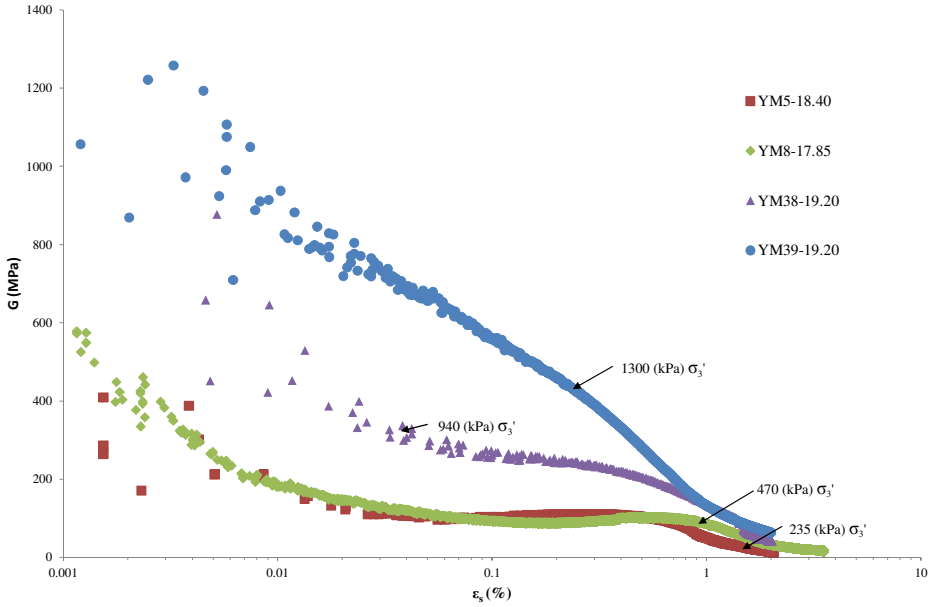

Figure 7.6: Small strain shear stiffness degradation with changing p' in Type A specimens.

All Type A samples display the highest shear stiffness at the lowest measurable shear strains. For the test consolidated to 235 kPa mean effective stress this G_{max} is approximately 350-400 MPa, whilst the 470, 940 and 1300kPa mean effective stress tests display a G_{max} of around 550, 650 and 1050MPa respectively (taken from the mean value within the data scatter). This high stiffness degrades rapidly with the onset of shear strains until at around 0.04% where upon a reasonably steady plateau is noted in all but the 1300kPa mean effective stress test.

Sample YM39-19.20, consolidated to 1300kPa does not display this stiffness plateau; instead it's stiffness degrades steadily from initial readings into small strains, perhaps indicating an isotropic de-bonding caused by the high effective confining pressure that

is not seen at lower stresses, corresponding to entirely contractant behaviour volumetrically. A further drop in shear stiffness is noted at between 0.6 – 1.2% shear strains, corresponding to the point immediately before peak deviator stresses are met. It is also at this point that samples consolidated to 235, 470 and 940 kPa (p'_0) shift from contractant to dilatant volumetric straining (ε_v).

Upon entering large strains all Type A sample stiffness's converge and samples display a similar residual shear stiffness.

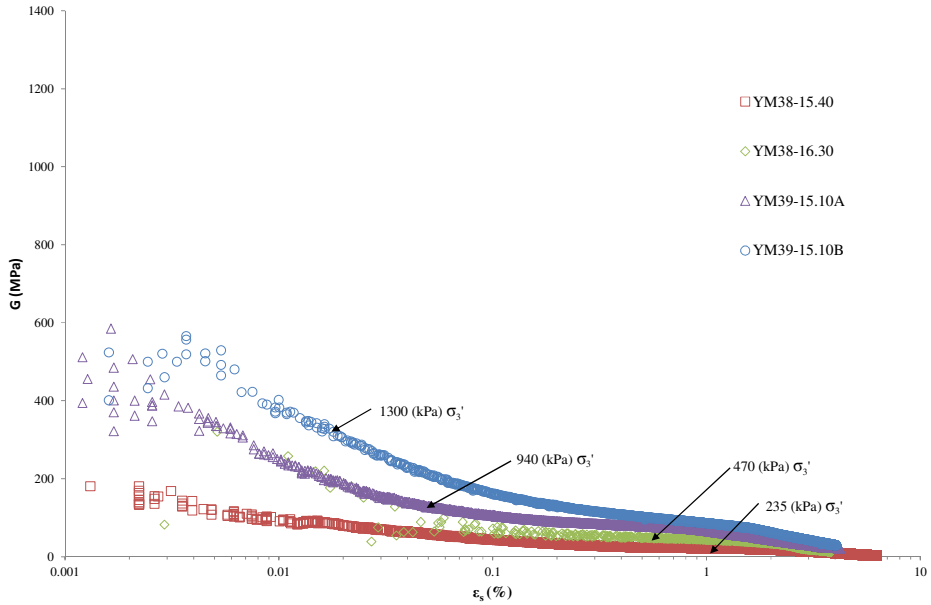

Figure 7.7: Small strain shear stiffness degradation with changing p' in Type B specimens.

Whilst Type B samples do display higher stiffness's relative to one-another as (p'_0) is increased, their (G_{max}) is much lower than those shown by Type A specimens for any equivalent (p'_0). The sample consolidated to 235kPa mean effective stress has a G_{max} of 180MPa, whilst the 470, 940 and 1300kPa tests display 300, 450 and 550MPa G_{max} respectively, almost half the shear stiffness of the Type A samples at any given initial mean effective stress state.

Type B samples do not show the stiffness plateau noted in the Type A samples, even at low mean effective stresses, instead their stiffness degrades at a relatively constant rate from their G_{max} until shear strains of between 0.02 – 0.05%, at which point they continue to degrade at a slower rate until entering large strains. Type B samples also converge to a nominal shear stiffness within the large strain range.

In terms of Mohr failure criterion, Type A materials have an effective cohesion (c') of 400 kPa and an effective angle of internal friction (φ') of 33°, as can be seen in Figure

7.8. The failure envelope is plotted linearly (as it would be from a soil mechanics perspective), however it is recognised that a certain degree of curvature is likely to be present due to the strong structure of the calcareous mudstone (parabolic failure envelopes are a common feature from a rock mechanics perspective (Hoek & Brown, 1988)). This linearity is likely to become more pronounced as higher mean effective stresses are encountered, particularly once materials begin to shift from brittle to ductile behaviours. This shift from brittle to ductile is beginning to occur during the 1300 kPa mean effective confining stress tests in the Type A materials and maybe as low as 940 kPa in the Type B materials (as seen in their stress – strain relationships earlier in this chapter).

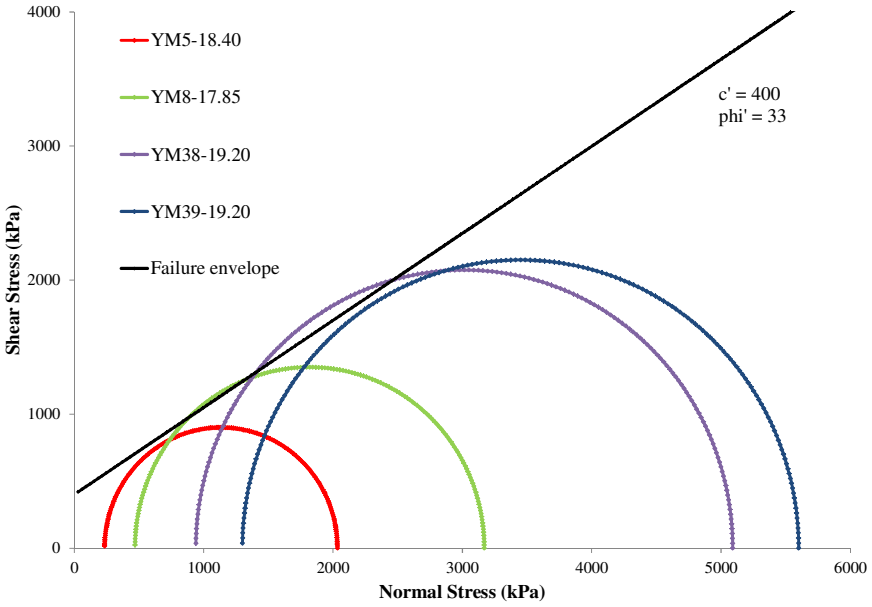

Figure 7.8: 'Best fit' Mohr circles of Type A specimens.

Type B materials display a similar φ' (of 33°) to that of Type A specimens, however have a significantly lower c' at only 200 kPa, as shown in Figure 7.9 (again with a linear failure envelope).

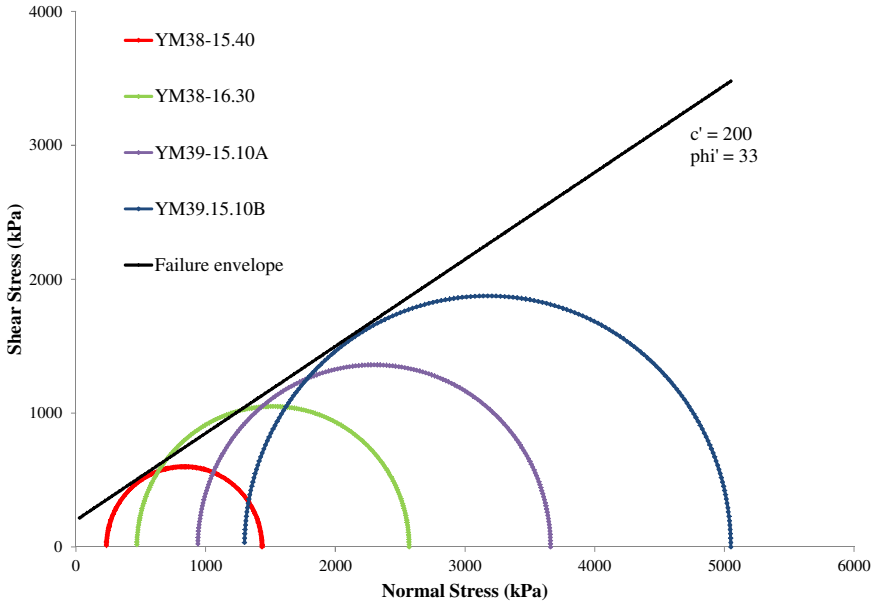

Figure 7.9: 'Best fit' Mohr circles of Type B specimens.

The lower cohesion in the Type B samples at failure is thought to be the mechanical expression of the poorer degree of bonding noted during SEM analysis in the previous chapter. This is similar to the findings of Sun, et al., (2006) who found that lower cohesions, but similar friction angles, were present in samples of similar composition but containing weaker structure.

Both data sets are superimposed upon one another as Figure 7.10 in order to contrast the behaviours between the specimen 'types'. It is thought that as the amount of in-situ re-crystallisation and precipitation of dolomite increases, the better bonded and more cohesive the material will become, forming the tightly bonded mosaics seen in the SEM study. The amount of Palygorskite present is likely to be a key factor in controlling the degree to which these in-situ processes are able to take place, with greater amounts of the clay mineral inhibiting these bonding mechanisms.

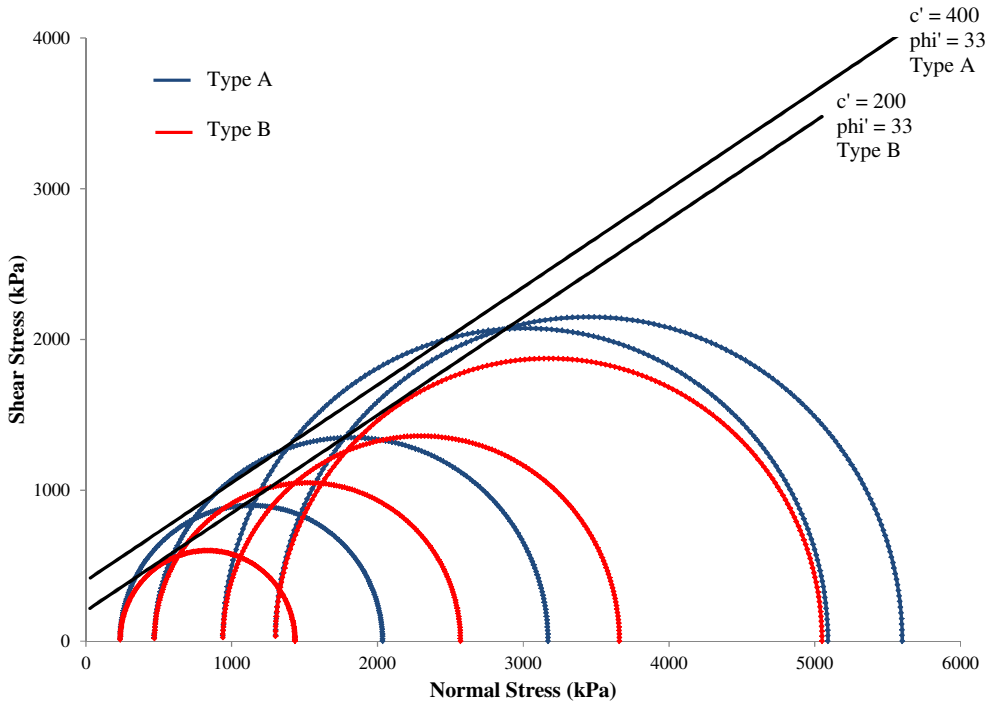

Figure 7.10: Mohr circles of both Type A and Type B specimens.

Figure 7.1 earlier in this chapter showed that samples of both Type A and Type B composition share similar residual strength behaviours post – peak. Figure 7.11 highlights this, in that, Type A and Type B samples share comparable critical state lines (CSL) in p' and q stress space.

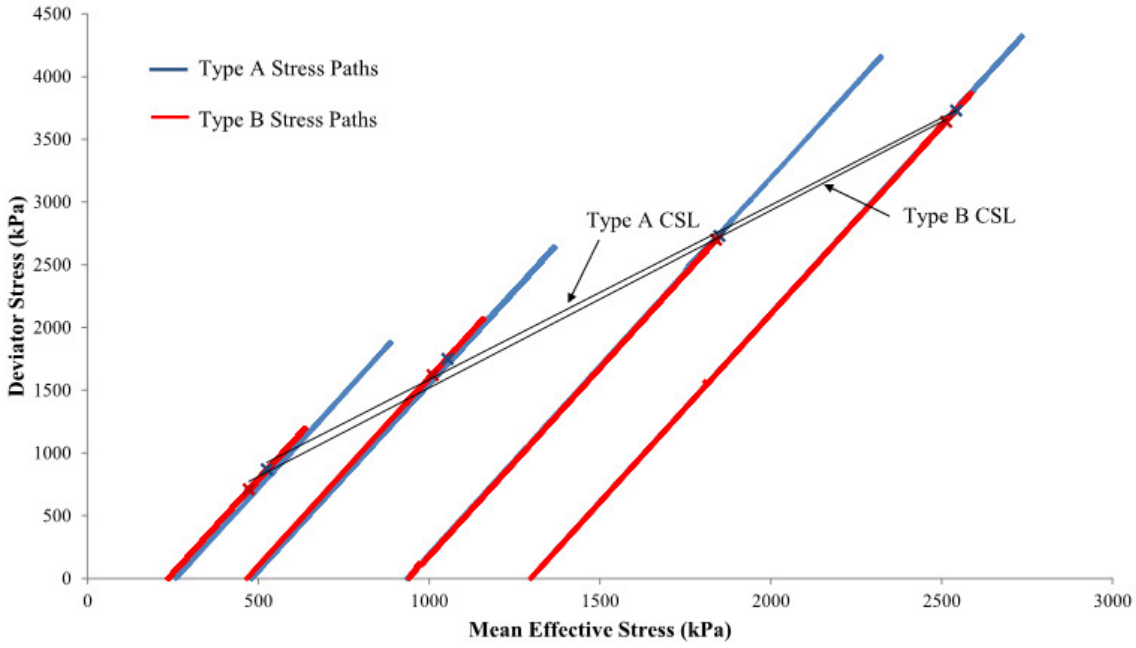

Figure 7.11: Drained stress paths of both Type A and Type B specimens with CSLs superimposed.

Examining the Type A and Type B sample sets failure envelopes not as 'best fit' behaviours of the total of their four respective Mohr circles, but as data sets of their own right, shows a strong agreement with the interpretation of the stress-strain and volumetric behaviour analysis with respect to degrading structure / bonding at the higher end of the mean effective stress tests undertaken.

The Type A samples were shown to change from contractant - dilatant (up to samples consolidated to 940kPa p'_0) to purely contractant (in the case of the sample consolidated to 1300kPa p'_0) as mean effective stress increased, with the sample consolidated to 1300kPa p'_0 not responding as stiffly or strongly to compressive stress relative to the increased stiffness response of those sheared at lower mean effective stresses, given the increase in effective confining stress between 940kPa and 1300kPa being 360kPa. This can clearly be seen in Figure 7.12, where an apparent loss of cohesion is noted between the 940kPa (YM38-1920) and 1300kPa (YM39-19.20) p'_0 tests.

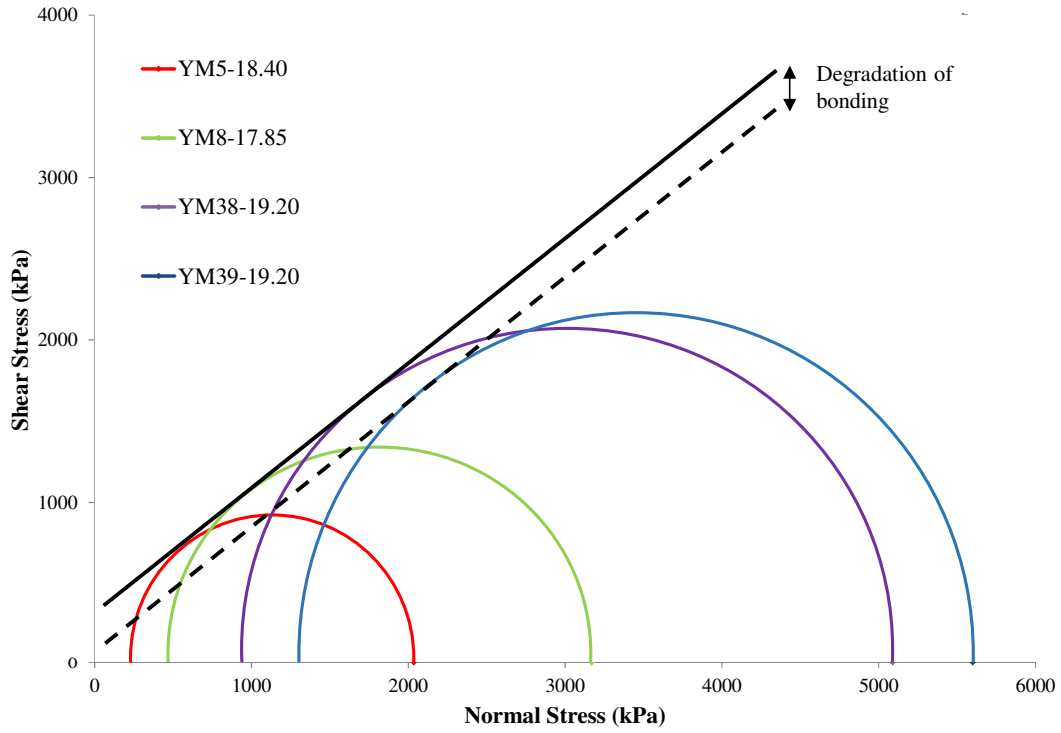

Figure 7.12: Mohr circles of Type A specimens pre- and post-destructuring.

This theorised loss of structure / bonding can be seen to occur at lower mean effective stresses in Type B samples (Figure 7.13), as highlighted in the interpretation of their volumetric strain and stress-strain behaviour, where the change from contractant - dilatant to purely contractant volumetric straining occurred at the lower mean effective stress of 940kPa. This good agreement between analyses increases the reliability of this hypothesis. Furthermore it is noted that the amount of apparent loss of bonding between

the 470kPa and 940kPa tests is less than that observed in the Type A samples (occurring between 940kPa and 1300kPa), perhaps due to Type B samples having lower degrees of initial bond strength compared to that of Type A samples.

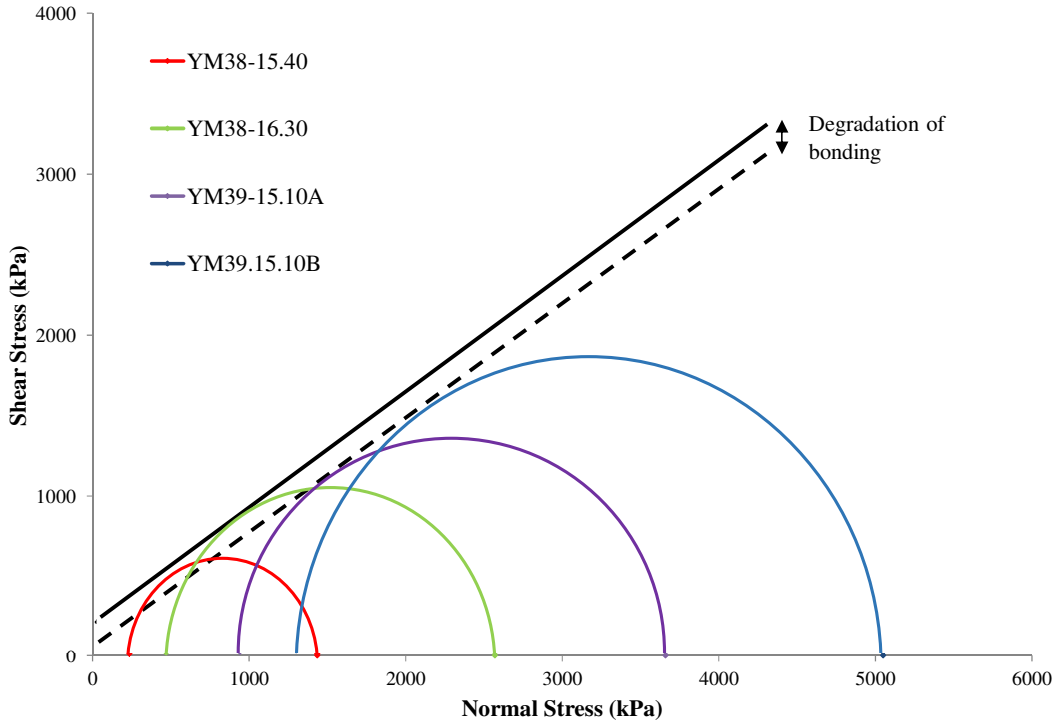

Figure 7.13: Mohr circles of Type B specimens pre- and post-destructuring.

Finally, sample NB02-40.00 was isotropically consolidated in a number of stages over the course of several weeks so that the role of mean effective stress on G_0 could be assessed using Bender Elements. Sample NB02-40.00 is of a Type A composition and so its stiffness at zero strain will be compared to that of the other Type A samples tested within this programme. Sample NB02-40.00 was prepared and saturated in the same manner as the other triaxial tests within this thesis, with the exception of the creation of a shallow trench at the centre of each sample end that houses the Bender Elements. This is covered in more detail in Chapter 4. The sample, once satisfactorily saturated, was consolidated to 150kPa then left until deformations ceased, at which point it was induced with a source S-wave via the Bender Elements and the associated received waveform was recorded and logged. The sample was then subjected to an isotropic rise in mean effective stress of 100kPa and the process repeated until a mean effective stress of 1250kPa was achieved.

In order to correctly interpret the results of the Bender Element tests, the bulk properties of the sample in question must be known at all times. This is achieved by monitoring

the amount of water entering or leaving the sample at all stages of testing as well as recording its axial and radial deformations, particularly during consolidation. As the consolidation stages were isotropic, an assumption is made that the sample deformed as a right cylinder, meaning that diametric measurements taken directly from the sample centre (local radial strain gauges) can be taken as representative of the sample whole. Figure 7.14 shows the raw back volume changes taken during the 12No. stages of consolidation.

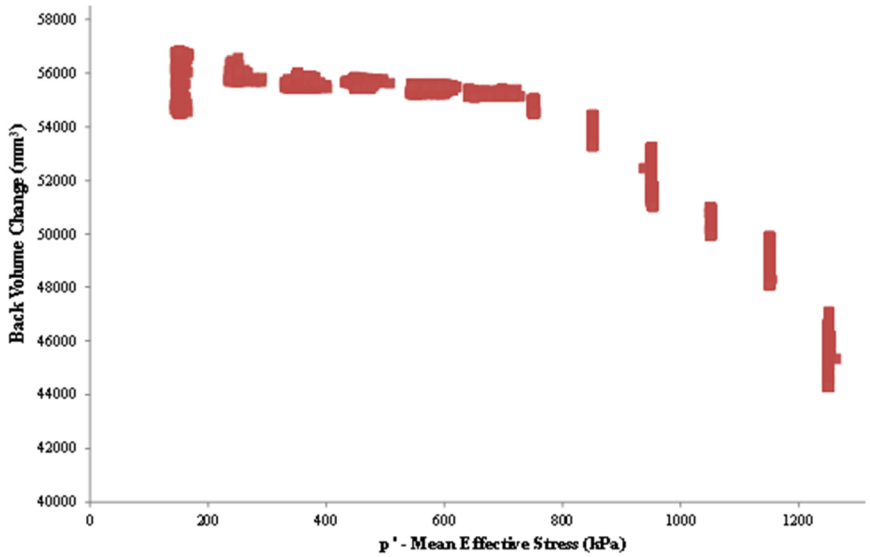

Figure 7.14: Back volume change in sample NB02-40.00 during Bender Element analysis.

Figure 7.15 shows the raw axial deformation of sample NB02-40.00 during consolidation:

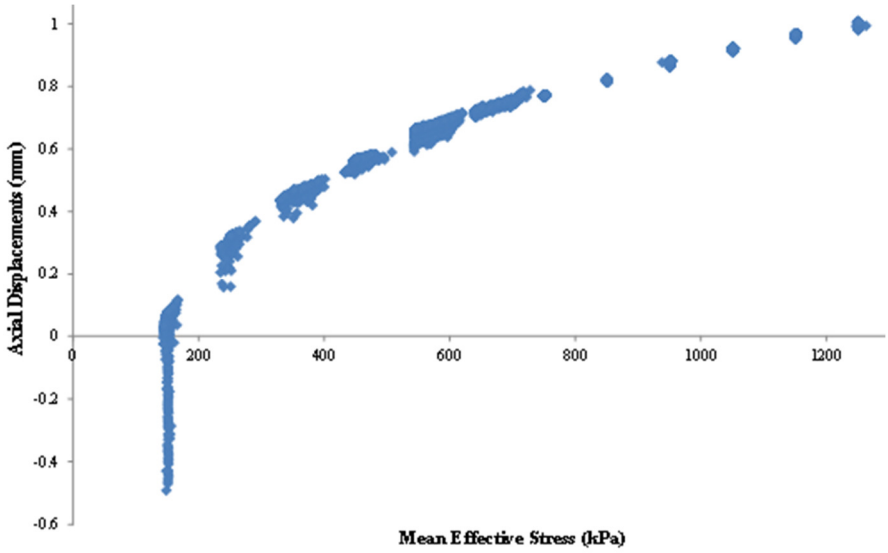

Figure 7.15: Axial deformation in sample NB02-40.00 during Bender Element analysis.

Figure 7.16 shows the raw diametric deformations.

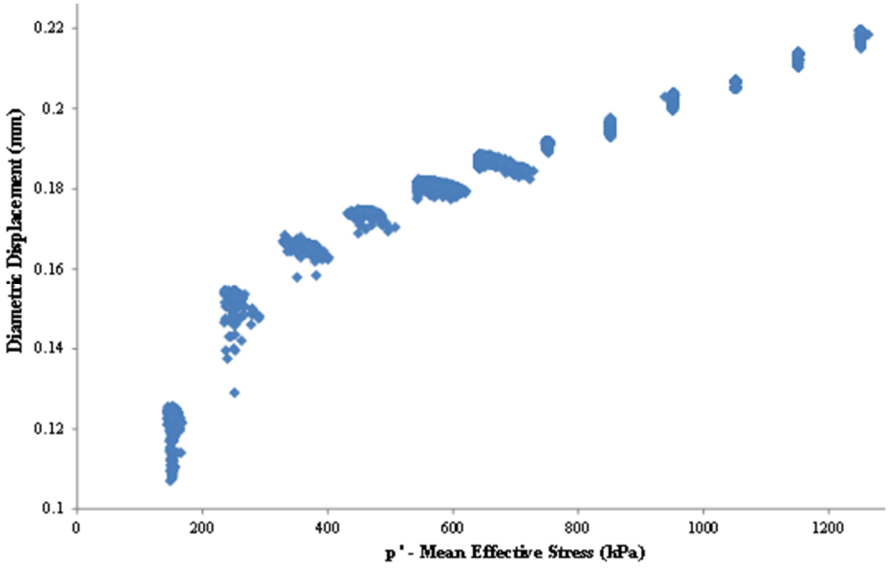

Figure 7.16: Diametric deformation in sample NB02-40.00 during Bender Element analysis.

From the relationship between these changing properties along with knowledge of the initial conditions, bulk density and distance between Bender Elements may be calculated for any point during the testing programme allowing first the seismic velocity (Vs) of the propagating wave to be calculated using:

$$V_s = \frac{L}{Ts} \qquad 4.6$$

Followed by the G_0 of the sample using:

$$G_0 = \rho \times {V_s}^2 \qquad 4.7$$

Again, these formula were covered more thoroughly in Chapter 4 along with an explanation of the four typical reference points from which to measure travel times upon the received waveform using the Time Domain method (namely, 1st deviation, 1st 'bump', zero crossing and 1st major peak), seen in Figure 7.17 as A, B, C and D respectively.

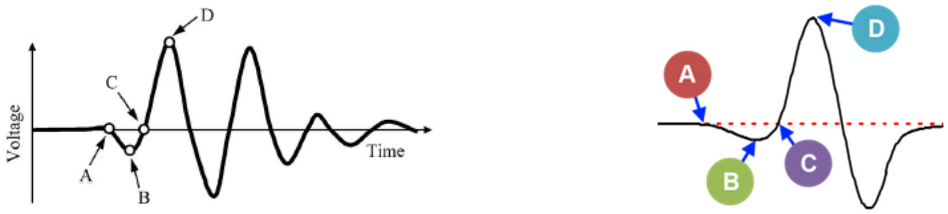

Figure 7.17: Idealised morphology of waveform showing points A – first deflection, B – first 'bump', C – zero crossing and D – first major peak. (Yamashita, et al., 2009); (Rees, et al., 2013)

As these four reference points are located at increasingly distant points along the time axis with respect to the source wave, the resultant calculated G_0 profiles appear to provide decreasingly stiff estimates. This can be seen on Figure 7.18.

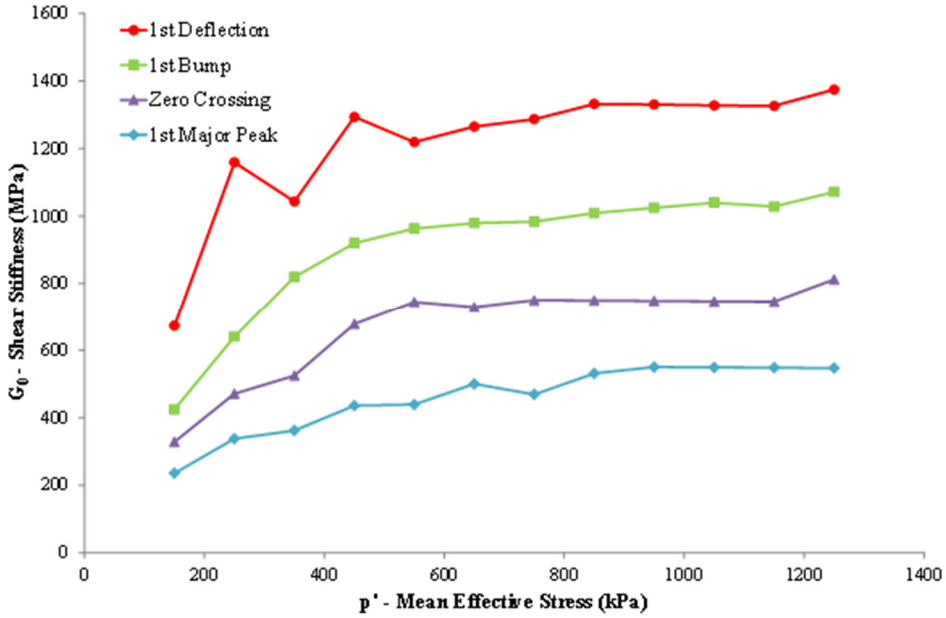

Figure 7.18: G_0 profile of sample NB02-40.00 with increase in p' using several reference points in the Time Domain.

Whilst all four methods provide similar curvilinear relationships between G_0 and p', the 1st 'bump' method is typically deemed to provide the best estimates of G_0 when comparisons are drawn from corresponding triaxial results at similar confining stresses. This is the method adopted by Viggiani & Atkinson (1995), Karg & Haegeman (2005), Camacho-Tauta, et al (2012) as well as a number of other authors (Fonseca, et al., 2009); (Chan, 2010) and can be seen as Figure 7.23 against existing Type A data.

Another reliable method that is also often considered is that of Peak to Peak, where the travel time difference between the source wave peak and arrival of the 1st major peak is used to calculate Vs (Figure 7.19) (Jovicic & Coop, 1996); (Black, 2009); (Chan, 2010).

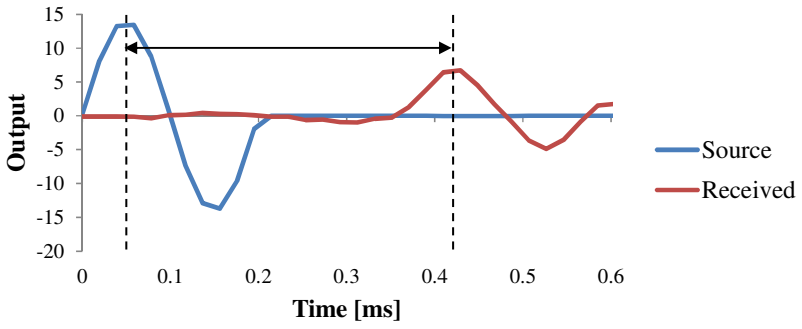

Figure 7.19: Schematic showing the travel time difference between source wave peak and received wave peak using the Peak to Peak method in the Time Domain.

This has the effect of raising estimates of G_0 compared to those generated using the raw Ts of the 1st Major Peak method, as seen in Figure 7.20.

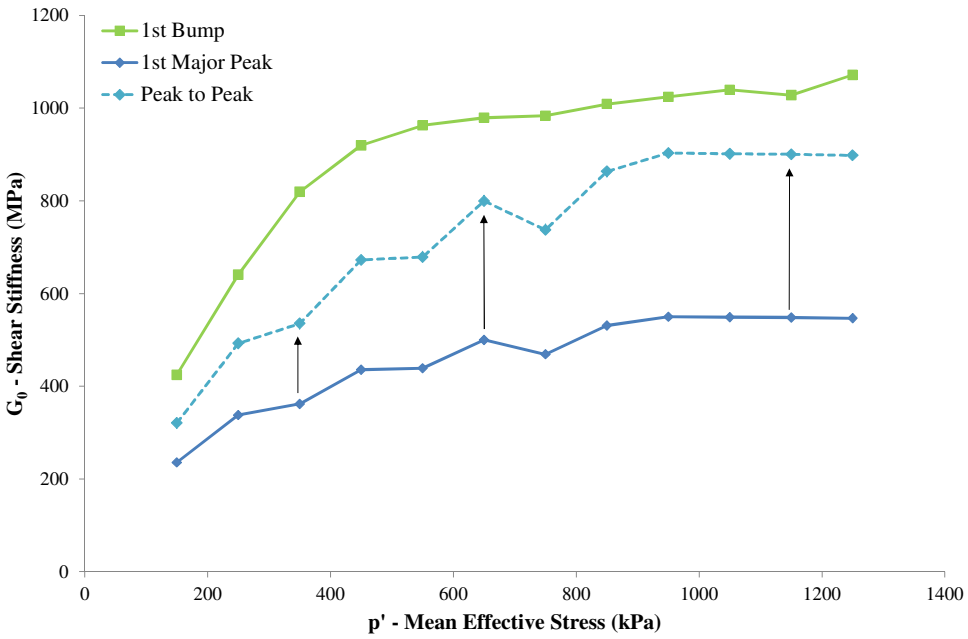

Figure 7.20: G_0 profile of sample NB02-40.00 with increase in p' using 1st 'bump', 1st major peak and a peak to peak method in the Time Domain.

The Peak to Peak method is often compared to the zero crossing results (sometimes called Start to Start method) as these two methods often present comparable G_0 estimates (Fonseca, et al., 2009); (Yamashita, et al., 2009); (Chan, 2010). Figure 7.21 shows these methods, often providing similar travel times and ultimately seismic velocities to one another.

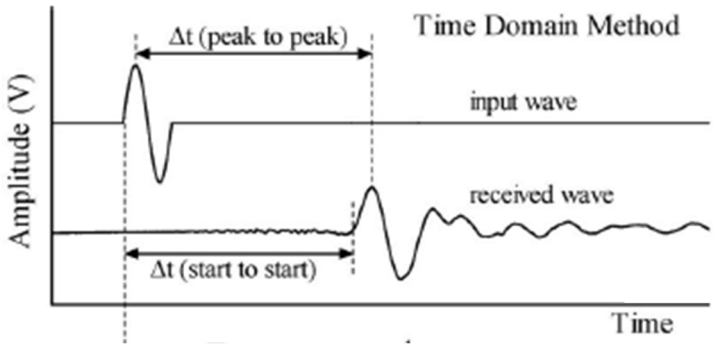

Figure 7.21: Two common Time Domain methods, Peak to Peak and Start to Start (Yamashita, et al., 2009);

The Peak to Peak and Start to Start methods are compared to one another in Figure 7.22 and show similar estimates of calculated G_0.

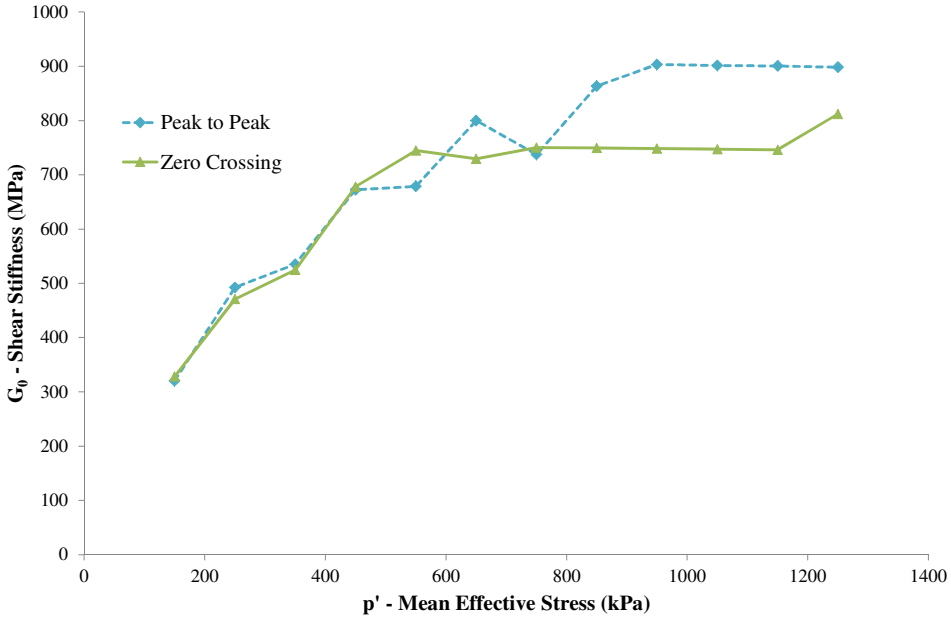

Figure 7.22: G_0 profile of sample NB02-40.00 with increase in p' using Peak to Peak method and Start to Start (zero crossing) method in the Time Domain.

Based on these results, the 1st 'bump' method provides what this thesis considers to be the upper boundary of G_0 estimates whilst the Peak to Peak / Start to Start method provides the lower boundary. These are shown in Figure 7.23 alongside Type A small strain stiffness degradation curves, with G_0 estimates being located at 0.0001% ε_s.

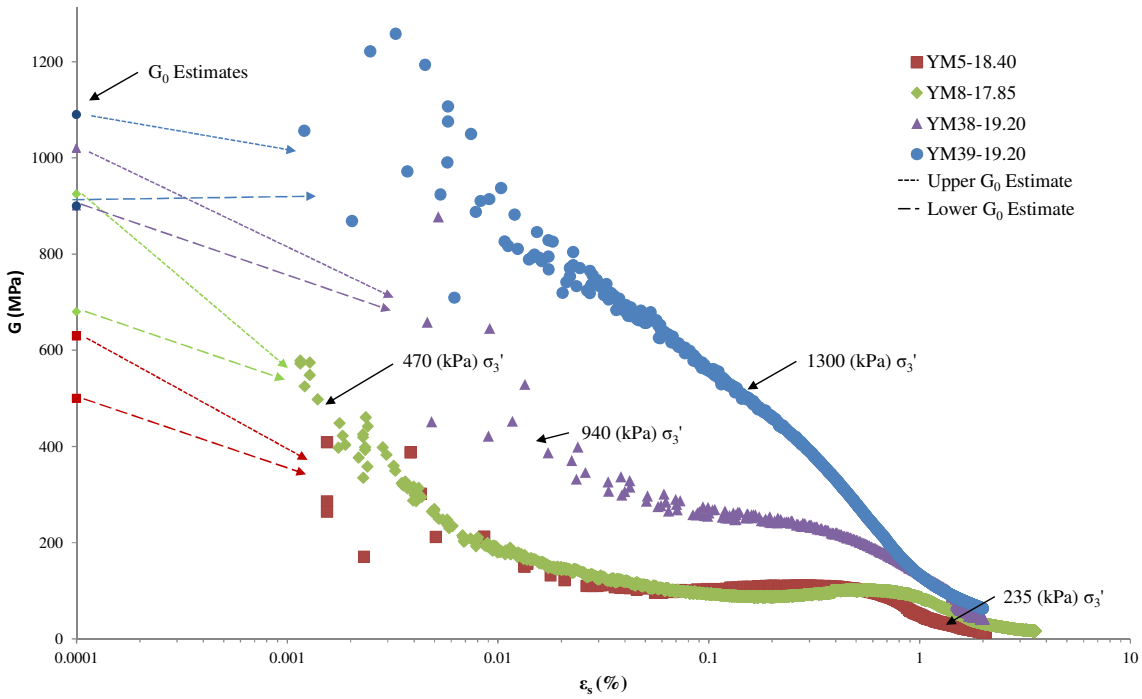

Figure 7.23: Upper and lower G_0 estimates superimposed upon corresponding Type A small strain stiffness degradation curves.

The range of G_0 indicated in Figure 7.20 is thought to serve as a good estimate for stiffness of Type A materials; with G_0 being approximately 20-40% greater than G_{max} measured using advanced triaxial testing employing local strain gauges. The exception to this are the apparently low estimates of G_0 for the 1300kPa mean effective stress tests, where G_0 is approximately equal to or even lower than the G_{max} derived from triaxial data depending upon if the upper or lower G_0 estimate is assumed. This may be due to the closure of micro-cracks at high confining stresses as shear strains develop, as observed by Clayton & Heymann (2001) in their testing of chalk, or may simply be due to the increase in data scatter at very small shear strains when using Hall Effect gauges.

7.2.2. *STUDY 2 - THE ROLE OF SHEARING RATE*

A total of 3No. core samples of calcareous mudstone were selected in order to assess the role of varying strain rate on sample stiffness and failure mechanisms. Due to limited availability of raw material, only Type B samples were selected, all sourced from the NBAD site at similar depths (within 10m of one another in the vertical stratigraphy) and all having similar initial index properties.

Drained testing was carried out on all samples, again to ensure consistency and comparability between both this set of tests and those from the mean effective confining stress study (study 1). Initial index properties of samples selected, along with the stresses and strain rates to which they were subjected are presented in Table 7.3.

Table 7.3: Summary of sample properties used during drained strain rate tests

	Strain Rate Tests			**Confining Pressure Tests**	
Strength Designation	Type B			Type A	Type B
Sample Reference	NB03-35.80	NB02-39.90	NB01-44.75	YM38-19.20	YM39-15.10A
Site Name	NBAD			Yas Mina	
Borehole No.	03	02	01	BH38	BH39
Depth Sample Taken (mbgl)	35.80	39.90	44.75	19.20	15.10
Initial Moisture Content (%)	21.1	19.8	20.2	17.80	20.5
Initial Bulk Density (Mg/m^3)	2.01	2.01	2.01	2.02	2.01
Initial Dry Density (Mg/m^3)	1.66	1.68	1.68	1.71	1.67
Initial Void Ratio	0.62	0.61	0.61	0.60	0.61
Initial Porosity (%)	38.4	37.8	37.9	37.7	38.2
Initial Degree of Saturation	91.4	88.0	89.3	81.04	89.5
Isotropic Mean Effective Stress (kPa)	940			940	
Shearing Rate (mm/min)	≈0.00014	≈0.0014	≈0.014	≈0.0014	
Strain Rate (%/min)	0.0001	0.001	0.01	0.001	

All samples were isotropically consolidated to a mean effective stress of 940 kPa. This stress state was selected as it represented the approximate change from brittle to ductile behaviour noted during the mean effective stress tests on Type B samples (and so a broader range of behaviours may be noted with changing strain rate), and to allow for direct comparison with both Type A and Type B samples from the previous study tested at this confining stress.

Samples examined during the mean effective stress tests were sheared at a set strain rate of 0.001% per minute (equating to approximately 0.0014mm/min). In order to ensure that the samples selected were not being controlled by their greater depth of origin, a repeat test at 0.001% axial strain was carried out as a control on sample NB02-39.90, to allow for cross comparisons with the mean effective stress tests.

To assess the effect of a slower strain rate, a test was carried out shearing the sample a factor of ten times slower (a rate of 0.0001% per minute) than the control and an additional test was carried out ten times faster (at a rate of 0.01% per minute).

Stress-strain plots show that the three rates of shearing present very differing mechanical behaviour (Figure 7.24).

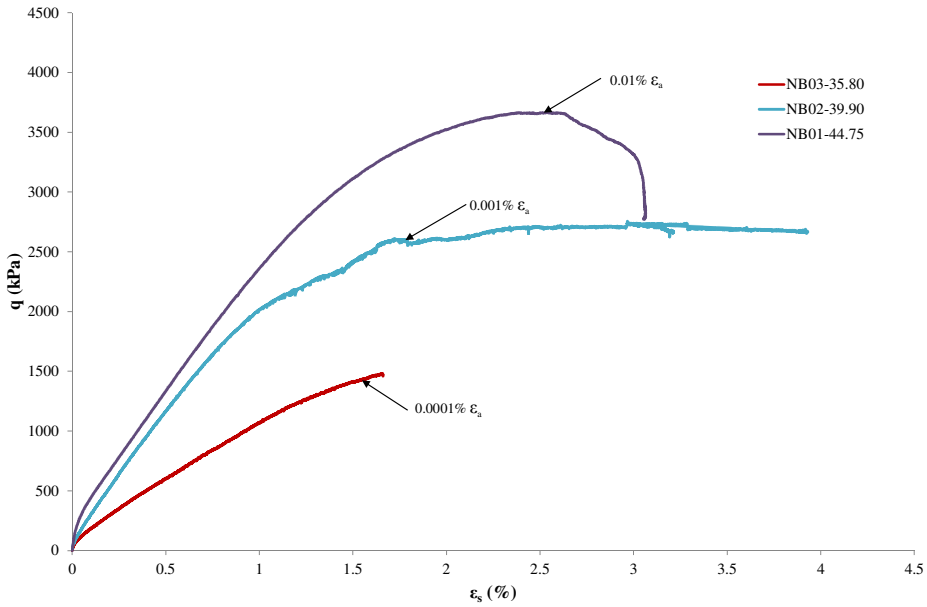

Figure 7.24: Stress – strain relationships with changing strain rate in Type B samples.

A markedly higher maximum deviator stress was observed in the faster 0.01%/min test than was seen in the 0.001%/min test, and the 0.0001%/min test showed the lowest maximum deviator stress (although it should be noted that the 0.0001% test had to be stopped prematurely due to computational errors brought about by the extended time

period over which it was carried out, however given the decreasing gradient of the stress-strain curve at 1.6% shear strain it is likely the sample was nearing its maximum deviator stress).

These findings indicate that rate of strain greatly effects the maximum devatoric stress this material can withstand for any given mean effective stress. It should be noted that the fastest rate (of 0.014mm/min) also caused peak deviatoric stress behaviour, despite the material being of Type B and consolidated to high p'_0 of 940kPa.

This data set can be compared to the results of both Type A and Type B materials from the 940kPa mean effective stress tests (Figure 7.25). The relationship between the three tests sheared at 0.001% axial strain (NB02-39.90, YM39-15.10 and YM38-19.20) is particularly noteworthy as it highlights that depth of sample origin is less of a controlling factor over strength and stiffness than material 'Type', as the two Type B sample plots show very similar behaviours despite having a 15 meter discrepancy in vertical separation (highlighting the reliability and repeatability of the testing undertaken and showing the lack of strength dependency upon depth of sample origin). The Type A sample (YM38-19.20) shows the overall stiffest response to deviatoric stress, even when compared to a Type B sample (NB01-44.75) sourced from a greater depth and sheared at a ten times faster rate.

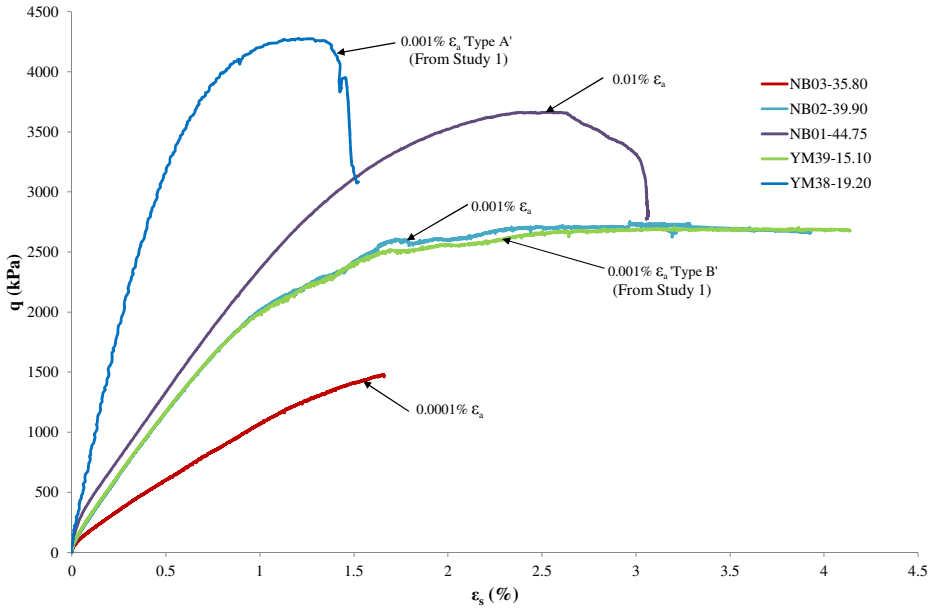

Figure 7.25: Comparing stress – strain relationships with changing strain rate between NBAD and Yas Mina samples.

The volumetric strain response to shear strains for the three rate tests are presented as Figure 7.26. Whilst all volumetric responses are overall contractant, the results show a gradual change in behaviour as shearing rate increases, with the slowest test (0.0001%, sample NB03-35.80) having a continuously contractant behaviour and the fastest test (0.01%, sample NB01-44.75) beginning to shift towards dilatant behaviour after achieving its maximum volumetric strain of 0.7% at approximately 1.5% shear strain.

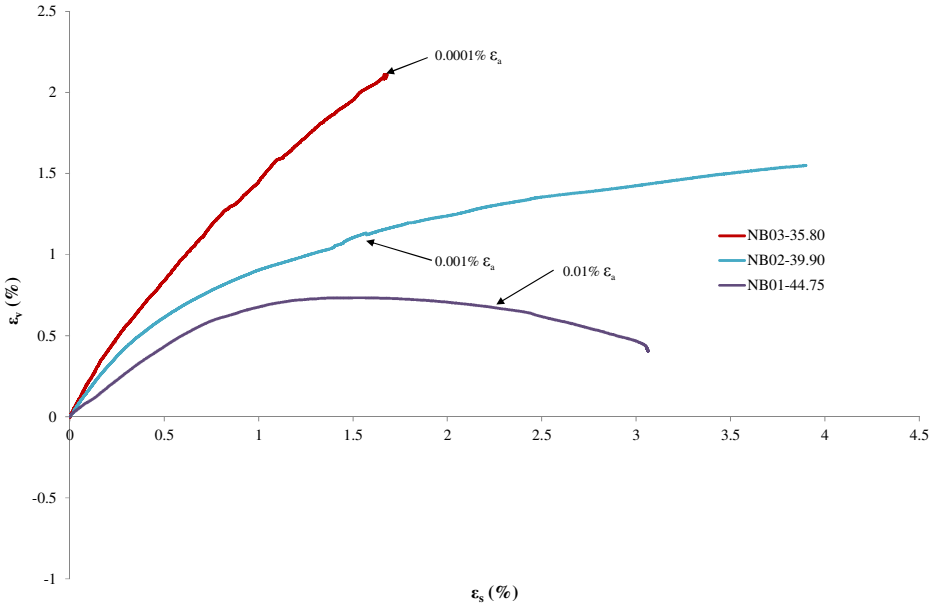

Figure 7.26: Volumetric strain behaviour with changing strain rate in Type B samples.

Comparing the rate of strain tests with samples YM39-15.10 and YM38-19.20 reveals very similar volumetric strain behaviour between YM39-15.10 and NB02-39.90, as shown on Figure 7.27, despite the difference in the depth of sample origin as has been previously established. Both are Type B samples sheared at 0.001% strain rate and consolidated to a p'_0 of 940kPa and so good comparisons can be made, again showing good repeatability between tests.

Once again the Type A sample (YM38-19.20) undergoes significantly lesser degrees of positive volumetric strain that any of the Type B tests, regardless of strain rate and is the only sample to become truly dilatant.

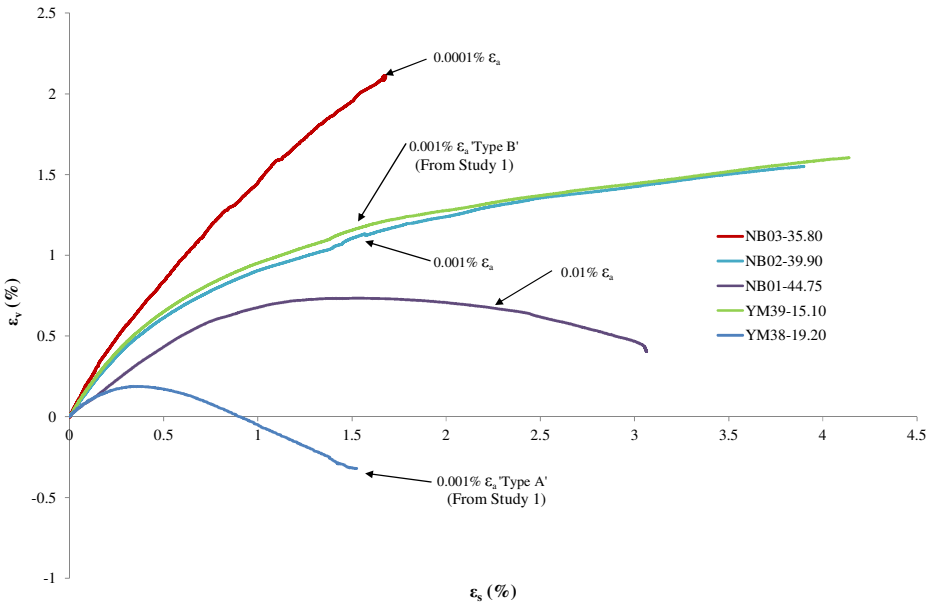

Figure 7.27: Comparing volumetric strain behaviour of rate tests with mean effective stress tests.

Small strain stiffness analysis of results (Figure 7.28) show a similar G_{max} (approximately 400MPa) for all three rates of strain, however the position at which stiffness begins to degrade is progressively shifted to the right, into higher levels of shear strain, as shearing rate increases. Number of data points taken below 0.01% shear strain also decrease as test speed increases as data was logged every 10 seconds throughout the duration of the tests.

As the tests progress, for any given amount of shear strain, measured shear stiffness decreases as shear strains develop, relative to shearing rate. For example, at 0.1% ε_s, shear stiffness is 146.1, 100.5 and 60.5MPa for the 0.01, 0.001 and 0.0001% strain rate tests respectively. This trend continues until shear strains of approximately 1.8-3.0% have developed, where upon all stiffness's converge to a similar value of around 30MPa.

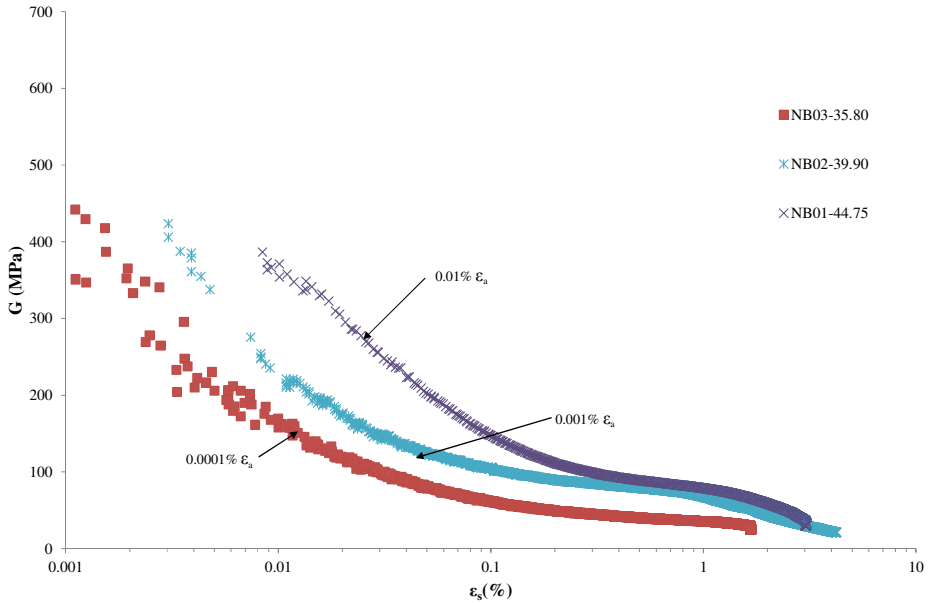

Figure 7.28: Shear stiffness against shear strain with changing strain rate in Type B samples.

By once again comparing these results to those taken from the mean effective stress study (at 940kPa) it can be seen that the Type B sample (YM39-15.10) is in good agreement with sample NB02-39.90 (carried out at similar strain rate and initial mean effective stress conditions), despite the influence of depth. The Type A sample shows stiffer behaviour throughout the test than all Type B specimens regardless of strain rate until it too converges at around 1.8% shear strains.

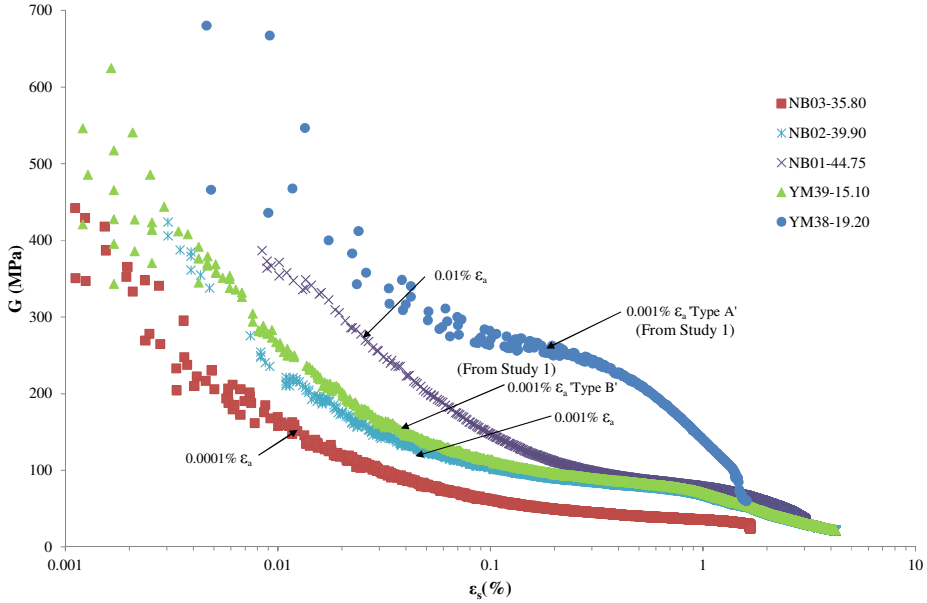

Figure 7.29: Comparing small strain stiffness of NBAD and Yas Mina samples.

7.2.3. *SUMMARY OF TRIAXIAL STUDIES*

Study 1 highlighted the importance of mean effective stress conditions on the overall strength and stiffness of samples of calcareous mudstone. Samples tested at in-situ mean effective stresses displayed peak strength behaviour along with pronounced failure planes, however as isotropic consolidation pressures were increased these features shifted towards a more ductile, strain hardening response to deviatoric stress. Volumetric behaviour also shifts from dilatant at low stresses to contractant as stresses increased.

These broad trends were noted for both the Type A and Type B specimens, however the transition from brittle to ductile behaviour occurred at lower stresses in the Type B samples. Type B samples were noted to fail in compression at lower deviatoric stresses than their Type A equivalent for any given initial mean effective stress state and at significantly higher values of shear strain, indicating a more ductile response to stress. Type B specimens were noted to be significantly less stiff within the small strain range and produced a gradual deterioration of secant shear stiffness as strain increased from G_{max} through to large strains, whereas Type A samples were repeatedly observed to produce two distinct stiffness deterioration curves with a plateaux of constant stiffness between, with the exception of sample YM39-19.20 which was consolidated to 1300kPa p'_0.

The brittle to ductile transition of these materials is thought to be linked to the gradual deterioration of structure as isotropic stress is increased, occurring more readily in the weaker, less well bonded Type B samples and at high stresses in Type A materials.

Both Type A and Type B materials showed similar angles of friction (of 33°), although Type A specimens being better bonded had much higher effective cohesion (of 400 kPa as opposed to 200 kPa in the Type B specimens). Both Type A and Type B materials showed similar post-failure behaviour, having very similar critical state lines.

Finally, study 1 was able to estimate G_0 of Type A specimens using Bender Elements, with the 1st 'bump' method providing the upper estimate of G_0 stiffness and the Peak to Peak / Start to Start method providing the lower estimate of G_0. Only Time Domain methods were assessed within this thesis. G_0 was shown to be curvilinear regardless of method chosen, with stiffness's 20-40% higher than G_{max} (from local small strain measurements) being calculated at low confining pressures and G_0 approximately equalling G_{max} at high confining pressures.

Study 2 saw a similar trend in sample behaviour by altering strain rate. Samples sheared at fast rates of strain (0.01%/min) displayed brittle peak behaviour and were becoming volumetrically dilatant, whereas slower strain rate tests (0.001 and 0.0001%/min) produced more ductile, strain hardening and volumetrically contractant behaviours.

Only Type B samples were tested within the strain rate study (study 2), however comparisons were made to two samples from study 1 that were sheared under similar mean effective stress and strain rates. These comparisons highlighted that depth of sample origin is a less important factor in controlling the mechanical behaviour of calcareous mudstones than those of sample 'type' (Type A and Type B) and the stress state / strain rate under which they are tested.

The comparison of samples between study 1 and study 2 (notably comparisons between samples NB02-39.90 and YM39-15.10) also allowed the reliability and repeatability of the testing procedure itself to be scrutinised, as well as providing a crude means of assessing inter-sample variability. The close agreement between the stress-strain, volumetric and small strain stiffness behaviour of these comparison samples indicate that the methodology and inter-sample quality are consistent enough that results may be discussed as part of an over-arching framework, despite variability in their depth and geographic location of origin.

7.3. BRAZILIAN TENSILE TESTING USING DIC

Indirect Brazilian tensile strength testing was carried out on samples of soft calcareous rock in order:

- To investigate the ultimate tensile strength at failure of the soft rock samples acquired from Abu Dhabi;
- To assess the use of DIC as a means of capturing the development of full field surface strains in real time, and;
- To assess the validity of indirect tensile strength results with respect to the origin of failure using both ASTM and flattened disk preparation and testing techniques on soft rocks.

Results from the Triaxial studies indicated that mineralogy and stress state during testing played a greater role on governing the behaviour of soft calcareous mudstones than that of depth of burial. In order to better understand these materials both Type A and Type B samples will be tested in tension. The role of other potential controlling factors such as depth of sample origin and moisture content will also be examined.

A total of forty two (42no.) Brazilian indirect tensile strength tests were carried out on samples of calcareous mudstone from both sites and from various depths, within this thesis. Chapter 4 covered the development of this test using samples of Springwell Sandstone as analogues for soft rocks, incorporating the DIC technique with findings concluding that tensile failures within disks in compression are significantly more likely to occur centrally if 'flattened' ends are introduced with a 2alpha angle of between 10 – 20 degrees. Ultimately a methodology tailored to calcareous mudstones was presented within Chapter 5, noting the benefit of using a 'contactless' strain gauge over more traditional gauges that require adhesion and that are typically unreliable in moisture sensitive and friable rocks.

Of the 42no. samples tested, approximately half (20no.) were prepared with 'flattened' ends (denoted by an -(F) at the end of their sample code), with the remaining 22no. samples being tested using ASTM suggested methods so that comparisons may be drawn between preparation techniques. In addition to this, samples displaying both the Type A and Type B characteristics were directly compared using both preparation methods in order to better understand how mineralogy and bonding affects these material's tensile strengths.

By necessity, multiple sub-samples were taken from each eligible core sample, meaning that a single core (for example YM5-18.40) may have multiple tests representing its characteristics. Where this occurs, individual tests are differentiated with capitalised letters directly following their depth (for example YM5-18.40A and YM5-18.40B).

7.3.1. *ASTM PREPARED SAMPLES*

A total of 22no. samples were prepared for indirect tensile testing using the ASTM approved method. Samples were selected that represented both Type A and Type B materials (determined using the results of Chapter 6 and correlations with previously discussed triaxial data). These tests used the samples summarised in Table 7.4, which also presents their ultimate tensile strength at failure.

It can immediately be noted that there exists a wide spread of ultimate tensile strength values for the materials tested, even within those sourced from a single length of core. For example sample YM5-18.40D displays a tensile strength of only 97kPa at failure, whilst YM5-18.40B, taken from the same length of core, provided 302kPa at failure.

Table 7.4: Samples selected for assessing the failure pattern of ISRM prepared tensile tests.

Sample Code	Site	Borehole No.	Sample Depth (mbgl)	Loading Rate (N/min)	Material 'Type' Designation	Tensile Strength at Failure (kPa)
YM5-18.40A	Yas Mina	5	18.40	150	Type A	107
YM5-18.40B	Yas Mina	5	18.40		Type A	302
YM5-18.40C	Yas Mina	5	18.40		Type A	188
YM5-18.40D	Yas Mina	5	18.40		Type A	97
YM5-18.40E	Yas Mina	5	18.40		Type A	200
YM38-16.30A	Yas Mina	38	16.30	150	Type B	231
YM38-16.30B	Yas Mina	38	16.30		Type B	149
YM38-16.30C	Yas Mina	38	16.30		Type B	174
NB01-44.75A	NBAD	01	44.75	150	Type B	109
NB01-44.75B	NBAD	01	44.75		Type B	119
NB01-44.75C	NBAD	01	44.75		Type B	158
NB01-44.75D	NBAD	01	44.75		Type B	108
NB01-44.75E	NBAD	01	44.75		Type B	96
NB01-44.75F	NBAD	01	44.75		Type B	154
NB02-23.50A	NBAD	02	23.50	150	Type A	243
NB02-23.50B	NBAD	02	23.50		Type A	75
NB02-23.50E	NBAD	02	23.50		Type A	225
NB02-23.50F	NBAD	02	23.50		Type A	221
NB02-23.50G	NBAD	02	23.50		Type A	195
NB02-23.50H	NBAD	02	23.50		Type A	336
NB03-29.00A	NBAD	03	29.00	150	Type A	379
NB03-29.00B	NBAD	03	29.00		Type A	355

Broadly speaking, the Type A samples have greater tensile strengths than Type B samples, which is to be expected of materials containing more bonding, with average ultimate tensile strengths of Type A samples being 225kPa and Type B samples being

only 144kPa. Whilst it is true that Type A samples have an overall higher average tensile strength than Type B samples, it is clear from the wide scatter of results that there is another factor controlling their measured maximum strengths.

Tensile strength at failure is plotted against depth of sample origin (Figure 7.30) in order to show that little relationship is observable. It is worth noting that samples obtained from the same length of core are plotted as having originated from the same depth, as the samples were generally only a few centimetres thick and the minor increase in depth of burial is unlikely to have affected their measured strengths.

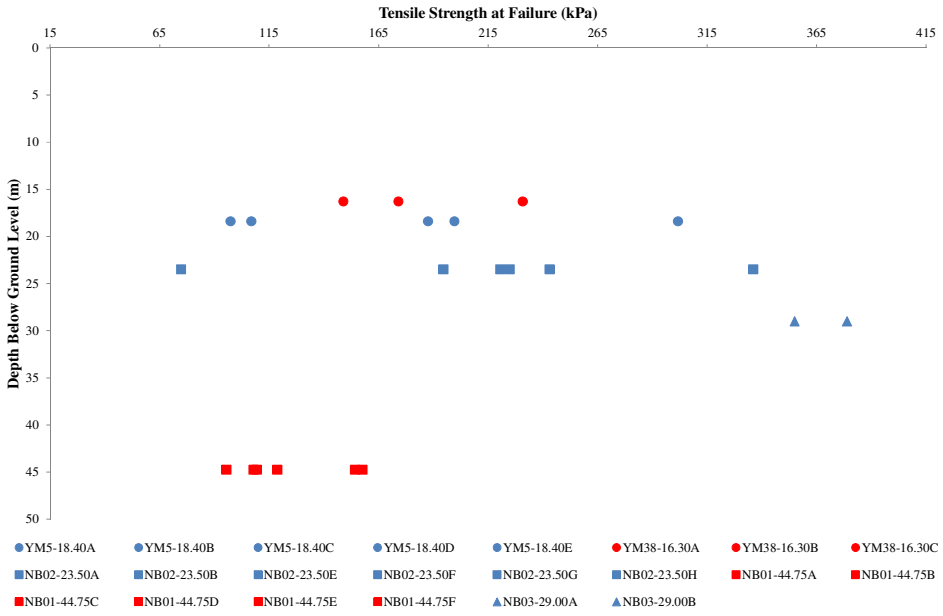

Figure 7.30: Tensile strength of samples vs depth using ASTM standard preparation.

It is clear from the range of tensile strengths obtained from testing that depth of origin is not a controlling factor. Tensile strengths measured using ASTM standard preparation and loading techniques range from 75 to 336kPa for Type A samples obtained between depths of 18.40 and 23.50mbgl for example, with no notable relationship between increasing depth and increasing tensile strengths.

This indicates that a variable other than depth of origin is contributing to the spread of results, the most likely being moisture content; as this material is highly susceptible to changing water contents, becoming clay like and disintegrating if immersed and becoming weak and friable if left to dry.

It should be noted that all samples were exposed to the air for the smallest time possible during preparation, being taken from their packaged state directly to cutting and then being re-covered once the DIC high contrast pattern was applied. Variable moisture

contents were noted between samples, despite having originated from very close to one another within a given core. This variability of moisture contents was observed on a number of occasions, including comparing the moisture content of sample off-cuts during triaxial testing with the back calculated initial moisture content of triaxial specimens. It is believed that the initial moisture distribution within a given core is highly heterogeneous, perhaps owing to localised concentrations of Palygorskite or Halite on a micro-scale or even to the distribution of micro-fractures (allowing non-homogenous drying to occur), which were not observable during pre-testing preparation. Once moisture content is plotted against tensile strength a rough trend emerges (Figure 7.31):

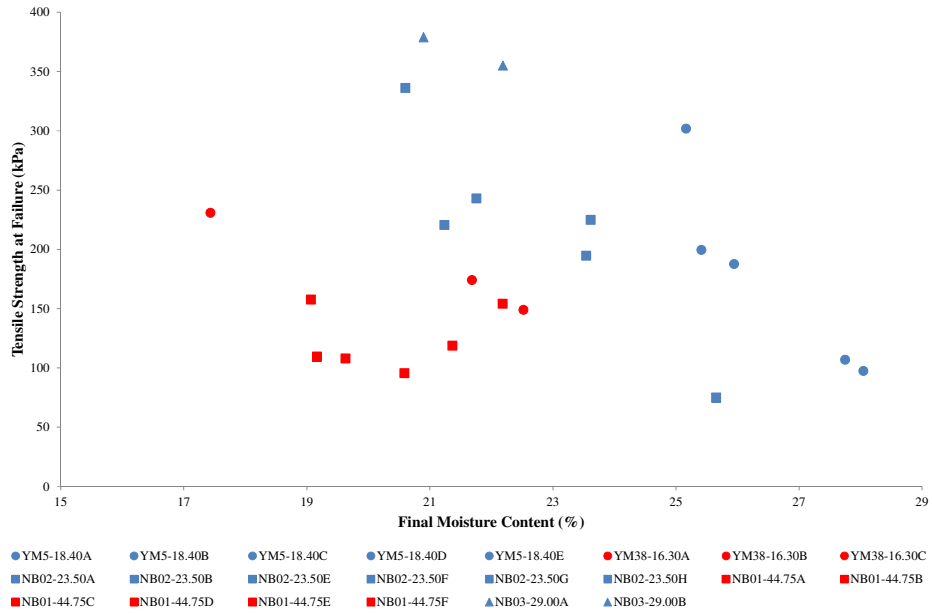

Figure 7.31: Tensile strength of samples vs moisture content using ASTM standard preparation.

Within a given material 'Type', ultimate tensile strengths are observed to decrease with increasing moisture content; with Type B samples plotting at lower tensile strengths for any given moisture content when compared to Type A samples. Type B samples are noted to be able to exist at slightly lower moisture contents than Type A samples, with results still being recordable between 17-20% moisture, whereas Type A samples within this range or lower were discarded prior to testing due to the presence of desiccation cracks and a powdery, friable surface.

All samples appeared to fail in a brittle manner with a vertically orientated fracture appearing and propagating suddenly (as opposed to a gradual propagation or crack opening slowly as the test progressed).

Following failure, several samples continued to be crushed due to the tests being load controlled and samples being held in place by the apparatus, resulting in a rapid increase in load being recorded. This post-failure behaviour can be seen in Figure 7.32 on sample NB02-23.50F and is not a representation of tensile strength parameters. This post-failure behaviour has therefore been omitted on all following graphics, with ultimate tensile strengths being derived from loads measured at a time directly preceding failure.

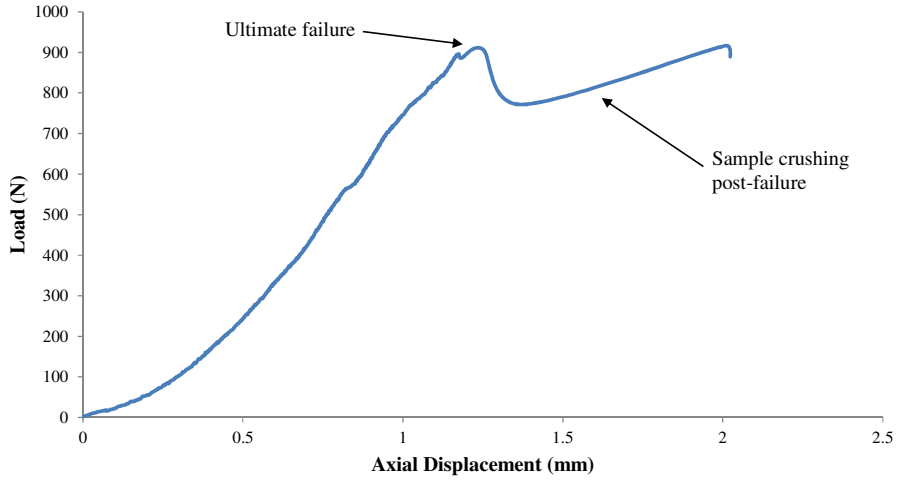

Figure 7.32: Example of post-failure Load vs Displacement behaviour of ASTM samples (using sample NB02-23.50F).

Figure 7.33 shows the stress strain relationships of all samples tested (with blue lines indicating Type A samples and red lines being Type B samples):

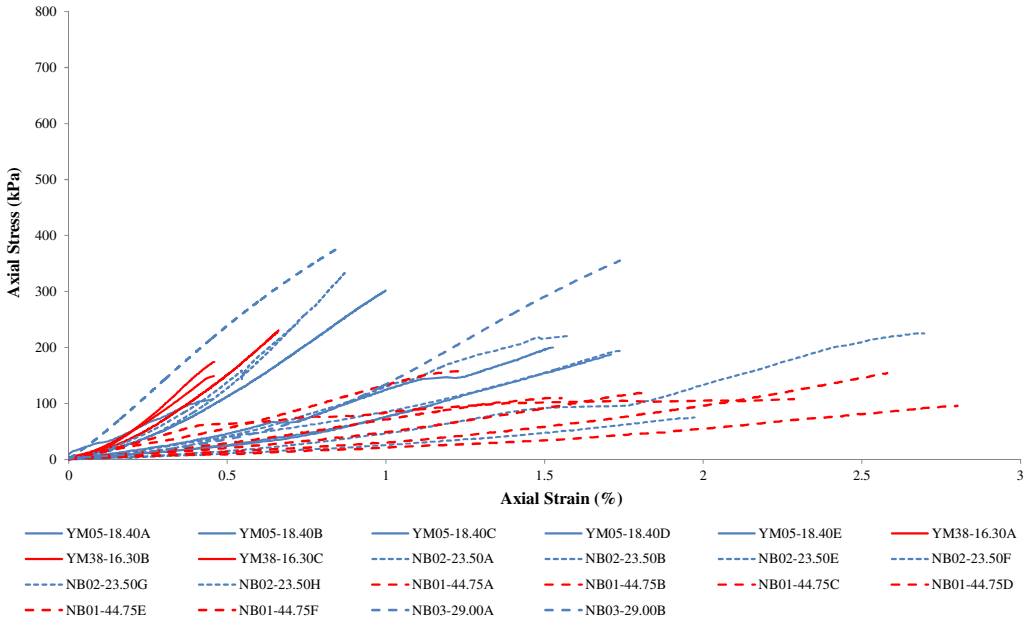

Figure 7.33: External stress strain relationships of ASTM samples.

Whilst the stiffest sample tested was indeed a Type A material and the least stiff was a Type B material, overall the stiffness of samples tested display a broad range, with no clear pattern of behaviour within either 'Type'. Type A samples fail at higher stresses

than Type B materials, however aside from this observation there are no significant trends. Instead it appears that moisture content is a more important controlling factor on the stress strain behaviour of samples of calcareous mudstone in Brazilian testing, and Figure 7.34 shows that, in general, samples become both stiffer and stronger as moisture content lowers (although samples from YM05-18.40 deviate slightly from this pattern).

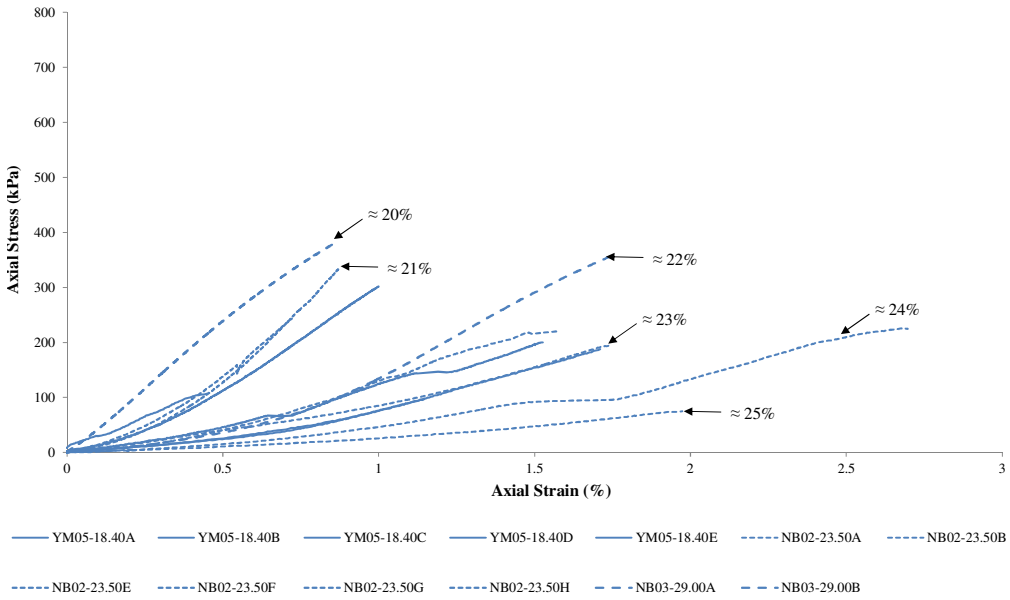

Figure 7.34: Stress strain relationships of Type A ASTM samples with moisture contents overlaid.

7.3.2. *ASTM SAMPLES ANALYSED USING DIC*

Throughout this section of the thesis, many references will be made to the outputs generated from the VIC-3D software. When referring to output images or samples tested the following terms will be used:

- The *Loading Area* will refer to the area of the sample in direct contact to the loading system, i.e. at the extreme top and bottom of the sample.
- The *Centre of the Sample* will refer to the middle of the rock sample, and where failure should occur as described by the Griffith criterion (Diyuan & Wong, 2013), as is assumed under the regulations of Brazilian Testing (both ASTM and ISRM standards).
- The *Outer Edges* refers to the left and right areas of the sample, the extreme ends of the axis perpendicular to the loading axis.

With regards to the qualitative and quantitative interpretation of outputs from the VIC-3D system, by default a colourised contour set is applied to all images with absolute values being presented in an associated scale of the same colour scheme. This scale

moves from red colours (indicating areas of tension) through blue and ultimately into purple (indicating areas of compression).

Images requiring only qualitative information are presented with contours only; whereas when quantitative interpretation is required the numerical scale is also shown, having positive numbers indicating tension and negative numbers indicating compression.

Whilst all samples tested using the ASTM method outwardly appeared to fail in a classical tensile manner, with a vertically orientated fracture and brittle stress-strain behaviour, the DIC technique reveals that the majority of samples tested using this setup did in fact not fail centrally. Instead, several samples are noted to have begun failure proximal to the loading area, generating strain concentrations around these zones as highlighted in Figure 7.35 (showing horizontal strain contours).

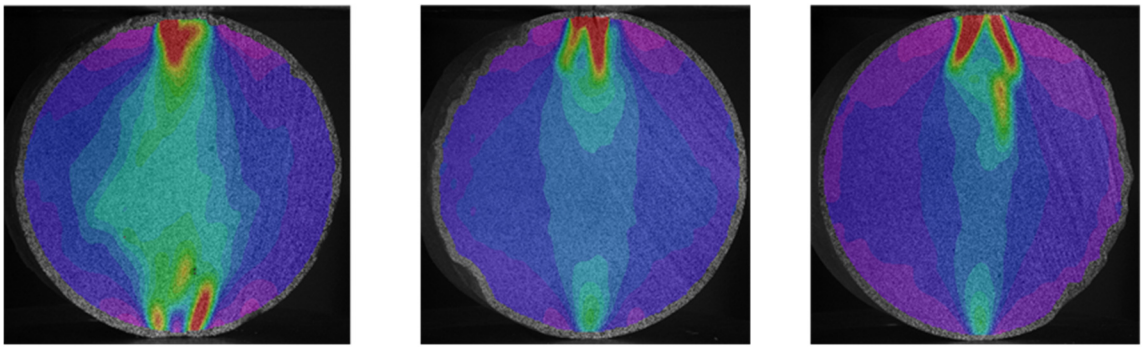

a) b) c)

Figure 7.35: Horizontal strain contours immediately prior to failure in samples a) NB01-44.75A, b) NB02-23.50F and c) NB02-23.50G.

These images are highly representative of the majority of samples tested using the ASTM setup, echoing the findings noted in Chapter 4 on Springwell Sandstone. Very little tensile straining is occurring away from the loading areas, and although these fractures propagated through the sample centres, they are interpreted as having originated from the loading points. More examples of this behaviour are given as Figure 7.36 along with absolute values of straining in the horizontal (exx) direction. In addition to this, a vertically orientated virtual strain gauge is also analysed and output graphically for comparison on each sample, forming the line i-ii..

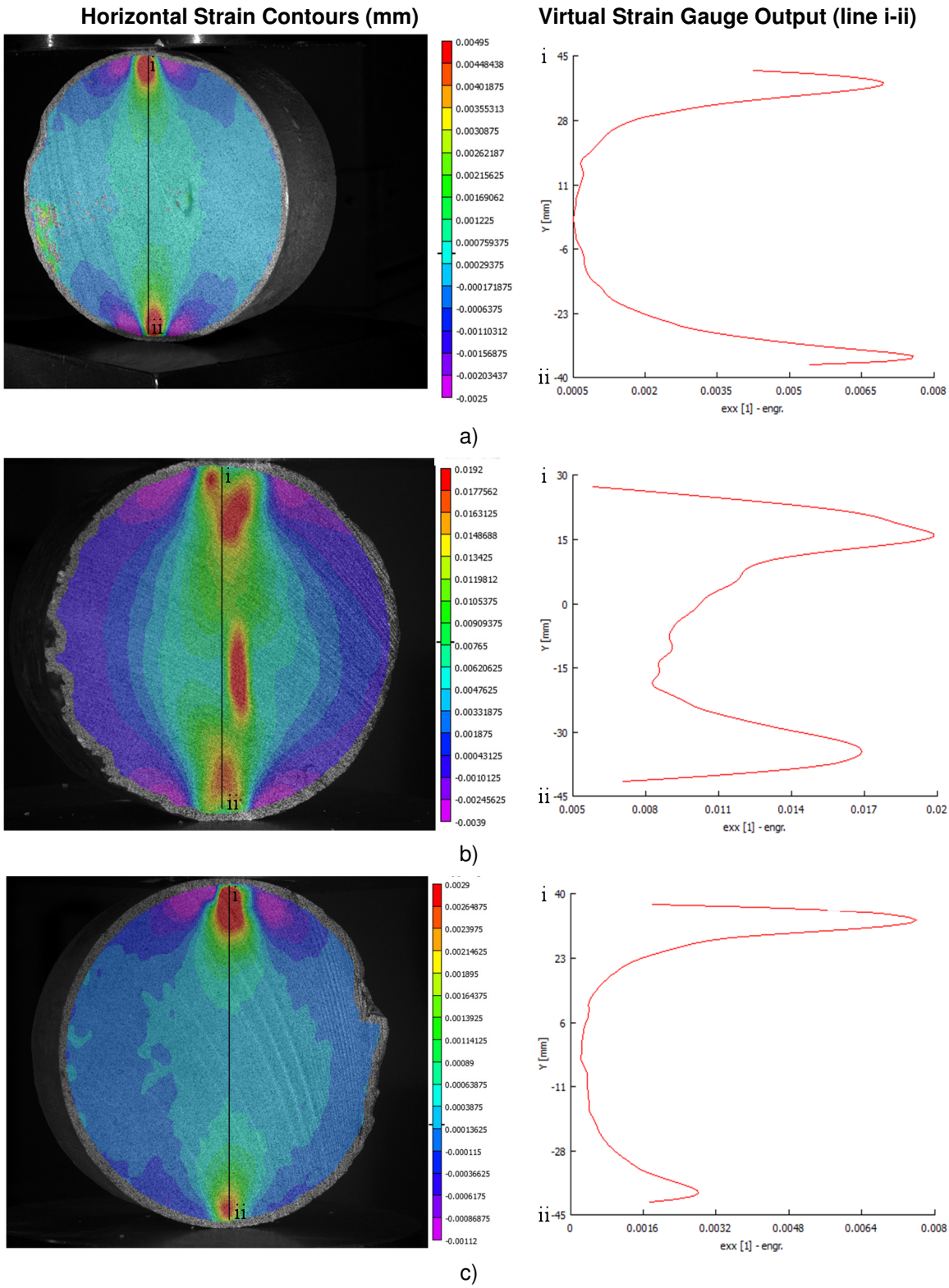

Figure 7.36: Horizontal strain contours and virtual strain gauge outputs immediately prior to failure in samples a) NB03-29.00A, b) NB01-44.75F and c) NB02-23.50B.

In addition to the majority of samples not failing in the centre using the ASTM method, many samples showed signs of localised shearing proximal to the loading areas (as shown in Figure 7.37). Tests displaying these characteristics ultimately failed at lower stresses than their maximum tensile strength.

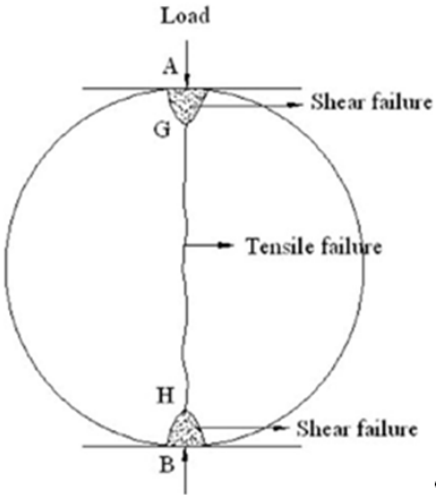

Figure 7.37: Diagram showing localised shear failures at loading areas in Brazilian indirect tensile testing (adapted from (Diyuan & Wong, 2013)).

Significant crushing at the loading ends of the samples also resulted in externally measured axial strains being high, and therefore stiffness's low, for any given sample, regardless of 'Type' or moisture content.

In all, only 2no samples from the 22no. tested using the ASTM preparation method failed centrally, meaning that a very high percentage of samples (93%) did not fail according to Griffith failure criterion for the indirect measurement of tensile strength, therefore not satisfying either ASTM or ISRM standards.

It should be noted that, were it not for the high frame rate, high resolution images captured and post-processing methods made available via the DIC, these tests would all have appeared to have failed in a classically brittle and tensile manner.

7.3.3. *SAMPLES PREPARED USING 'FLATTENED' GEOMETRY*

A total of 20no. samples were prepared for indirect tensile testing using the flattened geometry loading method first presented by Wang, et al (2004). Samples were again selected that represented both Type A and Type B materials (determined using the results of Chapter 6 and correlations with previously discussed triaxial data). Two samples (NB03-29.00C-(F) and NB03-35.80B-(F)) were unfortunately damaged during the process of flattening the sample ends to the desired 2α angle and needed to be discarded prior to testing. This is a noteworthy criticism of the flattened geometry method, especially if dealing with limited sample availability, as the added complication of grinding the specimen ends to be flat and parallel exposes them to unwanted disturbance if carried out incorrectly and can also instigate pre-emptive fracturing if pre-existing weaknesses exist.

Loading of the samples was carried out in much the same manner as the ASTM samples, and again all samples were prepared by applying a high contrast speckle pattern in readiness for the application of the DIC technique. Samples used are summarised in Table 7.5 along with their ultimate measured tensile strengths:

Table 7.5: Samples selected for assessing the failure pattern of flattened geometry tensile tests.

Sample Code	Site	Borehole No.	Sample Depth (mbgl)	Loading Rate (kN/min)	Material 'Type' Designation	Tensile Strength at Failure
NB02-23.50C-(F)	NBAD	02	23.50	150	Type A	487
NB02-23.50D-(F)	NBAD	02	23.50		Type A	521
NB02-39.90A-(F)	NBAD	02	39.90	150	Type B	422
NB02-39.90B-(F)	NBAD	02	39.90		Type B	363
NB02-39.90C-(F)	NBAD	02	39.90		Type B	267
NB02-39.90D-(F)	NBAD	02	39.90		Type B	386
NB02-39.90E-(F)	NBAD	02	39.90		Type B	512
NB02-40.00A-(F)	NBAD	02	40.00	150	Type A	583
NB02-40.00B-(F)	NBAD	02	40.00		Type A	491
NB02-40.00C-(F)	NBAD	02	40.00		Type A	583
NB02-40.00D-(F)	NBAD	02	40.00		Type A	651
NB03-29.00D-(F)	NBAD	03	29.00	150	Type A	408
NB03-29.00E-(F)	NBAD	03	29.00		Type A	522
NB03-29.00F-(F)	NBAD	03	29.00		Type A	669
NB03-29.00G-(F)	NBAD	03	29.00		Type A	420
NB03-35.80A-(F)	NBAD	03	35.80	150	Type B	620
NB03-35.80C-(F)	NBAD	03	35.80		Type B	534
NB03-35.80D-(F)	NBAD	03	35.80		Type B	364
NB03-35.80E-(F)	NBAD	03	35.80		Type B	511
NB03-45.50-(F)	NBAD	03	45.50	150	Type A	385

Immediately it can be seen that, regardless of depth or sample 'Type' the overall ultimate tensile strengths measured using the flattened geometries are significantly higher than during the previous study using ASTM methods. Once again average Type A samples display higher tensile strengths (of 520kPa) than Type B average tensile strengths (of 440kPa) and interestingly the difference between average strengths of Type A and Type B samples using the two methods is approximately 80kPa, suggesting a degree of repeatability of results and a fundamental rule that Type B specimens are likely to have lower tensile strengths than Type A specimens.

The following graph (Figure 7.38) once again shows that little relationship exists between sample depth of origin and ultimate tensile strength at failure:

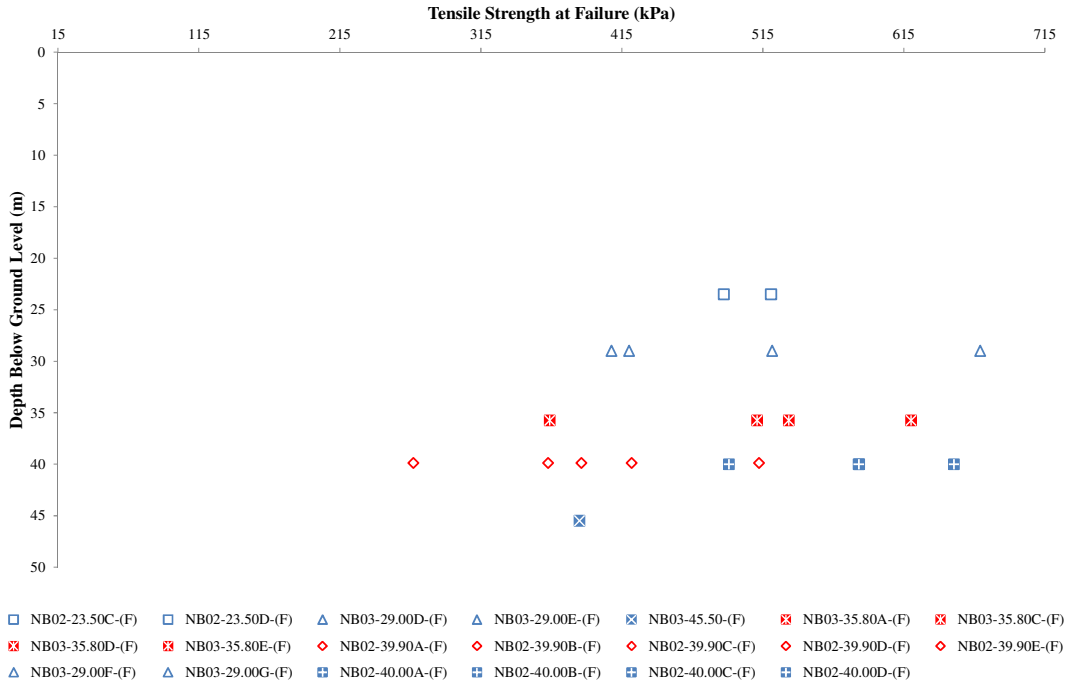

Figure 7.38: Tensile strength at failure vs depth of sample origin for samples prepared using flattened geometries.

As with the previous study, ultimate tensile strength at failure is compared to moisture content in Figure 7.39. Surprisingly the inversely proportional relationship that existed between moisture content and tensile strength is no longer apparent. It is possible that the previously recorded sensitivity to moisture content during indirect Brazilian testing only apparently existed in the ASTM prepared samples, effectively controlling the degree of localised crushing and shearing within the area proximal at the sample loading points (as indicated in Figure 7.34 that showed moister samples appearing to undergo significantly more axial straining than drier specimens).

DIC imagery supports this theory as the maximum amounts of axial straining occur close to the sample loading areas (as inferred from Figure 7.36). It should also be noted that a limitation of the DIC method is that the area directly at the contact points between the samples and the loading apparatus cannot be directly analysed (as complete 'squares' within the sub-set grid are required which are not achievable around the extreme circumference of samples with rounded geometries, as highlighted in Chapter 4), and as such the method is likely to underestimate the overall axial straining in these areas.

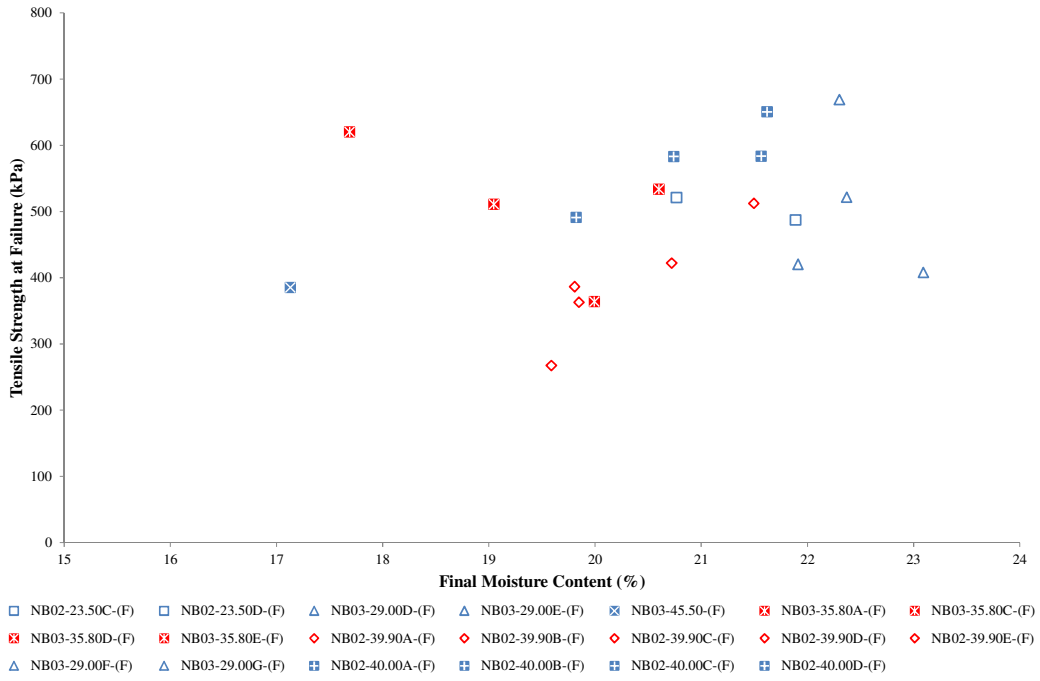

Figure 7.39: Tensile strength vs moisture content for samples prepared using flattened geometries.

Externally measured axial stress – strain diagrams indicate less crushing at the loading areas of samples, as overall less axial strains develop, resulting in significantly stiffer sample behaviour irrespective of 'Type', as seen in Figure 7.40. Once again red indicates Type B samples and blue indicates Type A samples.

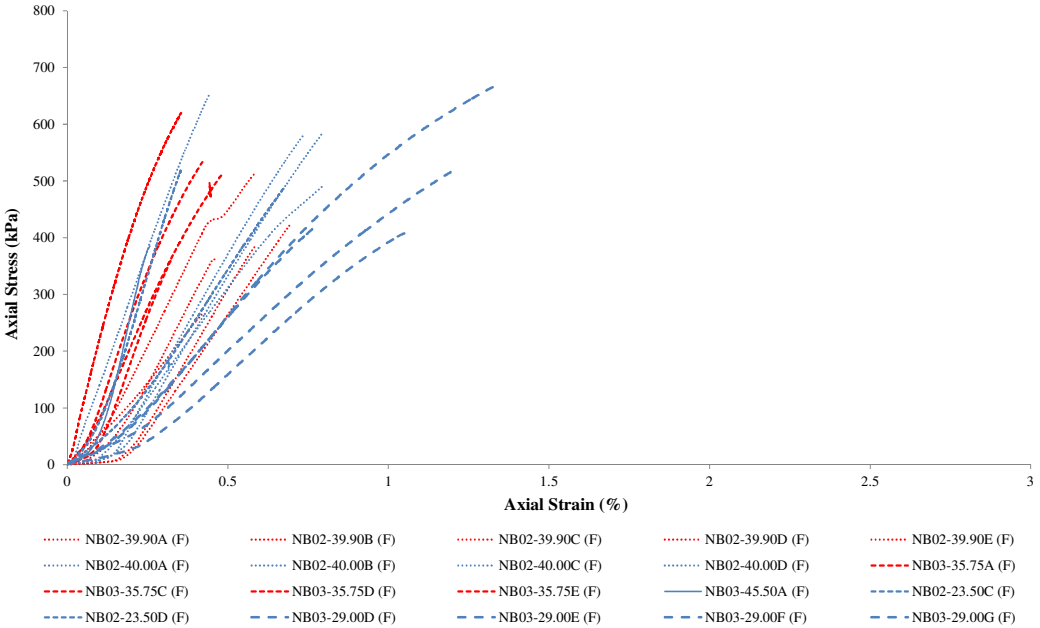

Figure 7.40: Axial stress vs axial strain for samples prepared using flattened geometries.

Figure 7.40 also indicates that on the samples selected, Type B specimens behave in a stiffer manner than their Type A equivalents, although their ultimate tensile strengths at

failure are consistently lower. This is counter-intuitive given the higher clay content of Type B specimens and their overall tendency to behave in a more plastic and ductile manner than Type A materials.

By comparing the stress – strain behaviour of samples prepared using the flattened loading geometries against those prepared using ASTM standards (Figure 7.41), it becomes very clear that the rounded ASTM methodology results in greater sample crushing / bedding errors, as they display significantly larger amounts of overall axial strain than those prepared using flattened sample ends.

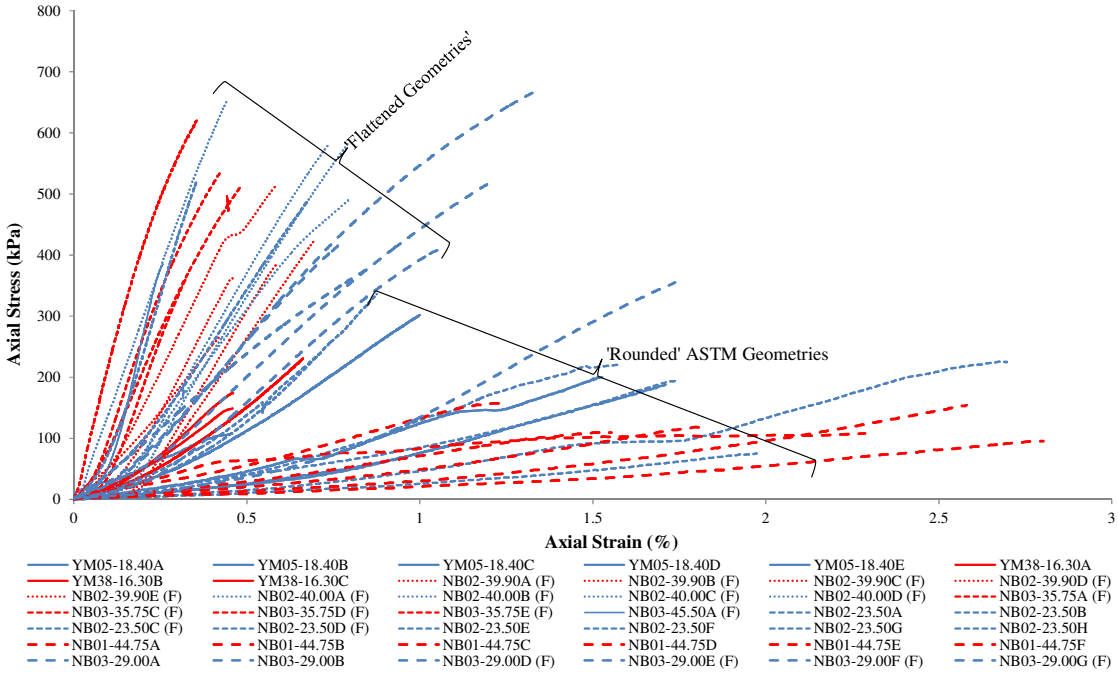

Figure 7.41: Axial stress vs axial strain diagram comparing samples prepared using ASTM and flattened loading geometries.

It is possible that this excessive bedding/crushing at the samples loading areas during ASTM testing is causing the true tensile strengths of these materials to be masked, as localised zones of shearing prompt pre-emptive fracturing.

7.3.4. *FLATTENED SAMPLES ANALYSED USING DIC*

In order to better understand the distribution of strains in the Flattened sample tests (and therefore infer stress distributions), samples were analysed using the VIC-3D software post failure.

Figure 7.42 presents some representative quantitative analysis of samples immediately prior to failure in order to show the pattern of horizontal strain localisation on sample

surfaces along with a graphical representation of horizontal strain distributions along the vertically orientated line i-ii.

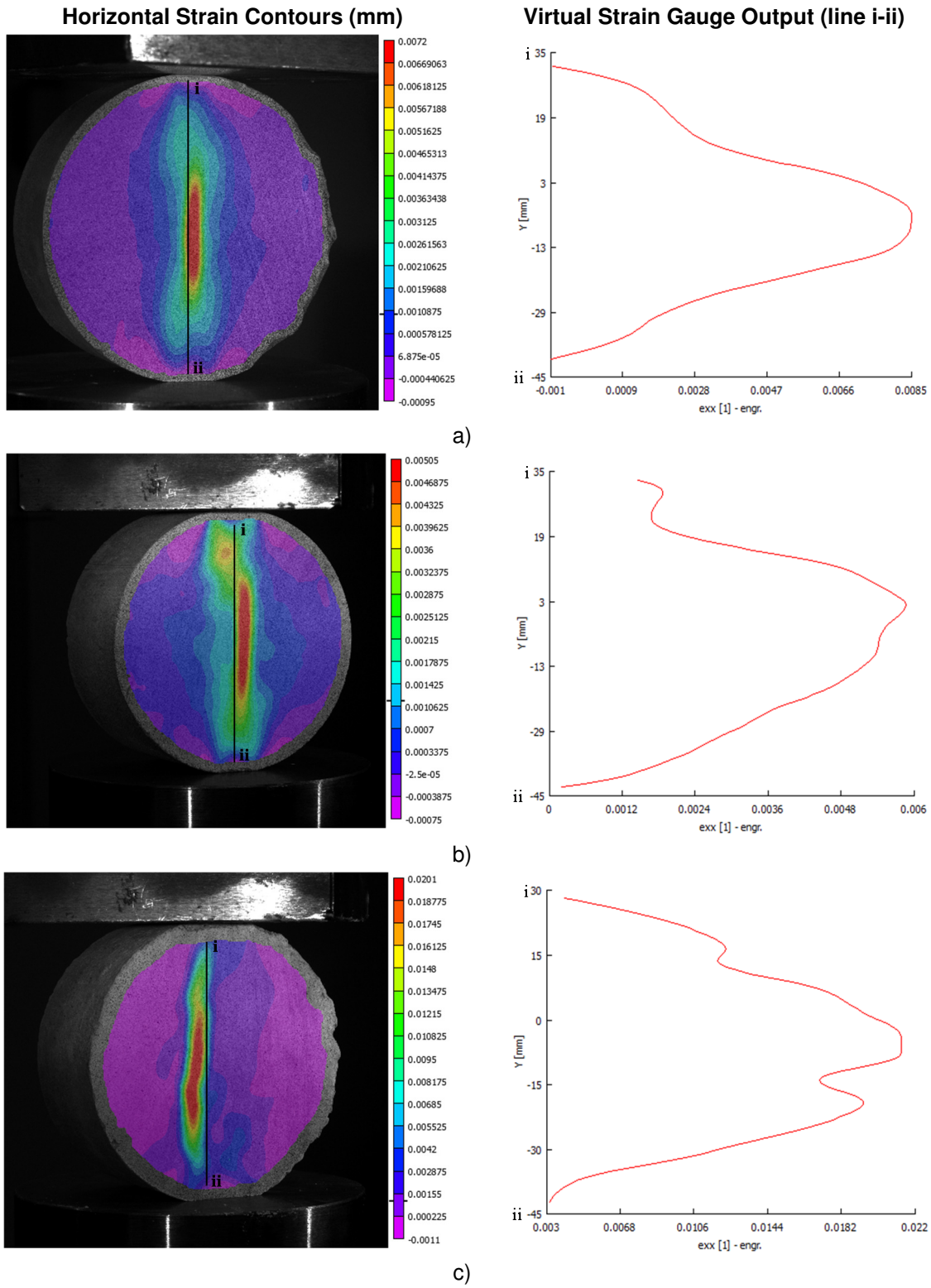

Figure 7.42: Horizontal strain contours and virtual strain gauge outputs immediately prior to failure in samples a) NB02-23.50D, b) NB03-35.75C and c) NB02-39.90D.

It is immediately apparent that samples compressed using flattened loading areas do not generate strains local to the loading points. Instead, maximum tensile strains are located

towards the centre of sample specimens, in keeping with the theory of Brazilian disk failures in tension. In fact very little straining occurs at the sample loading points at all, supporting the findings of the previous section (shown in Figure 7.41) that sample bedding / crushing errors are reduced significantly using this flattened geometry. These findings are similar to those noted in Chapter 4 on Springwell Sandstone.

Tensile failures occur at the point of highest tensile straining then propagate both upwards and downwards of the sample centre at high velocities, indicative of brittle fracturing. Figure 7.43 shows this sequence using the raw photographic images of the fracture propagation at the time of failure (Figure 7.43b), the image directly preceding it (Figure 7.43a at time of failure minus 100ms) and the image directly succeeding it (Figure 7.43c at time of failure plus 100ms). Due to the rapid propagation velocity of brittle fractures it is quite rare to capture images of this nature, even when using high frame rate cameras.

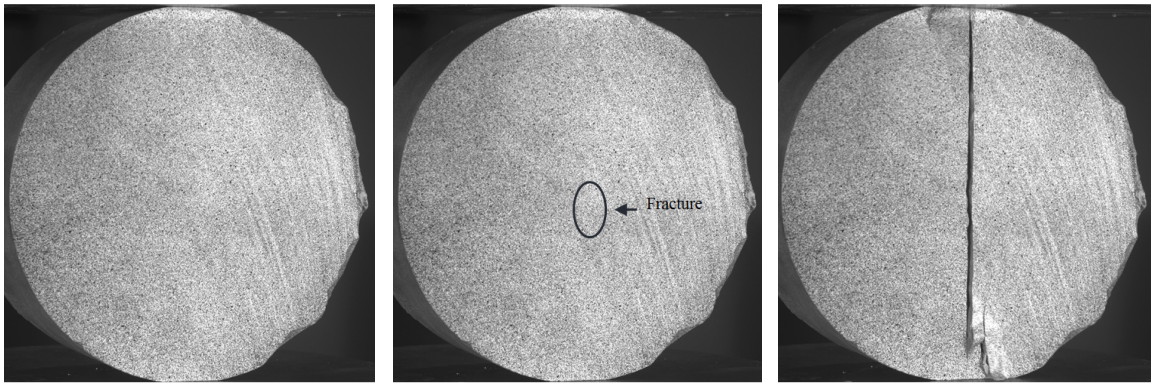

Figure 7.43: High velocity fracture propagation in samples NB02-23.50D at a) failure time -100ms, b) time of failure and c) failure time +100ms.

In total 70% of samples prepared using flattened loading geometries failed from centrally located fractures, instead of the 7% noted using the ASTM methodology.

7.3.5. *SUMMARY OF INDIRECT TENSILE TESTING PROGRAMME*

This part of the mechanical testing programme aimed to characterise the behaviour of samples of calcareous mudstone during indirect tensile testing (Brazilian method). The study was augmented via the use of DIC as a means of measuring full field strains as they developed in real time, with a focus on assessing the initiation point of failures using two loading geometries, a rounded geometry proposed by the ASTM standards and a flattened geometry proposed by Wang, et al (2004).

This study also aimed to better understand the behaviour of the two material sub-'Types' noted in previous sections, with respect to their ultimate tensile strengths.

It has been found that samples prepared using the ASTM guidance undergo localised crushing at the sample loading areas, resulting in pre-emptive failure via the formation of zones of shearing. Furthermore, the ASTM method causes significantly larger axial strains to develop than the flattened geometry method, producing considerably less stiff behaviours prior to failure.

Depth of sample origin was noted to be of little consequence to the individual sample's tensile strength. Instead, particularly in the ASTM study, moisture content at time of failure was deemed to be a much greater controlling factor, with samples of relatively high moistures having lower failure stresses than those of relatively low moisture contents. This observation was not seen in the samples prepared with flattened loading geometries to the same extent, leading to the interpretation that moisture was enabling the localised crushing / bedding errors seen at the extreme ends of the rounded ASTM samples.

Flattened loading geometries promoted more centralised tensile failures to occur without generating shearing failures within the sample loading areas, as was verified using DIC and VIC-3Ds post processing strain contour overlays. In total, the percentage of samples failing centrally increased from 7% using the ASTM method, to 70% using the flattened loading geometries proposed by Wang, et al (2004).

As well as encouraging centralised failures to occur when adopting the flattened methodology, an overall increase in measured tensile strengths was noted, raising from an average of 225kPa in Type A samples and 144kPa in Type B samples to 520kPa and 440kPa respectively. This increase is thought to be due to samples being able to achieve their maximum tensile strength before failure when using flattened loading, as opposed to failing prematurely due to the unwanted initiation of localised cracking at the sample loading points (as was the case in 93% of the ASTM tests).

Type A samples were noted to have an average of 80kPa higher tensile strengths than Type B samples using both loading methods, although their absolute tensile strength was considerably influenced depending upon the loading method adopted.

As no UCS testing was carried out during this thesis, only approximate ratios of UCS to tensile strength can be calculated (based upon UCS values annotated on the original site

investigation borehole logs provided by Buro Happold within the strata tested). UCS values from the Yas Mina logs taken within the calcareous mudstone layers indicated strengths of between 0.65-2.37MPa, meaning that UCS to tensile strength ratios (R) may be as low as 2.88 within Type A materials and as low as 4.48 within Type B materials using ASTM methods, which then reduce even further when using flattened loading geometries to 1.25 and 1.47 respectively. These findings are in keeping with those of published data concerning soft calcareous materials within evaporite rich areas (Coviello, et al., 2005); (Hoek, 2007); (Cai, 2010).

When comparisons are made between the tensile strength at failure Mohr Circles against those obtained from the triaxial testing program (for example in Figure 7.44, which shows the behaviour of averaged Type B specimens in tension against Type B samples in triaxial compression) it can be seen that the flattened samples appear to over-estimate tensile strength.

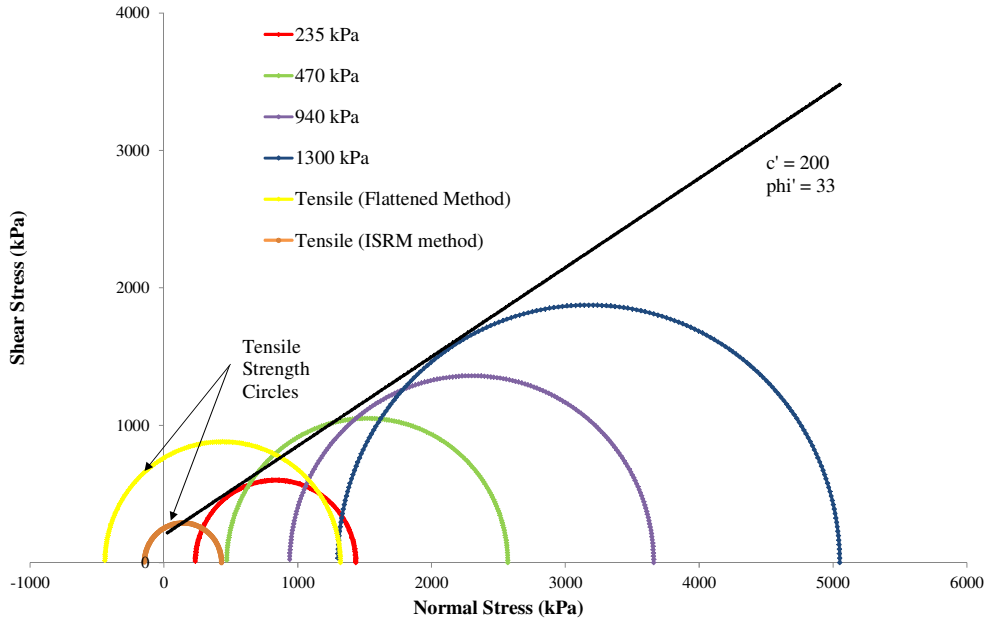

Figure 7.44: Tensile Mohr circles for Type B specimens plotted against Type B triaxial data

Brazilian disk Mohr circles are plotted using the following formula (Li & Wong, 2013), where (r) is the radius and (t) the thickness of the disk and (P) is the load at failure:

$$\sigma_3 = -P/\pi rt \qquad 7.2$$

$$\sigma_1 = 3P/\pi rt \qquad 7.3$$

The tensile testing programme, in contrast to the triaxial programme, was carried out in partially saturated conditions, meaning that direct comparisons with the results of the effective stress tests should be made cautiously. Whilst small changes in moisture

content did not affect the tensile strengths measured using flattened ends, it is likely that tensile strengths may drop significantly in fully saturated conditions. Inter-sample variability should also be taken into consideration.

7.4. ONE DIMENSIONAL CONSOLIDATION PROGRAMME

This phase of the mechanical testing programme was aimed at characterising the one dimensional consolidation characteristics of samples of calcareous mudstone, focusing on assessing the presence and effect of structure and the effect of using both saline and non-saline (deionised) water as a pore fluid (as described in section 4.9 of this thesis).

Three cores were sub-sampled and tested within this phase of the thesis, one Type B sample (YM39-14.40) and two Type A samples (NB01-33.10 and NB03-45.50) in order to compare the behaviour of the different material 'Types'. These tests are referred to as 'undisturbed', as they capture the behaviour of the calcareous mudstone following minimal alteration from their in-situ state. All undisturbed samples were tested using both deionised and saline water as pore fluids in order to understand the effect that salinity played on controlling consolidation and welling behaviour.

Finally, a set of fully de-bonded, remoulded samples were tested in order to establish the calcareous mudstones intrinsic compression behaviour, again using both saline and deionised pore water. These remoulded samples were prepared at moistures greater than their liquid limits, and are here on in referred to as 'slurry' samples.

Graphics are presented as both void ratio against vertical applied stress on a logarithmic scale (e-log P) and as normalised void ratios against applied stress (e/e_{max} – log P).

All samples initial properties are presented in tabular form preceding their respective analysis and both compression index (Cc) and swelling index (Cs) are reported following consolidation. These are calculated using:

$$\text{Cc or Cs} = \frac{e^1 - e^2}{log\ (P_2\ /\ P_1)} \qquad 7.4$$

Where e^1 is the void ratio at pressure P_1 and e^2 the void ratio at P_2, both being points along an approximately linear portion of the e-log P curve. For the Cc, these points are taken from the virgin compression line (or 1DCL, the one dimensional consolidation line), whereas for Cs (sometimes called Ce or expansion index) are taken from the unloading portions of the e-log P curve. This can be seen pictorially as Figure 7.45. Whilst the gradient of these lines is negative, they are reported as positive and unit-less:

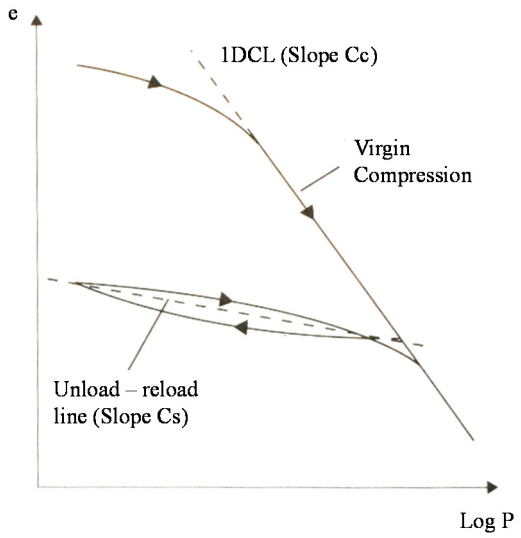

Figure 7.45: Void ratio – vertical pressure relationship. Adapted from (Craig, 2004).

7.4.1. *UNDISTURBED 'TYPE A' SAMPLES*

Two cores of Type A material (NB01-33.10 and NB03-45.50) were sub-sampled for testing in one dimensional consolidation. These were both taken from the NBAD site and are discussed in more detail below, starting with NB01-33.10.

Core NB01-33.10 was able to supply four undisturbed sub-samples for oedometer, two of which were compressed using deionised water as a pore fluid and two of which used synthetic saline pore water (the chemical makeup of which is described at the end of Chapter 4). These four sub-samples initial properties are summarised in Table 7.6.

Table 7.6: Sample NB01-33.10 properties for one dimensional consolidation tests

	Deionised Pore Water Tests		Saline Pore Water Tests	
Strength Designation	Type A		Type A	
Sample Reference	NB01-33.10		NB01-33.10	
Site Name	NBAD		NBAD	
Sub-sample ID	A	B	C	D
Depth Sample Taken (mbgl)	33.10		33.10	
Initial Moisture Content (%)	20.8	20.0	19.8	20.5
Initial Bulk Density (Mg/m^3)	2.03	2.03	2.02	2.02
Initial Dry Density (Mg/m^3)	1.68	1.69	1.68	1.68
Initial Void Ratio	0.60	0.59	0.59	0.60
Initial Porosity (%)	37.6	37.3	37.4	37.7
Initial Degree of Saturation	93.3	90.7	89.2	91.6
Swelling Pressure (kPa)	31	32	25	22
Saline Pore Water	No		Yes	

Similar initial properties are noted across all sub-samples, with average dry densities of 1.68Mg/m^3 and average void ratios of between 0.59 and 0.60. Swelling pressures were measured prior to consolidation by maintaining close to zero vertical strain, following the addition of pore waters, and recording the stress required to do so. Very low swelling pressures were noted in all samples; however sub-samples of NB01-33.10 that used saline pore waters were approximately 25% lower than those measured using deionised water.

Figure 7.46 shows that irrespective of initial void ratio (e^0), samples consolidated using saline water have steeper indices (both Cc and Cs) than those using deionised waters.

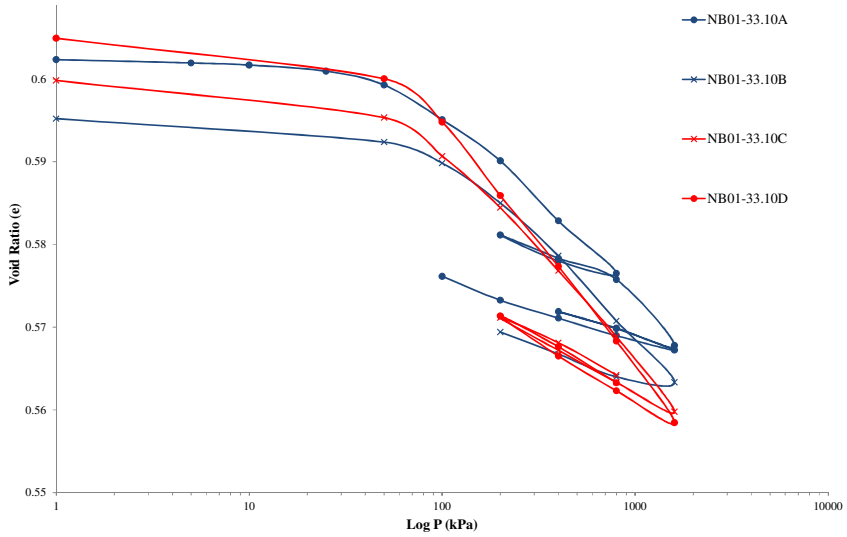

Figure 7.46: Void ratio vs axial pressure plot for Type A sample NB01-33.10 using deionised pore water (blue) and saline pore water (red).

Average Cc for deionised pore fluid samples is 0.0244 whilst the equivalent value for saline pore water samples is 0.0288, slightly steeper. Likewise average Cs for deionised pore water tests (0.0071) were lower than those of the saline pore water tests (0.0136). Compression and swelling indices are summarised in Table 7.7.

Table 7.7: Sample NB01-33.10 compression and swelling characteristics

	Deionised Pore Water Tests		Saline Pore Water Tests	
Strength Designation	Type A		Type A	
Test ID	NB01-33.10A	NB01-33.10B	NB01-33.10C	NB01-33.10D
Compression Index (Cc)	0.0244	0.0244	0.0277	0.0299
Swelling Index (Cs)	0.0066	0.0075	0.0131	0.0142
Saline Pore Water	No		Yes	

This trend becomes even more apparent once void ratios are normalised against e^{max} (maximum void ratio, synonymous to e^0 for the purposes of this testing programme), as shown in Figure 7.47.

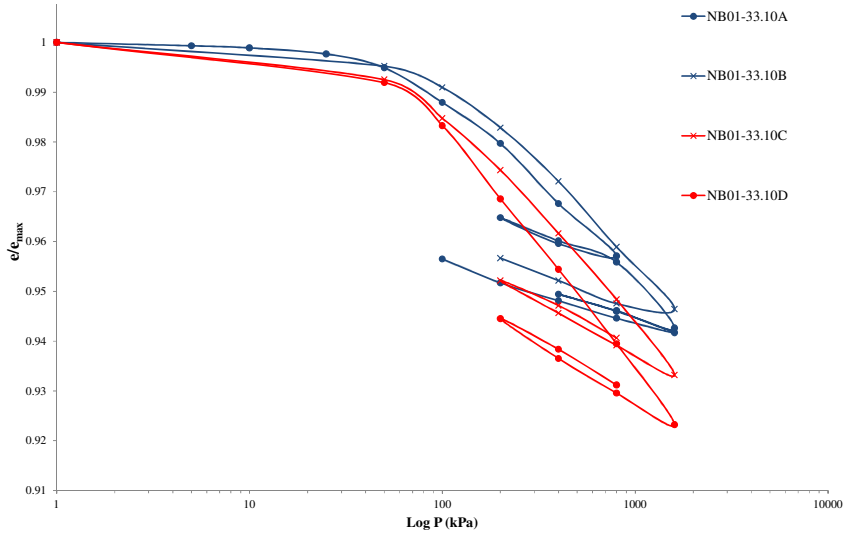

Figure 7.47: Normalised void ratio vs axial pressure plot for Type A sample NB01-33.10 using deionised pore water (blue) and saline pore water (red).

The normalised graph indicates that introducing saline pore water causes greater amounts of absolute consolidation to occur in both cases.

Core sample NB03-45.50 was also sub-sampled into four undisturbed specimens for testing, again half were compressed with saline pore water and half with deionised. Initial properties of the samples are presented as Table 7.8.

Table 7.8: Sample NB03-45.50 properties for one dimensional consolidation tests

	Deionised Pore Water Tests		Saline Pore Water Tests	
Strength Designation	Type A		Type A	
Sample Reference	NB03-45.50		NB03-45.50	
Site Name	NBAD		NBAD	
Sub-sample ID	A	B	C	D
Depth Sample Taken (mbgl)	45.50		45.50	
Initial Moisture Content (%)	20.5	20.1	20.0	19.8
Initial Bulk Density (Mg/m^3)	2.03	2.03	2.03	2.02
Initial Dry Density (Mg/m^3)	1.68	1.69	1.69	1.69
Initial Void Ratio	0.59	0.59	0.59	0.59
Initial Porosity (%)	37.4	37.4	37.3	37.3
Initial Degree of Saturation	92.3	90.9	91.0	89.8
Swelling Pressure (kPa)	27	28	22	25
Saline Pore Water	No		Yes	

Again, the initial properties of all sub-samples display little deviation from their mean values, allowing for good comparisons to be made regarding their mechanical behaviour. Average void ratios of 0.59 were calculated as were average dry densities of 1.69Mg/m^3. Once again low swelling pressures were noted in all samples, with those occurring in the samples exposed to saline waters being around 15% lower than those occurring in the deionised water samples. Their consolidation curves are presented as Figure 7.48.

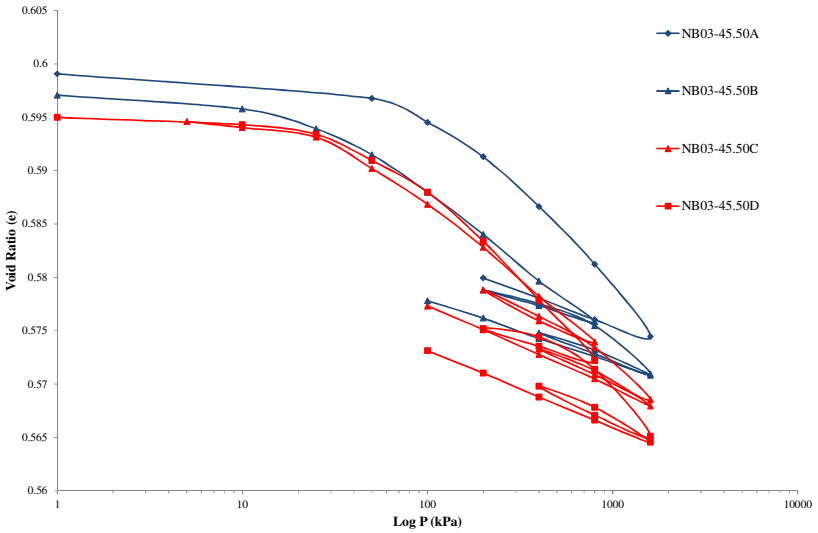

Figure 7.48: Void ratio vs axial pressure plot for Type A sample NB03-45.50 using deionised pore water (blue) and saline pore water (red).

Sample NB03-45.50 behaves in a similar way to sample NB01-33.10 in that, irrespective of initial void ratio, the samples tested using deionised water consolidated less than those using saline pore waters, displaying averagely shallower indices of both swelling (0.0061 compared to the saline 0.0066) and compression (0.0166 compared to 0.0177 using saline water). Summaries of this material's compression and swelling characteristics are presented as Table 7.9.

Table 7.9: Sample NB03-45.50 compression and swelling characteristics

	Deionised Pore Water Tests		Saline Pore Water Tests	
Strength Designation	Type A		Type A	
Test ID	NB03-45.50A	NB03-45.50B	NB03-45.50C	NB03-45.50D
Compression Index (Cc)	0.0188	0.0144	0.0155	0.0199
Swelling Index (Cs)	0.0066	0.0055	0.0066	0.0066
Saline Pore Water	No		Yes	

Figure 7.49 shows the normalised e-log P plots of all NB03-45.50 sub-samples, highlighting the greater absolute consolidation taking place in those samples compressed using saline pore waters.

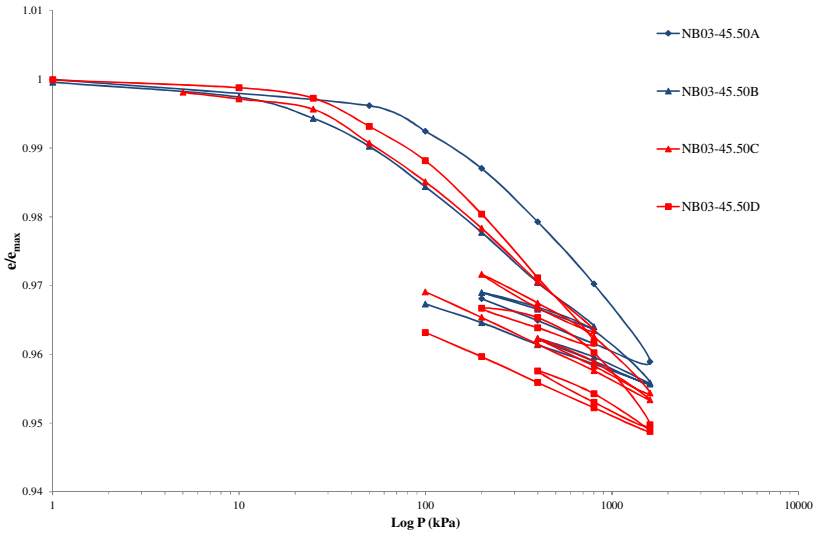

Figure 7.49: Normalised void ratio vs axial pressure plot for Type A sample NB03-45.50 using deionised pore water (blue) and saline pore water (red).

7.4.2. *UNDISTURBED 'TYPE B' SAMPLES*

Only one core of calcareous mudstone was tested that represented the Type B material type, namely sample YM39-14.40. Type B samples have been shown in Chapter 6 to contain greater quantities of the clay mineral Palygorskite than those of Type A specimens, meaning that they are likely to show greater amounts of consolidation for any given pressure, and may also display a more pronounced reaction to the presence of saline pore waters during compression.

YM39-14.40 was sub-sampled into two undisturbed one dimensional consolidation tests. Once again one of these tests used saline pore waters whilst the other used deionised water. The initial properties of these sub-samples are presented as Table 7.10.

Table 7.10: Sample YM39-14.40 properties for one dimensional consolidation tests

	Deionised Pore Water Tests	Saline Pore Water Tests
Strength Designation	Type B	Type B
Sample Reference	YM39-14.40	YM39-14.40
Site Name	Yas Mina	Yas Mina
Sub-sample ID	A	B
Depth Sample Taken (mbgl)	14.40	14.40
Initial Moisture Content (%)	20.6	20.1
Initial Bulk Density (Mg/m^3)	1.99	1.99
Initial Dry Density (Mg/m^3)	1.66	1.66
Initial Void Ratio	0.62	0.62
Initial Porosity (%)	38.6	38.6
Initial Degree of Saturation	88.1	86.5
Swelling Pressure (kPa)	24	19
Saline Pore Water	No	Yes

Higher average void ratios (of 0.62) are noted in this Type B material than observed in the Type A specimens, along with slightly lower average dry densities (of 1.66Mg/m^3). Unexpectedly lower swelling pressures were recorded however, despite the greater percentage of clay minerals being present. Once again, this swelling pressure was lower in the saline test (approximately 20% lower).

One dimensional consolidation plots for these two samples are presented as Figure 7.50, again showing that greater amounts of absolute consolidation take place in samples compressed using saline pore waters.

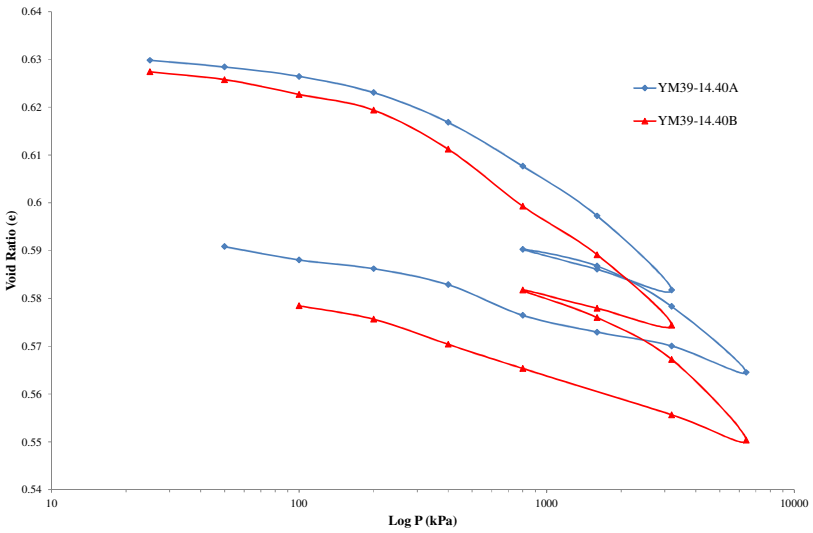

Figure 7.50: Void ratio vs axial pressure plot for Type B sample YM39-14.40 using deionised pore water (blue) and saline pore water (red).

As with the Type A samples, the compression index of the saline water test is once again higher than that of the deionised test, as is the swelling index (Table 7.11). Normalised e-Log P plots again clearly highlight this as well as showing the greater amounts of absolute consolidation occurring in the saline samples (Figure 7.51).

Table 7.11: Sample YM39-14.40 compression and swelling characteristics

	Deionised Pore Water Tests	Saline Pore Water Tests
Strength Designation	Type B	Type B
Test ID	YM39-14.40A	YM39-14.40B
Compression Index (Cc)	0.0266	0.0277
Swelling Index (Cs)	0.0089	0.0166
Saline Pore Water	No	Yes

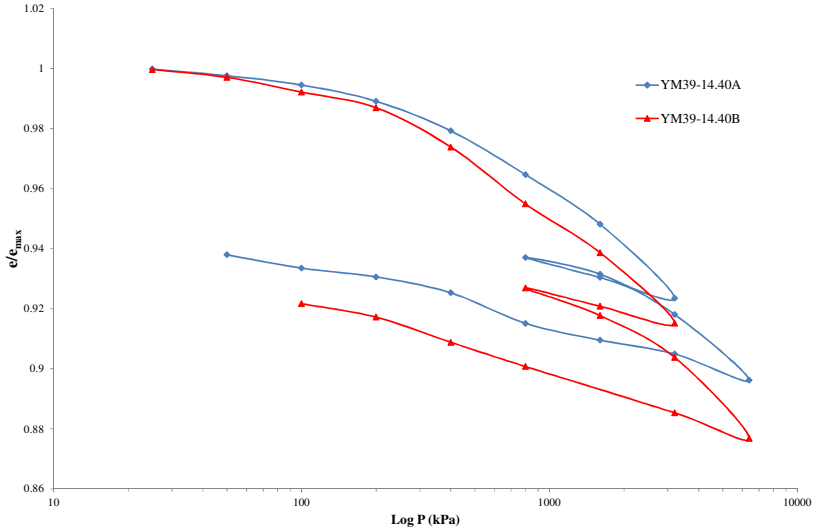

Figure 7.51: Normalised void ratio vs axial pressure plot for Type B sample YM39-14.40 using deionised pore water (blue) and saline pore water (red).

Normalised e-Log P plots of representative Type A samples superimposed onto the Type B sample show that both sample types have similar consolidation characteristics. Figure 7.52 shows the behaviour of Type A and Type B samples when consolidated using deionised water, and Figure 7.53 shows the same using saline pore water. Surprisingly, the Type B specimen behaviour falls between that of the two Type A samples, despite having higher initial void ratios and a greater percentage of Palygorskite.

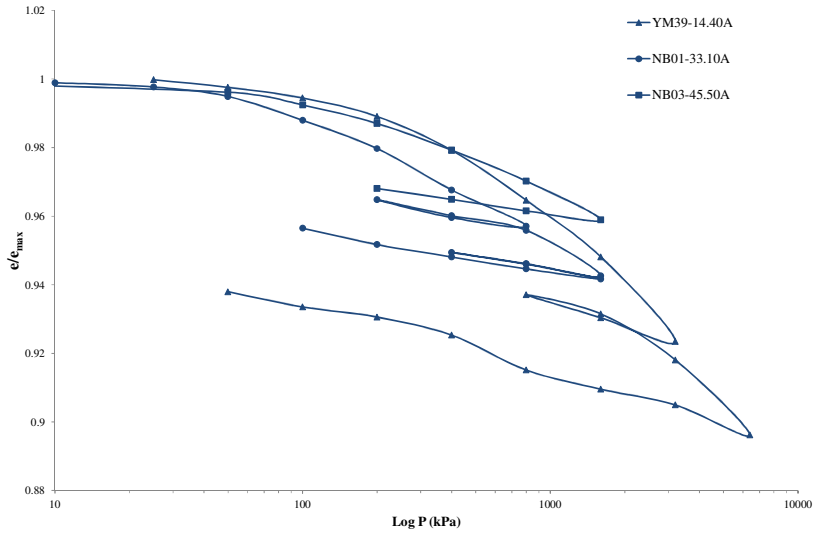

Figure 7.52: Normalised void ratio vs axial pressure plot comparing both Type A and Type B samples using deionised pore water.

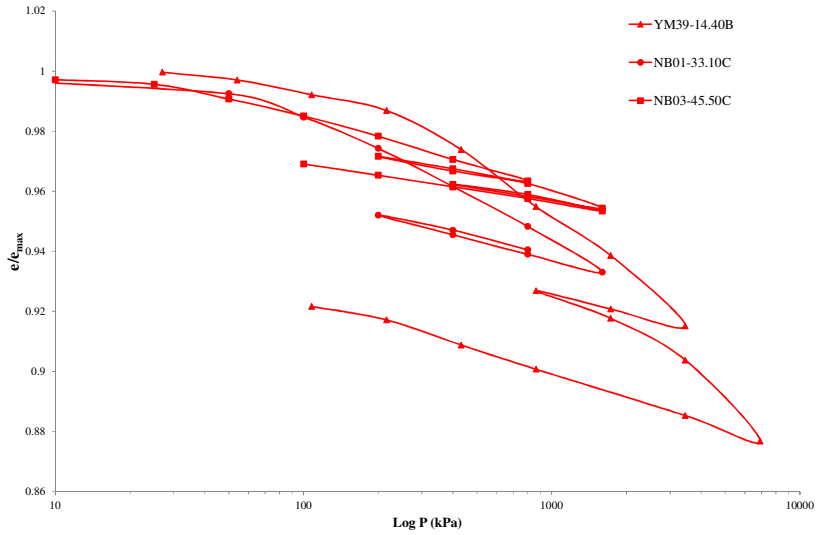

Figure 7.53: Normalised void ratio vs axial pressure plot comparing both Type A and Type B samples using saline pore water.

7.4.3. *INTRINSIC TESTS ON REMOULDED 'TYPE A' SAMPLES*

In order to quantify the amount of structure permitted space present in the calcareous mudstone specimens, it is first required that their intrinsic, de-structured behaviour be recorded.

A total of five tests were carried out to assess intrinsic behaviour, all samples were fully de-structured and wet of their liquid limits prior to loading. Three tests were undertaken on samples remoulded using deionised pore water and two using saline pore water. Initial properties of these samples are provided as Table 7.12.

Table 7.12: Remoulded sample properties for slurry (intrinsic) consolidation tests

	Deionised Pore Water Tests			Saline Pore Water Tests	
Strength Designation	Type A			Type A	
Sample Reference	Slurry Deionised			Slurry Saline	
Sub-sample ID	1	2	3	1	2
Initial Moisture Content (%)	62.7	62.8	57.3	66.5	63.7
Initial Bulk Density (Mg/m^3)	1.83	1.79	1.77	1.77	1.84
Initial Dry Density (Mg/m^3)	1.13	1.10	1.12	1.07	1.13
Initial Void Ratio	1.39	1.45	1.40	1.43	1.39
Initial Degree of Saturation	≈100*			≈100*	
Saline Pore Water	No			Yes	

**Samples prepared at moistures greater than their liquid limit*

Standard e-Log P plots for these tests are presented as Figure 7.54, along with normalised plots as Figure 7.55.

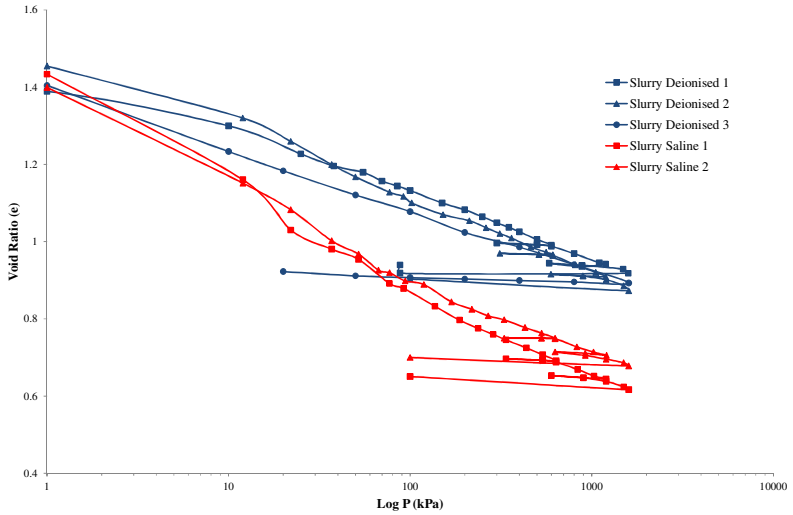

Figure 7.54: Void ratio vs axial pressure plot of remoulded (intrinsic) samples using both deionised pore water (blue) and saline pore water (red).

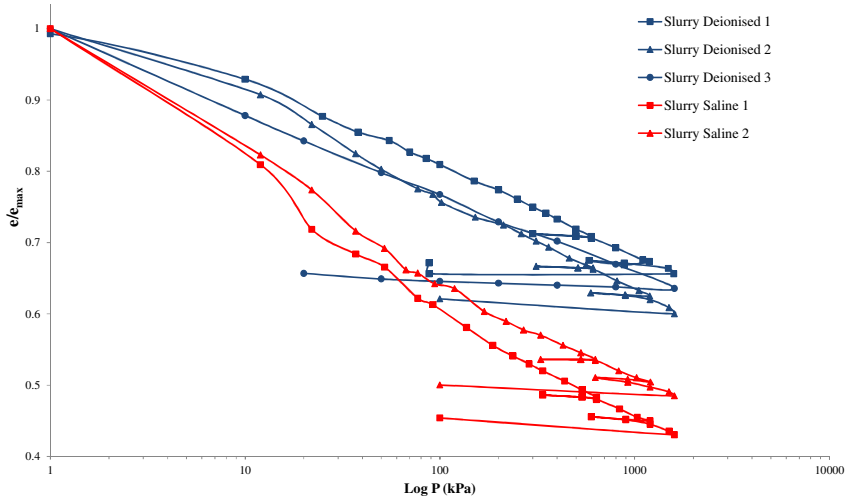

Figure 7.55: Normalised void ratio vs axial pressure plot of remoulded (intrinsic) samples using both deionised pore water (blue) and saline pore water (red).

These remoulded tests clearly show the effect of salinity; producing significantly steeper intrinsic compression lines (ICLs) than those tests prepared using deionised water. All samples were mixed to the same moisture content and were sourced from the same original sample (NB01-33.10).

However neither the deionised or saline pore water average ICL cross the consolidation lines of either the Type A or Type B natural undisturbed samples, as shown in Figure 7.56. An idealised structured sample is shown as Figure 7.57.

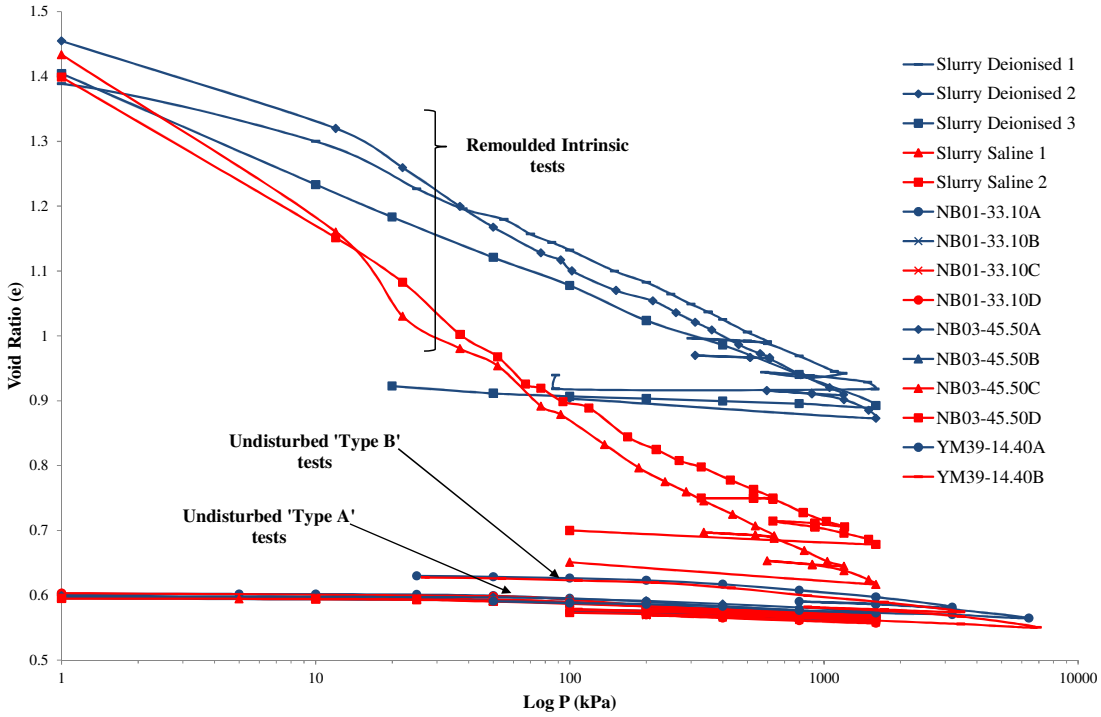

Figure 7.56: Void ratio vs axial pressure plot of all samples tested.

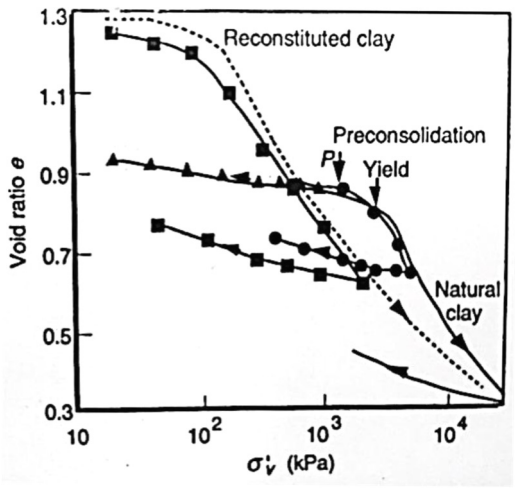

Figure 7.57: Idealised behaviour of a structured Clay against its remoulded equivalent. Adapted from (Leroueil, 2000)

By extrapolating the ICL lines to a point that they may intersect with the undisturbed sample compression lines it can be seen that pressures of between 4-400MPa would be required (depending if the saline or deionised ICL is extrapolated). This is significantly higher than would be expected; showing that the low in-situ void ratios of the undisturbed samples may have been caused by more than simply depth of burial and over-burden pressure. In-situ stresses are within the region of 100-500kPa depending upon the individual sample, its groundwater regime and its depth of burial and this is seen (via the intrinsic compression lines) to be insufficient to cause void ratios as low as 0.6 to occur.

It is therefore considered that the low void ratios may have been brought about by in-situ processes post-burial, for example precipitation of dolomite into void spaces, secondary precipitation of Palygorskite into void spaces and in-situ dissolution and re-crystallisation of dolomite grains making up the skeleton of the rock, allowing progressively denser configurations of constituent particles to be achieved.

This ties in well to the observations made in the SEM analysis in Chapter 6, where grains of dolomite could be seen to be fused into a tightly bonded mosaic, a configuration that would have required in-situ processes beyond overburden pressures to achieve.

7.4.4. *SUMMARY OF ONE DIMENSIONAL CONSOLIDATION PROGRAMME*

One dimensional consolidation tests on undisturbed samples of both Type A and Type B calcareous mudstones have revealed similar behaviours, despite Type B samples have higher percentages of clay minerals and higher initial void ratios.

The addition of a synthetic pore water, with salinity representative of in-situ groundwater's of coastal Abu Dhabi, have shown greater amounts of absolute consolidation to take place than in samples using deionised water. This was true in all samples, both Type A and B along with remoulded 'slurry' samples, causing a steepening of both compression and swelling indicies.

Intrinsic compression lines (ICLs) found via tests on de-bonded samples plot higher than undisturbed samples on a standard e-Log P curve for any given vertical stress (up to at least 1600kPa). This is interpreted as evidence that in-situ processes, such as

recrystallization and precipitation of secondary minerals, may be taking place to densify the materials to lower void ratios than possible by in-situ overburden pressures alone.

CHAPTER 8. CONCLUSIONS AND RECOMMENDATIONS

8.1. CONCLUSIONS

The coastline of Abu Dhabi is being widely urbanised and is home to some of the tallest buildings in the world and yet little published data exists that describes the properties of the underlying geology from a geotechnical standpoint. This lack of information has resulted in a requirement for a conservative approach to design.

The calcareous mudstones studied in this thesis are considered 'soft rocks', a material type that displays attributes of both soil and rock in terms of its performance characteristics and that requires a combined approach from both soil and rock mechanics disciplines in order to fully understand. They occur extensively both laterally and vertically within the underlying stratigraphy of Abu Dhabi Island and its surrounding landmasses and cannot be ignored if large developments are to continue being undertaken in this area. By gaining an understanding of these soft rocks' physical and mechanical properties, geotechnical designs upon or within them may be both more economical and safe. To this end, a suite of experimental procedures were undertaken in order to better characterise these widely occurring soft calcareous mudstones.

Initially, samples appeared to be broadly similar in terms of superficial appearance and bulk properties, however significant differences in mechanical performance that could not be accounted for solely by depth of origin began to emerge as experiments were undertaken, prompting a micro to macro scale investigation to be carried out in order to understand the key controlling factors affecting their behaviour. The results and interpretation of this investigation can be summarised as follows:

- XRD, ESEM and SEM analysis showed samples to consist of predominantly clay to silt sized Dolomite grains with minor constituents of Quartz and Feldspar (appearing as rare sand sized grains), Halite (often lining grain surfaces) and most notably Palygorskite (occurring within void spaces). Whilst the minerals present in samples were qualitatively similar, their relative abundances by percentage varied significantly, with samples displaying high quantities of Dolomite (88-89%) and low Palygorskite (4-9%) having distinctly different mechanical characteristics to samples with higher Palygorskite (10-23%) quantities and lower Dolomite (73-84%) quantities. This prompted the creation of two calcareous mudstone sub-

categories, namely Type A and Type B, which assisted in the correlation of material properties between samples sourced from the two site investigations during this thesis. It should be noted that a change from Type A to Type B can occur quite locally with respect to depth and that the change is not apparent by visual inspection.

- SEM of broken sections looked at the structure of the calcareous mudstones on a granular scale prior to shearing, identifying that the Type A samples displayed tightly bonded mosaics of Dolomite grains that appear chemically fused together, with small amounts of fibrous Palygorskite within voids and on the surface of Dolomite grains. It is believed that continuous dissolution and re-precipitation at the contact points between Dolomite grains has led to their interlocked appearance along with being a contributing factor for their higher strength and stiffness than Type B samples, as seen by Mazzullo, (1992) and Jameson, (2009).
- Type B samples showed a greater quantity of Palygorskite and a lesser degree of bonding between the Dolomite grains using SEM. The presence of clay minerals in calcareous rocks is thought to inhibit the processes of dissolution and precipitation, preventing the strong mosaics of Dolomite grains to form, meaning that weaker cementation can be expected in calcareous mudstone samples with higher Palygorskite contents. This is reflected in the findings of the mechanical study in terms of strength and stiffness, but also in that Type B samples typically have higher void ratios than Type A samples regardless of depth of origin, as less precipitation of Dolomite has occurred leaving void spaces more open.
- Atterberg limits and PSDs have been shown to provide good estimates of whether samples are likely to display Type A or Type B characteristics. Type A specimens typically have low to intermediate plasticity whilst Type B specimens have intermediate to high plasticity, reflecting their relative abundances of the mineral Palygorskite. PSD results also provide a good means of differentiating between the 'Types' in that Type B samples are typically comprised of a higher fraction of clay sized grains than Type A specimens. It is recommended that this be used as a means of estimating material 'type' where XRD and SEM techniques are not available.
- In triaxial compression, Type A samples displayed peak behaviour at all mean effective stresses, although the strength drop off post peak was noted to decrease as mean effective stress was raised, indicating a shift from brittle to ductile behaviour may be occurring similar to that seen in marine mudstones (Nygard, et al., 2006) and other hard rocks, as modelled by Schopfer, et al (2013) (albeit at a significantly

lower stresses due to the soft nature of the calcareous mudstone) along with other calcareous rocks including calcarenites (Carter, et al., 2000). It is theorised that if samples were sheared at increasingly higher mean effective stress conditions, this transition from brittle to ductile would become even more apparent, as shown diagrammatically as Figure 8.1:

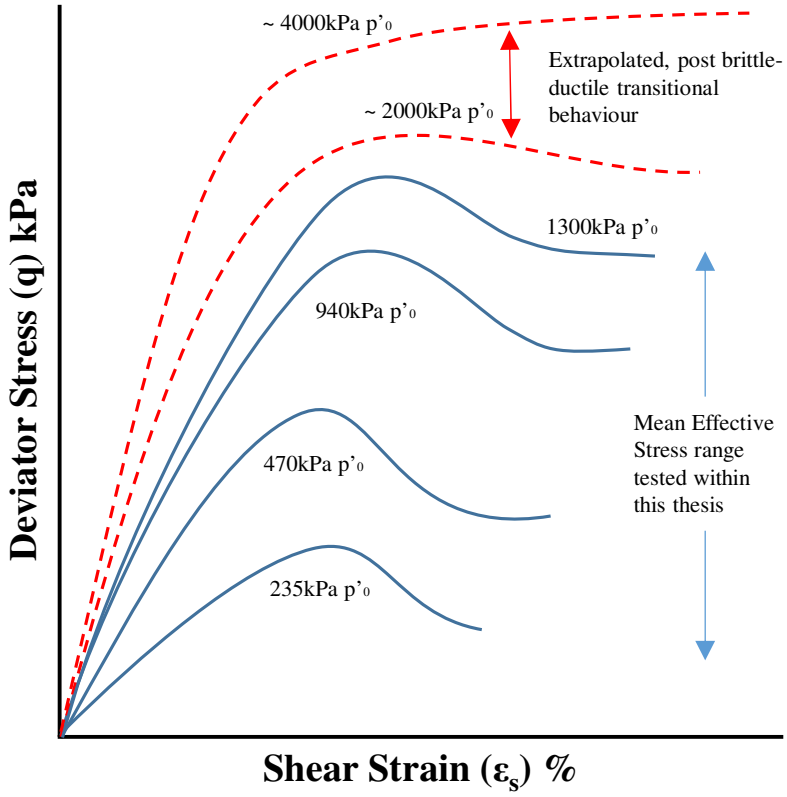

Figure 8.1: Conceptual model showing the role of mean effective stress on the brittle-ductile behaviour of calcareous mudstone (Type A).

- This was also noted in examination of the Type A Mohr failure envelope, which appeared to be starting to curve as high stresses were approached (in accordance with expected Hoek-Brown Failure Criteria (Eberhardt, 2012)), and as structural bonds begin to break. A high cohesion of 400kPa, likely due to the presence of strong Dolomite bonds, was recorded along with an average friction angle of 33°.
- Type B samples were both less stiff and strong than Type A samples in all tests, failing at a minimum of double the shear strains and displaying less peak behaviour, particularly at high mean effective stresses. Their response to stress was overall more plastic and they appeared to transition to ductile behaviour at much lower stresses than observed in Type A samples. In terms of Mohr failure criterion, Type B samples share Type A's average 33° friction angle, however have a cohesion of only 200kPa, due to their poorer bonding. Type B samples underwent significantly

greater amounts of volumetric strain during shearing, becoming purely contractant above 940kPa (as opposed to 1300kPa in Type A samples), supporting the hypothesis that they are becoming ductile at lower stresses.

- In addition to the overall differences in Mohr failure criteria between Type A and type B samples, the effect of structural breakdown with increasing mean effective stress can be observed to occur between 940kPa and 1300kPa p'_0 in Type A samples and 470kPa and 940kPa p'_0 in Type B samples, which may be expressed as a loss of cohesion, comparable to that noted to occur within weak weathered rock by Sun, et al (2006). This can be seen diagrammatically as Figure 8.2:

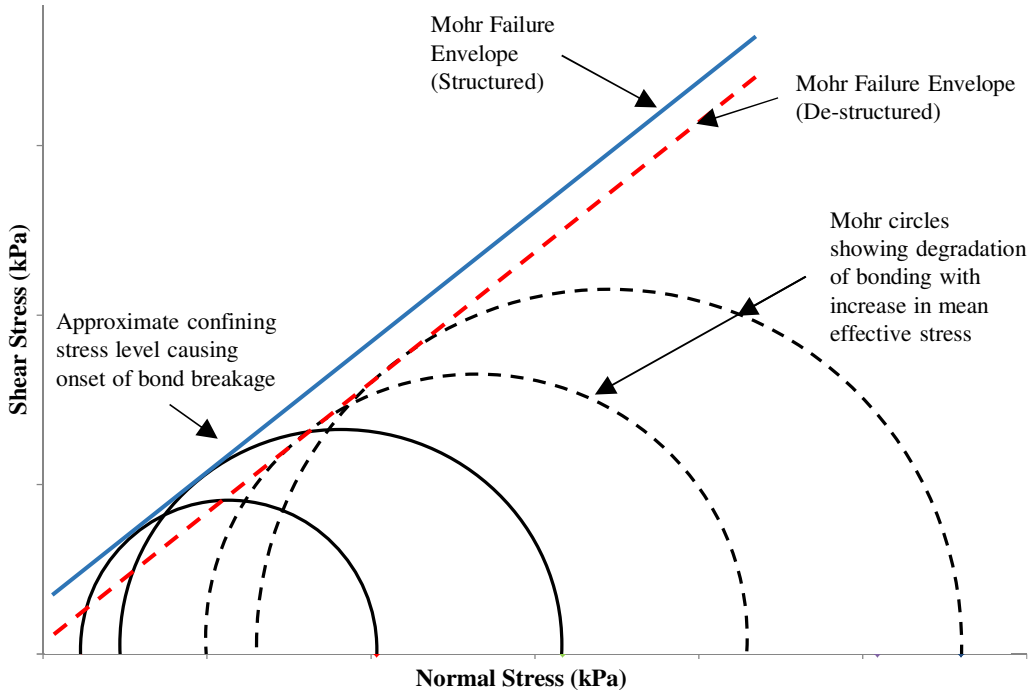

Figure 8.2: Conceptual model showing the effect of de-bonding on Mohr failure criteria with increase in mean effective stress.

- The role of strain rate was also examined, and results indicated a response typical of stiff soils (Sheng, et al., 1997) in that as strain rate increases, so too does the maximum stress at which a sample will fail in compression. This can be seen diagrammatically as Figure 8.3:

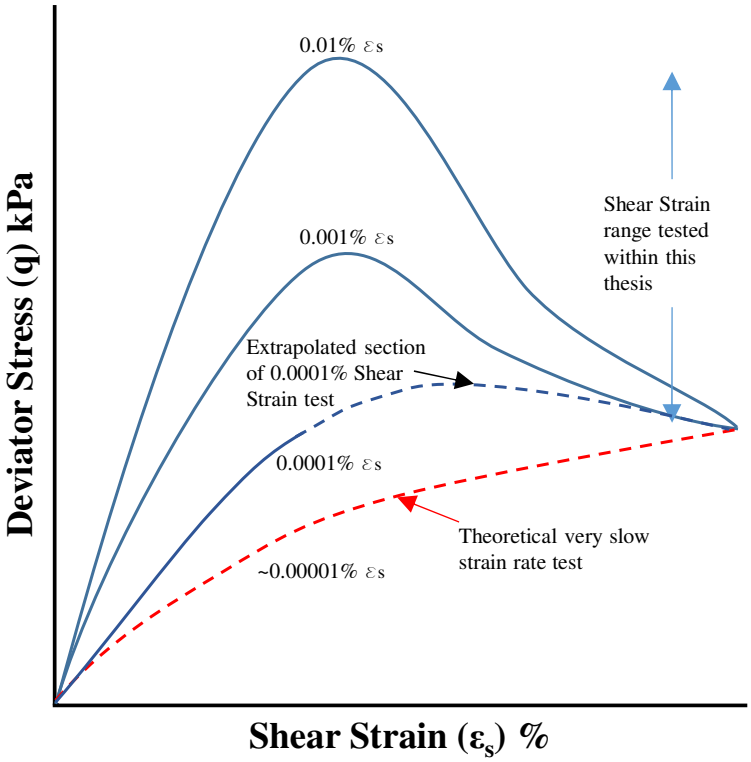

Figure 8.3: Conceptual model showing the role of strain rate on samples of calcareous mudstone.

- Palygorskite relative abundances are a key controlling factor on the overall behaviour of calcareous mudstone in compression. This can be seen diagrammatically as Figure 8.4:

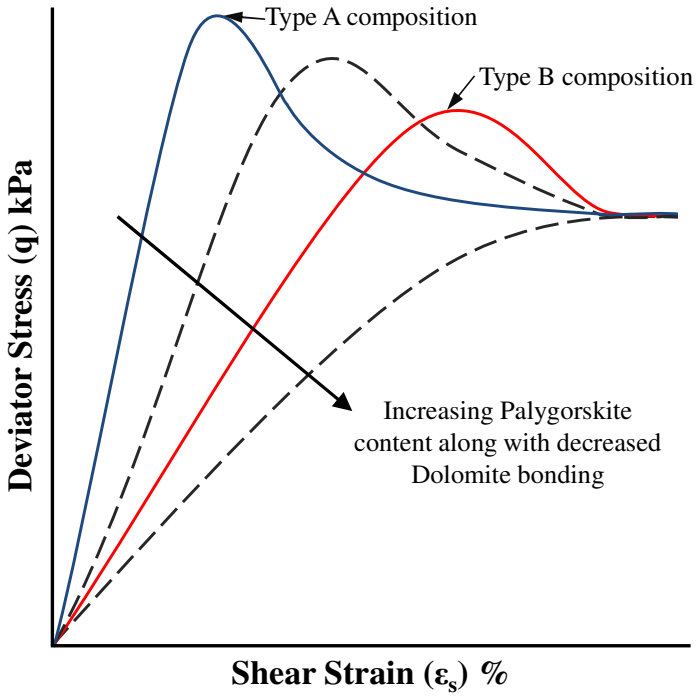

Figure 8.4: Conceptual model showing the role of Palygorskite content on the stress strain behaviour of calcareous mudstone.

- Both Type A and B samples share similar post failure strengths and CSL.
- All calcareous mudstone samples were noted to rapidly breakdown in water under unconfined conditions, displaying low first and second cycle durability values as well as being observed to disintegrate during dispersivity testing. This is not seen in triaxial testing where a positive mean effective stress (>50kPa) is applied, suggesting that the swelling of the mineral Palygorskite may be a key factor in the structural breakdown noted in unconfined conditions. The dissolution of soluble minerals such as Halite may also be contributing to the deterioration of bonding. It is advised that samples be prepared rapidly in the laboratory environment to stop them drying out prior to testing, and that excavations not be left open for prolonged periods of time during ground investigations within these materials.
- The stiffness of both Type A and Type B materials is shown to be highly non-linear from small through to large strains during triaxial compression, with the better bonded Type A samples being both stronger and stiffer than their Type B counterparts at any given mean effective stresses. This can be seen diagrammatically as Figure 8.5.

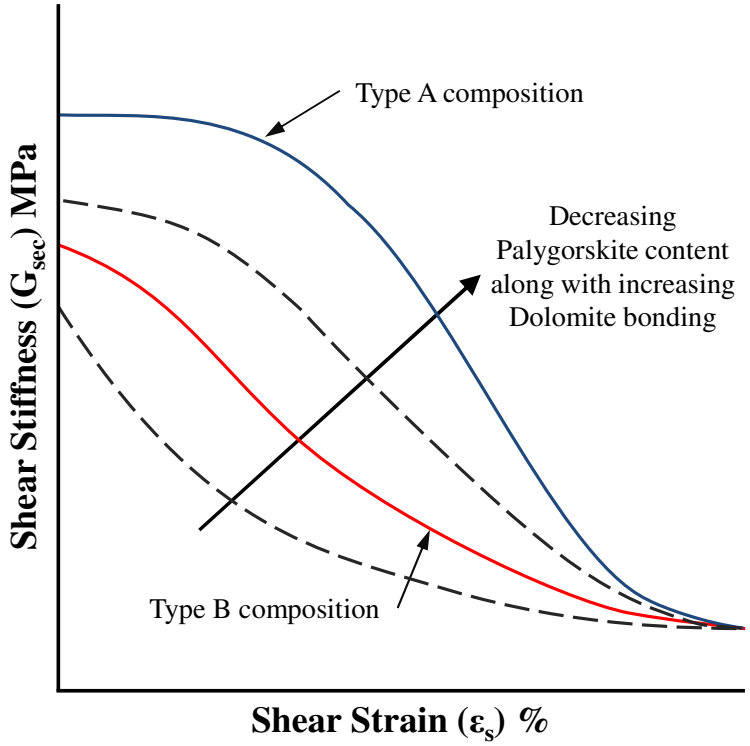

Figure 8.5: Conceptual model showing the role of Palygorskite content on the small strain shear stiffness behaviour of calcareous mudstone.

- G_0 profiles created using Bender Elements inducing shear waves at increasing mean effective stresses showed a strong agreement with the results of triaxial small strain

stiffness data, with low G_0 estimates being made via peak to peak methods and high estimates being obtained via 1st bump methods. G_0 at 1300kPa p' in Type A samples appear marginally lower than the G_{max} obtained from triaxial testing, possibly indicating the closure of micro-fissures as shear strains develop in high confining pressures.

- The overall increase in G_0 with increasing p'_0 is contrary to the findings of Trhlikova, et al (2012) who found a constant G_0 profile within calcarenites up until radial stresses were high enough to cause de-structuring. Whilst this behaviour may be common in rocks, (Mogi, 1974), soils and indeed soft rocks tend to show an increase in stiffness with increasing mean effective stress. This is likely due to the softer, less rigid nature of the bonding of materials tested within this thesis, allowing a degree of densification to occur as mean effective stress increases even at low levels of p'_0.
- The soft calcareous mudstones studied in this thesis are noted as having strength and stiffness that are highly dependent upon mean effective stress (similar to the behaviour of hard soils / soft rocks noted by Heymann, (1998) and soft sandstones by Kate & Gokhale (1998)), strain rate (comparable to structured soils as noted by Leroueil, (2000), hard soils (Silvestri & d'Onofrio, 2000) and indeed fine grained soils (Vardanega & Bolton, 2011)) as well as Palygorskite content.
- One dimensional consolidation tests showed that the low void ratios noted in all samples could not be replicated via compression alone, even with vertical stresses several times that of the materials in-situ stresses. This meant that the ICL could not be shown to intersect the normal compression line of undisturbed samples making quantifying structural permitted space impossible, however it does support the findings of the SEM analysis that suggests the Dolomite grains making up the calcareous mudstones are progressively fusing together via a means of dissolution and precipitation, effectively reducing void ratios (Palygorskite forming within voids will further reduce void ratios) as well as creating a fabric not possible by normal means of densification via overburden pressure.
- Calcareous mudstone samples were noted not to fail in tension when tested using standardised Brazilian methods, instead being seen to fail as a result of crushing induced fractures at the sample ends that propagate through the sample at high velocities. By adopting flattened loading geometries, sample disks fail at their centre in Brazilian indirect tensile tests, in keeping with Brazilian disk theory.

- Type A samples are shown to have tensile strengths approximately 80kPa higher than that of Type B samples, again due to their higher degree of Dolomite bonding. Tensile strengths measured during this thesis are high in comparison to the expected strengths predicted using triaxial Mohr failure envelopes. This is believed to be due to the degree of saturation of samples in Brazilian being lower than that of triaxial tests, coupled with the larger triaxial samples likely containing more micro-fissures and hidden imperfections than the smaller Brazilian disk specimens.

A general recommendation for the testing and interpretation of soft calcareous mudstones behaviour, is that they should be thought of as highly structured / bonded / cemented soils, similar to materials such as Vallericca Clay (Amorosi & Rampello, 2007), Pappadai Clay (Leroueil, 2000) or even London Clay (Gasparre, et al., 2007) in terms of the degree of additional strength and stiffness that is attributed to them due to the presence of structure (as discussed in Chapter 2 of this thesis), and methodologies should largely follow the similar frameworks in terms of triaxial and oedometric testing (with the exception of some recommendations specific to this lithology, as noted in the following section).

Deviations in behaviour from structured clays occurs in terms of the higher shear stiffness's and tensile strengths observed at lower mean effective stress, likely caused by the more developed bonding / cementation present in these calcareous mudstones than that which is seen in the structured clay materials previously mentioned, requiring more robust apparatus capable of applying / measuring stresses often not observed in soils.

In terms of routine, practical advice for their testing using common geotechnical laboratory testing apparatus, it is recommended that these materials be stressed mechanically using both triaxial and oedometer (modified to allow for higher applied stresses), as opposed to compressed in UCS, as removing their confining stress and allowing moisture contents to change throughout tested is unlikely to provide reliable results with respect to their compressive behaviour.

8.2. RECOMMENDATIONS FOR THE MECHANICAL TESTING OF SOFT ROCKS

In addition to characterising a calcareous mudstone from Abu Dhabi, this thesis also carried out experimentation in order to develop a repeatable testing methodology for soft and friable rocks within triaxial, Brazilian and characterisation tests. Some of these developments, such as the ground water salinity chemical composition recipe, are specific to the sites in question and would need adjusting for other potential users, however many of the developments made within this thesis (in particular within Chapter 4) would be suitable for other soft rock lithologies and even hard or structured soils testing.

It is important to reiterate that at this time, no standards exist that cover the application of local strain gauges for use with triaxial testing, nor do any standards exist with regards to Bender Element testing or DIC in Brazilian. Whilst many publications exist that incorporate such apparatus, methodologies are often lacking in specific information, making them difficult to replicate and open to interpretation. By being explicit with regards to the methods used in preparation and execution of tests, it is hoped that this thesis may provide a baseline methodology for the testing of these difficult materials.

What follows is a summary of findings and recommendations regarding practices of testing soft calcareous rocks in a geotechnical laboratory setting.

- It is recommended that moisture contents of soft calcareous rocks be found using ovens set to a constant 40ºC, as opposed to the 110ºC advised by BS1377. This is so as not to drive off water associated with halite or other hydrous minerals. Due to this lower temperature it should be noted that an increased time is required for drying to take place. It is recommended that samples be left within 40ºC ovens for not less than 10 days, again as opposed to the 48 hours recommended in BS1377.
- Where pore waters representative of in-situ ground water are required in impractically large quantities to be supplied direct from site, it is recommended that a synthetic solution comprising 15.6g magnesium chloride hexahydrate ($MgCl_2.6H_2O$), 10.74g sodium chloride (NaCl), 6.79g sodium nitrite ($NaNO_2$) 1.7g and potassium hydrogencarbonate ($KHCO_3$) per litre can be used. It should be noted that this is not a full representation of the chemistry of the natural groundwater at the NBAD and Yas Mina sites as determined via IC and ICP,

however it is of similar pH and consists of the major ingredients whilst retaining similar anion and cation balance. More complex mixtures that better matched the groundwater were found to be partially insoluble with unrepresentative pH, meaning that the simplified synthetic water is more repeatable and practical for experimentation purposes.

- It is recommended that the transfer of load from the triaxial apparatus into the sample should be made via a 'fixed' method, as opposed to using a traditional convex ram to concave topcap method or 'half ball' method. Using a 'fixed' docking method will significantly reduce the likelihood of rotational straining occurring during shearing and prevent misalignment of sample and ram during earlier stages. One draw-back of this method is that automated saturation / consolidation may not be undertaken using the GDS sat-con module, as unwanted loading of the sample will occur. It is instead advised that the advancedloading module be used, with deviatoric stress set to maintain a constant zero state throughout saturation and consolidation. Using a 'fixed' docking method with a submersible internal load cell will aid in the elimination of seating errors.
- Soft rocks are significantly stiffer than most soils, and so initial geometry of the sample and the degree of parallelism between the top and base of the sample is important for ensuring a strong fixed connection is possible. If the ram and topcap appear mal-aligned when the cell is constructed, this is a strong indicator that sample preparation was sub-standard. This is particularly true when using the 'fixed' docking method as any misalignment will result in having to disassemble the triaxial cell. It must be emphasised that attention to good sample preparation can reduce bedding errors, reduce seating errors and ultimately save time and increase the quality of results and the agreement between external and internal strain measurements.
- Saturation of samples of calcareous mudstone in triaxial tests can be adequately undertaken using a stepped approach with successive B-tests whilst maintaining mean effective stresses of not less than 50kPa to avoid swelling and not greater than the in-situ mean effective stress of a given sample. This often takes a number of days to achieve a B value of 0.95, however and so this must be factored into any testing programme. It is not recommended to attempt to speed up saturation by flushing the sample first with CO_2. This is impractical due to the low permeability of the rock along as well as its sensitivity to drying out,

however crucially any dissolved CO_2 may react with the dolomite causing inadvertent dissolution.

- Using an adhesive between the triaxial sample and its membrane at the location the gauge is to be adhered can form a strong fixing whilst also forgoing the need to perforate the membrane using pins (which itself may cause unwanted problems if carried out incorrectly), similar in methodology to Ismail, et al (2002) who used fixed foil footings to the same end. This proved reliable during the triaxial testing programme of this thesis and the fixing points remained adhered even after prolonged periods in full saturation. This is particularly useful for scenarios where few sample cores are available (as is often the case during post SI laboratory testing) as this is an non-destructive method. In addition to this (assuming that lightweight Hall Effect gauges are being utilised), it has been shown through experimentation that differential pressures of greater than 200kPa between the cell and pore pressures are sufficient to hold strain gauges in place without the need for pinning (or adhesive between sample and membrane) providing that axial strains of 2.5% are not exceeded and that membranes are fit for purpose with respect to core diameter. For tests assessing stress states lower than 200kPa mean effective stress, the issue of membrane-sample 'play' may become more pronounced however, and so pinning gauges is recommended at low stresses.
- Further to the previous recommendation, in all cases where local strain gauges are being implemented, it is important that in addition to initial gauge length being recorded, that any displacements that occur during setup, saturation and consolidation are taken into account when calculating axial and radial strains during shearing. It is also recommended that both local and external measurements be checked against one another in order to avoid any unrepresentative strain calculations caused by the development of localised shear plains of pre-existing localised weaknesses proximal to strain gauges. Likewise it is important to constantly measure volumetric change during these stages using both local gauges and back volume change in order to accurately calculate sample cross sectional area and bulk density so that stresses may be correctly derived, again cross checking both methods to ensure representative results are reported. Whilst the use of local strain gauges are generally encouraged, it must be reiterated that they too are subject to errors, especially during shearing where radial strains may be over-estimated due to 'barrelling'.

- Samples of soft calcareous rock are too stiff to allow Bender Elements to physically penetrate. In order to allow this technique to be carried out without damaging the Benders, it is recommended that narrow trenches be first created parallel to one-another at the centre of the sample ends and filled with a remoulded slurry of the host rock. This allows adequate contact to be maintained throughout isotropic consolidation.
- When using the GDSBES software and Bender Element hardware, a sampling frequency and sample time of 2000ksamp/sec and 5ms respectively are recommended along with a sinusoidal source wave with a period of 0.2ms and an amplitude of 14V. These initial settings were found to provide repeatable data with clear received waveforms that were relatively simple to derive time domain properties from.
- The GDS BEAT tool should not be used in isolation when analysing G_0 data, as it only recognises waveforms that adhere to an idealised pattern, making its selection of the four typical reference points within the time domain subject to error. It is recommended that the data set be manually checked and the output voltage sign reversed if need be in order for the BEAT tool to be most effective. The 1st deflection reference point is recommended to be manually identified, as the noise generated in a typical test is often misinterpreted by the BEAT tool.
- Upper bounds for the estimation of G_0 of soft rock within the time domain are recommended to obtain Ts and ultimately Vs using the '1st bump' method, whilst the lower bound for G_0 estimates should use the 'peak to peak' method (which generally has good agreement with the 'start to start' method for comparison purposes).
- DIC is a technique that overcomes the usual problems encountered when using traditional local strain gauges during the testing of soft calcareous rocks in unconfined conditions. Soft friable materials such as those tested within this thesis are poorly suited to local strain gauges being adhered to them in unconfined conditions due to their tendency to dry out and even deteriorate as a test is carried out, often precipitating a thin coating of halite on their surface and causing adhered gauges to become dislocated. Traditional strain gauges are also limited in that they cover only a single linear 2D section of a sample, whereas the strains being generated in Brazilian testing are complex and orientated in three dimensions. DIC, however, is contactless, rapid to prepare (especially if large batches of samples are to be tested) and 'full field' in that the whole of the

sample surface is included in the calculation of strains. Virtual local strain gauges may be placed on samples in post processing in any orientation and strain contours may be output that highlight strain localisation in 3D. DIC is recommended, where possible, for the capture of localised strain developments in soft rock testing due to these advantages over more traditional local strain gauges.

- DIC has highlighted that as sample thickness decreases in Brazilian tensile testing, the amount of unwanted straining at the loading points increases. When indirectly assessing the tensile strength of soft rocks it is advised that a 2:1 diameter to disk thickness ratio not be exceeded so as to prevent out of plane bending and/or crushing.
- Both the ISRM and ASTM methods have been shown through the use of DIC analysis to cause unwanted localised straining to occur proximal to the loading points during Brazilian testing. It is recommended that flattened areas at the top and bottom of the disk covering a 2α angle of 20^{o} be first cut in order to promote tensile failures to occur within the centre of the sample.

It should be reiterated that the testing programme undertaken within this thesis was carried out upon samples sourced using means outside of the authors control. As the materials tested behave broadly as highly structured / bonded soils, they are particularly susceptible to damage caused to them during recovery and transportation. Various sampling / drilling methods are discussed by Wright, et al (2000), with respect specifically to cemented calcareous soils, with push sampling, percussive drilling and rotary coring methods merits and limitations being compared and contrasted. Despite being thought of as structured soils in the context of laboratory testing and analysis, rotary coring is deemed to be the most reliable means of recovering samples of a high enough quality, and low enough sample disturbance, to allow meaningful testing to be undertaken. Using this method, however, one must remain aware of the flush medium / pressures used, so as not to cause unwanted core loss or damage to the samples bonding.

8.3. SUGGESTIONS FOR FURTHER WORK

Calcareous mudstones of the Abu Dhabi coastline are relatively unstudied from a geotechnical perspective, and as such there exists a limited pool of pre-existing information from which to draw upon and build upon when designing an experimental programme and developing any specific methodologies that may have been required to address their unique properties. It is hoped that this thesis forms an important first step in terms of better understanding the characteristics of these soft rock materials for use in design.

Whilst this research project was able to succeed in achieving its aim of characterising the calcareous mudstone from a micro through to macro scale, the breadth of its scope was limited due to a lack of available core samples, forcing the experimental testing programme to be economical with the raw materials upon which it was focused, and to be conservative with respect to risky preparation procedures that could have reduced the viable samples further. This was particularly true of samples scheduled for triaxial testing, due to the length of intact core required to form a 2:1 ratio with the cores' diameter.

Were further works to follow this thesis, there are several suggested research topics and experimental procedures that could be carried out to augment and build on the findings of this project. These include:

- X-Ray CT scanning of samples to assess the degree of micro-fractures present and examine intact structural features. This would also enable the location and orientation of Palygorskite to be assessed as it appears in-situ as opposed to on the surface of broken sections.
- Additional quantitative XRD analysis to corroborate findings of this research and correlate the behaviour of samples in compression and tension against their Dolomite and Palygorskite content by percentage.
- Additional tests assessing the effect of rate of strain on the behaviour of Type A samples.
- Additional tests incorporating Bender Element apparatus to corroborate the findings of this study as well as characterising Type B samples G_0 dependence upon mean effective stress.
- Assess the effect of long term creep on specimens in triaxial apparatus.
- Assess the response to cyclic stress in both Type A and Type B specimens.

- Extend the upper limits of the mean effective stress programme by undertaking experimentation within high pressure triaxial apparatus. This would allow the full brittle to ductile transition behaviour of samples to be observed, as well as better assessing the degree of curvature present in the Mohr failure envelopes.
- High pressure one dimensional consolidation tests would allow the upper limits of the oedometer programme to be extended, allowing an intersection between the ICL and the compression curve of undisturbed samples to be observed and characterised.
- Repeat of the triaxial testing programme carried out under undrained conditions using pressure / volume controllers of high capacity to examine pore pressure response.
- A programme of stress probing in order to characterise the anisotropy of samples and also to better understand the calcareous mudstones yielding behaviour (requiring multiple samples from a given depth, ideally cut from a single block sample).
- A programme of UCS testing using DIC as a means of measuring the development of local strains would expand on the Brazilian indirect tensile testing results.
- A study assessing the effect of saline pore waters (representative of in-situ conditions) on the response of samples in triaxial compression, comparing behaviours to those from this thesis using de-aired water.
- Attempt to capture the behaviour of soft calcareous mudstones using existing constitutive models designed for structured soils (for example that posed by Rouainia & Muir Wood, (2000)), using results and parameters obtained in this thesis to validate and calibrate results, albeit adapting the model to allow for the higher stiffness at lower strains noted in the laboratory testing results.

CHAPTER 9. REFERENCES

Abramson , l. W., Lee, T. S., Sharma, S. & Boyce , G. M., 2001. *Slope Stability and Stabilization Methods.* s.l.:John Wiley and sons.

Agustawijaya, D. S., 2007. *The uniaxial strength of soft rock,* Mataram: Civil Engineering Dimension.

Akazawa, T., 1953. RILEM Bull. *International association of testing and research laboratories for materials and structures,* Volume 13, pp. 13-23.

Al Suwaidi, A. S. et al., 2011. Carbonates and evaporites of the Upper Jurassic Arab Formation, Abu Dhabi: a petroleum exploration challenge. *International Association of Sedimentology,* Volume 43, pp. 421-430.

Alsayed, M. I., 2002. Utilising the Hoek triaxial cell for multiaxial testing of hollow rock cylinders. *International journal of rock mechanics and mining sciences,* Volume 39, pp. 355-366.

Alsharhan, A. S. & Kendall, C. G., 2011. Introduction to Quaternary carbonate and evaporite sedimentary facies and their ancient analogues. *International Association of Sedimentology,* Volume 43, pp. 1-10.

Amorosi, A. & Rampello, S., 1998. The influence of natural soil structure on the mechanical behaviour of stiff clay. *The geotechnics of hard soils - soft rocks,* Volume 1, p. 395.

Amorosi, A. & Rampello, S., 2007. An experimental investigation into the mechanical behaviour of a structured clay. *Geotechnique,* 57(2), pp. 153-166.

Andreev, G. E., 1991. A review of the Brazilian test for rock tensile strength determination. Part II: contact conditions. *Mining science and technology,* Volume 13, pp. 457-465.

Ansal, A., Iyisan, R. & Yildirim, H., 2001. The cyclic behavior of soils and effects of geotechnical factors in microzonation. *Soil dynamics and earthquake engineering,* Volume 21, pp. 445-452.

Arthur, J. R. & Phillips, A. B., 1975. Homogeneous and layered sand in triaxial compression. *Geotechnique,* 4(25), pp. 799 - 1815.

ASP, 2001. *ASP Review Oil Market Trends.* [Online]
Available at: http://www.thefreelibrary.com/ABU+DHABI+-+The+Geology.-a068710871

ASTM, 1984. Standard test method for splitting tensile strength of intact rock core specimens. *In annual book of ASTM standards,* pp. 336-341.

ASTM, 1990. Standard test method for slake durability of shales and similar weak rocks. In: *Annual Book of ASTM Standards Volumes 4.08.* Philadelphia: s.n., pp. 863-865.

Atkinson, J. H., 2000. Non-Linear soil stiffness in routine design. *Geotechnique,* 50(5), pp. 487 - 508.

Atkinson, J. H., Richardson, D. & Stallebrass, S. E., 1990. Effect of recent stress history on the stiffness of overconsolidated soil. *Geotechnique,* 40(4), pp. 531-540.

Atkinson, J. H. & Sallfors, G., 1991. *Experimental determination of soil properties. General report to session 1,* Florence: Proceedings of the 10th ECSMFE.

Aversa, S. & Evangelista, A., 1998. The mechanical behavior of a pyroclastic rock: Yield strength and "destructuration" effects. *Rock mechanics and rock engineering,* 31(1), pp. 25-42.

Aversa, S., Evangelista, A., Leroueil, S. & Picarelli, L., 1993. Some aspects of the mechanical behavior of 'structured' soils and soft rocks. *Geotechnical Engineering of Hard Soils - Soft Rocks,* pp. 359-366.

Baldi, G., Hight, D. W. & Thomas, G. E., 1988. A re-evaluation of conventional triaxial testing methods.. *Advanced triaxial testing of soil and rock. ASTM*, Volume STP 977, pp. 219 - 263.

Baranski, M., 2003. Laboratory measurement of the stiffness of normally consolidated till polluted by benzene with bender element tests. *Geological Quarterly,* 47(2), pp. 211-214.

Baranski, M., 2008. Engineering-geological properties of normally consolidated tills from Plock area. *Geologija,* Volume 50, pp. 40-48.

Barla, M. et al., 2000. *Stiffness of soft rocks from laboratory tests,* s.l.: s.n.

Barreto, D., Rouainia, M. & Simpson, D., 2014. *Significance of DEM input parameters on the modelling of low strength soft rock mechanical behavior.* s.l., s.n.

Been, K., Jefferies, M. G. & Hachey, J., 1991. The Critical State of Sands. *Geotechnique,* 41(3), pp. 365-381.

Bell, F. G., 2002. The geotechnical properties of some till deposits occuring along the coastal areas of eastern England. *Engineering Geology,* Volume 63, pp. 49-68.

Bell, F. G., 2004. *Engineering Geology and Construction.* s.l.:Spon Press.

Benaissa, R. et al., 2013. Comprehensive physicochemical study of dioctahedral Palygorskite-rich clay from Marrakech High Atlas (Morocco). *Physicochemical Minerals,* Volume 40, pp. 411-424.

Benz, T., 2007. *Small strain stiffness of soils and its numerical consequences,* Universitat Stuttgart: Ph.D Thesis.

Berest, P. et al., 2010. *Very Slow Creep Tests on Salt Samples,* Paris, France: EDP Sciences.

Berre, T., 2010. Triaxial Testing of Soft Rocks. *Geotechnical Testing Journal,* 34(1).

BGS, 2014. *British Geological Survey.* [Online]
Available at: http://www.bgs.ac.uk/home.html

Bica, A. V. D. et al., 2008. Anisotropic shear strength of a residual soil of sandstone. *Canadian Geotechnical Journal,* pp. 367-376.

Bieniawski, Z. T., 1973. Engineering classification of jointed rock masses. *Transactions of the south african institution of civil engineers,* Volume 15, pp. 335-344.

Bishop, A. W. & Henkel, D. J., 1964. The Measurement of Soil Properties in the Triaxial Test. In: s.l.:Edward Arnold.

Bishop, A. W. & Lovenbury, H. T., 1969. *Creep characteristics of two undisturbed clays.* s.l., s.n., pp. 29-37.

Bishop, A. W., Webb, D. L. & Lewin, P. I., 1965. Undisturbed samples of London Clay from the Ashford Common Shaft: Strength effective stress relationships. *Geotechnique,* Volume 15, pp. 1-31.

Black, J. A., 2009. Shear wave velocity measurment of kaolin during undrained unconsolidated triaxial compression. *GeoHalifax,* pp. 1-8.

Bontognali, T. R. et al., 2010. Dolomite formation within microbial mats in the coastal sabkha of Abu Dhabi. *Sedimentology,* Volume 57, pp. 824-844.

British Standards Institution; BS1377 - Part 7, 1990. *Methods of test for soils for civil engineering purposes.* s.l.:s.n.

British Standards Institution; BS5930, 1999. The code of practice for site investigations. In: s.l.:s.n.

Bromhead, E. N. & Patel, M. K., 2000. Triaxial testing in uncemented sandstone. *The geotechnics of Hard soils - Soft rocks,* pp. 63-70.

Brown, E. T., 1981. *Rock characterisation testing and monitoring ISRM suggested methods,* Oxford: Pergamon.

Brown, E. T., 1986. *Rock Characterization Testing and Monitoring: ISRM Suggested Methods.* s.l.:Pergamon Press.

BSI, 1990. *BS1377-8:1990 Methods of tests for soils for civil engineering purposes- Part 8: Shear strength tests (effective stress),* UK: British Standards Institution.

Burland, J. B., 1989. Small is Beautiful - the stiffness of soils at small strains.. *Canadian Geotech Journal,* 26(Ninth Lauritits Bjerrum Memorial Lecture), pp. 499 - 516.

Burland, J. B., 1990. On the compressibility and shear strength of natural clays. *Geotechnique,* 40(3), pp. 329-378.

Burland, J. B. & Hancock, R. J., 1977. Underground car park at the House of Commons: Geotechnical aspects. *Structural Engineer,* Issue 55, pp. 87 - 100.

Burland, J. B. & Lord, J. A., 1970. The load-deformation behaviour of Middle Chalk at Mundford, Norfolk: An comparison between full scale preformance and in-situ

laboratory measurments. *In situ investigations in soils and rocks, british geological society,* pp. 3-15.

Burland, J. B. & Symes, M., 1982. A simple axial displacement gauge for use in triaxial apparatus. *Technical Notes,* pp. 62-65.

Burnett, A. D. & Epps, R. J., 1979. The engineering geological description of carbonate suite rocks and soils. *Ground Engineering,* pp. 41-48.

Buro-Happold, 2007. 022179 Harvard Allston Science Complex Geotechnical Report. *Revision 04.*

Cai, M., 2010. Practical estimates of tensile strength and Hoek-Brown strength parameter mi of brittle rocks. *Rock Mechanics and Rock Engineering,* 43(2), pp. 167-184.

Calabresi, G. & Scarpelli, G., 1985. Effect of swelling caused by unloading in overconsolidated clays. *Proc 11th ICSMFE, San Francisco 1,* pp. 411-414.

Camacho-Tauta, J. F., Alvarez, J. D. & Reyes-Ortiz, O. J., 2012. A proceedure to calibrate and perform the bender element test. *Dyna,* 176(1), pp. 10-18.

Carneiro, F. & Barcellos, A., 1953. RILEM Bull. *International association of testing and research laboratories for materials and structures,* Volume 13, pp. 99-125.

Carter, J. P., Airey, D. W. & Fahey, M., 2000. A review of laboratory testing of calcareous soils. *Engineering for Calcareous Sediments,* pp. 401-431.

Cecconi, M. & Viggiani, G. M. B., 2001. Structural features and mechanical behaviour of a pyroclastic weak rock. *International journal for numerical and analytical methods in geomechanics,* Volume 25, pp. 1525-1557.

Chan, C.-M., 2010. Bender element test in soil specimens: identifying the shear wave arrival time. *EJGE,* Volume 15, pp. 1263-1276.

Chen, C. S. & Hsu, S. C., 2001. Measurement of indirect tensile strength of anisotropic rocks by the ring test. *Rock Mechanics and Rock Engineering ,* 34(4), pp. 293-321.

Chiu, H. K., Johnston, I. W. & Donald, I. B., 1983. Approptiate techniques for triaxial testing of saturated soft rock. *Int. J. Rock Mech,* 20(3), pp. 107 - 120.

Chu, T., Ranson, W. & Sutton, M., 1985. Applications of digital-image-correlation techniques to experimental mechanics. *Exp. Mech.,* Volume 25, pp. 232-244.

Clarke, A. R. & Walker, B. F., 1977. A proposed scheme for the classification and nomenclature for use in the engineering description of Middle Eastern sedimentary rocks. *Geotechnique,* 1(27), pp. 93-99.

Clarke, B. G., 1995. *Pressure-meter in Geotechnical Design.* s.l.:Chapman and Hall.

Clarke, B. G., Hughes, D. B. & Hashemi, S., 2008. Physical characteristics of subglacial tills. *Geotechnique,* 58(1), pp. 67-76.

Clayton, C. R., Gordon, M. A. & Matthews, M. C., 1994. Measurment of stiffness of soils and weak rocks using small strain laboratory testing and field geophysics. *Proceedings of the first international conference on prefailure deformation characteristics of geomaterials,* Volume 1, pp. 229-234.

Clayton, C. R. & Heymann, G., 2001. Stiffness of geomaterials at very small strains. *Geotechnique,* 51(3), pp. 245-255.

Clayton, C. R. I., 2011. Stiffness at small strain: research and practice. *Geotechnique,* 61(1), pp. 5-37.

Clayton, C. R. I. & Khatrush, S. A., 1986. A new device for measuring local axial strains on triaxial specimens. *Geotechnique,* Volume 36, pp. 593 - 597.

Clayton, C. R., Theron, M. & Vermeulen, N. J., 2004. *The effect of particle shape on the behavior of gold tailings.* London, Thomas Telford.

Comrie, R. J., 1998. The determination of non-linear stiffness and its application in predicting ground movements in retaining wall analysis. *MSc Thesis, Newcastle University.*

Cook, A. W., 1997. *Geotechnical engineering concerns with the weak calcareous rocks of the lower Arabian Gulf,* University of Surrey: Unpublished MSc Dissertation.

Cook, A. W., 1999. The rate of drying out of calcarenites. *Engineering for calcareous sediments,* Volume 1, pp. 229-232.

Cook, A. W., 1999. The soil to rock boundary for weak calcareous rocks. *Engineering for calcareous sediments,* Volume 1, pp. 131-137.

Cooke, R. W. & Price, G., 1974. Horizontal inclinometers for the measurment of vertical displacement in the soil around experimental foundations. In: *Field instrumentation in geotechnical engineering.* London: Butterworths, pp. 112 - 125.

Coop, M. R. & Atkinson, J. H., 1993. The Mechanics of Cemented Carbonate Sands. *Geotechnique,* 43(1), pp. 53-67.

Corp, E. T., 2010. *Epsilon Technology Corp.* [Online]
Available at: http://www.epsilontech.com/3544.htm

Correlated Solutions, 2010. *Vic-3D Testing Guide,* s.l.: s.n.

Cortesy, R., Leite, M. H., Gill, D. E. & Gaudin, B., 2003. Stress Measurement in Soft Rocks. *Engineering Geology,* Volume 69, pp. 381-397.

Corthesy, R., Leite, M. H., Gill, D. E. & Gaudin, B., 2003. Stress Measurement in Soft Rocks. *Engineering Geology,* Volume 69, pp. 381-397.

Coviello, A., Lagioia, R. & Nova, R., 2005. On the measurment of the Tensile Strength of Soft Rock. *Rock Mechanics and Rock Engineering,* 38(4), pp. 251-273.

Craig, R. F., 2004. *Craig's Soil Mechanics.* 7 ed. s.l.:CRC Press.

Cuccovillo, T. & Coop, M. R., 1997. The measurment of local axial strains in triaxial testing using LVDT's. *Geotechnique,* 47(1), pp. 167-171.

Cuccovillo, T. & Coop, M. R., 1997. Yielding and pre-failure deformation of structured sands. *Geotechnique,* 47(3), pp. 491-508.

Dave, E. V., Braham, A. F., Buttlar, A. G. & Paulino, G. H., 2011. Development of a flattened indirect tension test for asphalt concrete. *Journal of Testing and Evaluation,* 39(3).

Dixon, J. & Weed, S., 1989. *Minerals in the soil environments.* 2 ed. Madison: s.n.

Diyuan, L. & Wong, L. N., 2013. Rock Mechanics and Rock Engineering. *The Brazilian Disk Test for Rock Mechanics Applications: Review and New Insights,* 46(2), pp. 269-287.

Dobereiner, L. & Freitas, M. H., 1986. Geotechnical Properties of Weak Rocks. *Geotechnique,* 36(1), pp. 79-94.

Donaghe, R. T., Chaney, R. C. & Silver, M. L., 1988. *Advanced triaxial testing of soil and rock.* s.l.:ASTM.

d'Onofrio, A., Silvestri, F. & Vinale, F., 1999. Strain rate dependent behaviour of a natural stiff clay. *Soils and foundations,* 39(2), pp. 69-82.

Dreimanis, A., 1988. *Tills: Their genetic terminology and classification.* Rotterdam: A. A. Balkema.

Eberhardt, E., 2012. The Hoek-Brown failure criterion. *Journal of Rock Mechanics and Rock Engineering,* pp. 981-988.

Emerson, W. W., 1964. The slaking of soil crumbs as influenced by mineral composition. *Austrailian journal of soil research,* Volume 2, pp. 211-217.

Epps, R. J., 2010. Some engineering properties of the carbonate sediments of Abu Dhabi Island, United Arab Emirates. In: *Quaternary carbonate and evaporite facies and their ancient analogues.* s.l.:s.n., pp. 1-29.

Epps, R. J., 2011. Engineering properties of the carbonate sediments along the Abu Dhabi coast, United Arab Emirates. *International Association of Sedimentology,* Volume 43, pp. 221-242.

epsilontech, 2010. [Online]
Available at: http://www.epsilontech.com/3544.htm

Epsilontech, 2010. [Online]
Available at: http://www.epsilontech.com/3544.htm

ERYC, 2014. *East Riding Yorkshire Council.* [Online]
Available at: http://www.eriding.net/media/index.shtml

Eugster, H. P. & Hardie, L. A., 1978. Saline Lakes. In: *Physics and Chemsitry of Lakes.* New York: Springer-Verlag, pp. 237-293.

Evans , G. et al., 1973. The oceanography, ecology, sedimentology and geomorphology of parts of the Trucial Coast barrier island complex, Persian Gulf. In: B. Perser, ed. *The Persian Gulf.* s.l.:Springer Verlag.

Evans, G., 2011. An historical review of the Quarternary sedimentology of the Gulf (Arabian/Persian Gulf) and its geological impact. *International Accociation of Sedimentology,* Volume 43, pp. 11-44.

Ewald, P. P., 1962. *Fifty Years of X-Ray Diffraction.* s.l.:Springer US.

Fairbairn, E. M. R. & Ulm, F.-J., 2002. A tribute to Fernando L. L. Carneiro (1913-2001) engineer and scientist who invented the Brazilian test.. *Materials and Structures,* Volume 35, pp. 195-6.

Fairbairn, E. M. & Ulm, F. J., 2002. A tribute to Fernando L L Carneiro (1913-2001) engineer and scientist who invented the Brazilian test. *Material Structures,* Volume 35, pp. 195-196.

Fairhurst, C., 1964. On the validity of the 'Brazilian' test for brittle materials. *International journal of rock mechanics and mining sciences,* Volume 1, pp. 535-546.

Fang , H.-Y., 2002. *Foundation Engineering Handbook.* 2 ed. s.l.:Kluwer Academic Publishers.

Ferreira, C., Martins, J. P. & Correia, A. G., 2014. Determination of the small-strain stiffness of hard soils by means of bender elements and accelerometers. *Geotechnical and Geological Engineering,* Volume 32, pp. 1369-1375.

Finno, R. J. & Cho, W., 2010. Recent stress history effects on compressible chicago glacial clays. *Geotechnical and Geoenvironmental Engineering.*

Finno, R. J. & Cho, W., 2011. Recent Stress-History Effects on Compressible Chicago Glacial Clays. *Journal of geotechnical and geoenvironmental engineering,* pp. 197-207.

Finno, R. J. & Kim, T., 2011. Effects of stress path rotation angle on small strain responces. *Journal of Geotechnical and Geoenvironmental Engineering.*

Fonseca, A. V., Ferreira, C. & Fahey, M., 2009. A framework interpreting bender element tests, combining time-domain and frequency-domain methods. *Geotechnical Testing Journal,* 32(2), pp. 1-17.

Fookes, P. G., French, W. J. & Rice, S. M., 1985. The influence of ground and groundwater chemistry on construction in the Middle East. *Quarterly Journal of Engineering Geology and Hydrogeology,* Volume 18, pp. 101-128.

Fookes, P. G. & Higginbottom, I. E., 1975. The clasification and description of near shore carbonate sediments for engineering purposes. *Geotechnique,* 2(25), pp. 406-411.

Fortuna, S., Callisto, L. & Rampello, S., 2006. Small Strain Stiffness of a Soft ClayAlong Stress Paths Typical of Excavations. *Geotechnical Symposium in Roma.*

Franklin, J. A. & Chandra, A., 1972. The slake durability test. *International Journal of Rock Mechanics and Mineral Sciences,* Volume 9, pp. 325-341.

Fugro Middle East, 2013. *NBAD Global Headquarters Building, Geotechnical Investigation Factual Report,* Abu Dhabi: Unplublished.

Galan, E., 1996. Properties and applications of palygorskite-sepiolite clays. *Clay Miner,* Volume 31, pp. 443-453.

Gasparre, A., 2005. *Advanced Laboratory Charactorisation of London Clay,* s.l.: Imperial College London.

Gasparre, A. & Coop, M., 2006. Techniques for performing small strain probes in the triaxial apparatus. *Geotechnique,* 56(7), pp. 491-495.

Gasparre, A., Nishimura, S., Coop, M. R. & Jardine, R. J., 2007. The influence of structure on the behavior of London Clay. *Geotechnique,* 57(1), pp. 19-31.

Gasparre, A. et al., 2007. The stiffness of natural London Clay. *Geotechnique,* 57(1), pp. 33 - 47.

Gens, A., 1982. *Stress-strain charactoristics of a low plasticity clay,* University of London: Ph.D Thesis.

GeoCongress, 2012. *State of the Art and Practice in Geotechnical Engineering.* Oakland Marriott City Center, Oakland, California USA, s.n.

Goto, S. et al., 1991. A simple gauge for local mall strain measurments in the laboratory. *Soils and foundations,* 31(1), pp. 169-180.

Graham, J. & Houlsby, G. T., 1983. Anisotropic elasticity of a natural clay. *Geotechnique,* 33(2), pp. 165-180.

Grisso, R. D., Johnson, C. E., Bailey, A. C. & Nichols, T. A., 1984. Influences of Soil Sample Geometry on Hydrostatic Compaction. *American Society of Agricultural Engineers.*

Haberfield, C. M., 2000. Panel report: Towards a universal approach to soil and rock engineering: Fact or fallacy?. *The geotechnics of hard soils - soft rocks,* pp. 1403-1409.

Hawkes, I. & Mellor, M., 1970. Uniaxial testing in rock mechanices laboratories. *Engineering Geology,* 1(4), pp. 177-285.

Hawkins, A. B., 2000. *General report: The Nature of hard rocks / soft soils.* Rotterdam, ISBN, pp. 1391-1402.

Hawkins, A. B. & Pinches, G. M., 1992. Engineering description of mudrocks. *Engineering Geology,* Volume 25, pp. 17-30.

Hayano, K., Tatsuoka, F. & Yoshiizumi, N., 1999. Modeling Pre-Failure Stress-Strain Properties of Sedimentary Soft Rock Based on Very Small Strain Stiffness. *ASTM.*

Haydn, H., Murray & Huitang, Z., 2005. *Palygorskite and Sepiolite (Hormites),* s.l.: s.n.

Heymann, G., 1998. *The Stiffness of Soils and Weak Rocks at Very Small Strains,* University of Surrey Department of Civil Engineering: Thesis.

Heymann, G., Clayton, C. R. & Reed, G. T., 2005. Triaxial Ultra-Small Strain Measurments Using Laser Interferometry. *Geotechnical Testing Journal,* 28(6), pp. 1-9.

Hird, C. & Chan, C., 2008. One-dimensional compression tests on stabilized clays incorporating shear wave velocity measurments. *Geotechnique,* 31(2), pp. 166-174.

Hoek, E., 1965. Rock fracture under static stress conditions. *MEG 303, CSIR, Pretoria, South Africa.*

Hoek, E., 2007. *Practical Rock Engineering.* s.l.:s.n.

Hoek, E. & Brown, E. T., 1988. The Hoek-Brown failure criterion - a 1988 update. *Rock engineering for underground excavations, Proceedings 15th Canadian Rock Mechanics Symposium, Toronto,* pp. 31-38.

Hoek, E., Marinos, P. & Benissi, M., 1998. Application of the geological strength index (GSI) classification for very weak and sheared rock masses. *The case of the Athens Schist Formation,* 57(2), pp. 151-160.

Ho, E. W., Atkinson, J. H. & Lewin, P. I., 1990. A simple inner cell for triaxial tests using corrosive water. *Geotechnique,* 40(1), pp. 131-132.

Holden, J. M. & Yilmaz, M., 1988. *Penetration Testing in the UK: Chapter 6.* s.l.:Thomas Telford.

Hondros, G., 1959. The evaluation of Poisson's ratio and the modulus of materials of low tensile resistance by the brazilian (indirect tensile) test with particular reference to concrete. *Australian journal of applied science,* Volume 10, pp. 243-268.

Houlsby, G. T. & Wroth, C. P., 1991. The variation of shear modulus of a clay with presure and over-consolidation ratio. *Soils and Foundations,* 31(3), pp. 138-143.

Huat, B. B., Toll, D. G. & Prasad, A., 2012. *Handbook of tropical residual soils engineering.* London: Taylor and Francis Group.

Hudson, J. A., Brown, E. T. & Rummel, F., 1972. The colntrolled failure of rock discs and rings loaded in diametral compression. *International Journal of Rock Mechanics and Mining Science,* Volume 9, pp. 2241-48.

Hughes, P. N. et al., 2009. Full-Scale Testing To Assess Climate Effects on Embankments. *Engineering Sustainability.*

Ibrahim, K., Bunce, G. & Murrells, C., 2009. Foundation Design for the Pentominium Tower in Dubai, UAE. *Proceedings of ICE,* Volume 162, pp. 25-33.

Inglès, M. & Anadón, P., 1991. Relationship of clay minerals to depositional environment in the non-marine eocene pontils group, SE Ebro basin (Spain). *Journal of Sedimentary Petrology,* 61(6), pp. 926-939.

Interact, U., 2010. *UAE Interact.* [Online]
Available at: http://www.uaeinteract.com/nature/geology/fos01.asp

Interact, U., 2011. *UAE Interact.* [Online]
Available at: http://www.uaeinteract.com/nature/geology/fos01.asp

Ismail, M. A., Joer, H. A., Sim, W. H. & Randolph, M. F., 2002. Effect of cement type on shear behavior of cemented calcareous soil. *Journal of Geotechnical and Geoenvironmental Engineering,* 128(6), pp. 520-529.

Ismail, M. A., Sharma, S. S. & Randolph, M. F., 2001. *Small and large strain behaviour of a calcareous soil lithified by different cements.* s.l., s.n.

Isphording, W. C., 1973. Discussion of the occurrence and origin of sedimentary palygorskite-sepiolite deposits. *Clays and Clay Minerals,* 21(1), pp. 391-401.

ISRM, 1978. Suggested methods for determining tensile strength of rock materials. *International Journal of Rock Mechanics and Mining Sciences,* pp. 99-103.

Izumi, K., Ogihara, M. & Kameya, H., 1997. Displacements of Bridge Foundations on Sedementary Soft Rock: A case study on small strain stiffness. *Geotechnique,* 46(3), pp. 619-632.

Jameson, J., 2009. Dolomite neomorphism and porosity evolution. *AAPG Search and Discovery Article*, June, pp. 22-25.

Jardine , R. J., Brooks, N. J. & Smith, P. R., 1985. The use of electrolevel transducers for strain measurements in triaxial tests on weak rocks. *International Journal of Rock Mechanics,* Volume 22, pp. 331-337.

Jardine, R. J., Potts, D. M., Fourie, A. B. & Burland, J. B., 1986. Studies of the influence of non-linear stress strain characteristics in soil-structure interaction. *Geotechnique,* 36(3), pp. 377 - 396.

Jardine, R. J., Symes, M. J. & Burland, J. B., 1984. The measurement of soil stiffness in the triaxial apparatus. *Geotechnique,* 34(3), pp. 323 - 340.

Jardine, R. L., 1992. Some observations on the kinematic nature of soil stiffness. *Soils and Foundations,* 32(2), pp. 111-124.

Jianhong, Y., Wu, F. Q. & Sun, J. Z., 2009. Estimation of the tensile elastic modulus using Brazilian disc by applying diametrically opposed concentric loads. *International journal of rock mechanics and mining sciences,* Volume 46, pp. 568-576.

Johnston, I. W., 1991. Geomechanics and the Emergence of Soft Rock Technology. *Australian Geomechanics,* pp. 3-13.

Johnston, I. W. & Haberfield, C. M., 1992. *Piling: European Practice and Worldwide Trends: Chapter 8.* s.l.:Thomas Telford.

Jovicic, V. & Coop, M. R., 1996. Objective criteria for determining Gmax from bender element tests. *Geotechnique,* 46(2), pp. 357-362.

Jovicic, V. & Coop, M. R., 1997. Stiffness of coarse-grained soils at small strains. *Geotechnique,* 47(3), pp. 545-561.

Karg, C. & Haegeman, W., 2005. Advanced Cyclic Triaxial and Bender Element Test Equipment. *Innovatie Forum Geotechniek,* pp. 1-10.

Karman, T. V., 1911. Festigkeitsversuche unter allseitigern Druck. Zeit. *Vereines Deutch,* Volume 55, pp. 1749-1757.

Kate, J. M. & Gokhale, C. S., 1998. Influence of moisture on triaxial compression behaviour of soft sandstone. *The geotechnics of hard soils - soft rocks,* Issue 1, pp. 245-252.

Kavvandas, M. J. & Anagnostopoulos, A. G., 1998. *A framework for the mechanical behaviour of structured soils.* Naples, Italy, 2nd international conference on the geotechnics of hard soils and soft rocks.

Kendall, C. & Alsharhan, A., 2011. Coastal Holocene carbonates of Abu Dhabi, UAE: depositional setting, sediment distribution, and role of cyanobacteria in micritization. *International association of sedimentology,* Volume 43, pp. 205-220.

Kim, T. & Finno, R., 2011. Anisotropy evolution and irrecoverable deformation in triaxial stress probes. *Journal of geotechnical and environmental engineering.*

Kim, Y. S., Tatsuoka, F. & Ochi, K., 1994. Deformation characteristics at small strains of sedimentary soft rocks by triaxial compression tests. *Geotechnique,* 44(3), pp. 461-478.

Kirkham, A., 2011. Halite, sulphates, sabkhat and salinas of the coastal regions and Sabkha Matti of Abu Dhabi, United Arab Emirates. *International Association of Sedimentology,* Volume 43, pp. 265-276.

Kogel, J. E., Trivedi, N. C., Barker, J. M. & Krukowski, S. T., 2006. *Industrial Minerals and Rocks. Commodities, markets and uses.* 7 ed. s.l.:SME.

Krauskopf, K. B. & Bird, D. K., 1995. *Introduction to Geochemistry.* 3 ed. s.l.:McGraw-Hill International Editions.

Kung, G. T. & Juang, C. H., 2009. Modelling small strain behavior of Taipei clays for finite element analysis of braced excavations. *Computers and Geotechnics,* Volume 36, p. 304.

Last, W. M., 1990. Lacustrine Dolomite: An Overview of Modern, Holocene and Pleistocene Occurrences. *Earth Science Reviews,* Volume 27, pp. 221-263.

Lehane, B., 2000. Post-symposium written discussion: A new local instrumentation system for triaxial tests. *The geotechnics of hard soils - soft rocks,* pp. 1433-1434.

Leonards, G. A. & Ramiah, B. K., 1959. Time effects in the consolidation of clays. *ASTM Special Technical Publication,* Volume 254, pp. 116-130.

Leroueil, S., 2000. Contribution to the round table: Peculiar aspects of structured soils. *The geotechnics of hard soils - soft rocks,* pp. 1669-1678.

Leroueil, S. & Hight, D. W., 2002. *Behaviour and properties of natural soils and soft rocks.* Singapore, Symposium on Characterisation and Engineering Properties of Natural Soils.

Leroueil, S., Tavenas, F. & Locat , J., 1984. Discussion on corrolations between index tests and the properties of remoulded clays. *Geotechnique,* 35(2), pp. 223-226.

Leroueil, S. & Vaughan, P. R., 1990. The General and Congruent Effects of Structure in Natural Soils and Weak Rocks. *Geotechnique,* pp. 467-488.

Li, D. & Wong, L. N. Y., 2013. The Brazilian disc test for rock mechanics applications: Review and new insights. *Journal of Rock Mechanics and Rock Engineering,* Volume 46, pp. 269-287.

Lo, K. Y. & Milligan, V., 1967. Shear strength properties of two stratified clays. *ASCE, SMFD, SM1,* pp. 1-15.

Long, M. & Menkit, C. O., 2007. Geotechnical Properties of Dublin Boulder Clay. *Geotechnique,* 57(7), pp. 595-611.

Machel, H. G., 2001. Bacterial and thermochemical sulfate reduction in diagenetic settings - old and new insights. *Sedimentary Geology,* Volume 140, pp. 143-175.

Macklin, S. et al., 2011. *The engineering geological characterisation of the Barzaman Formation, with reference to coastal Dubai, UAE,* London: ARUP.

Malandraki, V. & Toll, D. G., 1996. The definition of yield for bonded materials. *Geotechnical and Geological Engineering,* 14(1), pp. 67-82.

Malandraki, V. & Toll, D. G., 2001. Triaxial tests on weakly bonded soil with changes in stress path. *Journal of geotechnical and geoenvironmental engineering,* pp. 282-291.

Matthews, M., Simons, N. E. & Menzies, B., 2006. *A short course in geology for civil engineers.* s.l.:Thomas Telford.

Mazzullo, S. J., 1992. Geochemical and neomorphic alteration of dolomite: a review. *Carbonates and Evaporites,* 7(1), pp. 21-37.

Mechanics, I. S. o. R., 1981. Commission on classification of rock and rock messess. *International journal of rock mechanics, mining sciences and geomechanics,* pp. 85-110.

Merkl, R. S., 1989. *A sedimentological, mineralogical and geochemical study of the fuller's earth deposits of the Miocene Hawthorne Group of south Georgia-north Florida,* Bloomington: Indiana University.

Mesri, G., Feng, T. W. & Benak, J. M., 1990. Postdensification penetration resistance of clean sands. *Journal of Geotechnical Engineering,* Volume 116, pp. 1095-1115.

Messerklinger, S. & Springman, S. M., 2010. Non-Linear Elasto-Plastic Behaviour of Lacustrine Clay. *Geotech Geol Eng.*

Mitchell, J. K., 1976. *Fundamentals of Soil Behaviour.* New York: John Wiley & Sons.

Mitchell, J. K., 1993. *Fundamentals of Soil Behaviour.* 2 ed. New York: John Wiley & Sons.

Mogi, K., 1974. On the pressure dependence of strength of rocks and the Coulomb-fracture criterion. *Tectonophysics,* Volume 21, pp. 273-285.

Mohsin, A. K., 2008. *Automated Gmax measurement to explore degredation of artificially cemented carbonate sand,* s.l.: The University of Sydney.

Muir Wood, D., 1990. *Soil behaviour and critical state soil mechanics.* 1st ed. Cambridge: Cambridge University Press.

Neaman, A. & Singer, A., 2000. Rheological Properties of Aqueous Suspensions of Palygorskite. *The Soil Science Society of America,* pp. 427-436.

Nguyen, T. L., Hall, S. A., Vacher, P. & Viggiani, G., 2011. Fracture mechanisms in soft rock: Identification and quantification of evolving displacement discontinuities by extended digital image correlation. *Tectonophysics,* Volume 503, pp. 117-128.

Niemunis, A., Wichtmann, T., Petryna, Y. & Triantafyllidis, T., 2004. Stochastic modelling of settlements due to cyclic loading for soil-structure interaction. *Institute of soil mechanics and foundation engineering.*

Niemunis, A., Wichtmann, T. & Triantafyllidis, T., 2005. Long term deformations in soils due to cyclic loading. *Institute of soil mechanics and foundation engineering.*

Nishi, K., Ishiguro, T. & Kudo, K., 1989. Dynamic properties of weathered sedimentary soft rocks. *Soils and foundations,* 29(3), pp. 67-82.

Nova, R. & Montrasio, L., 1991. Settlements of Shallow Foundations on Sand. *Geotechnique,* 41(2), pp. 243-256.

Nova, R. & Parma, M., 2011. Effects of bond crushing on the settlements of shallow foundations on soft rocks. *Geotechnique,* 61(3), pp. 247-261.

Nygard, R., Gutierrez, M., Bratli, R. K. & Hoeg, K., 2006. Brittle-ductile transition, shear failure and leakage in shales and mudrocks. *Marine and Petroleum Geology,* 23(1), pp. 201-212.

Okubo, F. & Fukui, K., 1996. Complete stress-strain curves for various rock types in uniaxial tension. *International journal of Rock Mechanics,* pp. 549-556.

Pennington, D. S., Nash, D. F. T. & Lings, M. L., 1997. Anisotropy of G0 shear stiffness in Gault Clay. *Geotechnique,* 47(3), pp. 391 - 398.

Peters, W. H. & Ranson, W. F., 1982. Digital imaging techniques in experimental stress analysis. *Optical Engineering,* 21(3), pp. 427-431.

Peth, S. & Horn, R., n.d. *The mechanical behavior of soil under cyclic loading - implications for soil deformation and stress distribution,* Kiel, Germany: Institute for plant nutrition and soil science.

Pierre, C. & Rouchy, J. M., 1988. Carbonate replacements after sulfate evaporites in the middle Miocene of Egypt. *Journal of Sedimentary Petrology,* Volume 58, pp. 446-456.

Potts, D. M. & Zdravkovic, L., 2001. *Finite element analysis in geotechnical engineering - Application.* s.l.:Thomas Telford.

Powell, J. J. & Butcher, A. P., 2003. Characterisation of a Glacial Till at Cowden, Humberside.. *Proceedings of the international conference on the characterisation and engineering properties of natural soils,* pp. 983-1019.

Puzrin, A. M. & Burland, J. B., 1998. Non-linear model of small-strain behaviour of soils. *Geotechnique,* 48(2), pp. 217-233.

Rees, S., Le Compte, A. & Snelling, K., 2013. *A new tool for the automated travel time analyses of bender element tests.* Paris, s.n.

Reeves , G. M., Sims, I. & Cripps , J. C., 2006. *Clay materials used in construction.* 21 ed. s.l.:The geological society publishing house.

Richardson, A. M. & Whitman, R. V., 1963. Effect of strain-rate upon undrained shear resistance of a saturated remoulded fat clay. *Geotechnique,* 13(4), pp. 310-324.

Richart, F. E., Woods, J. D. & Hall, J. R., 1970. *Vibrations of soils and foundations,* New Jersey: Prentice - Hall.

Rietveld, H. M., 1969. A profile refinement method for nuclear and magnetic structures. *Journal of Applied Crystallography,* 2(2), pp. 65-71.

Rodriguez-Navarro, C., Sebastian, E., Doehne, E. & Ginell, W. S., 1998. The role of sepiolite-palygorskite in the decay of ancient Egyption limestone sculptures. *Clays and Clay Minerals,* 46(4), pp. 414-422.

Rolo, R., 2003. *The anisotropic stress-strain-stiffness behavior of brittle sediments,* PhD Thesis: Imperial College London.

Roscoe, K. H., Schofield, A. N. & Thurairajah, A., 1963. An evolution of test data for selecting a yield criterion for soils. *ASTM,* Volume STP 361, pp. 111 - 128.

Rouainia, M. & Muir Wood, D., 2000. A kinematic hardening constitutive model for natural clays with loss of structure. *Geotechnique,* 50(2), pp. 153-164.

Rouili, A., 2007. Stress History effect on the Small Strains Behavior of Re-compacted Clay. *Twelfth International Colloquium on Structural and Geotechnical Engineering.*

Sanz-Montero, M. E., Rodriguez-Aranda, J. P. & Calvo, J. P., 2006. Mediation of Endoevaporitic Microbial Communities in Early Replacement of Gypsum by Dolomite: A Case Study from Miocene Lake Deposits of the Madrid Basin, Spain. *Journal of Sedimentary Research,* Volume 76, pp. 1257-1266.

Sarsfield, B. A. et al., 2006. Powder X-ray diffraction detection of crystalline phases in amorphous pharmaceuticals. *JCPDS-International Centre for Diffraction Data,* pp. 322-327.

Scherf, A. & Rullkotter, J., 2009. Biogeochemistry of high salinity microbial mats - Part 1: Lipid composition of microbial mats accross intertidal flats of Abu Dhabi, UAE. *Organic Geochemistry,* Volume 40, pp. 1018-1028.

Scholtes, L. & Donze, F. V., 2013. A DEM model for soft and hard rocks: role of grain interlocking strength. *Journal of the mechanics and physics of solids,* 61(2), pp. 352-369.

Sepmstrata, 2011. *Sepmstrata.* [Online]
Available at: http://sepmstrata.org/UAE/AbuDhabi.html

Sheng, D., Westerberg, H., Mattsson, H. & Axelsson, K., 1997. Effects of End Restraint and Strain Rate in Triaxial Tests. *Computers and Geotechnics,* 21(3), pp. 163-182.

Sides, G. & Barden, L., 1970. The microstructure of dispersed and flocculated samples of kaolinite, illite and montmorillonite. *Canadian Geotechnical Journal,* Volume 8, pp. 391-399.

Silvestri, F. & d'Onofrio, A., 2000. Panel report: Advanced procedures in laboratory stress-strain testing on hard soils. *The geotechnics of hard soils - soft rocks,* pp. 1415-1427.

Simpson, B., O'Riordan, N. J. & Croft, D. D., 1979. A computer model for the analysis of ground movements in London Clay. *Geotechnique,* Issue 29, pp. 149 - 175.

Simpson, D. & Rouainia, M., 2011. *Non-Linear Small Strain Stiffness of Glacial Till.* Newcastle University CEG, s.n.

Simpson, D. & Rouainia, M., 2012. *Non-Linear Small Strain Stiffness of Glacial Till.* San Francisco, GeoCongress 2012, pp. 2234-2243.

Singer, A., 1981. The texture of Palygorskite from the Rift Valley, Southern Israel. *Clay Minerals,* Volume 16, pp. 415-419.

Skempton, A. W., 1953. The colloidal "activity" of clays. *International conference on soil mechanics and foundation engineering,* 1(3), pp. 57-61.

Skempton, A. W., 1961. *Effective stress in soils concrete and rock.* London, Butterworths, pp. 4-16.

Specification, G., 2010. *Global Specification.* [Online]
Available at:
http://www.globalspec.com/Specifications/Engineering_Services/Geotechnical_Services

Stephenson, P., Skinner, M. & Richmond, A., 2009. *Numerical Modeling in Geotechnical Practice and Research.* Newcastle, ARUP.

Stirling, R. A., 2014. *Multiphase modelling of desiccation cracking in compacted soil.* Newcastle: Newcastle University.

Stirling, R. A., Simpson, D. J. & Davie, C. T., 2013. The application of digital image correlation to Brazilian testing of sandstone. *The international journal of rock mechanics and mining sciences,* Volume 60, pp. 1-11.

Sun, D. A. et al., 2004. Deformation and strength characteristics of weathered soft rock using triaxial tests. *International journal of rock mechanics and mineral science,* 41(3), pp. 1-6.

Sun, D., Feng, T. & Matsuoka, H., 2006. Stress-strain behaviour of weathered weak rock in middles-sized triaxial tests. *Canadian Geotechnical Journal,* Volume 43, pp. 1096-1104.

Sutton, M. A., 1983. Determination of displacements using a digital correlation method. *Image and vison computing,* 1(3), pp. 133-139.

Sutton, M. A., McNeill, S. R., Helm, J. D. & Chao, Y. J., 2000. Advances in two-dimentional and three-dimentional computer vision. *Photomechanics, Topics Applied Physics,* Volume 77, pp. 323-372.

Symes, M. J. & Burland, J. B., 1984. The determination of local displacements on soil samples. *ASTM Geotech. Test. J. In Press.*

Szymakowski, J., 2006. Shear Testing of Soft Rock Masses. *Geotechnical Testing Journal,* 30(2).

Takahashi, A., Jardine, R. J. & Dennis, W. H., 2005. Swelling effects on mechanical behavior of natural London Clay. *Soil Mech. Osaka in print.*

Tatsouka, F. et al., 1998. Some new aspects of time effects on the stress-strain behavior of stiff geomaterials. *2 HSSR, Napoli.*

Tatsuoka, F., 1996. A note on the use of a local gauge in consolidated undrained triaxial compression tests on sedimentary soft rock. *Stress strain testing of geomaterials in the laboratory ISSMGE.*

Tatsuoka, F. & Kohata, Y., 1995. Stiffness of hard soils and soft rocks in engineering applications. *Pre-failure deformation of geomaterials,* Volume 2, pp. 947-1063.

Teller, J. T., Glennie, K. W., Lancaster, N. & Singhvi, A. K., 2000. Calcareous dunes of the United Arab Emirates and Noah's Flood: the postglacial reflooding of the Persian (Arabian) Gulf. *Quaternary International,* Volume 68-71, pp. 297-308.

Terzagi, K., Peck, R. B. & Mesri, G., 1996. *Soil Mechanics in Engineering Practice.* 3 ed. s.l.:Wiley-Interscience Publication.

Thompson, R. P. & Leach, B. A., 1988. *Penetration Testing in the UK: Chapter 7.* s.l.:Thomas Telford.

Tobin, M. P., 1980. Factors Influencing Road Design, Construction and Maintenance in the United Arab Emirates. *Proc. Instn Civ. Engrs, Part 1,* Volume 68, pp. 27-38.

Trhlikova, J., Masin, D. & Bohac, J., 2012. Small-strain behaviour of cemented soils. *Geotechnique,* 62(10), pp. 943-947.

Truong, Q. H., Lee, C., Kim, Y. U. & Lee, J. S., 2012. Small strain stiffness of salt-cemented granular media under low confinement. *Geotechnique,* 62(10), pp. 949-953.

uaetourguide, 2011. *uaetourguide.* [Online]
Available at: http://uaetourguide.blogsome.com/

UBW, 2014. *University of Bristol Website.* [Online]
Available at: http://environment.uwe.ac.uk/geocal/SoilMech/compression/default.htm

Vardanega, P. J. & Bolton, M. D., 2011. Practical methods to estimate the non-linear shear stiffness of fine grained soils. *International symposium on deformation characteristics of geomaterials,* pp. 33-40.

Vatsala, A., Nova, R. & Srinivasa Murthy, B. R., 2001. Elastoplastic model for cemented soils. *Journal of geotechnical and geoenvironmental engineering,* pp. 679-687.

Vaughan, P. R., 1993. Engineering Behavior of Weak Rocks: Some Answers and Some Questions. *Geotechnical Engineering of Hard Soils - Soft Rocks,* pp. 1741-1765.

Venkatramaiah, C., 2006. *Geotechnical Engineering.* s.l.:New age international publishers.

Viggiani, G. & Atkinson, J. H., 1995. Interpretation of bender element tests. *Geotechnique,* 45(1), pp. 149-154.

Viggiani, G. & Atkinson, J. H., 1995. Interpretation of Bender Tests. *Geotechnique,* Volume 45, pp. 149 - 154.

Viggiani, G. & Atkinson, J. H., 1995. Stiffness of fine-grained soil at very small strains. *Geotechnique,* 45(2), pp. 249-265.

Walkden, G. M. & Williams, A. H., 1998. Carbonate Ramps and the Pliestocene-Recent Depositional Systems of the Arabian Gulf. In: S. Publications, ed. *Carbonate Ramps.* London: Geological Society.

Walker, M. J., 2012. *Hot Deserts: Engineering, Geology and Geomorphology: Engineering Group Working Party Report.* s.l.:Geological Society of London.

Waltham, T., 2012. Soluble Ground. In: J. Burland, T. Chapman, H. Skinner & M. Brown, eds. *ICE manual of geotechnical engineering: Volume 1.* s.l.:ICE Publishing, pp. 533-545.

Wang, Q. Z. et al., 2004. The flattened Brazilian disc specimen used for testing elastic modulus, tensile strength and fracture toughness of brittle rocks; analytical and numerical results. *International Journal of Rock Mechanics and Mining Sciences,* Volume 41, pp. 245-253.

Wang, Q. Z. & Xing, L., 1999. Determination of fracture toughness by using the flattened Brazilian disc specimen for rocks. *Engineering and fracture mechanics,* Volume 64, pp. 193-201.

Wanjei, C. & Richard, J. F., 2010. Stress Strain responce of block samples of compressible chicago glacial tills. *Journal of geotechnical and geoenvironmental engineering.*

Whitlow, R., 2001. *Basic Soil Mechanics.* 4 ed. s.l.:Prentice Hall.

Wijk, G., 1978. Some new theoretical aspects of indirect measurments of the tensile strength of rocks. *International journal of rock mechanics, mining sciences and geomechanics,* Volume 15, pp. 149-160.

Wissa, A. E. Z., Fuleihan, N. F. & Ingra, T. S., 1982. *Evaluation of Phosphatic Clay Disposal and Reclaimation Methods,* s.l.: s.n.

Wright, A. C., Burgraeve, A. R. & Cathie, D. N., 2000. State of practice for site investigation in calcareous sediments. *Engineering for Calcareous Sediments,* pp. 433-442.

Wu, B., King, M. S. & Hudson, J. A., 1991. Stress-induced Ultrasonic wave velocity anisotropy in a sandstone. *International journal of rock mechanics and mining sciences,* 28(1), pp. 101-107.

Wyllie, D. C. & Mah, C. W., 2004. *Rock Slope Engineering, Civil and Mining.* 4 ed. s.l.:Spon Press.

Yamashita, S. et al., 2009. Interpretation of international parallel test on the measurement of Gmax using bender elements. *Soils and Foundations,* 49(4), pp. 631-650.

Yanagidani, T., Sano, O., Terada, M. & Ito, I., 1978. The observation of cracks propagating in diametrically-compressed rock discs. *International journal of rock mechanics, mining sciences and geomechanics,* Volume 15, pp. 225-235.

Yin, Z. Y., Chang, C. S. & Hicher, P. Y., 2010. A micro-structural approach for modelling the mechanical behaviour of structured clays. *Soil behaviour and geo-micromechanics. Geotechnical special publication,* Volume 200, pp. 172-177.

Yoshinaka, R. & Osanda, M., 1995. The comparison between dynamic and static strength of soft sedimentary rocks. *In Rock Foundation,* pp. 109-114.

Yu, Y., Zhang, J. & Zhang, J., 2009. A modified Brazilian disk tension test. *International journal of rock mechanics and mining sciences,* Volume 46, pp. 421-425.

Zdravkovic, L., Potts, D. M. & John, H. D., 2005. Modelling of a 3D excavation in finite element analysis. *Geotechnique,* Volume 55, pp. 497-513.

Zhang, S. et al., 2010. Tempurature-controlled triaxial compression/creep test device for thermodynamic properties of soft sedimentary rock and corresponding theoretical prediction. *Journal of rock mechanics and geotechnical engineering,* 2(3), pp. 255-261.